DIRECT ESTIMATION OF ACOUSTIC SOURCE CHARACTERISTICS OF THE INTERNAL COMBUSTION ENGINE EXHAUST SYSTEM AND ANALYSIS OF COMPLEX MUFFLER CONFIGURATIONS

A Thesis

Submitted for the degree of

Doctor of Philosophy

IN THE FACULTY OF ENGINEERING

By

Krishna Mohan Kumar

Department of Mechanical Engineering

Indian Institute of Science

BANGALORE-560012

JULY 2018

Dedicated

to

my Parents

ACKNOWLEDGEMENTS

First of all, I would like to express my sincere gartitude to my mentor **Prof. M. L. Munjal** for his constant encouragement and motivation which played a pivotal role in making this thesis possible. He taught the subjects Industrial Noise Control and Acoustics of Ducts and Mufflers not only in the class to me but in every discussion meeting. Moreover, his teachings to me were not limited to the technical subjects, they helped me to carry out any work in a systematic way. I have been convinced by him that every hurdle is an oppourtunity in disguise, and I hope that it will encourage me to tackle any problem in my research career ahead.

I thank **Prof. V. R. Sonti** for accepting me as a PhD student and for his valuable discussions from time to time. He taught me two subjects, namely, Fundamentals of Acoustics and Structural Acoustics which proved to be the foundation stone for my research work. I have been inspired by his dedication and passion for teaching. The series of assignments in these two courses helped me to develop better understanding of the subject.

I take this opportunity to sincerely acknowledge **Prof. R. Narasimhan** (Chairman when I joined the department) and **Prof. Pradip Dutta** (present Chairman) for making all the facilities and financial assistance freely avaialable to me.

I thank the instructors of the subject Computational Fluid Flow and Heat Transfer, **Prof. R.V. Ravikrishna, Dr. Ratnesh Shukla** and **Dr. Gaurav Tomar** who made me do several assignments that helped me to develop better computational skills.

I also wish to acknowledge the **Ministry of Human Resources and Development (MHRD), India** for supporting my research through a substantial scholarship throughout these five years.

The pleasant journey of my PhD research has been a result of the support I got from the staff of the Department of Mechanical Engineering. I wish to acknowledge **Mrs. Somavathi Devi**, **Mrs. Devaki, Mrs. F. S. Banu, Mr. P. Sampath, Ms. Chinnamma, Ms. Mangala R., Mr. Dileep and Mr. Raja**. I would like to acknowledge the technical help provided to me by **Mr. C. Srinivasa** in the laboratories of the Facility for Research in Technical Acoustics (FRITA).

Srijan, Dinesh, Venkatapathy, Subhojit, Somnath, Yogendra, Kundan, Keshav, Vivek and **Chandrashekhar** have seen me through several ups and downs in the entire journey, I would like to thank all of them. I also wish to thank my labmates to whom I have been very

close, namely, **Dr. Arup Nandy, Dr. Manish Agrawal, Abhishek Verma, E Ramya, S. Kaushik, Vikas Kumar, Anoop Mappa, Reginald Lourd Raj, Vachan Rao E** and **Biswajit Bharat**. I especially acknowledge **Abhishek Verma** for teaching me to do simulations in LMS Virtual Lab, and **E Ramya** for demonstrating how to take measurements with PULSE acquisition system. I have been greatly benefited in my understanding of duct acoustics while discussing with my colleagues **Vidya Sagar** and **Vikas Kumar**. **Reginald Lourd Raj** and **E Vachan Rao** have done the proofreading for me with joy.

I would like to express my sincere thanks to the **anonymous OEMs** who shared with me the measured values of the unmuffled exhaust noise of their diesel engines. I am grateful to **AVL AST, Austria** who provided me free licences of their BOOST software through these years.

It is my personal belief that whatever I have been able to do till date is due to the teachings of **my former teachers**. I thank all of them from the bottom of my heart.

Last, but not the least**, I bow my head before Lord Shiva who has been constantly giving me courage as well as guidance.**

(Krishna Mohan Kumar)

ABSTRACT

Reduction in noise radiated from the internal combustion (IC) engines is needed to meet the ever increasingly stringent noise regulations. The unmuffled exhaust noise of an IC engine is the biggest contributor to the overall engine noise. Prediction of the unmuffled as well as muffled sound pressure level (SPL) spectrum calls for prior estimation of both the source characteristics, namely, source pressure and source impedance, whereas prediction of the insertion loss (IL) spectrum of a muffler needs only source impedance. The present study aims at estimation of both these source characteristics using a novel direct evaluation method.

The source impedance just downstream of the valve throat is the sum of the cylinder volume compliance and valve impedance (resistance and inertance). The cylinder compliance depends on the in-cylinder gas temperature and the valve resistance depends on the exhaust gas mass flow rate, and both vary with respect to the crank angle. Computation of source impedance and exhaust gas mass flow rate calls for the aero-thermodynamic computation in the time-domain making use of the values of pressure and temperature of the in-cylinder gas at the exhaust valve opening (EVO) along with the basic geometrical details of the cylinder, intake and exhaust valves and ports. Equivalent source impedance of time-varying source is estimated by taking the reciprocal of the crank-angle-area-weighted average of the admittance of the source, where at every crank angle step the instantaneous cylinder volume is taken for estimation of the compliance of cylinder and the instantaneous valve flow area and mass flow rate for the valve impedance. The source impedance of a single-cylinder engine is estimated at different engine speeds and it is shown that the little variations in it due to different engine speeds do not matter for the IL estimation. Further a simple, albeit approximate, parametric expression of source impedance is derived in terms of cylinder capacity for ready reference of the muffler designers.

This novel direct evaluation method is now applied to the naturally aspirated (NA) two-cylinder engine exhaust system by estimating the source characteristics of each cylinder assuming that the other cylinder is not exhausting at the same time. Source pressure of each cylinder is the product of acoustic mass velocity at the source-load junction and the sum of the source impedance and the load impedance. The estimated source characteristics for each cylinder at the downstream of the exhaust valve are then transferred downstream to the end of the runner. The source characteristics so obtained are combined for the two cylinders. These values are then transferred to the beginning of the acoustic test load (exhaust pipe or exhaust muffler). The estimation of source characteristics is dependent on the exhaust gas mass flow

rate which depends on the exhaust system to which the cylinders are discharging. Thus, the IC engine acoustic source is load-dependent, not unique. Yet, the resultant source characteristics help to predict unmuffled sound pressure level (SPL) spectra that are shown to agree reasonably with the measured spectra.

Using the transfer matrix of the turbine of a turbocharger the source characteristics of a turbocharged engine exhaust system are estimated making use of the novel direct evaluation method developed in the present study. Transfer matrices of the turbine and compressor of an automotive turbocharger are derived using the mass continuity upstream and downstream of the turbine and compressor along with the pressure ratios. The acoustic source characteristics of each cylinder at the source-load junction downstream of the exhaust valve are computed assuming that the cylinder discharges to the ideal pressure release boundary condition with the constant pressure being the product of the turbine pressure ratio and mean pressure in the exhaust pipe. Source characteristics of each cylinder are used to estimate the source characteristics downstream of the exhaust manifold. The source characteristics are further estimated at the source-load junction downstream of the turbine using the derived transfer matrix of the turbine. Finally, the estimated source characteristics of the engine downstream of the turbine are used to predict the unmuffled sound pressure level (SPL) spectrum which is shown to compare reasonably well with the experimentally measured values. Importance of acoustic modelling of the turbine is highlighted by comparing the SPL spectra predicted using the estimated source characteristics with and without the turbine. The estimated source characteristics and unmuffled approximate SPL spectrum of a turbocharged engine being thus known at the engine's inception stage, the present study can be used for the possible integration of design and analysis of the engine and muffler.

Efficient mufflers are needed to comply with the stringent noise regulations as well as the requirement of low backpressure to ensure low brake specific fuel consumption. Design and analysis of some commercial complex mufflers are therefore studied here. The mufflers are analysed using the 1-D integrated transfer matrix (ITM) approach and validated against the 3-D finite element analysis. Three different types of mufflers; double flow-reversal muffler with a few holes in pipes and baffles, multiply-connected co-axial (MCCA) perforated element muffler, and side-inlet side-outlet (SISO) perforated element muffler are investigated here. To predict the IL spectrum of mufflers used in multi-cylinder engines, source is assumed anechoic.

Mufflers for automotive engine require adequate overall insertion loss (IL) in dBA, low backpressure to ensure low brake specific fuel consumption (BSFC) of the engine, and a low

muffler volume to engine capacity ratio, all at the same time. In the present research work, the role of mean flow on the flow-acoustic performance of four different multiply-connected co-axial mufflers (MCCA) is illustrated. The parametric studies on one of the configurations highlight the importance of the bias and grazing mean flow Mach number. The automotive engines operate over a wide range of engine speeds, which demands a wideband transmission loss (TL) and insertion loss (IL) rather than sharp peaks at certain frequencies. In the literature, a higher mean flow Mach number has been associated with more jet-noise as well as backpressure. However, in this thesis, it is shown that higher mean flow can be used to advantage in the MCCA mufflers by making use of the inline flow-acoustic resistance which raises the TL curve over the entire frequency range. In the present study some design guidelines for the mufflers with higher specific insertion loss (ratio of overall insertion loss (in dBA) to the muffler to engine volume ratio) as well as modest backpressure.

In general, large volume of the muffler for a diesel generator (DG) set engine is not a concern, but logistics of an acoustic enclosure require mounting of the exhaust muffler on the top of the enclosure with side-inlet and side-outlet. Four different, yet somewhat similar, side-inlet side-outlet (SISO) perforated element muffler configurations with almost same backpressure have been investigated. It has been shown that the 1-D plane wave analysis is adequate for the first few harmonics of the engine speed order that are of prime interest for muffler designers. The 1-D plane wave analysis, however, becomes too approximate at higher frequencies, and for that reason, one has to rely on the 3-D FEA for evaluation of the overall four-pole parameters of the muffler. Finally, some design guidelines have been evolved for similar mufflers.

LIST OF CONTENTS

LIST OF FIGURES

LIST OF TABLES

NOMENCLATURE AND ABBREVIATIONS

Although most of the mathematical symbols or notations as well as the abbreviations have been defined at the first instance of their occurrence in the text; in this section we define the most commonly occurring mathematical symbols as well as abbreviations for the sake of clarity and completeness.

Roman Letters

$B_{i,j-k}$	Transfer matrix of perforated baffle between j^{th} section and k^{th} section of i^{th} domain
c_0	Sound speed in exhaust gas medium
c_a	Sound speed in ambient gas medium
C_D	Coefficient of discharge
d_{ep}	Diameter of exhaust pipe
d_{tp}	Diameter of tail pipe
D_{vi}	Valve seat inner diameter
F	Frequency (Hz)
ID_{i,j,k_l}	Transfer matrix of interacting ducts of domain i and j between sections k and l
J	$\sqrt{-1}$
k_0	Wave number
M_b	Bias flow Mach number
M_{ex}	Mean flow Mach number in exhaust pipe
M_g	Mean grazing flow Mach number
M_{tp}	Mean flow Mach number in tail pipe
$\dot{m}_c$	Rate of change of in-cylinder gas
$\dot{m}_{ex}$	Exhaust gas mass flow rate from exhaust valve/s cylinder
P	Acoustic pressure
$p_{i,j}$	Acoustic pressure in i^{th} domain at j^{th} section

P_{i,j_k}	Transfer matrix of pipe element between j^{th} section and k^{th} section of i^{th} domain
p_s	Source pressure
P_{ep}	Transfer matrix of exhaust pipe
P_{tp}	Transfer matrix of tail pipe
Q_0	Volume discharge rate
R_0	Radiation resistance
r_0	radius of orifice at the radiation end
R_{eq}	Equivalent flow resistance
S_{ep}	Cross-sectional area of exhaust pipe
$S_{i,j}$	Acoustic state variables of i^{th} domain at j^{th} station
$T_{11},\ T_{12},\ T_{21},\ T_{22}$	Four pole parameters of transfer matrix of an element
v	Acoustic mass velocity
v_0	Acoustic mass velocity at radiation end
$v_{i,j}$	Acoustic mass velocity of i^{th} domain at j^{th} section
v_s	Source velocity
VP_{i,j_k}	Transfer matrix of variable area conical pipe excluding inner pipe/s
Y_0	Characteristic impedance of a pipe
Y_{tp}	Characteristic impedance of tail pipe
Z_0	Radiation impedance
Z_L	Load impedance
Z_p	Perforate impedance
Z_s	Source impedance
$Z_{s,eq}$	Equivalent source impedance

Greek Letters

α_c	Compressor static pressure ratio
α_t	Turbine static pressure ratio

γ	Ratio of specific heat capacities of gas
ε	Loss factor
ΔP	Backpressure of a muffler
ΔP_{ep}	Stagnation pressure drop across the exhaust pipe of a muffler
ΔP_{MP}	Stagnation pressure drop across the muffler proper
ΔP_{t}	Stagnation pressure drop across the complete muffler
ΔP_{tp}	Stagnation pressure drop across the tail pipe of a muffler
η_{v}	Volumetric efficiency of engine
θ	Crank angle; Normalized specific impedance of a perforate
λ	Wavelength
μ	Dynamic viscosity
ν	Kinematic viscosity
ρ_{a}	Density of air
ρ_{ex}	Density of exhaust gas
σ	Porosity of perforated pipe/baffle
ϑ	Normalized perforate reactance
χ	Normalized perforate resistance
ω	Angular frequency (rad/s)

Abbreviations

0-D	0-dimensional (Lumped Element)
1-D	1-dimensional
3-D	3-dimensional
B1, B2, B3	Baffle 1, Baffle 2, Baffle 3, respectively
BDC	Bottom Dead Centre
BEM	Boundary Element Method
C1, C2, C3	Chamber 1, Chamber 2, Chamber 3, respectively
C-1, C-2, C-3, C-4	Configuration nos. 1, 2, 3, and 4 of MCCA and SISO mufflers, respectively
CFD	Computational Fluid Dynamics
CPU	Central Processing Unit
CTR	Concentric Tube Resonator

DG	Diesel Generator
DTEC	Double Tuned Expansion Chamber
EV	Exhaust Valve
EVC	Exhaust Valve Closing
EVO	Exhaust Valve Opening
FEA	Finite Element Analysis
FEM	Finite Element Method
HAW	Holes Attached with Wall of Muffler Shell
HBM	Harmonic Balance Method
IC	Internal Combustion
IL	Insertion Loss
ISO	International Organization for Standardization
ITM	Integrated Transfer Matrix
IV	Intake Valve
IVC	Intake Valve Closing
IVO	Intake Valve Opening
MCCA	Multiply-Connected Coaxial
NA	Naturally Aspirated
NR	Noise Reduction
OAR	Open Area Ratio
PWH	Plug with Hole
RPM	Shaft speed in Revolutions Per Minute
SEC	Simple Expansion Chamber
SISO	Side-Inlet and Side-Outlet
SPL	Sound Pressure Level
SSL	Source Strength Level
T/C	Turbocharged
TDC	Top Dead Centre
TL	Transmission Loss
TMM	Transfer Matrix Method

Chapter 1

Introduction and Literature Review

1.1 Introduction

Internal combustion engines are considered as one of the most useful inventions which have changed the world we see today. Its application ranges from small agricultural pump engines to the large size marine engines. However, noise pollution due to the internal combustion (IC) engines has been a concern for almost every application. Day-by-day, the regulations for noise due to IC engines are becoming increasingly stringent across the globe. The unmuffled exhaust noise of an internal combustion engine is the greatest contributor to the overall engine noise. Thus, the problem of reducing overall engine noise calls for better attenuation of the exhaust noise. Stricter noise limitations can be satisfied by means of quieter sources (IC engines) and the mufflers with better attenuation characteristics.

Flow processes in an IC engine running at constant shaft speed (RPM) can be modelled in the time domain as well as frequency domain. Periodic nature of the IC engine processes makes the frequency domain modelling a preferable tool for a fast and simple analysis over the relatively time consuming and cumbersome time domain analysis. The exhaust mass flux $\left(\dot{m}_{ex}\left(t\right)\right)$ discharged by a cylinder of an IC engine during one thermodynamic cycle can be represented as the sum of Fourier series

$$\dot{m}_{ex}\left(t\right)=\sum_{n=-\infty}^{\infty}v_{c,n}\left(n\omega_0\right)e^{jn\omega_0 t},\quad \omega_0=\frac{2\pi}{T_0},\ T_0=\frac{60}{N}\times\frac{n_{st}}{2} \tag{1.1}$$

where T_0 is the time period of engine crankshaft to complete one thermodynamic cycle, N is the engine crankshaft speed in revolutions per minute (RPM), n_{st} is number of strokes in a thermodynamic cycle, ω_0 is the circular frequency, n is the harmonic number, ω/ω_0, and $v_{c,n}(n\omega_0)$ along with its complex conjugate are the Fourier coefficients of the n^{th} harmonic. Here, $v_{c,0}$ is the mean exhaust mass flow rate which is given by

$$v_{c,0}=\frac{1}{T_0}\int_0^{T_0}\dot{m}_{ex}\left(t\right)dt. \tag{1.2}$$

The fundamental frequency of the discharged exhaust gas mass flux of a cylinder is called the firing frequency of an individual cylinder which is given by

$$F_{cyl} = \frac{N}{60} \times \frac{2}{n_{st}}. \tag{1.3}$$

Thus, the firing frequency of a multi-cylinder engine is given by

$$F_{eng} = \frac{N}{60} \times \frac{2}{n_{st}} \times n_{cyl}, \tag{1.4}$$

where n_{cyl} is the number of cylinders in the engine.

The firing frequency and its multiples can also be represented by a non-dimensional frequency parameter which is known as Speed Order. It is defined as ratio of frequency (f) and engine crankshaft frequency (revolutions per second), which is mathematically represented by

$$\text{Speed Order (SO) of frequency } f = \frac{f}{RPM/60}. \tag{1.5}$$

Thus, the speed orders corresponding to individual cylinder firing frequency (F_{cyl}) and multi-cylinder engine firing frequency (F_{eng}) are $2/n_{st}$ and $n_{cyl} \times 2/n_{st}$, respectively.

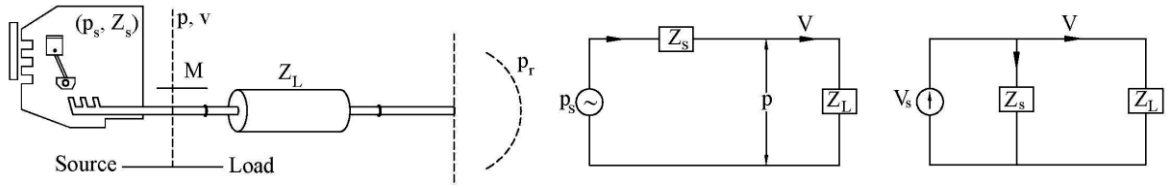

(a) (b) (c)

Figure 1.1. Schematic of the typical IC engine exhaust system: (a) Acoustic source-load system, (b) Electro-acoustic circuit with pressure representation of the source, (c) Electro-acoustic circuit with velocity representation of the source.

The frequency domain analysis of the IC engine's exhaust system is based on the electro-acoustic analogy where the engine (to be more specific, each cylinder) is assumed to be an alternating potential (pressure) source, p_s, or an alternating current (mass velocity) source, v_s, with certain internal impedance (acoustic source impedance), Z_s, for each harmonic of the firing frequency [1]. In the electro-acoustic analogy, the acoustic pressure (p) and the acoustic mass velocity (v) are analogous to the electric potential and the electric current, respectively.

This can be seen in Fig. 1.1. The representations of source given in Figs. 1.1 (b) and 1.1 (c) would be equivalent (yielding same v) provided $v_s = p_s/Z_s$.

Frequency domain analysis using the electro-acoustic analogy does not consider the contribution of shock noise and flow generated noise from the exhaust valve and ports. It was shown by Jones [2] that the propagating pressure waves caused by variations in the mass flow rate at the exhaust port of a single-cylinder, 2-stroke engine is the most significant factor for noise radiation. Jones [2] also showed experimentally the relative insignificance of noise contribution due to shock and turbulent mixing mechanisms to the overall radiated noise.

Generally, there are three performance measures of a muffler, namely, transmission loss (TL), noise reduction (NR) and insertion loss (IL). TL is defined as the difference between the acoustic power level incident on to the muffler and that transmitted to an anechoic termination, NR is the difference between sound pressure levels at two arbitrary selected points upstream and downstream of the muffler proper, and IL is the difference between the radiated acoustic power levels or the sound pressure levels (SPL) in the far field at the same distance from the exhaust orifice with and without muffler. Therefore, IL is the true performance measure of any muffler. It depends on the source impedance, the muffler and the radiation impedance with and without the muffler [1].

Table 1.1. Different source impedance assumptions in literature

Assumption	Source impedance value	Used in literature
Constant pressure source	0	Davis *et al*. [3]
Constant velocity source	∞	Fukuda [4]
Anechoic source	$Y_0\left(=c_0/S_{ep}\right)$	Harris [5]
Compliance of cylinders and engine manifold	$-jc_0^2/\left(\omega V_m\right)$	Sreenath and Munjal [6]
Equal magnitude of source resistance and reactance	$Y_0(0.7-j0.7)$	Callow and Peat [7]

To meet the norms of noise regulations, knowledge of the unmuffled SPL is needed. Then only the design of an appropriate muffler can be carried out. It is well known that the prediction of unmuffled SPL requires apriori knowledge of both the source characteristics, namely, source pressure p_s and source impedance Z_s shown in Fig. 1.1. However, estimation of IL needs only the source impedance. In literature, three approximations of an acoustic source are mentioned, namely, constant pressure source (zero source impedance), constant velocity source (infinite

source impedance), and anechoic source (source impedance equal to characteristic impedance of the connecting pipe). In one of the first papers, the source impedance of a multi-cylinder engine was assumed as the compliance of half of cylinder cavity and exhaust manifold volume [6], and it showed that in the low frequency region the source behaves as a constant velocity source and in the high frequency region it is very close to constant pressure source. None of the above mentioned models assume the source to have complex source impedance with real and imaginary parts. Callow and Peat [7] proposed another model of source impedance which has equal values of normalized positive resistance and negative reactance, and its magnitude is equal to the charcteristic impedance of the exhaust pipe. The different models of source impedance mentioned in the literature are given in Table 1.1.

Probably, the first attempt to compute the IL considering source impedance and radiation impedance was made by Sreenath and Munjal [6]. Later, an algebraic algorithm was developed to compute velocity ratio and thence the IL of an acoustic filter, and in general a one-dimensional dynamic filter [8,9]. The algorithm brings out the significance of dominating factors and highlights the importance of source impedance as well. However, these references did not include the effect of mean flow on wave propagation, and most importantly, the role of mean flow on the radiation of noise. It was shown by Alfredson and Davies that the consideration of mean flow leads to a better prediction of noise radiated from the tail pipe [10]. However, this study was carried out with measured values of acoustic pressure upstream of the tail pipe. A systematic application of transfer matrix method (TMM) with mean flow effect was demonstrated by Munjal [11], where the aeroacoustic (or convective) variables (pressure and mass velocity) were introduced. In that study, the convective state variables were related to the classical acoustic state varibles in terms of the mean flow Mach number and characteristic impedance of the pipe. Later, relations between the convective source parameters (source pressure, source velocity and source impedance) and the corresponding classical acoustic source parameters were derived by Munjal and Doige [12].

In the following section, computation of radiated exhaust SPL and IL of a muffler in terms of source characteristics and transfer matrices of the reference pipe element and the muffler are presented for ready reference.

1.2 Radiated exhaust SPL and IL of a muffler

The electro-acoustic circuit of a load with pressure representation of the source and the four-pole parameters of the acoustic load is shown in Fig. 1.2.

The relation between the acoustic state variables at the source load and the acoustic load in Fig. 1.2 is given by

$$\begin{bmatrix} p_s \\ v \end{bmatrix} = \begin{bmatrix} 1 & Z_s \\ 0 & 1 \end{bmatrix} \begin{bmatrix} T_{11} & T_{12} \\ T_{21} & T_{22} \end{bmatrix} \begin{bmatrix} Z_0 v_0 \\ v_0 \end{bmatrix} \tag{1.6}$$

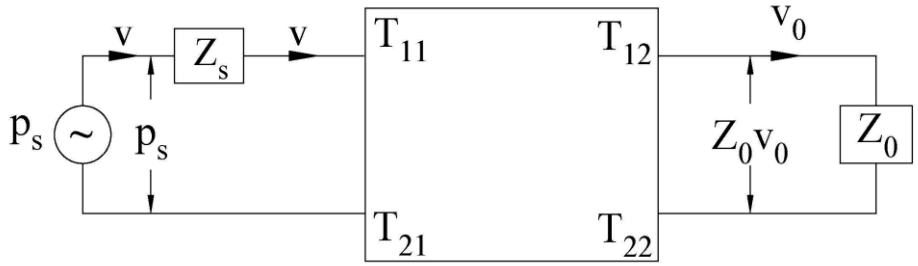

Figure 1.2. Electro-acoustic circuit with four-pole parameters of an acoustic load

From Eq. (1.1), the acoustic mass velocity at the radiation end is given in terms of source characteristics, four-pole parameters of load, and radiation impedance by

$$v_0 = \frac{p_s}{Z_0\left(T_{11} + T_{21}Z_s\right) + \left(T_{12} + T_{22}Z_s\right)} \tag{1.7}$$

The acoustic power at the radiation end (just inside the tail pipe) is given by [1]

$$W_T = \frac{|v_0|^2}{2\rho_{ex}}\left[R_0\left(1 + M_{tp}^2\right) + M_{tp}\left(\frac{|Z_0|^2}{Y_{tp}} + Y_{tp}\right)\right] \tag{1.8}$$

where ρ_{ex} is the exhaust gas density, M_{tp} is the mean flow Mach number in the tail pipe, Y_{tp} is characteristic impedance of the tail pipe, $Z_0 = R_0 + jX_0$ is the radiation impedance, and R_0 is the radiation resistance.

The relation between acoustic power available in the far field W_F and total acoustic power in the tail pipe W_T is given by [13]

$$W_F = W_T \frac{\left(k_0 r_0\right)^2}{2M_{tp} + \left(k_0 r_0\right)^2} \tag{1.9}$$

where $k_0 = \omega / c_0$ is the wave number and r_0 is radius of the tail pipe.

Assuming a point source for the acoustic radiation available in the far field, the relation between power available in free-field, root mean square pressure (p_{rms}) at the surface of a hypothetical sphere of radius *r*, ambient gas density ρ_a and speed of sound in ambient medium c_a is given by

$$W_F = \frac{\left(p_{rms}\right)^2}{\rho_a c_a} 4\pi r^2 \tag{1.10}$$

Combining Eqs. (1.2) – (1.5) gives the value of p_{rms} as

$$p_{rms} = \left| \frac{p_s}{Z_0\left(T_{11} + T_{21} Z_s\right) + \left(T_{12} + T_{22} Z_s\right)} \right| \sqrt{\frac{\rho_a c_a}{4\pi r^2} \frac{1}{2\rho_{ex}} \frac{W_F}{W_T} \left[R_{0,1}\left(1 + M_{tp}^2\right) + M_{tp}\left(\frac{\left|Z_0\right|^2}{Y_{tp}} + Y_{tp} \right) \right]} \tag{1.11}$$

Finally, the SPL at a distance *r* from the source is given by

$$\text{SPL} = 20 \log_{10}\left(\frac{p_{rms}}{2 \times 10^{-5}} \right), \quad \text{dB} \tag{1.12}$$

The SPL would represent unmuffled or muffled sound depending on the four-pole parameters of acoustic load used in Eq. (1.11).

Insertion loss (IL) is usually defined either with respect to a reference pipe (a simple pipe inserted between the source and atmosphere) or without any reference pipe (source-load junction opening directly into the atmosphere). Electro-acoustic circuit representations with a muffler and a uniform pipe are shown in Figs. 1.3 (a) and 1.3 (b), respectively.

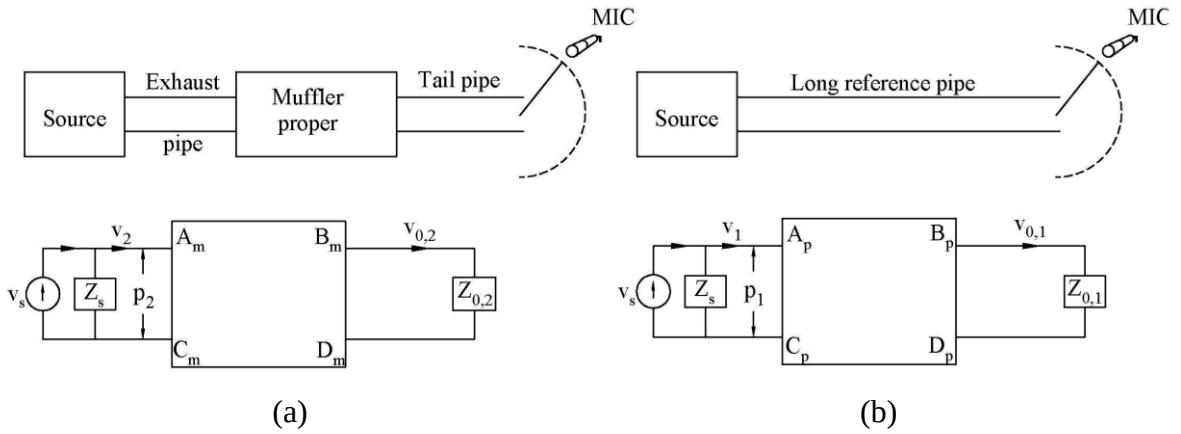

(a) (b)

Figure 1.3. Electro-acoustic circuit representation of exhaust system (a) with muffler, (b) with reference pipe (the four-pole parameter subscripts *m* and *p* denote 'muffler' and 'reference pipe', respectively).

As per the definition of IL:

$$IL = 10\log_{10}\left(W_1/W_2\right), \quad dB \tag{1.13}$$

where subscripts 1 and 2 denote 'without muffler' and 'with muffler', respectively.

Acoustic power through a pipe cross-section in the presence of incompressible mean flow is given by Eq. (1.3). Using Eqs. (1.7) and (1.13) along with the transfer matrix relation between the upstream and downstream state variables, in accordance with Fig. 1.3, the expression of IL of a muffler with respect to a reference pipe in the presence of mean flow (Mach number, *M*) is given by

$$IL = 20\log_{10}\left[\frac{A_m Z_{0,2} + B_m + \left(C_m Z_{0,2} + D_m\right) Z_s}{A_p Z_{0,1} + B_p + \left(C_p Z_{0,1} + D_p\right) Z_s}\left(\frac{\rho_{0,2}}{\rho_{0,1}}\frac{R_{0,1}\left(1+M_{ep}^2\right) + M_{ep}\left(\left|Z_{0,1}\right|^2 / Y_{ep} + Y_{ep}\right)}{R_{0,2}\left(1+M_{tp}^2\right) + M_{tp}\left(\left|Z_{0,2}\right|^2 / Y_{tp} + Y_{tp}\right)}\right)^{1/2}\right] \tag{1.14}$$

where subscripts *ep* and *tp* denote exhaust pipe and tail pipe, respectively.

Eq. (1.14) gives a generalized expression for IL with incompressible mean flow. One can get the IL without any reference pipe if the transfer matrix of the pipe is substituted by the unity matrix. Further, one can obtain the IL of a muffler without mean flow by letting the values of mean flow Mach numbers in the exhaust pipe and tail pipe tend to zero. The prediction of IL requires the source impedance, $Z_s\left(=R_s + jX_s\right)$. However, both the source characteristics (p_s and Z_s) are required for prediction of the unmuffled and muffled sound pressure levels [1].

1.3 Estimation of acoustic source characteristics

There are two different categories of methods in literature for acoustic source characterization, namely, Indirect Multi-load methods and Direct measurement methods for source impedance. A detailed discussion on these two methods is concisely presented in the following sub-sections.

1.3.1 Indirect Evaluation Methods

Theoretically, for a linear time-invariant acoustic source, the experimentally measured or numerically computed (through time-domain cycle simulation) values of acoustic pressure for two known load impedances can give the values of both source characteristics. This method is known as the two-load method [14,15]. Mathematically, both source characteristics can be computed by Eq. (1.15), where p_i and $Z_{L,i}$ are acoustic pressure at source-load junction and load impedance for the i^{th} load.

$$\begin{bmatrix} Z_{L,1} & -p_1 \\ Z_{L,2} & -p_2 \end{bmatrix} \begin{bmatrix} p_s \\ Z_s \end{bmatrix} = \begin{bmatrix} p_1 Z_{L,1} \\ p_2 Z_{L,2} \end{bmatrix} \tag{1.15}$$

Thus, the estimated source characteristics using the two-load method depends on the selected pair of loads, and it is clear from Eq. (1.10) that the measured acoustic pressures with phase information for two different loads at source-load junction are needed. A numerical study was carried out by Gupta and Munjal [16] to get the acoustic pressure at source-load junction for a number of sets of two different loads. They observed that the different pairs of selected loads yield different values of source characteristics, which highlights the fact that the unique source characteristics, *i.e.*, independent of load do not exist for the IC engine exhaust systems.

Since the acoustic pressure measurements inside the duct with hostile conditions with a reference signal are very difficult, a four-load method was proposed by Prasad which yielded the source impedance using the magnitude of sound pressure levels measured outside the duct [17]. Although the source used was a loudspeaker in a duct, yet the source resistance turned out to be negative at all frequencies. Besides, the inherent error in the implicit reduction of nonlinear equations to linear equations in the four-load method proved to be unacceptably high [18].

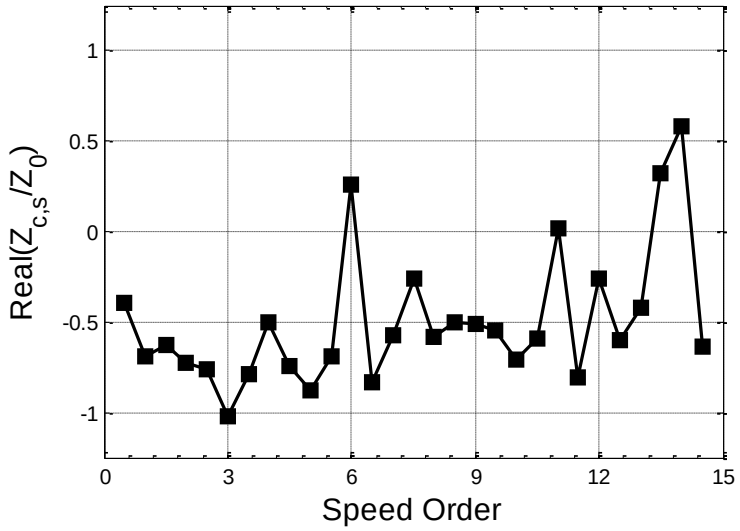

Figure 1.4. Measured source resistance of the exhaust of an IC engine operating at 2500 rpm (adopted from Ref. [19]).

The least squares method used by Desmons and Hardy [20] for estimation of the acoustic source characteristics of a loudspeaker source by solving an overdetermined system of linear equations for minimizing an error function proved to be better (less prone to errors) than the four-load method. Desmons *et al*. determined the acoustic source characteristics of a 4-cylinder, 4-stroke IC engine with 1798 cc swept volume using the least squares method with several calibrated loads [21]. A direct least squares method using the four loads only, however, was shown to be less sensitive to input errors [22] as compared to the four-load method [17] and the least squares method [20,21]. A new multi-load method proposed by Jang and Ih [19] was shown to perform better than the methods presented in Refs. [17,20–22] in terms of sensitivity to the input errors. A numerical investigation on the selection of loads for the refined multi-load method to have less sensitivity to the input errors was carried by Jang and Ih [23]. An analytical study on the load selection was done by Zheng *et al*. to estimate accurate source impedance values, which led to the conclusion that the resistances of selected loads should be of the same order in magnitude, and it should also avoid the frequency range of impedance load peaks [24]. However, multi-load indirect methods [17,19–22] result in negative source resistance for most of the frequencies, as can be observed from Fig. 1.4, which is physically untenable. This also casts a shadow on the estimated values of X_s, reactance of the source, and p_s, the source pressure. The possible causes of negative source resistance were reviewed by Ih and Peat [25].

The Indirect Multi-load methods applied in Refs. [16,17,19–22] are based on the assumption that the source is linear and time-invariant. However, an IC engine is a non-linear and time-variant source. A multi-load method was used for measuring the source characteristics of a time-variant modified compressor source [26]. Acoustic impedance of a time-varying source (a cylinder which discharges through a varying open area of the valve which is not a realistic model of an IC engine) was estimated analytically using multi-load indirect method [27]. A modified multi-load method was proposed by Rämmal and Bodén [28] for nonlinear source characterization. The nonlinear term is caused by the pressure drop over the constriction. Due to the one non-linear term, minimum three loads for the source characterization are required, in contrast to the two-loads for a linear time invariant source. Later, many non-linear and time-variant terms were introduced in a simplified exhaust system of a fluid machine, and the effect of different sets of terms on the prediction of acoustic pressure at the source-load junction was investigated [29]. Kim et al. [29] have explained about the origin of non-linear terms and showed that the inclusion of N non-linear terms requires at least $N+2$ number of loads for the estimation of source characteristics.

If the source is linear then the estimated characteristics from the overdetermined set of linear equations using either the pressure representation of the source or the velocity representation of the source must be same [28]. A linearity test based on a linearity coefficient for overdetermined set of linear equations was introduced by Lavrentjev *et al*. [30] and Bodén and Albertson [31]. The internal consistency of the linear source identification for IC engine exhaust system was checked by Macián *et al.* [32], where an over-determined set of linear equations was solved using both representations of source applying a least-square fitting criterion to the modulus or to the real and imaginary parts separately.

1.3.2 Direct Measurement of Source Impedance

The acoustic source impedance of any source can be measured directly by deactivating all active sources and placing an auxiliary source somewhere in the load section which drives the waves on to the inactive source. The impedance measured just downstream of the auxiliary source is the source impedance of the primary source under test. Direct method for estimation of source impedance of the exhaust system of the same V-8 IC engine under running conditions was applied by Prasad and Crocker [33] using the transfer function method (with a random excitation source) [34,35], and Ross and Crocker [36] using the standing wave tube technique. The schematic diagram of their direct measurement method [33] is shown in Fig. 1.5. Their

study showed that the experimentally measured source resistance was positive. Moreover, the IL of a muffler and muffled SPL predicted using the estimated source characteristics were shown to compare well with measured values in contrast with those obtained through assumption of constant pressure source and constant velocity source [37]. However, the direct method reported in the literature [33,36] has certain limitations as follows:

a. The purpose of a strong enough secondary (or auxiliary) source cannot be met by a normal electroacoustic driver; one has to use an electro-pneumatic driver, but even this cannot produce strong enough sound that would dominate the noise produced by the engine (primary source) at very low frequencies (of the order of the firing frequency of the engine) that are of primary interest to the muffler designers.

b. One can use a motored engine instead of the firing engine with an auxiliary source, but this would alter the flow conditions across the exhaust valve (for example, there would be no choked-sonic condition). Because of it, the source impedance so predicted would be unrealistic or erroneous.

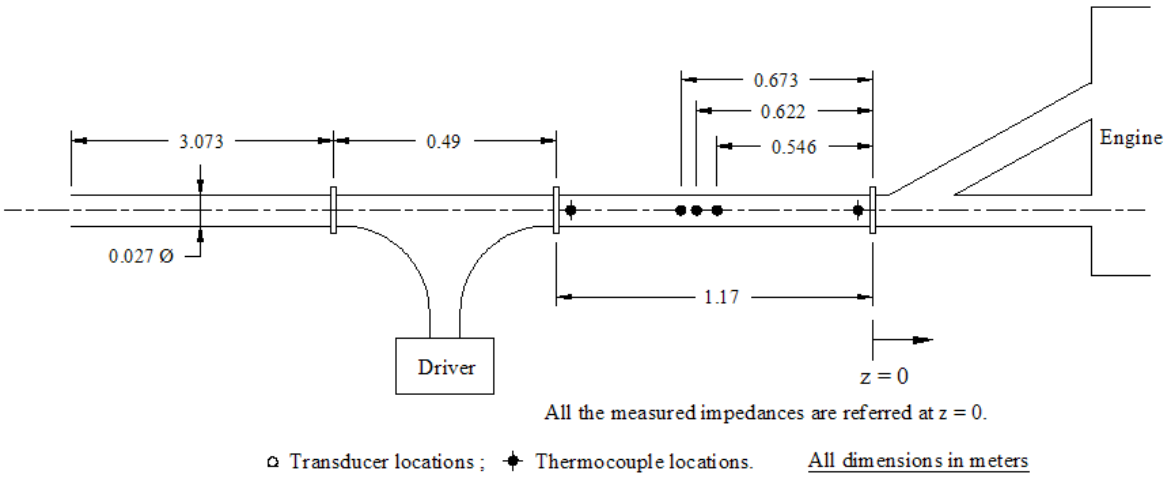

Figure 1.5. Diagram of the setup for engine impedance measurement by direct method (adapted from Ref. [33])

An analytical investigation of the direct measurement of the source impedance of a linear time-variant source was carried by Peat [38]. However, the engine model studied by Peat [38] is not a realistic one, and thus it cannot be applied to an actual IC engine.

1.4 Hybrid approach

Acoustic analysis of mufflers is preferred in the frequency domain; however, the unique source characteristics of an IC engine do not exist because it is a non-linear and time-variant

source [16]. It is well known that the source can be better described in the time domain and the muffler in the frequency domain. Hybrid approaches, for example, Sathyanarayana and Munjal [39] and Hota and Munjal [40], combine the advantage of time-domain modelling of source and frequency domain modelling of acoustic load through a Fourier transform pair. The hybrid approach proposed by Hota and Munjal [40] showed the capability to predict the unmuffled/muffled exhaust SPL spectrum of a 4-stroke single cylinder engine. However, when they attempted to extend this approach to predict radiated noise from multi-cylinder engines, results were not satisfactory [41]. The implicit assumption that one cylinder is firing at a time, and thus, the Fourier transform of pressure time-histories of cylinders differs only in phase was attributed to unreasonable prediction of exhaust noise radiated from a multi-cylinder engine. Further, Hota [41] argued that when one cylinder exhaust valve/s are open then others are not fully closed which in turn disturbs the wave pattern because of the mixing of exhaust gases from other cylinders. Therefore, the hybrid approach could not be extended to multi-cylinder engines [41].

1.5 Parametric study on the acoustic source strength level

The problems associated with application of hybrid approach to the multi-cylinder engines were circumvented by relying upon the frequency domain analysis [41]. Parametric expressions of the source strength level (SSL) of exhaust system of compression ignition engines [42] and spark ignition engines [43] were proposed by Hota and Munjal. Parametric expression of source strength level as a function of speed order were given in terms of the number of cylinders, engine capacity (swept volume), engine shaft speed and air-fuel ratio. The source characteristics were derived using the multi-load indirect methods which results in negative source resistance at most of the speed orders which is physically untenable. Therefore, the expression given in Ref. [7] was adopted. Moreover, the same source impedance was used for estimation of source pressure (or source strength level). The parametric expression was derived for engines having exhaust runners of equal length meeting at one junction, therefore, the resulting parametric expression for SSL cannot be applied to engines having unequal runner lengths.

1.6 Acoustic modelling of turbochargers

In Ref. [42], the selected source-load junction was at the downstream end of the turbine of the turbocharger. The engine load determines the noise radiated by a turbocharged engine. The engine load was not considered for parametric expression of SSL of the turbocharged engines. If acoustic source characteristics of each cylinder of a T/C engine were known then source characteristics could be combined and transferred, if needed [44], and for that matter, the passive acoustic properties of a turbocharger must be known.

Probably, the first attempt to study the passive acoustic effect of the turbine of an automotive turbocharger and to compute the transfer matrix using numerical simulation was made by Peat *et al*. [45]. They considered the turbine composed of three separate sections, namely, volute, rotor and diffuser. At first, they solved the full nonlinear time-dependent equations of conservation of mass, momentum and energy to obtain the flow properties as functions of spatial coordinates throughout the turbine section. Matching boundary conditions, i.e. continuity of pressure, temperature and mass flow were enforced at the volute-rotor and rotor-diffuser boundaries. The same set of conservation equations were taken for the fluid properties as the sum of a steady-flow value and an acoustic value, and the steady flow equations were subtracted to obtain the equations in terms of acoustic perturbations. Acoustic disturbance was assumed isentropic which obviated the need of energy equation.

A test-rig based on the principle of modified impulse method was designed by Peat *et al*. [46] to measure the direct and inverse transmission and reflection coefficients. In the direct case, the acoustic excitation travels in the same direction as the mean flow, whereas in the inverse case, in the opposite direction. The experimental investigation was carried out for the static and running rotor conditions. It was shown that the transmission loss (TL) of turbine predicted through a numerical study compares well with the experimentally measured values for the inverse cases for the rotor speed up to 54,000 RPM. However, the differences between the predicted and the experimentally measured TL values were found to increase with the increasing rotor speeds for the direct case.

Probably, the first attempt to make a systematic experimental investigation on the complete passive acoustic characterization of turbochargers working in several different operating conditions was made by Tiikoja *et al*. [47]. They evaluated the scattering matrix and used it to measure the TL spectra of the turbine and compressor, in the upstream and downstream

directions. Later, Tiikoja *et al*. [48] did experimental investigation in order to measure generation of sound from automotive turbochargers.

1.7 Analysis and design considerations related to commercial mufflers

Noise can be controlled, either at its origin or in the propagation path. For a noise control solution, it is desirable to quieten the source itself, however exhaust noise radiated by an engine mostly depends on the acoustic load on the engine and crankshaft speed. Thus, efficient mufflers are needed to ensure adequate noise control in the transmission path.

Mufflers have been used to control the exhaust noise radiated by IC engine since its inception. However, for a long time it depended on the empirical knowledge of muffler designers. Using the electro-acoustical analogies, a systematic investigation of muffler designs was done in Refs. [49–51]. However, this analysis was for the estimation of transmission loss which is not the true measure of a muffler applied to the source. Prediction of actual attenuation parameter of a muffler, i.e. IL was attempted by Fukuda [4], who however, assumed the radiation impedance and source impedance to be zero and infinity, respectively. Later, IL of mufflers was computed using the radiation impedance without mean flow and source impedance as the compliance of the engine exhaust manifold and cylinders by Sreenath and Munjal [6]. There have been several developments in the design and analysis of mufflers in the last fifty years as discussed below.

1.7.1 Analysis of cascaded element mufflers

Cascaded element mufflers are ideally suited for the transfer matrix method (TMM). An algebraic algorithm to evaluate the IL spectrum of such kind of mufflers without having to solve a number of algebraic equations was developed by Munjal *et al*. [8,9]. This algorithm was shown to be specially suited for a rational synthesis of one-dimensional acoustic filters [52], and was extended to exhaust mufflers with incompressible mean flow by means of convective state variables [11].

1.7.2 Analysis of perforated element mufflers

In the literature, use of the perforated element mufflers has been reported since a long time. For the first time, an analytical study of the concentric tube resonator (CTR) was done by Sullivan and Crocker [53]. Later, a segmentation procedure to model all types of perforated

elements, namely, through-flow element, cross flow element, and reverse flow element was presented by Sullivan [54,55]. In this segmentation approach, the uniformly perforated pipe is discretized arbitrarily, and one has to increase the number of segments for better predictions.

The need to check the convergence of the solution in Sullivan's segmentation approach [54,55] was avoided by the decoupling approach proposed by Jayaraman and Yam [56]. But, the method proposed in Ref. [56] has a flaw in its assumption that the mean flow Mach numbers in the two interacting ducts are equal, which is not the case in an actual muffler system where the two Mach numbers are inversely proportional to the cross-sectional areas of the respective ducts. Later, Munjal *et al.* [57] presented a generalised decoupling approach for the analysis of two and three interacting duct element mufflers with perforated pipes. In the generalised decoupling approach [57], or the distributed parameter approach, the mean flow Mach number in any tube is taken as constant along the entire perforate. However, this would vary along the length of the perforate, because the flow through the cross elements is distributed along it. This variation of mean flow can be taken into account in the segmentation approach [54,55]. However, the average values of the grazing and bias flow Mach numbers used in Ref. [57] are a good approximation, as confirmed by Peat in his numerical approach to the decoupling making use of an eigenvalue formulation [58].

Later, Dokumaci [59] proposed the matrizant approach for evaluation of transfer matrices of perforated pipe mufflers incorporating the effect of axially varying mean flow, and showed that the distributed parameter approach could be used for accurate prediction of the effect of mean flow velocity gradients.

Using the distributed parameter approach, Gogate and Munjal [60] analysed two new configurations of perforated element mufflers, namely, single-chamber three-duct open-ended perforated element muffler, and the two-chamber three-duct open-ended perforated element muffler. These two configurations are known for combining relatively higher acoustic TL with moderate backpressure. Kar and Munjal [61] proposed a method for acoustic analysis of a muffler with any number of perforated interacting ducts.

In the early days of usage of the perforated element mufflers, CTR was used with perforation on the entire length of the inner pipe. The CTR has the advantage of low backpressure compared to the double tuned expansion chamber (DTEC), which tunes out or lifts up three-fourths of the troughs of a simple expansion chamber (SEC) [62]. Ramya and Munjal [63] developed parametric expressions for the length of perforated pipes as a function

of different geometrical and environmental parameters to design a tuned CTR, which combines the advantage of wide-band TL with low backpressure and little aerodynamic noise generation.

1.7.3 Analysis of multiply-connected perforated element mufflers

The methods presented in Refs. [53–57,59–61] however cannot be applied for acoustic analysis of a muffler with perforated baffle placed inbetween the two perforated pipe sections. It is because the use of perforated baffles makes the sound field in different chambers multiply-connected. Nowadays, most of the commercial mufflers used for multi-cylinder or even high capacity single-cylinder engines have perforated baffles. These baffles are wisely located to reduce the backpressure without compromising the acoustic attenuation characteristics. Elnady *et al.* [64] analysed such a muffler using a new version of Sullivan's segmentation approach [54]. They used their two-port transfer matrices to model both the perforated branches and the intermediate hard pipe segments. This method [64] is capable of analysing complicated commercial mufflers with single inlet and single outlet.

An analytical alternative to the Elnady *et al.*'s two-port technique [64] was proposed by Vijayasree and Munjal [65], making use of a novel integrated transfer matrix (ITM) approach. The ITM approach does not need segmentation of the perforated sections.

1.7.4 3-D analysis of mufflers

In general, the shell diameter (or major axis of elliptical shell mufflers, and largest transverse dimension for rectangular shell mufflers) is such that the first higher-order mode gets cut on beyond the frequency range of interest to muffler designers. However, in the case of sudden area discontinuities, the evanescent higher modes affect considerably the muffler performance by shifting the TL peaks. This can be verified through experimental investigation or finite element or boundary element (FE/BE) analysis. Moreover, the small and medium shell diameter mufflers are synthesized using 1-D analysis. However, at middle and higher frequencies the results are generally validated by the FEM/BEM computations.

Size of muffler depends on the swept volume of the engine. For large swept volume engines, applicability of plane wave analysis does not hold beyond very low frequency region even though the inlet and outlet pipes may permit plane waves only. However, the FEM/BEM can be used to compute the transfer matrix of the muffler proper up to the frequency limit of plane wave analysis in the inlet and outlet pipes.

Probably, Young and Crocker [66] were the first to apply FEM for analysis of 3-D wave propagation in simple expansion chamber. Later, 3-D wave propagation in flow-reversal chamber mufflers were analysed by Young and Crocker using FEM [67]. Probably, for the first time in literature, 3-D FEM was used by Ross [68] to analyse the perforated element mufflers. Evaluation of the four-pole parameters of ducts with flow using FEM were illustrated by Peat [69].

Pre-computational effort as well as the computational cost is always a concern for application of numerical analysis. BEM requires discretization of the boundary surfaces, which saves considerable time and labour as compared with the FEM. Axisymmetric and asymmetric simple expansion chamber and extended inlet/outlet chamber mufflers were analysed using BEM by Wang *et al*. [70]. Later, the BEM was applied to the CTR using the specific acoustic impedance of the perforate by Wang *et al*. [71]. Successful application of the BEM to the perforated intruding tube mufflers was done in Ref. [72]. The BEM computation were validated against the measurements in Refs. [70–72]. Formulation of the BEM of axisymmetric and asymmetric simple expansion chamber and extended inlet/outlet chambers with mean flow was done by Ji *et al*. [73]. Effect of length to diameter ratio of simple expansion chamber on TL were investigated using 2-D axisymmetric analytical solution by Selamet and Radavich [74]. It was shown in Ref. [74] that for axially short expansion chamber mufflers with length to diameter ratio less than 0.5, 1-D plane wave analysis fails well before the cut-on frequency whereas the axisymmetric analytical solution and BEM computations compared well with the measured TL spectrum. A 3-D analytical approach was developed by Selamet and Ji [75] to study the effect of the length to diameter ratio of the offset inlet/outlet ports of a simple expansion chamber. In the companion paper of Ref. [75], BEM was shown to compare well with analytical solution as well as measurements [76]. Acoustic analysis of three-pass perforated duct mufflers was done by Ji and Selamet [77] using the 1-D plane wave analysis and the substructure BEM. TL spectrum of a three-pass perforated duct muffler computed by the 1-D plane wave analysis and BEM was shown to compare well with the measured TL spectrum. Later, hybrid expansion chamber silencers were analysed using the substructure BEM by Ji [78].

1.7.5 Constraints on design of an appropriate muffler

Low backpressure and adequate IL (dBA) of a muffler are the two design criteria for mufflers. In the recent past, some studies [79–81] have been done for designing mufflers with

better acoustic attenuation characteristics and low backpressure. Sagar and Munjal [80] analysed a novel muffler, which is a three-pass muffler with tubular bridges. This muffler has less backpressure as compared to its counterpart without tubular bridges as well as the advantage of reduced flow-induced noise. The tubular bridges can reduce the flow impingement on the end plates in both the end chambers. Using this configuration, Sagar and Munjal [81] have analysed the fork muffler with H-connections. The dual or fork mufflers are used in commercial mufflers to meet the constraints of space under the vehicle.

The perforated element mufflers can raise the back pressure if there is a plug in between [82]. Kumar and Munjal [83] carried out the acoustic analysis of modified plug-mufflers for low backpressure and improved acoustic performance.

In some places, the location of inlet and outlet pipes can be also a constraint, e.g. the side-inlet side/axial-outlet pipes for mufflers applied on DG sets. Lumped element (0-D) analysis, plane wave (1-D ITM) analysis and 3-D finite element analysis of such mufflers were carried out by Kumar and Munjal [84,85].

1.8 State of the art

Acoustic source characteristics of IC engines are needed to predict the unmuffled SPL and IL of a muffler. Parametric expressions of SSL of IC engines are given in literature, and assuming a source impedance value these expressions can be used to predict the unmuffled/muffled SPL spectrum. However, in literature, to the best of author's knowledge, there is no parametric expression for a single-cylinder engine source impedance.

Direct evaluation methods result in measurement/estimation of positive source resistance, however, in the indirect evaluation methods, source resistance turns out to be negative at most of the speed orders. The reason for negative source resistance estimation/measurement by multi-load indirect methods are discussed in literature, yet negative source resistance is physically untenable and casts a shadow of doubt on the predicted values of both the source characteristics p_s and Z_s.

Till now, in case of multi-cylinder engines complete engine has been regarded as a black-box acoustic source and their characteristics were estimated/measured. However, each cylinder of an engine is an independent acoustic source, and its characteristics are not estimated/measured in isolation.

Harmonic balance method has been applied to a simple one-cylinder 'piston-restriction' cold engine [86]; however, its application to real single-cylinder engine and multi-cylinder engine is not found in the literature.

In literature, acoustical modelling of turbochargers involved either the numerical analysis or experimental measurement of the four-pole parameters of turbine. However, to the best of author's knowledge, analytical expressions of transfer matrices of the turbine and compressor in terms of respective static pressure ratios are not reported in the literature.

Generally, adequate value of overall IL calls for sufficiently large muffler volume. As a rule of thumb, small size muffler volume is approximately five times the engine swept volume. This much volume is sometimes not available for reasons of logistics and cost-effectiveness. A systematic investigation on judicious use of perforated pipes and baffles in multiply-connected ultra-small mufflers (volume less than twice of engine swept volume) with less backpressure and moderate overall IL (dBA) have not been carried out. Often, the advantage of high mean flow Mach number has been associated with more jet noise; however, there is no approximate relation between mean flow Mach number, mass flow rate and jet noise reported in the literature.

Applicability of the 1-D ITM approach to acoustic analysis of the side-inlet side-outlet (SISO) mufflers with perforated inlet/outlet pipes has been limited to very low frequency region due to the lumped element modelling of the chambers with side inlet/outlet [84,85]. The one-dimensional plane wave propagation modelling in the end chamber of the SISO mufflers with perforated inlet/outlet pipes are not found in the literature.

1.9 Scope of the present investigation

The equivalent internal impedance (source impedance) of a time-variant single-cylinder internal combustion engine is estimated making use of the cylinder thermodynamics and hypothetical auxiliary source in Chapter 2. The variation of source impedance for different engine speeds is investigated. Further, for a range of different capacities of a single-cylinder engine, a parametric expression of impedance is derived, which is probably the first of its kind in the literature. These expressions can be used for the estimation of IL of mufflers applied to single-cylinder internal combustion engines.

The direct evaluation method developed in Chapter 2 for a single-cylinder engine is applied for a two-cylinder naturally aspirated diesel engine in Chapter 3. Harmonic balance method is

applied when one cylinder of the engine is discharging to the typical exhaust system while other is not exhausting. The source characteristics estimated using the two different discharge conditions, namely, discharging directly to the atmosphere and a typical exhaust system are shown to predict reasonably well the unmuffled SPL spectra as compared with measured spectrum. In Chapter 4, the direct estimation method is extended to a multi-cylinder turbocharged engine by deriving and incorporating transfer matrix of the turbine.

Acoustical analysis of a typical double flow-reversal commercial muffler of a motorcycle engine is done by means of the 1-D ITM approach and validated against the 3-D FEA in Chapter 5. The effect of mean flow on the attenuation characteristics is investigated and commented upon.

The jet noise generated by the mean flow jet emerging from the tail pipe imposes a limit on the maximum net IL achievable in the muffler. To ensure a certain minimum IL, an approximate expression of the limiting Mach number is derived in Chapter 6, and the effect of mean flow on multiply-connected coaxial perforated element mufflers is studied.

Plane wave analysis of SISO mufflers with perforated inlet/outlet has been carried out in Chapter 7. Perforated inlet and outlet pipes of the large SISO perforated element mufflers are replaced by their lumped resistances and 1-D plane waves are assumed on the both sides of the perforated inlet/outlet pipes. This rather novel approach is shown to have considerable advantage in applying 1-D ITM approach to large SISO perforated element mufflers. Furthermore, rational design guidelines are developed in Chapter 7 for large SISO mufflers.

Chapter 2

Direct Estimation of the Acoustic Source Characteristics of Single-Cylinder NA Engine*

As indicated in Chapter 1, the indirect (two-load or multi-load) method often leads to the prediction of negative source resistance which is obviously absurd. In fact, it casts a shadow of doubt on the accuracy of the reactive part of the source impedance and the source strength as well. On the other hand, the direct method always gives positive source resistance. However, the direct method reported in the literature, carried out experimentally or analytically, has certain limitations which make the method unsuitable for estimation of source impedance of internal combustion (IC) engines [1].

In this chapter, the equivalent internal impedance (source impedance) of a time-variant IC engine is estimated making use of a hypothetical auxiliary source. The variation of source impedance for different engine speeds is investigated. Further, for a range of different capacities of a single-cylinder 4-stroke, naturally aspirated (NA) gasoline engine, a parametric expression is derived for source impedance, which is probably the first of its kind in the literature. This expression can be used for the estimation of IL of mufflers applied to the single-cylinder IC engines.

2.1 Theory of direct estimation of source impedance

It is evident from Fig. 1.1(b) that if there were an auxiliary source put somewhere in the load section and the real source were made inactive, then the ratio of acoustic pressure and acoustic mass velocity, p/v, at the source-load junction would be the source impedance, Z_s [44]. The schematic diagram for the application of direct method and corresponding electro-acoustic circuit representation are shown in Figs. 2.1(a) and (b).

The volume of the acting cylinder and flow passage area of the exhaust valve vary with the crank angle while the cylinder is exhausting. Thus, the geometry of the source is changing with respect to time. In the present study, following Prasad and Crocker [33] and Ross and Crocker

* A preliminary version of this chapter was presented at International Congress on Sound and Vibration (ICSV-24) held in London during 23rd –27th July 2017.

[36], the actual cylinder is made inactive. In other words, the inactive cylinder is motored; thus, the variation of the source geometry is considered. The hypothetical auxiliary source transmits waves into the inactive real source. At every crank angle step, the piston of the cylinder is assumed to be momentarily stationary, and the cylinder volume and exhaust valve flow passage area remain constant. The variation in the configuration of the source is periodic and repeats after one thermodynamic cycle.

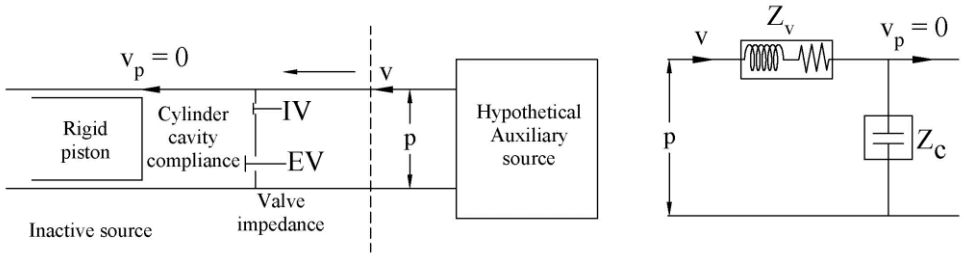

(a) (b)

Figure 2.1. Application of the direct evaluation method for estimation of source impedance: (a) Schematic diagram with auxiliary source transmitting waves into the inactive real source, and (b) the electro-acoustic circuit representation thereof.

It is evident from Fig. 2.1 that the source impedance for the source configuration at a particular crank angle is sum of the valve passage impedance (inertance and resistance in series) and cylinder cavity compliance. The valve flow passage may be modeled as a hole whose area is the valve flow minimum area. The resistance of the valve is due to the aerodynamic losses of the bias flow of exhaust gas through it. The valve resistance due to the mean bias flow is taken from the Elnady *et al.* [64] expression of perforate impedance. Mathematically, the expression for source impedance at a particular crank angle θ is given by

$$Z_s(\theta) = -j\frac{c_c^2(\theta)}{\omega V_c(\theta)} + j\omega\frac{t_{v,eff}(\theta)}{S_v(\theta)} + 1.15M_v(\theta)\frac{c_v(\theta)}{S_v(\theta)}, \quad \omega = n\omega_0, \quad \omega_0 = \frac{2\pi}{120/N} \tag{2.1}$$

where $M_v(\theta)$ is given by

$$M_v(\theta) = \frac{\dot{m}_{ex}(\theta)}{\rho_v(\theta)S_v(\theta)c_v(\theta)} \tag{2.2}$$

In Eqs. (2.1) and (2.2), ω_0 is fundametal angular frequency in rad/s, n is the harmonic number, N is the engine shaft speed in revolutions per minute, $V_c(\theta)$ is the instantaneous cylinder volume, $S_v(\theta)$ is the valve flow minimum area, $\dot{m}_{ex}(\theta)$ is the exhaust gas mass flow

rate, $t_{v,eff}(\theta)$ is the effective acoustic length of the valve for inertance, $c_v(\theta)$ is the sound speed in the valve, $c_c(\theta)$ is the sound speed of the in-cylinder gas, $\rho_v(\theta)$ is the exhaust gas density at the valve, and $M_v(\theta)$ is the Mach number of bias flow through the exhaust valve. The parameters associated with the valve and cylinder vary with crank angle θ.

The speed of sound of the in-cylinder gas and the exhaust gas passing through the valve are given by

$$c_c(\theta) = \sqrt{\gamma R T_c(\theta)} \tag{2.3}$$

$$c_v(\theta) = \sqrt{\gamma R T_v(\theta)} \tag{2.4}$$

where $T_c(\theta)$ is the in-cylinder gas temperature and $T_v(\theta)$ is the gas temperature at the valve throat at the crank angle θ.

The effective valve thickness $t_{v,eff}(\theta)$ is given by

$$t_{v,eff}(\theta) = t_v + 0.85\sqrt{A_m(\theta)/\pi} \tag{2.5}$$

It is clear from Eqs. (2.1) – (2.5) that the source impedance value for the source configuration at a particular crank angle depends on the in-cylinder gas variable and mass flow rate through exhaust valve. Therefore, the cycle simulation must use the thermodynamics of the cylinder along with the quasi-steady one-dimensional isentropic flow through valves. The thermodynamics of cylinder and flow through valves are discussed briefly in Appendix A. The variation of minimum valve flow area (A_m) with respect to the valve lift is given in Appendix B.

There are three different possibilities of flow through exhaust valve, namely, forward choked flow, forward subsonic flow and reverse subsonic flow.

For the forward choked flow, the Mach number of mean flow at the valve is unity. Assuming isentropic flow, Eqs. (2.6) and (2.7) give the density and temperature of the exhaust gas flow at the valve throat.

$$\rho_v = \rho_c \left(\frac{2}{\gamma + 1} \right)^{1/(\gamma - 1)} \tag{2.6}$$

$$T_v = T_c\left(\frac{2}{\gamma+1}\right) \tag{2.7}$$

In the case of subsonic forward flow, Eqs. (2.8) and (2.9) give the density and temperature of the exhaust gas at valve throat:

$$\rho_v = \rho_c\left(1+\frac{\gamma-1}{2}M_v^2\right)^{-1/(\gamma-1)} \tag{2.8}$$

$$T_v = T_c\left(1+\frac{\gamma-1}{2}M_v^2\right)^{-1} \tag{2.9}$$

where the value of mean flow Mach number at valve section is of the previous time step, and is given by

$$M_v = \frac{|\dot{m}_{ex}|}{\rho_v A_m c_v} \tag{2.10}$$

For reverse subsonic flow, Eqs. (2.11) and (2.12) give the density and temperature of the exhaust gas at the valve throat:

$$\rho_v = \rho_{ex}\left(1+\frac{\gamma-1}{2}M_{ex}^2\right)^{1/(\gamma-1)}\left(1+\frac{\gamma-1}{2}M_v^2\right)^{-1/(\gamma-1)} \tag{2.11}$$

$$T_v = T_{ex}\left(1+\frac{\gamma-1}{2}M_{ex}^2\right)\left(1+\frac{\gamma-1}{2}M_v^2\right)^{-1} \tag{2.12}$$

where the mean flow Mach number in the exhaust runner (of cross-sectional area A_{er}) just downstream of the exhaust valve is given by

$$M_{ex} = \frac{|\dot{m}_{ex}|}{\rho_{ex}A_{er}\sqrt{\gamma RT_{ex}}} \tag{2.13}$$

At the end of the time domain simulation of every crank angle step the source impedance assuming the configuration of the source at that step is computed using Eq. (2.1). Reciprocal of the source impedance of a particular frequency at a crank angle step is the source admittance corresponding to that frequency and crank angle step. The equivalent source admittance corresponding to each harmonic of the fundamental frequency of a time varying source is evaluated here as the average source admittance over different crank-angle steps. In the present method, the equivalent or effective source impedance is evaluated as reciprocal of the source

admittance averaged over one complete thermodynamic cycle. Symbolically, it is represented by

$$\frac{1}{Z_{s,eq}} = \frac{1}{N}\sum_{i=1}^{N}\frac{1}{Z_s(\theta_i)} \tag{2.14}$$

where N is the number of the crank-angle steps in one thermodynamic cycle. In the present analysis, a complete cycle of thermodynamic processes is divided into 2^{11} or 2048 crank-angle steps. When the exhaust valve is closed, the source impedance would tend to infinity. In order to simplify a time-variant source as a time-invariant source, the equivalent source impedance is considered as reciprocal of the average admittance over different crank-angle steps, because the average of source impedance at different crank-angle steps would yield the infinite source impedance for all harmonics of the fundamental frequency. It is well established in literature that the constant velocity source, or an infinite impedance source is not a good approximation, as illustrated later in this chapter. The hypothesis of the equivalent source impedance model is not only justified, but it also reduces the complexity of frequency domain analysis of time-variant sources [26,27,38,87]. In Refs. [26,87], a time-variant source was described by linear differential equations with time-varying coefficients. Periodic time-variant parameters for linear time-variant source model were represented as infinite sum of Fourier series, however, the computation requires the truncation of series on the basis of convergence study [26,27,38,87]. Thus, the acoustic pressure is related to acoustic volume velocity or mass velocity by an impedance matrix, where the non-diagonal elements of impedance matrix reflects the coupling between different frequency components at the source.

In the following section, the algorithm for the time-domain simulation for computation of the in-cylinder gas variables, properties of flowing fluid at the exhaust valve throat section, exhaust port and intake port as well as the mass flow rates through intake and exhaust valves are discussed.

2.2 Algorithm for time-domain simulation of aero-thermodynamics

The history of the exhaust gas mass flow rate through the valve depends on the exhaust system (or load) to which the cylinder is exhausting. Equations involved in calculation of the in-cylinder gas variables and mass flow rate through the exhaust and intake valves are described in Appendix A. In this section, the application of the predictor-corrector scheme for

before and after the intake valve opening (IVO) is described. The cylinder is assumed to be directly discharging into the atmosphere.

The time-domain simulation for the in-cylinder gas properties and the mass flow rate through valves requires the following steps:

i. Input the essential variables: RPM (N) of the engine, bore diameter (B), length of stroke (L_s), compression ratio (CR), connecting rod length (l), exhaust and intake valve diameters, lift-profiles and discharge coefficients for flow through valves, crank angle corresponding to the exhaust valve opening, intake valve opening and exhaust valve closing, and the in-cylinder gas pressure and temperature at the exhaust valve opening.
ii. Compute the array of crank-angle steps in between the exhaust valve opening EVO and exhaust valve closing EVC as well as the intake valve opening IVO and EVC. Compute the effective exhaust valve flow area during EVO to EVC and effective intake valve flow area during IVO to EVC, the volume of the in-cylinder gas and its rate of change corresponding to each of the crank angle steps, as given in Appendix A.
iii. The in-cylinder pressure at the current time step is computed by Eq. (A.11). First, the current step in-cylinder pressure is computed from the previous step net mass flow rate and the in-cylinder mass value. This pressure is used now to compute the mass flow rate. With this, the net mass flow rate and the in-cylinder gas mass are computed. The values of the previous step in-cylinder pressure, the current step mass flow rate and the net in-cylinder gas mass are used for computing the corrected value of the in-cylinder gas pressure. This is used to find out the corrected value of the net mass flow rate, which in turn is used to estimate the corrected in-cylinder gas mass.

2.3 Effect of source impedance on IL

It can be noted that the estimation of exhaust mass flow rate requires the values of pressure at the downstream of the exhaust valve and upstream of the intake valve (during the valve overlap period) which vary with crank angle. One may assume a constant mean pressure (say 1.06 bar) at the downstream of exhaust valve to compute the average source impedance. It is clear from Fig. 2.2 that the assumption is reasonable for the source impedance prediction. In the valve overlap period the pressure at upstream of the intake valve is also assumed constant (say 0.98 bar). These assumptions avoid the complete time-domain analysis of the cylinder

along with waves in the intake and exhaust systems by means of a commercial software like AVL-BOOST.

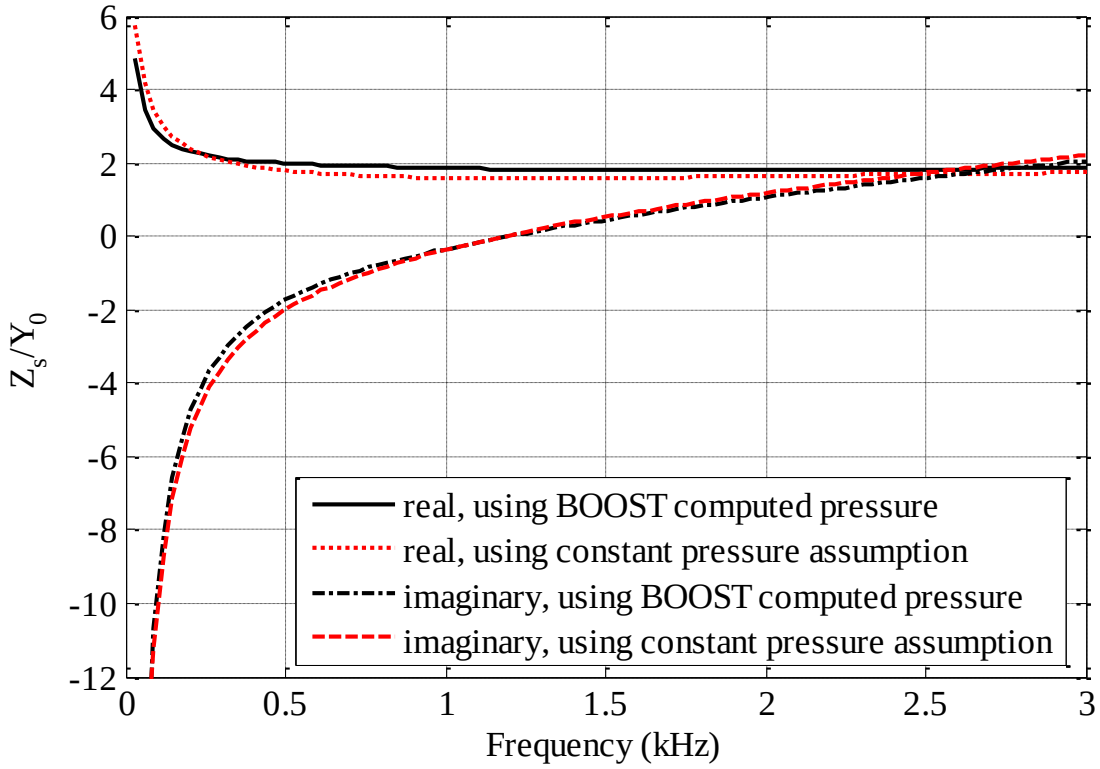

Figure 2.2. Effect of pressure at the downstream of exhaust valve on the estimated value of the normalized real and imaginary components of the source impedance of the engine running at 3500 RPM

The small variations in the prediction of source impedance practically donot matter for the prediction of IL. This is illustrated for a simple expansion chamber (Fig. 2.3) in Fig. 2.4. IL spectrum of a simple expansion chamber (SEC) is with respect to a 1 metre long reference pipe of 31 mm diameter.

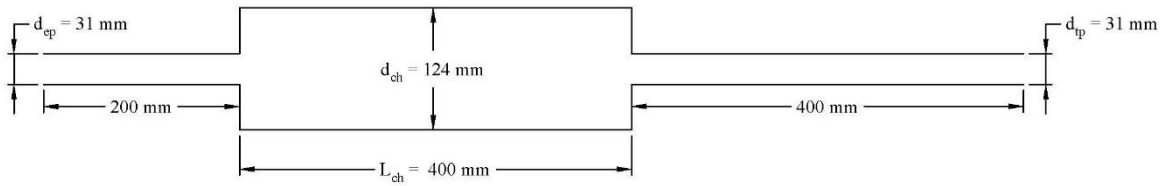

Figure 2.3. Schematic diagram of the simple expansion chamber muffler

The present study is done on the BOOST Example Manual single-cylinder 500 cc gasoline engine. The specifications of this engine are given in Appendix C. Figure 2.5 represents the BOOST model of the engine.

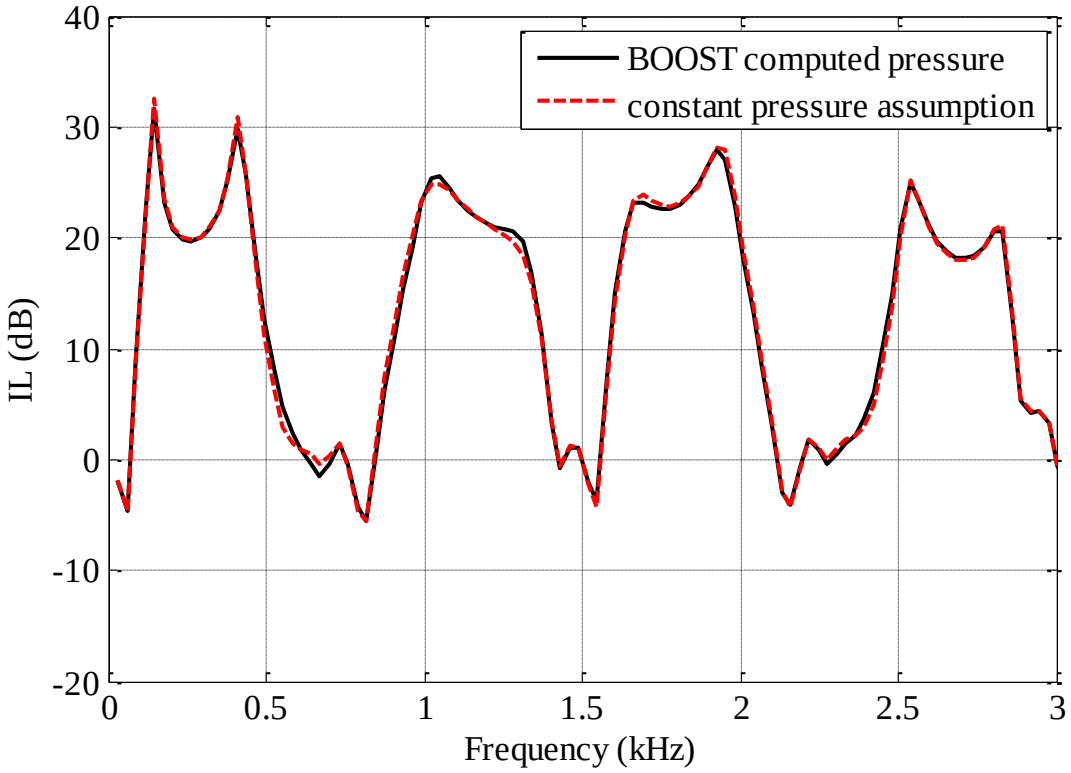

Figure 2.4. Effect of the static pressure at the downstream of exhaust valve on the estimated insertion loss of the simple expansion chamber muffler when the engine is running at 3500 RPM

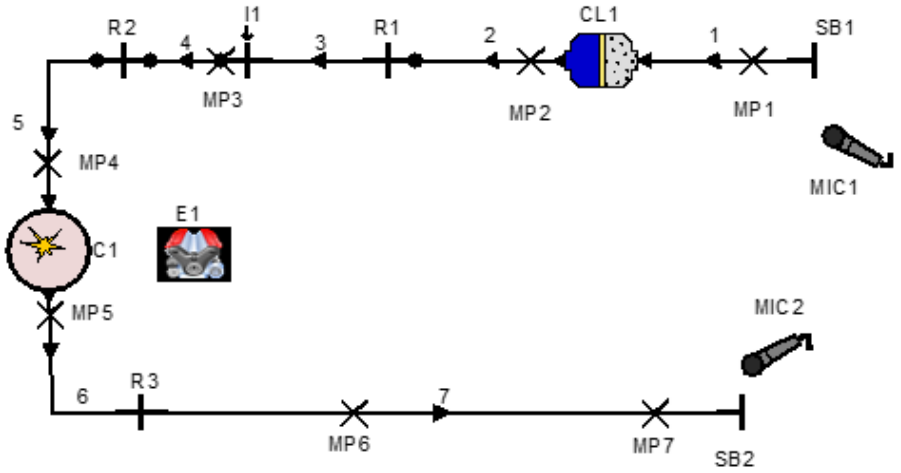

Figure 2.5. AVL BOOST model of the 500 cc single-cylinder gasoline engine

Now, the different values of source impedance used in the literature, such as infinite impedance i.e. constant velocity source, characteristic impedance (anechoic source), source impedance expression proposed by Callow and Peat [7] along with the source impedance computed in the present study are investigated for estimating IL of the simple expansion chamber (Fig. 2.3). The effect of the source impedance on IL is shown in Fig. 2.6. It may be observed that assumptions of infinite impedance result in large variation in IL whereas the

characteristic impedance (anechoic source) assumption and the source impedance expression proposed by Callow and Peat [7] yields IL values that are reasonably close to those predicted from the source impedance computed here by means of the direct method, especially at mid frequencies. However, the IL values computed by assuming infinite source impedance tally well at very low frequencies only. The reason for this fact is that the cylinder compliance is quite high in the low frequency region as may be observed from Fig. 2.2.

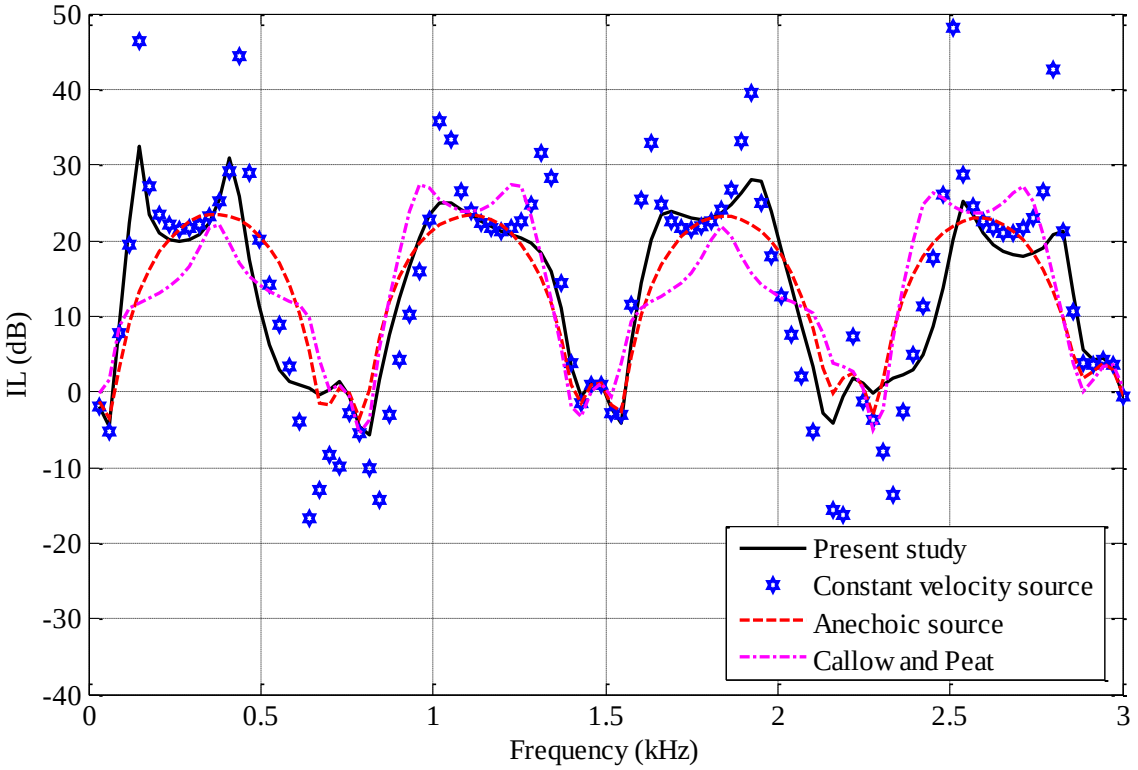

Figure 2.6. Effect of different source impedance expressions on the insertion loss of the simple expansion chamber muffler when the engine is running at 3500 RPM

Similarly large variations in prediction of IL spectra of simple expansion chamber (SEC) were also shown by Zhang *et al*. in Ref. [88] for the engine running at different conditions.

2.4 Parametric study of source impedance

The difference in IL of the muffler with different source impedance expressions indicates the importance of the correct estimation of the source impedance. It motivated the Author to do a parametric study of the source impedance. First, speed of the engine is varied to see the changes in the source impedance. As shown in Fig. 2.7, the effect of RPM is not significant on the source impedance and a common fitted value can serve the purpose of estimating the IL with sufficient accuracy, and its adequacy and efficacy for IL is shown in Fig. 2.8.

Curve fitting for the normalized source impedance is done in the form

$$\frac{Z_s}{Y_0} = \frac{a_R + b_R f}{1 + c_R f + d_R f^2} + j\frac{a_X + b_X f}{1 + c_X f + d_X f^2}, \quad 30\,\text{Hz} \le f \le 3000\,\text{Hz} \tag{2.15}$$

where coefficients are listed in the last column of Table 2.1.

Table 2.1. Table of coefficients used in the curve fit in Eq. (2.15) for different values of the cylinder capacity

Coefficients	Cylinder Capacity				
	100 cc	200 cc	300 cc	400 cc	500 cc
a_R	9.615	8.587	8.524	8.438	8.761
b_R	3.11×10^{-2}	4.27×10^{-2}	4.07×10^{-2}	5.27×10^{-2}	6.42×10^{-2}
c_R	3.33×10^{-2}	3.23×10^{-2}	3.31×10^{-2}	3.522×10^{-2}	4.013×10^{-2}
d_R	3.72×10^{-7}	-1.47×10^{-7}	-9.32×10^{-7}	-13.33×10^{-7}	-16.25×10^{-7}
a_X	-207.08	-152.51	-135.01	-107.70	-96.84
b_X	9.75×10^{-2}	9.09×10^{-2}	8.92×10^{-2}	8.46×10^{-2}	8.36×10^{-2}
c_X	11.2×10^{-2}	9.97×10^{-2}	9.21×10^{-2}	7.98×10^{-2}	7.51×10^{-2}
d_X	-2.9×10^{-5}	-2.55×10^{-5}	-2.30×10^{-5}	-1.94×10^{-5}	-1.80×10^{-5}

It is clear from Fig. 2.8 that the single fitted value for all the engine speeds for an engine is good enough to predict the IL at different engine speeds. This further motivated the author to extend the parametric analysis of source impedance of single-cylinder gasoline engine to incorporate the effect of cylinder capacity.

If the cylinder capacity is varied, then the lengths and areas in the model are changed as given below [40-42]:

i. $L_n = L_o\left(V_c/500\right)^{1/3}$ where V_c is the capacity of the cylinder in cc. L_n and L_o are characteristic lengths; that is, diameters of cylinder, valves and pipes; length of stroke, connecting rod-length, intake and exhaust valve lifts of the new capacity engine, and the base engine of 500 cc, respectively.

ii. $A_n = A_o\left(V_c/500\right)^{2/3}$ where A_n and A_o are areas of intake and exhaust port areas of the new capacity engine, and the base engine of 500 cc, respectively.

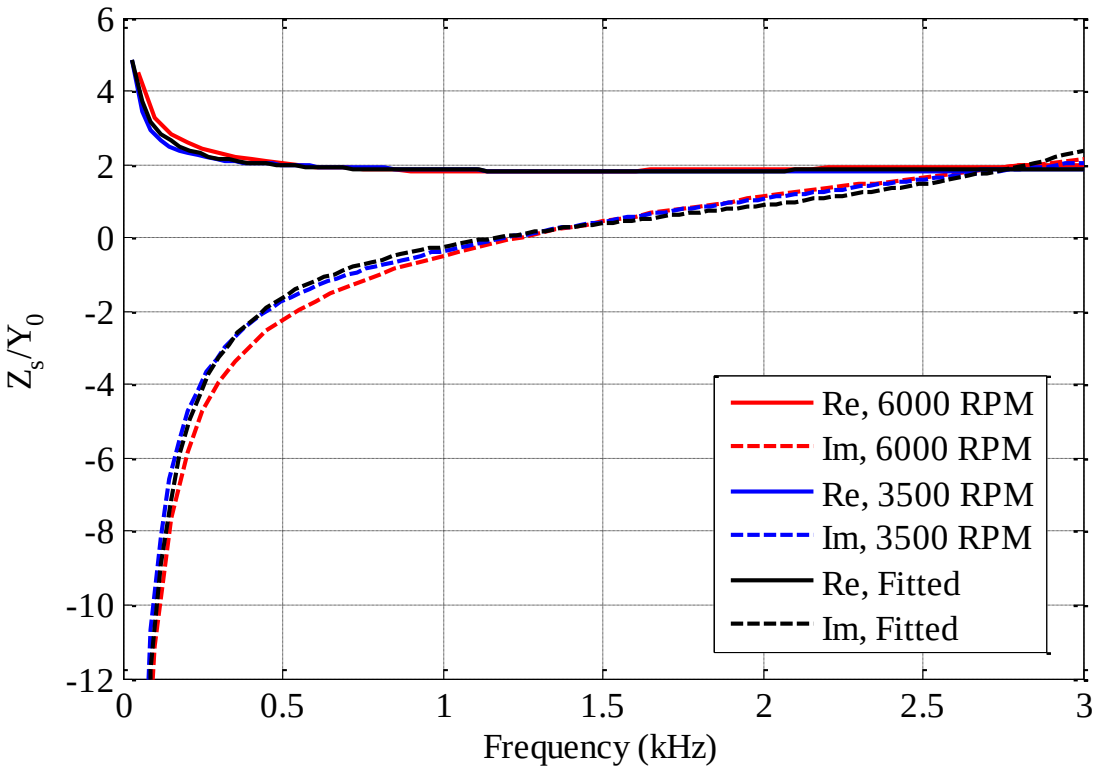

Figure 2.7. Effect of the engine RPM on the source impedance

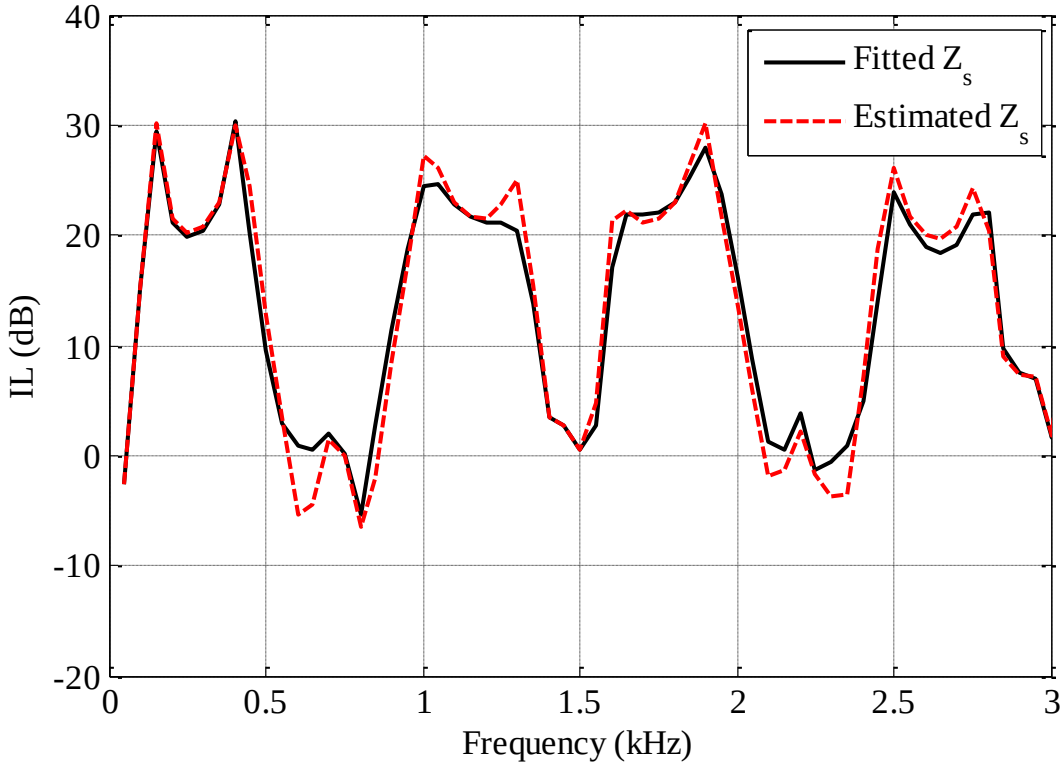

Figure 2.8. Comparison of the estimated insertion loss with the single fitted source impedance value and the computed value of source impedance, for the engine running at 6000 RPM

These coefficients are fitted by the least squares polynomial fit as a function of cylinder capacity. Expressions for normalized resistance and reactance in the frequency range 30 Hz to 3000 Hz are given below in Eqs. (2.16) and (2.17).

$$\frac{R_s}{Y_0} = \frac{\left(10.68 - 1.33v + 0.19v^2\right) + \left(2.35 + 0.76v\right)\times 10^{-2} f}{1 + \left(3.647 - 0.398v + 0.094v^2\right)\times 10^{-2} f + \left(8.21 + 5.18v\right)\times 10^{-7} f^2} \tag{2.16}$$

$$\frac{X_s}{Y_0} = \frac{\left(-258.19 + 59.80v - 5.53v^2\right) + \left(10.36 - 0.70v + 0.06v^2\right)\times 10^{-2} f}{1 + \left(12.51 - 1.387v + 0.075v^2\right)\times 10^{-2} f + \left(-3.404 + 0.477v + 0.031v^2\right)\times 10^{-5} f^2} \tag{2.17}$$

$$v = \frac{V(\text{in cc})}{100} \tag{2.18}$$

Finally, the expression for the normalized source resistance and reactance given by Eqs. (2.16) and (2.17) may be used for estimating the IL of a given exhaust muffler for a single-cylinder gasoline engine, without having to follow the algorithm detailed above in Section 2.2.

2.5 Conclusion

In this chapter, a novel scheme has been presented for direct evaluation of the source impedance of a single-cylinder firing engine. It is free from the anomalous behaviour of the indirect methods that make use of two or more arbitrary loads and result in negative source resistance. It makes use of a hypothetical auxiliary source and does not require the engine bed measurements or complete numerical simulations over several thermodynamic cycles. Both resistance and reactance components of the resulting source impedance turn out to be smooth functions of frequency that allow simple algebraic fits. The source impedance is shown to be more or less independent of the engine speed.

Parametric studies have been conducted for different capacities of a single-cylinder gasoline engine, so as to derive a general expression of the source impedance as a function of the engine displacement as well as frequency. This expression should come handy for muffler designers who can predict the IL of a given muffler. This simple direct approach is extended to multi-cylinder engines in Chapters 3 and 4.

Chapter 3

Estimation of the Source Characteristics of Multi-Cylinder NA Engine*

Application of the novel direct evaluation method presented in Chapter 2 is extended here to the two-cylinder naturally aspirated (NA), 4-stroke-cycle diesel engine. Exhaust mass flow rate produced by each cylinder is required for estimation of the source characteristics, and for that matter, two different exhaust systems are considered; one, directly discharging into the atmosphere, and the other discharging to a typical two-cylinder engine exhaust system excluding muffler. These mass flow rates are assumed to be produced by a hypothetical auxiliary source, and these are used first for estimating the source impedance of each cylinder. Then, the acoustic source pressure is estimated by multiplying the acoustic mass velocity with the summation of the acoustic source impedance and load impedance.

In the case of cylinders discharging to a typical two-cylinder engine exhaust system excluding muffler, the ratio of acoustic pressure and acoustic mass velocity must satisfy the load impedance, and that calls for use of harmonic balancing method (HBM).

3.1 Harmonic Balance Method

Application of the predictor-corrector scheme for the cylinders discharging to a typical exhaust system is the same as illustrated in Chapter 2 for the ideal pressure release boundary condition except that the pressure downstream of the valve varies here. Computation of exhaust gas mass flow rate ($\dot{m}_{ex}(t)$) in the time domain requires the corresponding value of pressure ($p_{ex}(t)$) downstream of the exhaust valve. Initially, the simulation can be started with the initial guess value of $p_{ex}(t)$. The algorithm for the HBM is given in Fig. 3.1.

At the end of every loop, the difference between the current step and the previous step classical acoustic mass velocity vector are computed. Mathematically, Eq. (3.1) gives the condition for harmonic balance:

* This chapter is generally based on the Author's publication in Applied Acoustics, vol. 135, pp. 70 –84, 2018.

$$\left|\frac{v_{curr}\left(n\omega_0\right)-v_{prev}\left(n\omega_0\right)}{v_{prev}\left(n\omega_0\right)}\right|\leq 10^{-6},\quad n\leq 16 \tag{3.1}$$

where $v_{curr}\left(n\omega_0\right)$ and $v_{prev}\left(n\omega_0\right)$ are the n^{th} harmonic acoustic mass velocities of the current step and previous step, respectively.

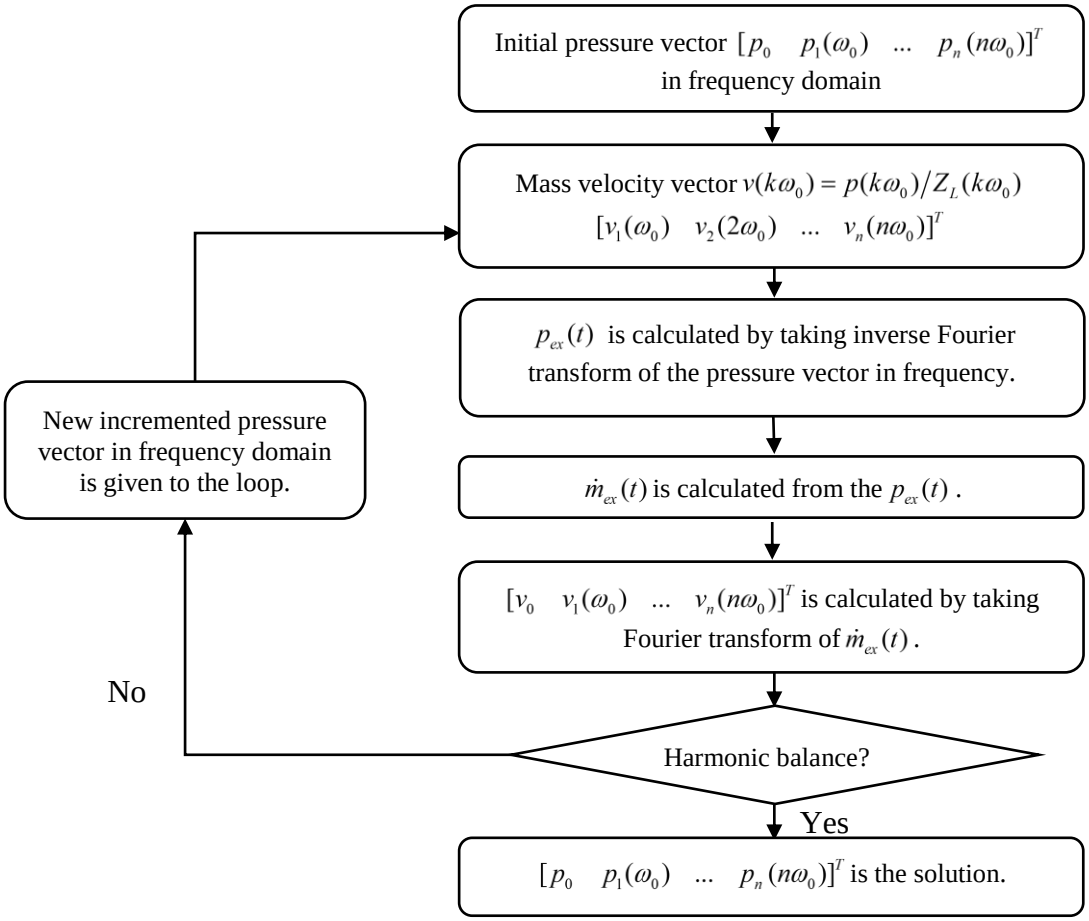

Figure 3.1. Flow chart of the Harmonic Balance Method [89,90]

For starting the computation, the initial pressure at the downstream of the valve is taken as the mean pressure in the exhaust port which is equal to the sum of atmospheric pressure and backpressure of the exhaust system. The Fourier transform of the mass flow rate gives the aeroacoustic or convective mass velocity which is converted to classical acoustic mass velocity by Eq. (3.2) [1]:

$$v\left(n\omega_0\right)=\frac{v_c\left(n\omega_0\right)}{1+M\,Z_L\left(n\omega_0\right)/Y_0} \tag{3.2}$$

where *M* is the mean flow Mach number, *v* is acoustic mass velocity, v_c is the aeroacoustic or convective mass velocity, Z_L is the load impedance and Y_0 is the characteristic impedance of the pipe.

3.2 Estimation of source characteristics of engine exhaust system

Equivalent (average) source impedance of a single cylinder is computed as described in Chapter 2. It is clear from Fig. 1.1(b) that the classical acoustic source pressure can be given by

$$p_s\left(n\omega_0\right) = v\left(n\omega_0\right)\left(Z_s\left(n\omega_0\right) + Z_L\left(n\omega_0\right)\right) \tag{3.3}$$

where $v\left(n\omega_0\right)$ is given by Eq. (3.2). Equations (2.14) and (3.3) give the classical acoustic source impedance and source pressure of a single cylinder as a source where only the cylinder and valves constitute the acoustic source.

Estimation of the source characteristics of a multi-cylinder engine requires transfer of source characteristics from just downstream of the exhaust valves to the upstream of exhaust manifold junction and then a combination of these characteristics to give the source characteristics at the downstream of the manifold junction. The relation between source characteristics at two different source-load junctions for the same source, and combined source characteristics of two different sources with source characteristics of individual sources are given in Appendix D.

Acoustic source characteristics of the exhaust system of two-cylinder naturally aspirated, 4-stroke diesel engines are estimated in this chapter. Exhaust mass flow rate history of cylinder # 1 and cylinder # 2 of a two-cylinder 4-stroke engine for a single thermodynamic cycle can be represented by Eqs. (3.4) and (3.5), respectively.

$$\dot{m}_{ex,C1}\left(t\right) = \sum_{n=-\infty}^{\infty} v_{1,c,n}\left(n\omega_0\right)e^{jn\omega_0 t}, \quad \omega_0 = \frac{2\pi}{T_0},\ T_0 = \frac{120}{N} \tag{3.4}$$

$$\dot{m}_{ex,C2}\left(t\right) = \dot{m}_{ex,C1}\left(t - \frac{T_0}{2}\right) = \sum_{n=-\infty}^{\infty} v_{1,c,n}\left(n\omega_0\right)e^{jn\omega_0\left(t-\frac{T_0}{2}\right)} = \sum_{n=-\infty}^{\infty} v_{1,c,n}\left(n\omega_0\right)e^{jn\omega_0 t}e^{-jn\pi} \tag{3.5}$$

Variables in Eqs. (3.4) and (3.5) carry usual meaning and these are also mentioned in Chapter 1 below Eq. (1.1). Here, $v_{1,c,n}$ and its complex conjugate are the Fourier coefficient of the perturbations on the average exhaust mass flow rate downstream of the exhaust valve/s

discharged by cylinder # 1. In other words, $v_{1,c,n}$ is the aeroacoustic mass velocity corresponding to the n^{th} harmonic of fundamental frequency at the downstream end of exhaust valve/s of cylinder # 1. In accordance with Eq. (3.4), the mass flow rate history downstream of the exhaust valve/s of cylinder # 2 can also be represented by

$$\dot{m}_{ex,C2}(t) = \sum_{n=-\infty}^{\infty} v_{2,c,n}(n\omega_0) e^{jn\omega_0 t}. \tag{3.6}$$

Using Eqs. (3.5) and (3.6), the relation between aeroacoustic mass velocity downstream of exhaust valve/s of cylinder # 1 and cylinder # 2 is given by

$$v_{2,c,n}(n\omega_0) = v_{1,c,n}(n\omega_0) e^{-jn\pi}. \tag{3.7}$$

Using Eqs. (3.2) and (3.7), the relation between acoustic mass velocity at the downstream of the exhaust valve of cylinder # 2 and that of cylinder # 1 for a symmetric exhaust manifold is given by

$$v_{2,n}(n\omega_0) = v_{1,n}(n\omega_0) e^{-jn\pi}. \tag{3.8}$$

Similarly, the source pressure (at the downstream end of the exhaust valve) of cylinders 1 and 2 are related as

$$p_{s,2}(n\omega_0) = p_{s,1}(n\omega_0) e^{-jn\pi}. \tag{3.9}$$

Using Eqs. (D.1), (D.3) and (3.5), it is found that the source pressure of a two-cylinder engine at the downstream of the exhaust manifold junction is negligibly weak for odd multiples of the single cylinder firing frequency as compared to the even multiples, provided the runners of the two cylinders are identical.

The range of source pressure (real as well as imaginary part) is large, so it is expressed in terms of the source strength level (SSL), which is defined as

$$\text{SSL} = 20\log\left(\left|\frac{p_s/\sqrt{2}}{p_{th}}\right|\right), \quad \text{dB} \tag{3.10}$$

where p_{th} denotes the standard hearing threshold pressure, 20 μPa $\left(2\times10^{-5}\,\text{Pa}\right)$.

3.3 Application of direct estimation method to the DG-Set engines

Two diesel generator set (DG-Set) engines are taken for the application of this novel direct method for estimation of their source characteristics in this chapter. The nominal power of these engines is 15 kVA and 20 kVA, and hereafter these are referred as 15 kVA engine and 20 kVA engine, respectively. The specifications of these engines are given in Appendix C. In subsequent subsections 3.3.1 and 3.3.2, the computed source characteristics of one cylinder at just downstream of the exhaust valve and complete engine at downstream end of the manifold junction and just upstream end of the applied acoustic load are presented.

3.3.1 Acoustic source characteristics of 15 kVA engine

The mass flow rate history at the downstream end of exhaust valve for the cases when the cylinder is discharging directly into the atmosphere and to the exhaust system (schematic diagram is shown in Fig. 3.2) of engine excluding muffler are shown in Fig. 3.3. It is evident that the mass flow rate history has to be different for different exhaust systems, and it can indeed be observed from Fig. 3.3. The comparison of static pressure downstream of exhaust valve for the two cases is shown in Fig. 3.4.

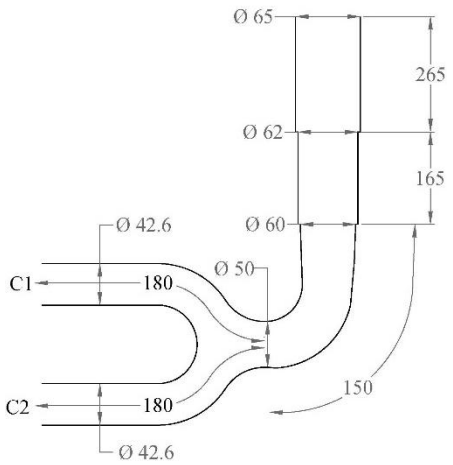

Figure 3.2. Schematic diagram of the exhaust system of 15 kVA engine

It is evident from Figs. 3.5 and 3.6 that the acoustic source characteristics of the IC engine of each cylinder are dependent on the exhaust system, although the source impedance is relatively less dependent. However, the apparent dependence of source strength level is because it largely depends on the acoustic load impedance as well as the acoustic mass velocity. This confirms the non-uniqueness of source characteristics as predicted by Gupta and Munjal [16].

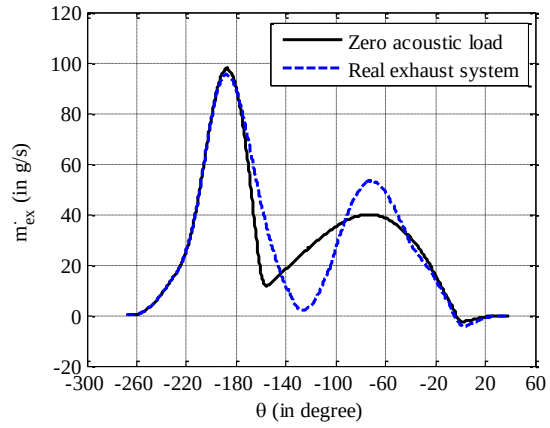

Figure 3.3. Comparison of mass flow rate history at downstream end of exhaust valve of 15 kVA engine

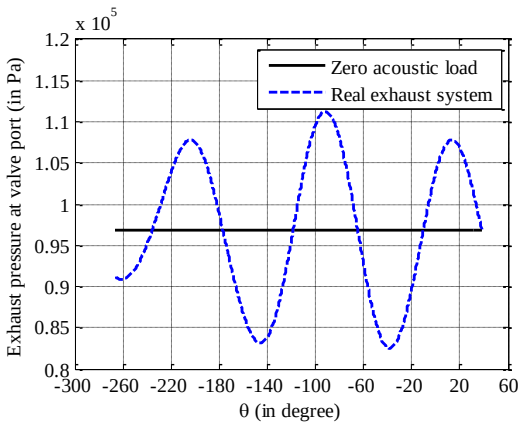

Figure 3.4. Comparison of static pressure at downstream end of exhaust valve of 15 kVA engine

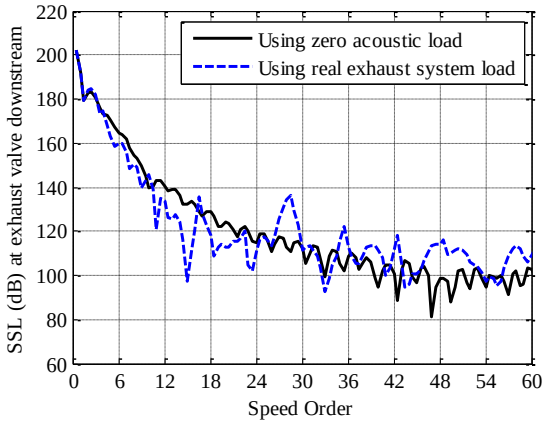

Figure 3.5. Comparison of source strength level at the downstream end of exhaust valve of 15 kVA engine

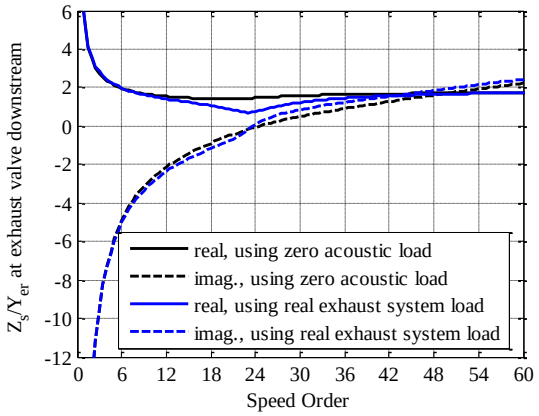

Figure 3.6. Comparison of normalised source impedance at the downstream end of exhaust valve of 15 kVA engine

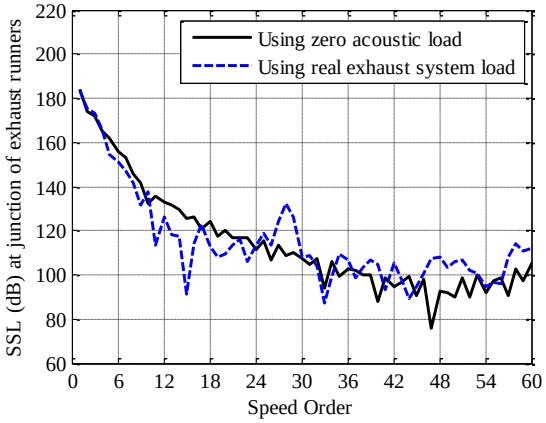

Figure 3.7. Comparison of source strength level at the downstream end of exhaust manifold junction of 15 kVA engine

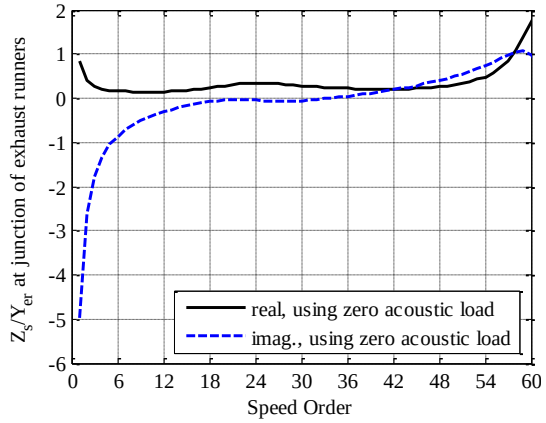

Figure 3.8. Normalized source impedance at the downstream end of exhaust manifold junction of 15 kVA engine

Because of the weaker dependence of acoustic source impedance on the acoustic load with which the exhaust gas mass flow rate history is computed, the values of source impedance at the exhaust manifold junction downstream end and upstream end of the acoustic load are not compared in Figs. 3.8 and 3.10. In Figs. 3.7 and 3.9 the source strength level at the exhaust manifold junction and the upstream of acoustic load are shown, respectively. The SSL spectra shown in Figs. 3.7 and 3.9 do not contain the odd multiples of half speed order.

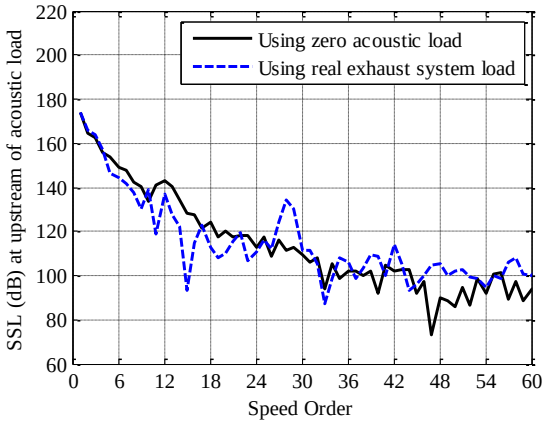

Figure 3.9. Comparison of source strength level at the upstream end of the acoustic load of 15 kVA engine

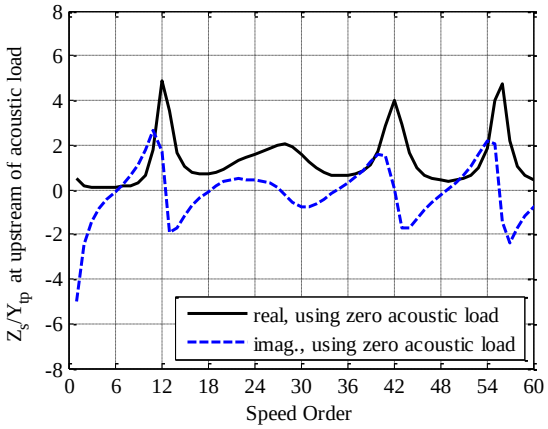

Figure 3.10. Normalized source impedance at the upstream end of the acoustic load of 15 kVA engine

After the source impedance of the engine at the downstream end of the manifold junction is obtained, it is transferred to the upstream end of acoustic load (section 3'-3' of Fig. D.2). It is shown in Fig. 3.10. Effect of components in the exhaust system downstream of the manifold junction can be observed in Fig. 3.10. It is evident from Figs. 3.7 and 3.9 that the shifting of the source-load junction in the downstream of acoustic load weakens the source strength, as would indeed be expected because of the acoustic attenuation of elements.

3.3.2 Acoustic source characteristics of 20 kVA engine

Corresponding to the plots shown in Figs. 3.3–3.10 for 15 kVA engine, Figs. 3.12–3.19 relate to 20 kVA engine (schematic diagram is shown in Fig. 3.11). The trends are all similar and therefore do not call for a separate discussion.

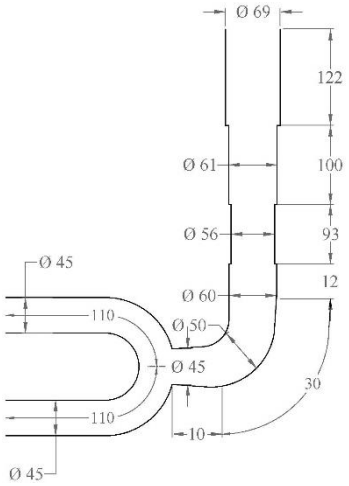

Figure 3.11. Schematic diagram of the exhaust system of 20 kVA engine

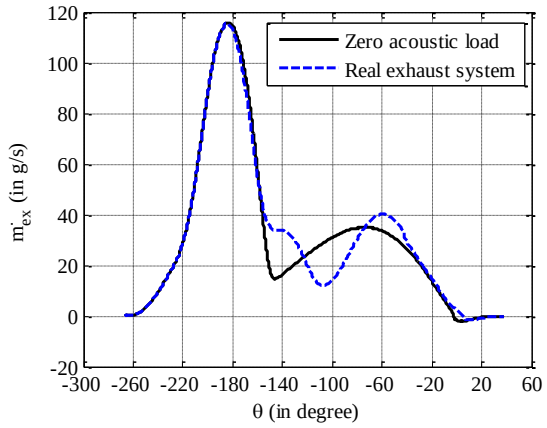

Figure 3.12. Comparison of mass flow rate history at the downstream end of exhaust valve of 20 kVA engine

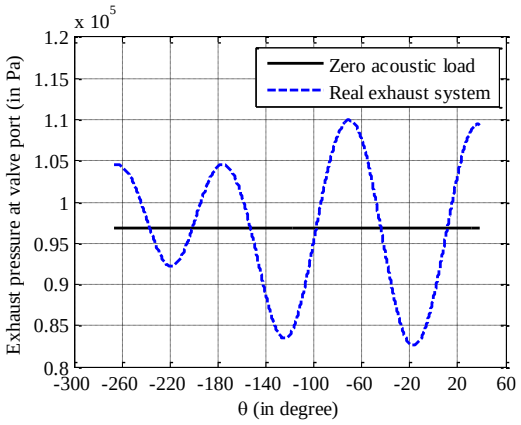

Figure 3.13. Comparison of static pressure at the downstream end of exhaust valve of 20 kVA engine

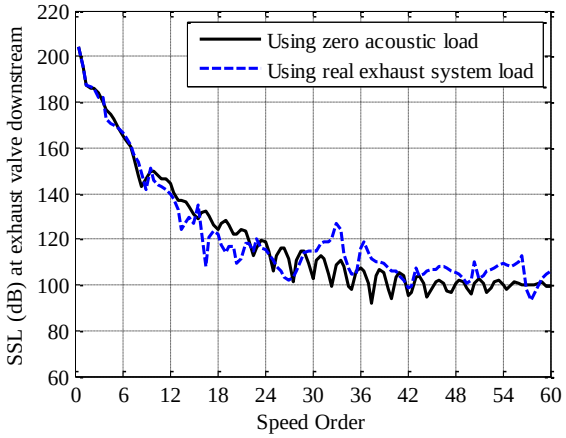

Figure 3.14. Comparison of source strength level at the downstream end of exhaust valve of 20 kVA engine

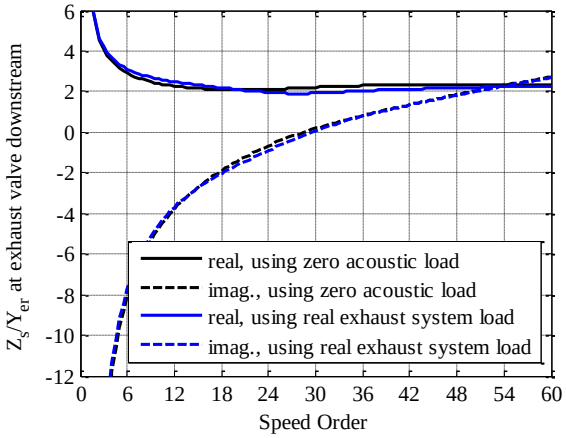

Figure 3.15. Comparison of normalised source impedance at the downstream end of exhaust valve of 20 kVA engine

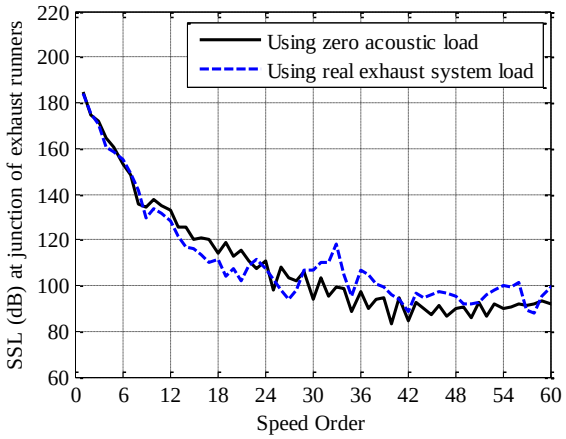

Figure 3.16. Comparison of source strength level at the downstream end of exhaust manifold junction of 20 kVA engine

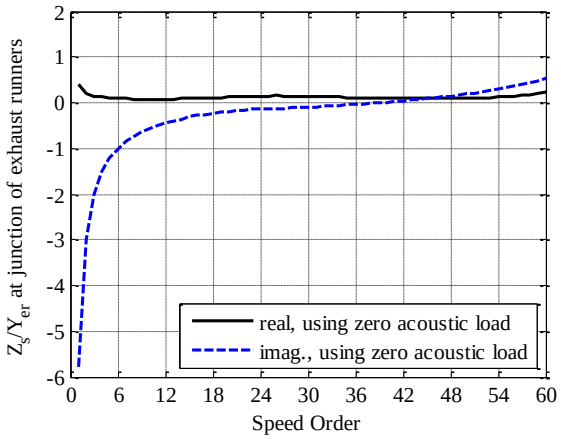

Figure 3.17. Normalized source impedance at the downstream end of exhaust manifold junction of 20 kVA engine

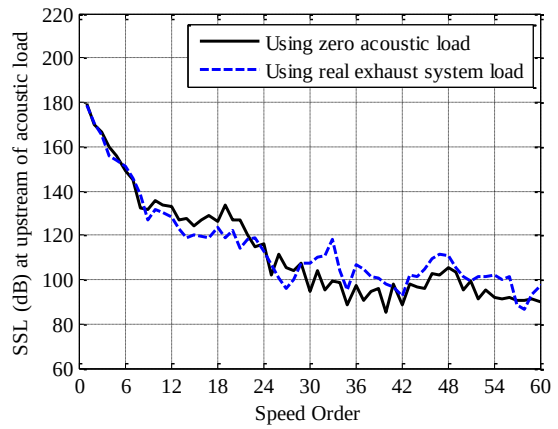

Figure 3.18. Comparison of source strength level at the upstream end of the acoustic load of 20 kVA engine

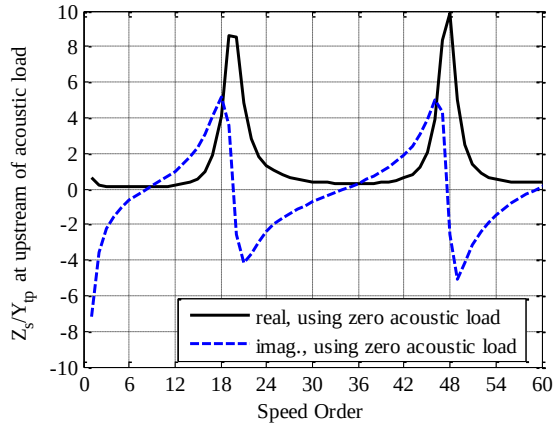

Figure 3.19. Normalized source impedance at the upstream end of the acoustic load of 20 kVA engine

3.4 Experimental validation of the estimated source characteristics

Using the values of the source characteristics, the unmuffled sound pressure level (SPL) at a distance of 0.5 metre from the exhaust orifice is predicted for the 15 kVA DG-Set engine and the 20 kVA DG-Set engine. Unmuffled noise SPL spectra for 15 kVA DG-Set engine and 20 kVA DG-Set engine are plotted in Figs. 3.20 and 3.21.

It is clear from Figs. 3.20 and 3.21 that the comparison of the experimentally measured overall SPL with those predicted in the present study is reasonable. The engine exhaust system is highly nonlinear (because of high pressure blowdown) and time variant (because of the

exhaust valves and cylinder cavity as discussed in Chapter 2). However, the source characterization procedure adopted here (based on Thevenin theorem and/or Norton theorem for the electrical wave filter theory) is applicable for linear time-invariant systems only. Therefore one has to accept discrepancies of as high as 5 to 10 dB.

Both the figures show that the predicted SPL spectra have similar trends to the experimentally measured SPL spectra. The SPL values predicted by using the source characteristics if the cylinder is assumed to discharge directly into the atmosphere and if the cylinder is assumed to discharge into a typical exhaust system, are similar for the first four speed orders, but start deviating at the higher speed orders.

The experimentally measured SPL spectra also contain the casing noise outside the acoustic enclosure. In Figs. 3.20 and 3.21, the casing noise which comes out from the enclosure is added to the estimated unmuffled exhaust noise (using the estimated source characteristics) to predict the noise at the microphone location (used in experimental measurement).

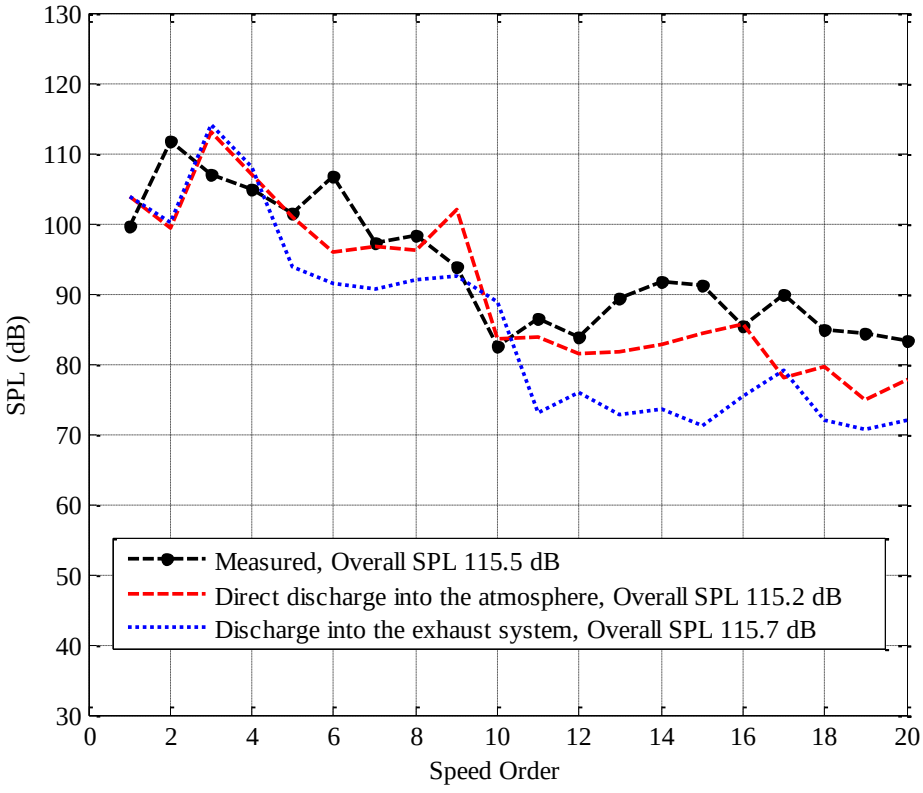

Figure 3.20. Comparison of unmuffled SPL radiated by 15 kVA engine: experimentally measured, predicted using estimated source characteristics while cylinder is assumed to discharge directly into the atmosphere, and predicted using estimated source characteristics while cylinder is assumed to discharge to the exhaust system

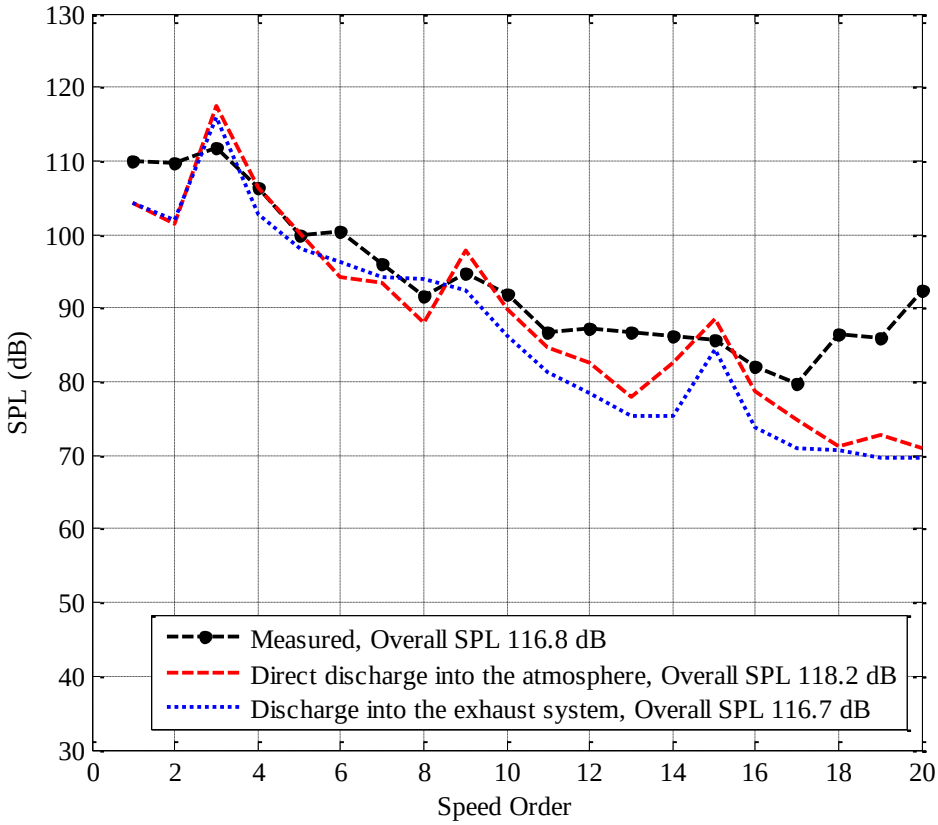

Figure 3.21. Comparison of unmuffled SPL radiated by 20 kVA engine: experimentally measured, predicted using estimated source characteristics while cylinder is assumed to discharge directly into the atmosphere, and predicted using estimated source characteristics while cylinder is assumed to discharge to the exhaust system

The casing noise is assumed as the logarithmic average of the values of the muffled SPL picked up by the microphones (at different locations on a hypothetical parallelopiped outside the acoustic enclosure of DG-Set) as per the survey method (ISO 8528-10 [91]). The microphones will pick up the casing noise as well as the exhaust noise. The experimentally measured values of the overall casing noise for 15 kVA engine and 20 kVA engine are 72.8 dBA and 73.0 dBA, respectively. To evaluate the octave band frequency spectrum of the diesel engine casing noise in dBA the frequency adjustments given in the second row of Table 3.1 are subtracted from the overall casing noise outside the enclosure.

Table 3.1. Frequency adjustments to be subtracted for evaluation of the octave band spectrum of casing noise of reciprocating engines [92–94]

Octave band centre frequency (Hz)	31.5	63	125	250	500	1000	2000
Correction to be subtracted from the overall casing noise	14	9	7	8	7	7	9

SPL spectrum in dB is obtained by subtracting the A-weighting correction which is given by [95,96]:

$$\mathrm{A}(f) = 2 + 20\log\left(\frac{12200^2 \cdot f^4}{\left(f^2 + 20.6^2\right)\sqrt{\left(f^2 + 107.7^2\right)\left(f^2 + 737.9^2\right)}\left(f^2 + 12200^2\right)}\right) \quad (3.11)$$

The difference between the overall casing noise outside the acoustic enclosure of 15 kVA engine and 20 kVA engine is 0.2 dB which is negligible. The SPL spectrum of casing noise outside the enclosure (with 72.8 dBA overall SPL) is shown in Fig. 3.22.

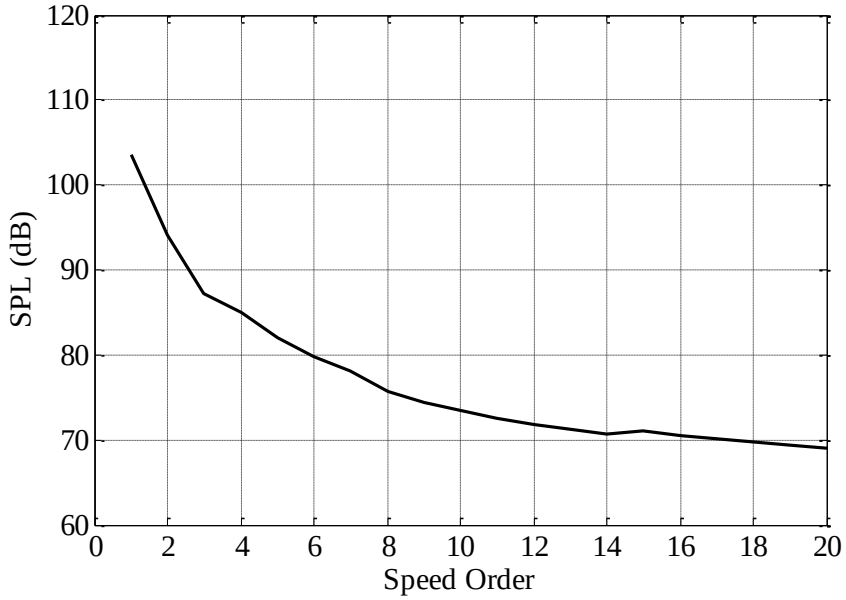

Figure 3.22. SPL spectrum of casing noise outside the acoustic enclosure of a DG-Set

Figures 3.23 and 3.24 show the effect of source impedance on prediction of the unmuffled SPL spectra of 15 kVA engine and 20 kVA engine, respectively. In Figs. 3.23 and 3.24, the unmuffled exhaust SPL spectra were computed using the estimated source pressure while cylinder is exhausting directly into the atmosphere. It is evident from Figs. 3.23 and 3.24 that the assumption of anechoic source just upstream of the acoustic test load is a good approximation to predict the unmuffled exhaust SPL spectrum. Therefore, in the case of unavailability of the measured source impedance or the estimated source impedance by the present method, anechoic source can be assumed to predict the unmuffled exhaust SPL spectrum of multi-cylinder naturally aspirated engines and the IL spectrum of mufflers applied on the multi-cylinder naturally aspirated engines. However, one must remember that the computed value of source pressure is implied here.

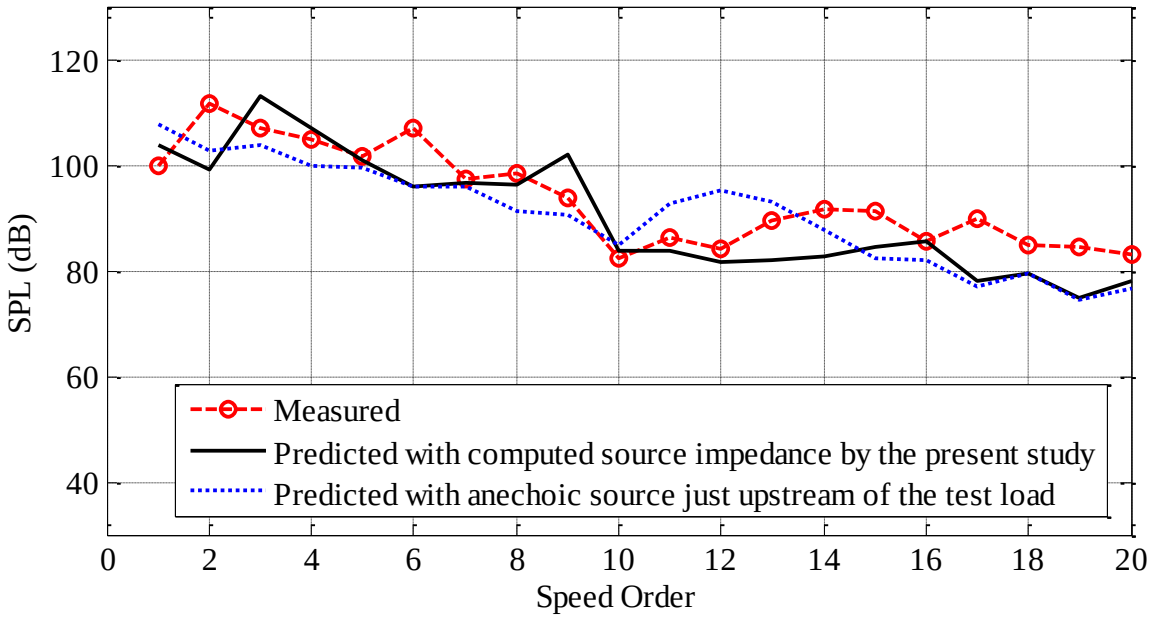

Figure 3.23. Effect of source impedance on prediction of unmuffled exhaust SPL spectrum of the 15 kVA engine (source pressure, however, is the computed values in both the cases)

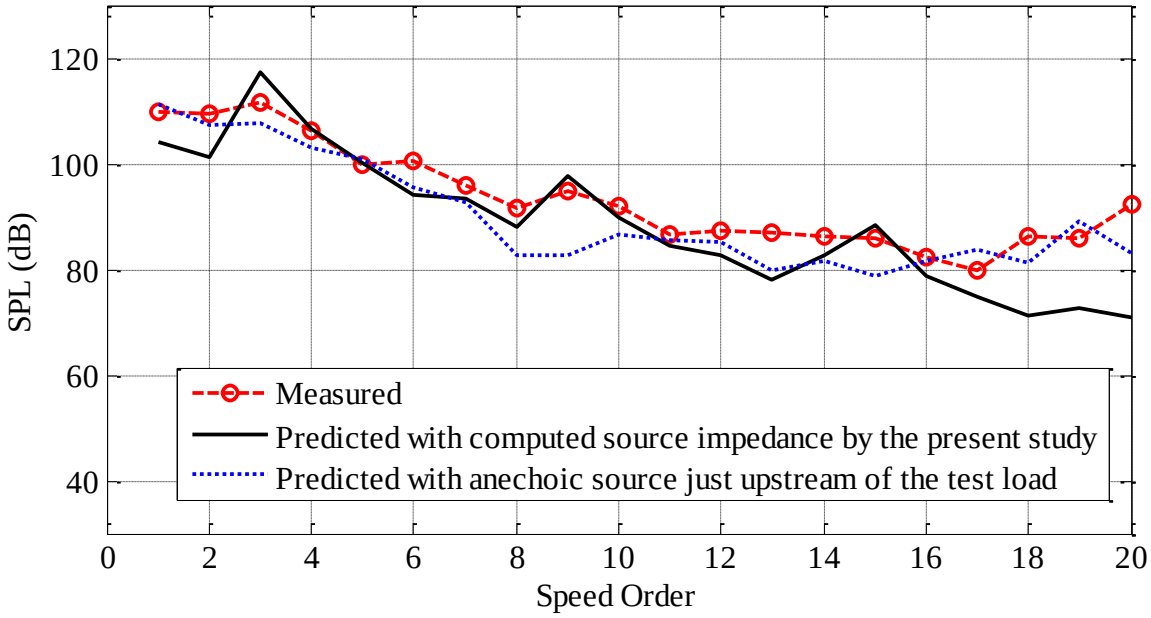

Figure 3.24. Effect of source impedance on prediction of unmuffled exhaust SPL spectrum of the 20 kVA engine (source pressure, however, is the computed values in both the cases)

3.5 Conclusion

A procedure to obtain the source characteristics of a two-cylinder engine is shown in this chapter which obviates the need of experiments as well as the complete time domain simulation over several engine cycles. The values of source resistance at all speed orders are shown to be

positive, and this is one of the biggest merits of the present approach over the conventional multi-load indirect methods which predict negative source resistance at most of the speed-orders. Non-uniqueness of the source characteristics of IC engines is observed in the framework of the direct method presented here because of the time-variant and non-linear nature of the exhaust system/process. However, the unmuffled SPL predicted with the estimated source characteristics considering two different loads are in reasonable agreement with the experimentally measured SPL spectra. Moreover, the estimated source characteristics using zero acoustic load termination is adequate for predicting the unmuffled SPL, and this simplifies the process. Thus, the method presented here with zero acoustic load termination can be used to predict the unmuffled SPL spectrum and design an appropriate muffler for an IC engine even before it is prototyped. Thus, the design and analysis of engine and muffler can be integrated.

Chapter 4

Estimation of the Source Characteristics of Multi-Cylinder T/C Engine*

Application of novel direct method illustrated in Chapters 2 and 3 for naturally aspirated (NA) engines is extended to the turbocharged (T/C) engine's exhaust system for estimation of acoustic source characteristics in this chapter. All the preceding studies on acoustic modelling of turbochargers [45–48], involved either the numerical analysis or experimental measurement of the four-pole parameters of a turbine. However, the method of direct evaluation of source characteristics presented in Chapters 2 and 3 can be extended to the turbocharged engines only if the transfer matrix of the turbine is known analytically in terms of the significant operating parameter the static pressure ratio. In the present study, acoustic modelling (analytical derivation of four-pole parameters) of the turbine and compressor is done as a point model where the isentropic expansion and compression takes place, respectively. Transfer matrices of the turbine and compressor of an automotive turbocharger are derived using the mass continuity upstream and downstream of the turbine and compressor along with the static pressure ratios. The acoustic source characteristics of each cylinder for the source-load junction downstream of the exhaust valve is computed assuming that the cylinder discharges to an ideal pressure release boundary condition with the constant pressure being product of the turbine pressure ratio and mean pressure in the exhaust pipe downstream of the turbine. Source characteristics of each cylinder are used to estimate the source characteristics downstream of the exhaust manifold. Using the derived transfer matrix of the turbine, the source characteristics are further estimated at the source-load junction downstream of the turbine.

4.1 Derivation of transfer matrices of turbine and compressor of a turbocharger

Primary job of the turbocharger is to extract the exhaust gas waste energy to run the common shaft of a turbine and compressor which in turn compresses the intake air to a higher

* This chapter is generally based on the Author's publication in Applied Acoustics, vol. 149, pp. 171 –180, 2019.

density. The compressed air allows more air to burn more fuel and thus produces more power as compared to the naturally aspirated engine of the same size. Thus, the turbocharged engines are commonly used in many applications to fulfil the demands of the downsizing of automotive engines, increase in fuel efficiency and reduction in noise pollutants.

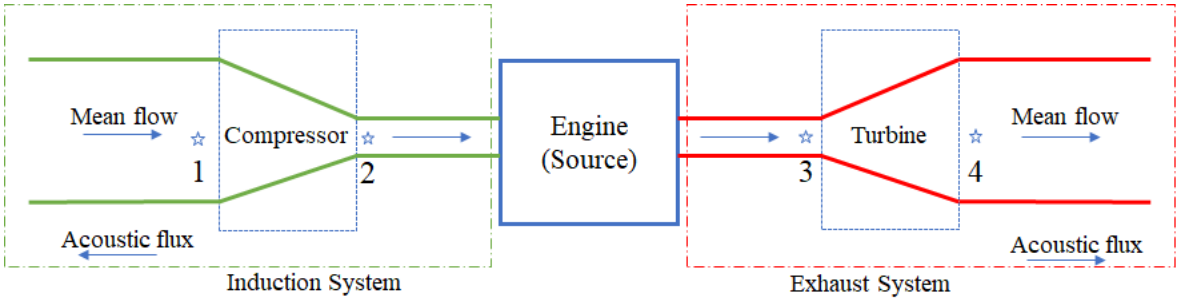

Figure 4.1. Schematic of a turbocharged engine's exhaust system indicating directions of mean flow as well as acoustic flux

A schematic of the engine, turbine and compressor including the direction of mean flow and acoustic flux is shown in Fig. 4.1. In the compressor, the acoustic wave propagation is in the opposite direction to the mean flow direction, whereas in the turbine both acoustic wave propagation and mass flow are in the same direction (i.e. going away from the engine).

4.1.1 Transfer matrix of the turbine of the turbocharger

The static pressure ratio of the turbine is α_t. Thus

$$P_{3,0} = \alpha_t P_{4,0}, \tag{4.1}$$

where $P_{3,0}$ and $P_{4,0}$ are the static pressure at the upstream and downstream ends of the turbine. Equation (4.1) would hold also for the case with acoustic perturbations (i.e. with waves). Therefore,

$$P_{3,0} + p_3 = \alpha_t \left(P_{4,0} + p_4 \right). \tag{4.2}$$

Subtraction of Eq. (4.1) from Eq. (4.2) yields the relation between the acoustic pressures at the upstream and downstream ends of the turbine:

$$p_3 = \alpha_t p_4. \tag{4.3}$$

The mass continuity between the upstream and downstream of a turbine holds with and without waves yielding Eqs. (4.4) and (4.5), respectively.

$$\rho_{0,3}U_3S_3 = \rho_{0,4}U_4S_4 \tag{4.4}$$

$$\left(\rho_{0,3}+\rho_3\right)\left(U_3+u_3\right)S_3 = \left(\rho_{0,4}+\rho_4\right)\left(U_4+u_4\right)S_4 \tag{4.5}$$

Subtracting Eq. (4.4) from Eq. (4.5) and neglecting second-order (nonlinear) terms yields

$$\rho_3U_3S_3 + \rho_{0,3}u_3S_3 = \rho_4U_4S_4 + \rho_{0,4}u_4S_4. \tag{4.6}$$

Neglecting entropy fluctuations in view of incompressible mean flow $\left(M_3^2, M_4^2 \ll 1\right)$, we apply the isentropicity relations

$$\rho_3 = \frac{p_3}{c_3^2}, \tag{4.7}$$

$$\rho_4 = \frac{p_4}{c_4^2}. \tag{4.8}$$

Noting that acoustic mass velocity, $v = \rho_0 Su$, the characteristic impedance of a pipe, $Y = c_0/S$, and the mean flow Mach number, $M = U/c_0$, and applying these relations in Eq. (4.6)

$$v_3 + \frac{M_3}{Y_3}p_3 = v_4 + \frac{M_4}{Y_4}p_4. \tag{4.9}$$

Equations (4.3) and (4.9) may be rearranged in the required transfer matrix form for the turbine:

$$\begin{bmatrix} p_3 \\ v_3 \end{bmatrix} = \begin{bmatrix} \alpha_t & 0 \\ \left(M_4/Y_4\right) - \alpha_t\left(M_3/Y_3\right) & 1 \end{bmatrix}\begin{bmatrix} p_4 \\ v_4 \end{bmatrix}. \tag{4.10}$$

The product of M_3/M_4 and Y_3/Y_4 in terms of turbine pressure ratio (α_t) is

$$\frac{M_3}{M_4}\frac{Y_4}{Y_3} = \frac{U_3S_3}{U_4S_4}\frac{T_4}{T_3} = \frac{\rho_{0,4}}{\rho_{0,3}}\frac{T_4}{T_3} = \left(\alpha_t\right)^{-1/\gamma}\left(\alpha_t\right)^{(1-\gamma)/\gamma} = \alpha_t^{-1}. \tag{4.11}$$

Using Eqs. (4.10) and (4.11), transfer matrix of the turbine can be represented as:

$$\begin{bmatrix} p_3 \\ v_3 \end{bmatrix} = \begin{bmatrix} \alpha_t & 0 \\ 0 & 1 \end{bmatrix}\begin{bmatrix} p_4 \\ v_4 \end{bmatrix}. \tag{4.12}$$

The transfer matrix derived above does not consider the wave propagation inside the turbine, and it shows that the transmission properties are independent of frequency. It is interesting to note that the acoustic pressure downstream of the turbine is $1/\alpha_t$ times the upstream acoustic pressure.

4.1.2 Transfer matrix of the compressor of the turbocharger

A similar procedure to that for the turbine can be carried out to derive the transfer matrix of compressor given by Eq. (4.13)

$$\begin{bmatrix} p_2 \\ v_2 \end{bmatrix} = \begin{bmatrix} \alpha_c & 0 \\ (M_1/Y_1) - \alpha_c (M_2/Y_2) & 1 \end{bmatrix} \begin{bmatrix} p_1 \\ v_1 \end{bmatrix}, \tag{4.13}$$

where α_c is the compressor pressure ratio.

Transfer matrix of the compressor given by Eq. (4.13) can be further simplified as done in Eq. (4.11) for the turbine, and it yields

$$\begin{bmatrix} p_2 \\ v_2 \end{bmatrix} = \begin{bmatrix} \alpha_c & 0 \\ 0 & 1 \end{bmatrix} \begin{bmatrix} p_1 \\ v_1 \end{bmatrix}. \tag{4.14}$$

It is interesting to note that the acoustic pressure upstream of the compressor is $1/\alpha_c$ times the downstream acoustic pressure. Transfer matrix of the compressor can be used in the acoustic analysis of the induction system of turbocharged engines.

4.2 Estimation of the source characteristics of a T/C diesel engine exhaust system

The measured values of average exhaust temperature and the pressure downstream of exhaust valve are 768 K and 0.96 bar (because the atmospheric pressure at the place of the experiment is 0.95 bar), respectively. The temperature of the exhaust gas in the exhaust runners (manifold) is computed by assuming isentropic expansion through the turbine:

$$T_{er} = T_{ex} \left(\alpha_t \right)^{(\gamma-1)/\gamma} \tag{4.15}$$

where α_t , γ, T_{ex} and T_{er} are the turbine pressure ratio, isentropic exponent of exhaust gas, mean exhaust gas temperature downstream of the turbine, and the mean exhaust gas temperature in the exhaust runners, respectively. The temperature of exhaust gas in the exhaust runners turns out to be 942 K.

Significant mass flow through the valves occurs after a reference valve lift, usually termed as clearance valve lift. In the present study, 0.2 mm is taken as the reference valve lift for both the intake and exhaust valves. The in-cylinder gas temperature is computed using the ideal gas equation corresponding to the in-cylinder gas mass required for the desired exhaust gas mass

flow rate. The pressure (experimentally measured) and temperature (computed with assumptions) of the in-cylinder gas at the blowdown are 9.8 bar and 1042 K, respectively. It is interesting to note that the summation of the mean mass flow rate of all the cylinders for one engine cycle turns out to be 281 g/s which is very close to the experimentally measured value of 283.3 g/s.

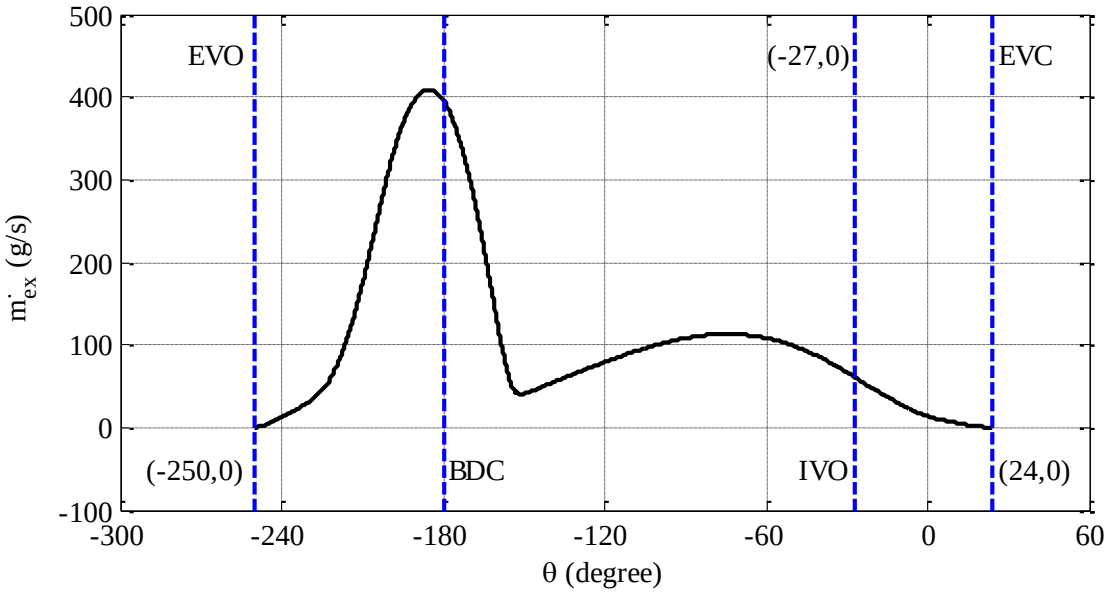

Figure 4.2. Mass flow rate history downstream of the exhaust valve of a cylinder.

Figure 4.2 shows the mass flow rate history at the downstream end of exhaust valve for one cylinder. It can be observed from this figure that the blowdown process continues almost up to the BDC in expansion process where the mass flow occurs due to the difference of pressure despite the piston moving in the opposite direction. Moreover, most of the exhaust gas flow occurs in the blowdown process. In the exhaust stroke, from BDC to TDC the mass flow rate occurs due to the displacement process where the piston is pushing out the gas. There is no backflow occurring in the overlap period of the intake and exhaust valve because of the assumption of constant pressure in the intake and exhaust runners. The pressure in the intake runners in the exhaust valve is more than that of the exhaust runners. Therefore the forward flow through exhaust valve occurs in the overlap period.

Exhaust mass flow rate history of the m^{th} cylinder (in order of firing) of a six-cylinder 4-stroke engine for a single thermodynamic cycle can be represented by

$$\dot{m}_{ex,Cm}(t)=\dot{m}_{ex,C1}\left(t-(m-1)\frac{T_0}{6}\right)=\sum_{n=-\infty}^{\infty}v_{1,c,n}(n\omega_0)e^{jn\omega_0\left(t-(m-1)\frac{T_0}{6}\right)}=\sum_{n=-\infty}^{\infty}v_{1,c,n}(n\omega_0)e^{jn\omega_0 t}e^{-jn\frac{2\pi(m-1)}{6}} \quad (4.16)$$

where subscripts *Cm* and *C1* denote the m^{th} cylinder and 1st cylinder, respectively.

The Fourier transform of the mass flow rate downstream of the exhaust valve/s of a cylinder gives the aeroacoustic or convective mass velocity. $v_{m,c,n}(n\omega_0)$ and its complex conjugate are the Fourier coefficients of aeroacoustic mass velocity at the downstream end of the exhaust valve/s of the m^{th} cylinder (in order of firing). Thus, the relation between aeroacoustic mass velocity downstream of the exhaust valve/s of the m^{th} cylinder (in order of firing) of a six-cylinder engine and that of the 1st cylinder is given by

$$v_{m,c,n}(n\omega_0) = v_{1,c,n}(n\omega_0)e^{-jn\frac{2\pi(m-1)}{6}} \tag{4.17}$$

The aeroacoustic mass velocity $v_{m,c,n}(n\omega_0)$ is converted to classical acoustic mass velocity $v_m(n\omega_0)$ by means of Eq. (3.2). The relation between the acoustic mass velocity downstream of the exhaust valve of the m^{th} cylinder (in order of firing) of a 6-cylinder engine and that of the 1st cylinder for ideal pressure release boundary condition is given by

$$v_m(n\omega_0) = v_1(n\omega_0)e^{-jn\frac{2\pi(m-1)}{6}}. \tag{4.18}$$

Similarly, the source pressures (downstream of exhaust valve) of the m^{th} cylinder (in order of firing) of a 6-cylinder engine and the 1st cylinder are related as

$$p_{s,m}(n\omega_0) = p_{s,1}(n\omega_0)e^{-jn\frac{2\pi(m-1)}{6}}. \tag{4.19}$$

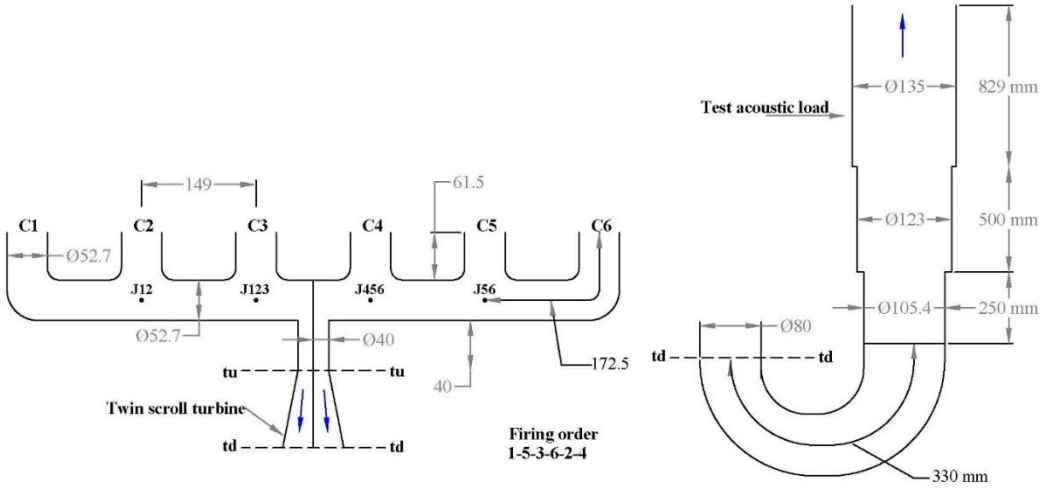

(a) (b)

Figure 4.3. Schematic diagram of the turbocharged engine exhaust system. (a) exhaust manifold and turbine; (b) exhaust system downstream of the turbine.

The specifications of the turbocharged engine are given in Appendix C. In the subsequent sub-sections, the estimation of source characteristics of each cylinder downstream of the exhaust valve, and the complete engine downstream of the exhaust manifold and turbine are shown. Schematic diagram of the exhaust system is shown in Fig. 4.3.

4.2.1 Acoustic source characteristics of a single cylinder

Estimation of the source characteristics of each cylinder of the engine is carried out as illustrated in Section 3.3.

It can be observed from Fig. 4.4 that the source resistance and reactance values are large in the low frequency region because the cylinder cavity compliance is inversely proportional to the frequency. In the low frequency region (up to speed order 12), the source reactance is mainly due to the cylinder cavity compliance, whereas in the mid and high frequency regions, the source reactance is mainly governed by valve inertance which is proportional to frequency. It is also interesting to note that the source resistance becomes almost constant whereas the source reactance varies linearly with respect to frequency after speed order 12 (300 Hz). Figure 4.5 shows the exponential decay of source strength level with respect to speed order.

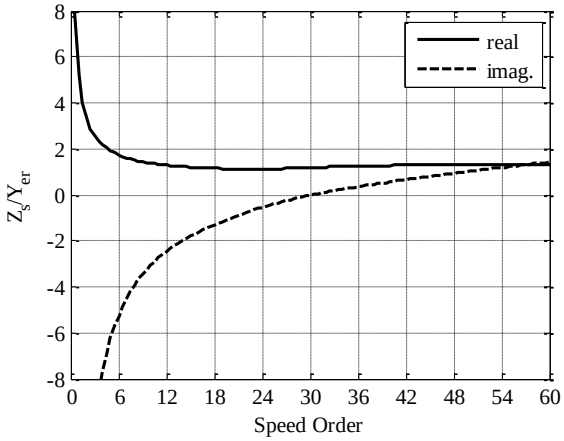

Figure 4.4. Normalized source impedance (with respect to the characteristic impedance of exhaust runner) downstream of the exhaust valve

Figure 4.5. Source strength level of a cylinder downstream of exhaust valve

4.2.2 Acoustic source characteristics of the engine downstream of the exhaust manifold

After estimating the source characteristics of each cylinder downstream of the exhaust valve, the source characteristics are transferred to downstream of exhaust runners making use of Eqs. (D.1) and (D.2) of Appendix D. The equivalent source characteristics of cylinder # 1

and cylinder # 2 at junction J12 are obtained by combining the source characteristics downstream of respective exhaust runners by means of Eqs. (D.3) and (D.4). Similarly, equivalent source characteristics of the cylinder # 1 and cylinder # 2 are transferred to the junction J123, and it is combined with the transferred source characteristics downstream of cylinder # 3 runner to give the equivalent source characteristics of three cylinders (# 1, # 2 and # 3). Further, this equivalent source characteristics are transferred to the downstream of the exhaust manifold (i.e. the section tu-tu upstream of the turbine).

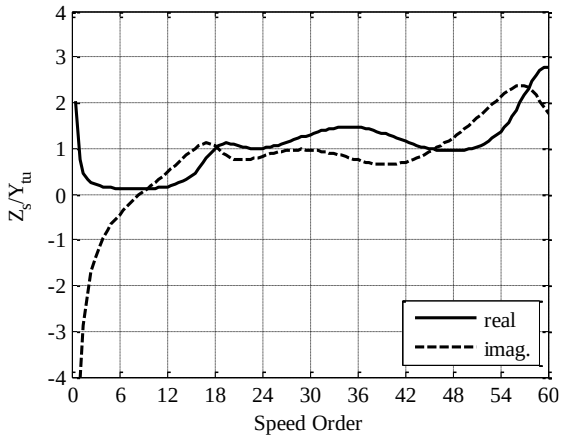

Figure 4.6. Normalized source impedance (with respect to the characteristic impedance of the turbine upstream pipe) of each side of cylinders upstream of turbine

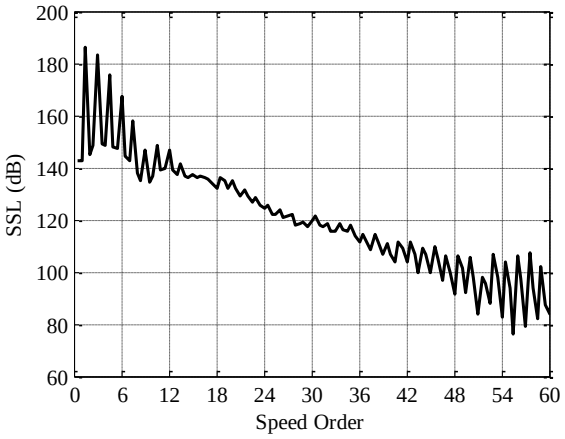

Figure 4.7. Source strength level of each side of cylinders upstream of turbine (i.e. downstream of exhaust manifold)

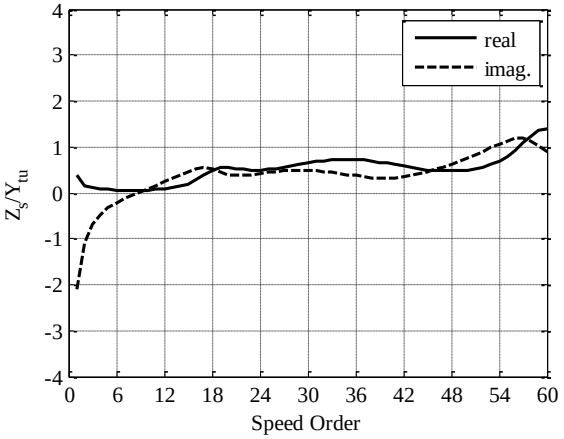

Figure 4.8. Normalized source impedance (with respect to the characteristic impedance of the turbine upstream pipe) of combination of all six cylinders upstream of turbine

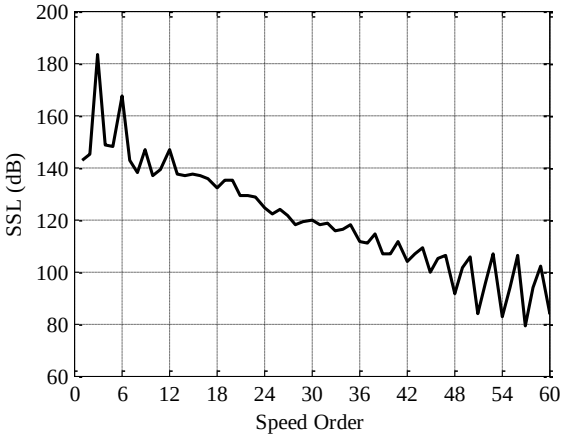

Figure 4.9. Source strength level of combination of all six cylinders upstream of turbine (i.e. downstream of exhaust manifold)

Figures 4.6 and 4.7 show the source characteristics downstream of the exhaust manifold for one side of the cylinders (either right or left). It is interesting to note that the combined source pressure of cylinders (# 1, # 2 and # 3) shows dominant peaks at harmonics of speed order 1.5 up to speed order 12, even though the runner lengths are unequal. This observation says that the role of phase differences due to such small path differences become substantial in the mid and high frequency region only.

The firing order of cylinders is 1-5-3-6-2-4. Thus, from the mid-section of the exhaust manifold the equidistant cylinders are having a difference of 360^0 between firing of the relevant cylinders, and consequently, the combined source pressures of the right-side cylinders and the left-side cylinders are equal in magnitude. The equivalent source characteristics of all six cylinders combined are shown in Figs. 4.8 and 4.9. The source impedance of the right side and the left side cylinders are in parallel combination, and that is why the equivalent source impedance downstream of the manifold for harmonics of speed order is half of the value of each side, as can be observed from Figs. 4.6 and 4.8. The source pressure values of each side of cylinders are out of phase for the odd harmonics but in phase with each other for the even harmonics of the 0.5 speed order. Thus, the equivalent source pressure values at the odd harmonics of the 0.5 speed order are negligible compared to the even harmonics. Therefore, the SSL spectrum in Fig. 4.8 contains only the even harmonics of the 0.5 speed order. The foregoing discussion can be appreciated using Eq. (4.17). The value of combined source pressure for all even harmonics is same as that of the one-side cylinders combined. This is evident from Figs. 4.7 and 4.9, and can be appreciated using Eq. (D.3) of Appendix D. It can also be noted from Fig. 4.8 that up to speed order 12, dominant peaks are at the multiples of speed order 3 (the speed order corresponding to the engine firing frequency).

4.2.3 Acoustic source characteristics of the engine downstream of the turbine

The source characteristics downstream of the exhaust manifold (i.e. upstream of the turbine) are then transferred downstream of the turbine (section td-td). These are shown in Figs. 4.10 and 4.11. Significantly, comparison of Figs. 4.9 and 4.11 shows a reduction in source strength level of about 7 dB due to the turbine in the entire frequency range. Incidentally, this reduction of 7 dB is in concurrence with the TL spectrum of the turbine of an automotive turbocharger shown in Fig. 2 of Ref. [45] for the engine running at 1500 RPM.

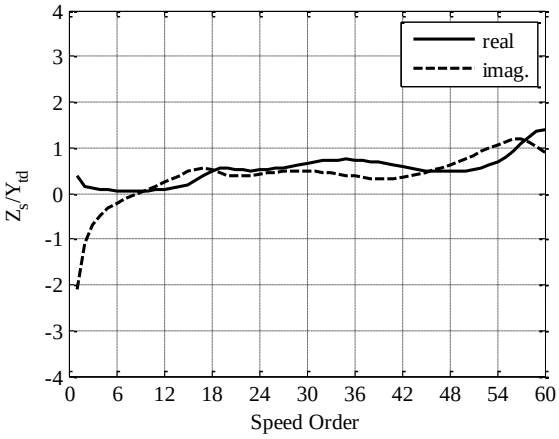

Figure 4.10. Normalized source impedance (with respect to the characteristic impedance of the turbine downstream pipe) of combination of all six cylinders downstream of turbine

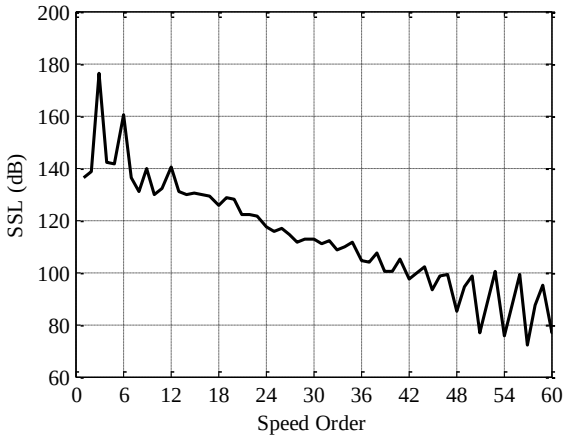

Figure 4.11. Source strength level of combination of all six cylinders downstream of turbine

4.3 Experimental validation of the estimated source characteristics

The SPL spectra predicted with and without acoustic modelling of the turbine and their comparison with the measured SPL spectrum are shown in Fig. 4.12. The casing noise (shown in Fig. 3.22) coming outside the acoustic enclosure is added to the unmuffled SPL spectrum as done in Chapter 3, and it is significant only up to speed order 2.

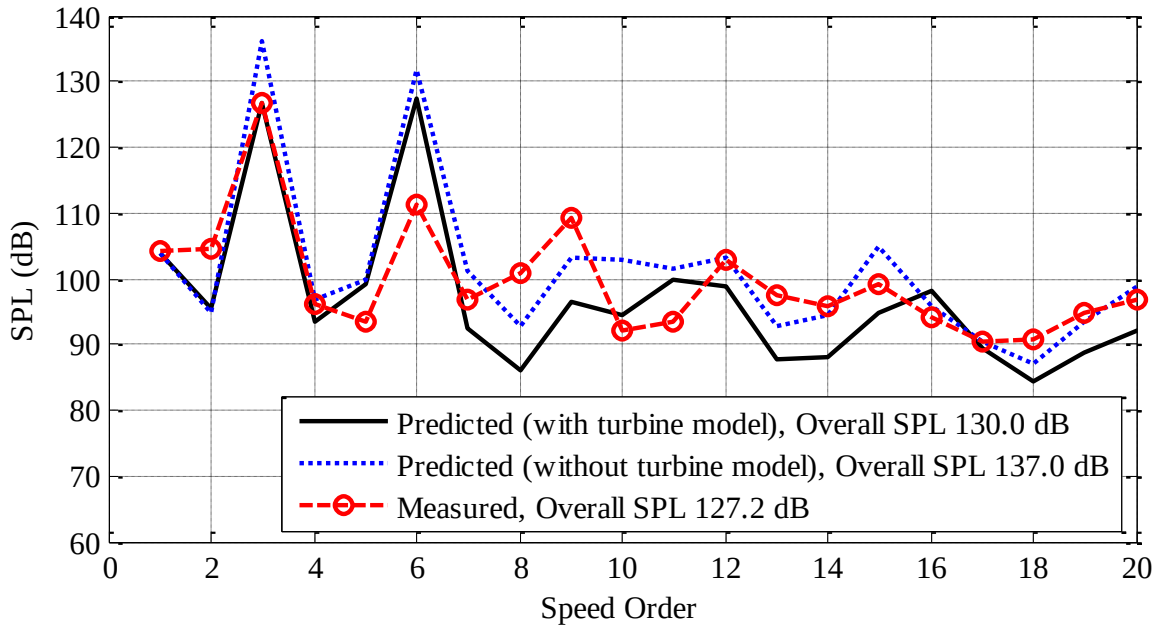

Figure 4.12. Comparison of the predicted and measured values of the unmuffled exhaust sound pressure level of 200 kVA T/C DG-Set engine.

The maximum difference in SPL values at low speed orders is observed at the speed order of 6. However, the turbine model proposed here has been able to reduce the difference in SPL from 21 dB to 14 dB at speed order 6. 14 dB difference is too high, but in view of the strong nonlinearity and time variance of the source, the difference is reasonable. One probable cause of such difference may be the neglect of wave propagation inside the turbine. However, one must accept such kind of differences because this study implicitly presumes that the source is linear and time-invariant, whereas an IC engine source is neither linear nor time-invariant.

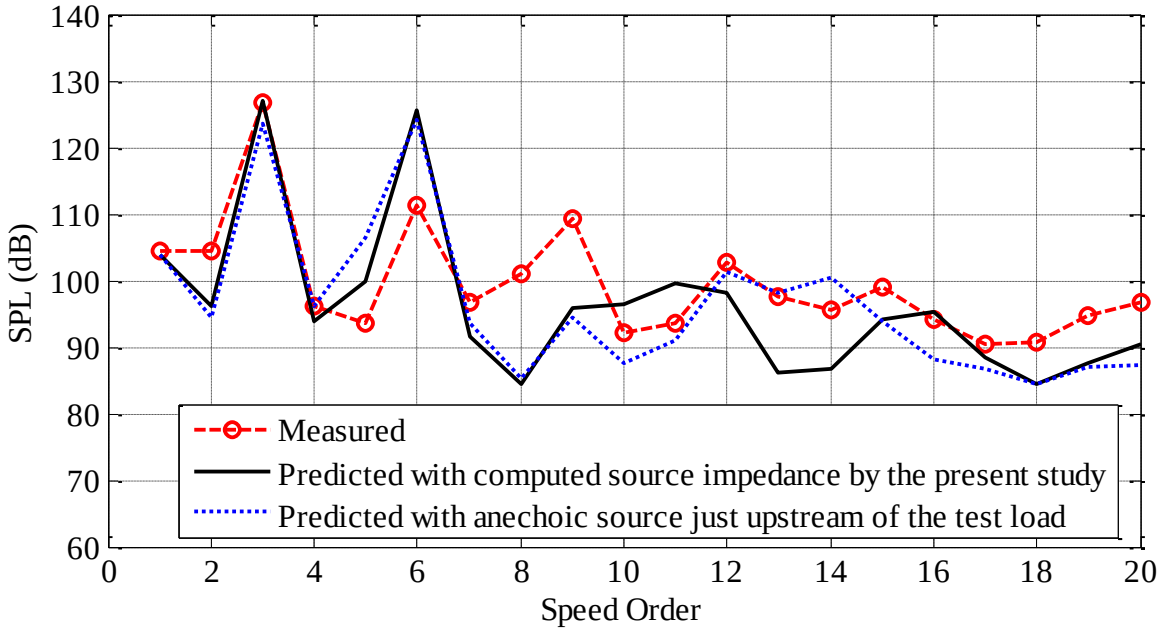

Figure 4.13. Effect of source impedance on prediction of unmuffled exhaust SPL spectrum of 200 kVA DG-Set engine (source pressure, however, is the computed values in both the cases)

It can be observed from Fig. 4.13 that the assumption of anechoic source just upstream of the acoustic test load is a good approximation to predict the unmuffled exhaust SPL spectrum. Therefore, in the case of unavailability of the measured source impedance or the estimated source impedance by the present method, anechoic source can be assumed to predict the unmuffled exhaust SPL spectrum of multi-cylinder turbocharged engines and the IL spectrum of mufflers applied on the multi-cylinder turbocharged engines.

4.4 Conclusion

The direct evaluation method developed in Chapters 2 and 3 for the naturally aspirated engines is extended in this chapter for estimation of the acoustic source characteristics of a turbocharged diesel engine using the derived transfer matrix of a turbine, which is modelled as

a black box wherein the isentropic expansion takes place. However, such simple analytical expression for the transfer matrix of a turbine is not reported in the literature to the best of Author's knowledge. The source resistance of either one cylinder, or a combination of some cylinders, or the complete engine at any source-load junction is found to be consistently positive. This finding is the biggest merit of the direct evaluation method over the extant indirect methods. The unmuffled SPL spectrum predicted using the estimated source characteristics using the transfer matrix of the turbine derived here tallies reasonably with the measured spectrum. Now, the direct method can be used to predict the unmuffled SPL spectrum and design an appropriate muffler for a turbocharged engine even before the engine is prototyped. In particular, the method described in this paper has the ability to make available the estimated source characteristics data of exhaust system of internal combustion engines for those designers who have no access to commercial internal combustion engine simulation codes. Thus, the design and analysis of engine and muffler can be integrated at the inception stage itself.

Chapter 5

1-D Analysis of a Typical Commercial Muffler of a Motorcycle Engine and 3-D Validation Thereof*

Estimation of the source characteristics of an internal combustion (IC) engine has been illustrated in Chapters 2, 3, and 4. However, the estimated source characteristics can be used to predict the unmuffled/muffled exhaust sound pressure level (SPL) spectrum of an engine and insertion loss (IL) spectrum of a muffler. But, the design and analysis of efficient mufflers are needed to comply with ever increasingly stringent noise regulations. One of most commonly used muffler in many automobile engine exhaust systems is flow-reversal chamber muffler which ensures higher acoustic attenuation in limited space. Muffler designers have used flow reversal chamber mufflers since a long time [67]. Young and Crocker [67] used the finite element method to do acoustic analysis of several flow reversal chamber mufflers because of the limitations of the 1-D transfer matrix approach developed until that time [11].

Double flow-reversal mufflers with holes (one or two generally) in baffles are the common type of mufflers that are applied in an exhaust system of small capacity motorcycle engines. The holes in baffles make all chambers of the muffler proper multiply-connected for flow as well as acoustics. The 1-D integrated transfer matrix (ITM) approach is used for the acoustic analysis of a complex double flow-reversal perforated-element muffler of a single-cylinder motorcycle engine. In the 3-D analysis as well as the 1-D analysis, the convective effect of mean flow is neglected, but the dissipative effect of mean flow is duly incorporated at the area discontinuities as well as the perforated elements. Transmission loss (TL) spectrum computed using 1-D ITM approach is shown to have good agreement with 3-D computed TL spectrum up to about 1600 Hz which covers the frequency range of interest.

5.1 Flow network analysis

The presence of mean flow in mufflers affects the acoustical transmission properties of a muffler in three ways, namely, the convective effect of mean flow in straight pipe which

* This chapter is generally based on the Author's conference paper presented at 4th Automotive Noise and Vibration Congress held in Pune during 8th–9th November 2017.

changes the wave numbers of the forward and the reflected progressive waves, introduction of aeroacoustic losses at sudden discontinuties, and the change in impedances of perforates due to either grazing flow, bias flow, or a combination of the two [64]. The change in perforate impedances due to the flow in mufflers has a significant effect on its attenuation properties. In order to investigate the effect of the mean flow on muffler's acoustical attenuation characteristics, it is necessary to know the flow distribution through the different paths. In the present study, the flow distribution analysis is carried out with electrical analogy as described by Elnady *et al.* [64] and Munjal *et al*. [97]. Here, the stagnation pressure drop is analogous to voltage drop, the volume flow rate is analogous to electric current, and the flow resistances are analogous to electrical resistances, except that the flow resistance is defined as the stagnation pressure drop across the element divided by square of the volume flow rate through the element.

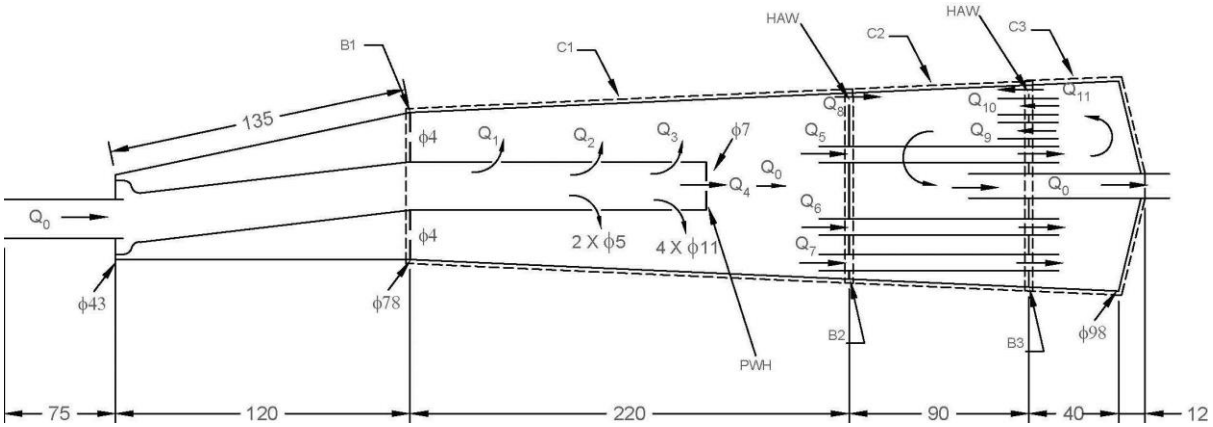

(a)

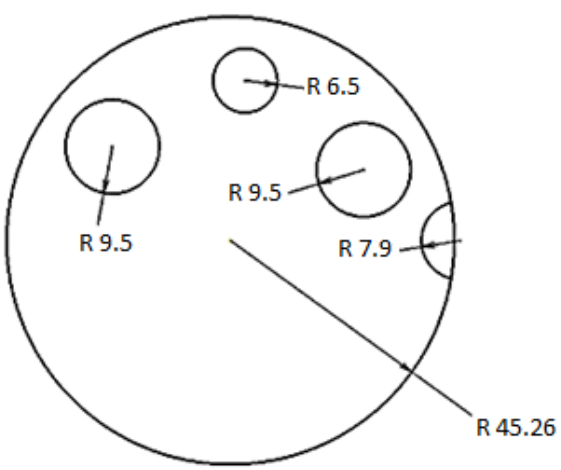

(b)

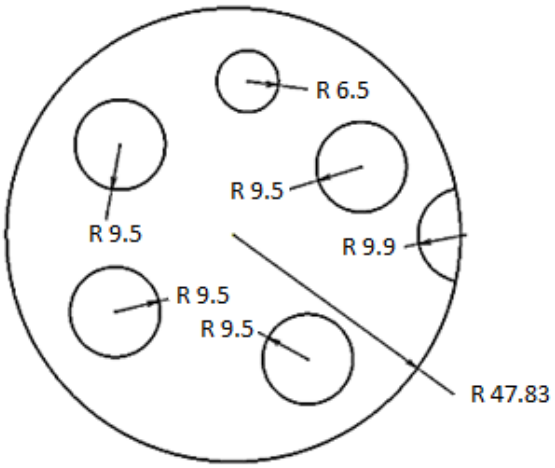

(c)

Figure 5.1. Schematic diagram of the double flow-reversal interacting chambers muffler with salient dimensions in mm (a) Muffler proper with flow distribution through different flow resistances; (b) Baffle 2; and (c) Baffle 3

Schematic diagram of the muffler investigated here is shown in Fig. 5.1. In Fig. 5.1(a), abbreviations PWH and HAW stand for plug with hole, and hole attached with wall of muffler shell, respectively. Abbreviations B1, B2, and B3 represents Baffle 1, Baffle 2 and Baffle 3, respectively. Abbreviations C1, C2, and C3 stand for Chamber 1, Chamber 2 and Chamber 3, respectively.

Figure 5.2 shows the flow network diagram corresponding to the flow-distribution in the muffler of Fig. 5.1, with the volume flow rate Q through different paths. In this muffler, there are two types of flow resistances, namely, the flow losses at the open end, either in the inlet or outlet ducts connected to large volumes, and the losses due to holes in baffles or pipes. Expressions for these two kinds of flow resistances are given by Eqs. (E.1)–(E.3) of Appendix E.

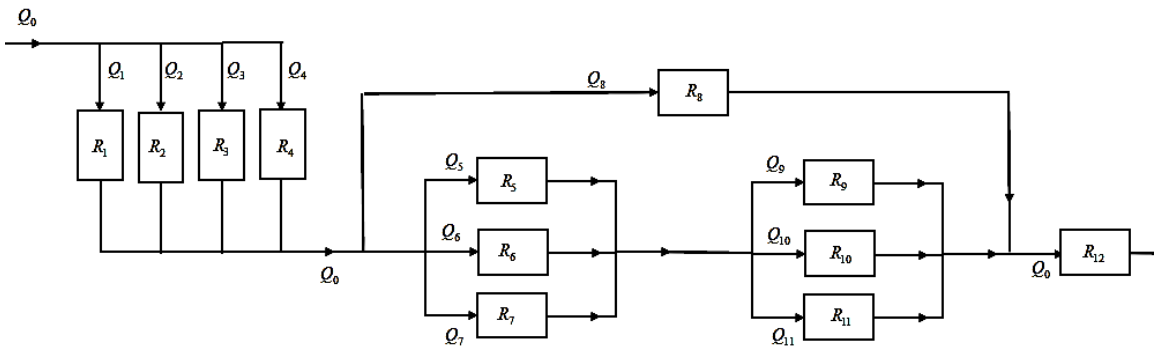

Figure 5.2. Flow network diagram of the muffler

In Fig. 5.2, flow rates Q_1, Q_2, Q_3, Q_4, Q_8 and Q_{11} face only the losses due to holes and flows Q_5, Q_6, Q_7, Q_9 and Q_{10} face flow losses due to open ends of both kinds, inlet and outlet ducts connected to large volumes. The value of flow resistances R_1 to R_{12} calculated by means of Eqs. (E.1)–(E.3) of Appendix E and are given in Table 5.1.

Equivalent resistances of R_1 to R_4, R_5 to R_7 and R_9 to R_{11} are given by

$$R_{1,2,3,4} = \frac{1}{\left(\sum_{i=1}^{4} \sqrt{1/R_i}\right)^2} \tag{5.1}$$

$$R_{5,6,7} = \frac{1}{\left(\sum_{i=5}^{7} \sqrt{1/R_i}\right)^2} \tag{5.2}$$

$$R_{9,10,11} = \frac{1}{\left(\sum_{i=9}^{11} \sqrt{1/R_i}\right)^2} \tag{5.3}$$

The equivalent resistance of the complete network is given by

$$R_{eq} = R_{1,2,3,4} + \frac{1}{\left(\sqrt{1/\left(R_{5,6,7} + R_{9,10,11}\right)} + \sqrt{1/R_8}\right)^2} + R_{12}. \tag{5.4}$$

Table 5.1. Flow resistances

Resistances	R_1	R_2	R_3	R_4	$R_5 / R_9 / R_{10} / R_{12}$	R_6	R_7	R_8	R_{11}
Values (in 10^6 kg/m^7)	727.9	181.9	1.942	189.4	3.351	15.29	3.351	65.41	23.05

The 1-D and 3-D acoustical analysis are carried out on an acoustic source of 100 cc internal combustion engine running at 3120 RPM. The exhaust gas mass flow rate will be the same as the mass flow rate of fresh charge (sucked air) and the fuel burnt. The expression for the volume flow rate of exhaust gas is given by

$$Q_0 = \frac{\rho_a V_d N \eta_v}{120 \rho_{ex}} \left(1 + \frac{F}{A}\right) \tag{5.5}$$

where ρ_a, V_d, N, η_v, ρ_{ex} and F/A are density of ambient air, capacity of cylinder, engine shaft speed in RPM, volumetric efficiency of cylinder, exhaust gas density and fuel-air ratio, respectively. The values of these parameters are, 1.0523 kg/m^3, 10^{-4} m^3, 3120 RPM, 0.95, 0.3592 kg/m^3, and 0.069, respectively. The volume flow rate of exhaust gas turns out to be 0.0077 m^3/s, which gives the flow velocity and Mach number in the tail pipe as 27.3 m/s and 0.047, respectively. Distribution of volume flow through different resistances is given in Table 5.2.

Table 5.2. Flow distribution inside the muffler, in percentage of Q_0

Q_1	Q_2	Q_3	Q_4	Q_5	Q_6	Q_7	Q_8	Q_9	Q_{10}	Q_{11}
4.11	8.22	79.61	8.06	35.79	16.75	35.79	11.66	37.09	37.09	14.14

The flow resistance due to the frictional losses in pipe is not considered in the analysis. Thus, flow rates Q_1 to Q_4 are in parallel and these values are given by

$$Q_i = Q_0\sqrt{R_{1,2,3,4}/R_i}, \quad \text{for } i = 1,2,3, \text{ and } 4 \tag{5.6}$$

Flow rates Q_5 to Q_7 are in parallel and the combination of these again are divided in Q_9 to Q_{11}. Thus, flow rates Q_9 to Q_{11} are in parallel. The combinations Q_5 to Q_7 and Q_9 to Q_{11} are in series and they are in parallel with the flow rate Q_8. The flow rate Q_8 and $Q_0 - Q_8$ are given by

$$Q_8 = Q_0\sqrt{\frac{1}{\left(\sqrt{1/\left(R_{5,6,7}+R_{9,10,11}\right)}+\sqrt{1/R_8}\right)^2}\frac{1}{R_8}} \tag{5.7}$$

$$Q_0 - Q_8 = Q_0\sqrt{\frac{1}{\left(\sqrt{1/\left(R_{5,6,7}+R_{9,10,11}\right)}+\sqrt{1/R_8}\right)^2}\frac{1}{\left(R_{5,6,7}+R_{9,10,11}\right)}} \tag{5.8}$$

Flow rates Q_5 to Q_7 and Q_9 to Q_{11} are given by

$$Q_i = \left(Q_0 - Q_8\right)\sqrt{R_{5,6,7}/R_i}, \quad \text{for } i = 5,6, \text{ and } 7 \tag{5.9}$$

$$Q_i = \left(Q_0 - Q_8\right)\sqrt{R_{9,10,11}/R_i}, \quad \text{for } i = 9,10, \text{ and } 11 \tag{5.10}$$

Total backpressure of the muffler is given by Eq. (5.11) which turns out to be 3.24 kPa.

$$\Delta p = R_{eq}Q_o^2 \tag{5.11}$$

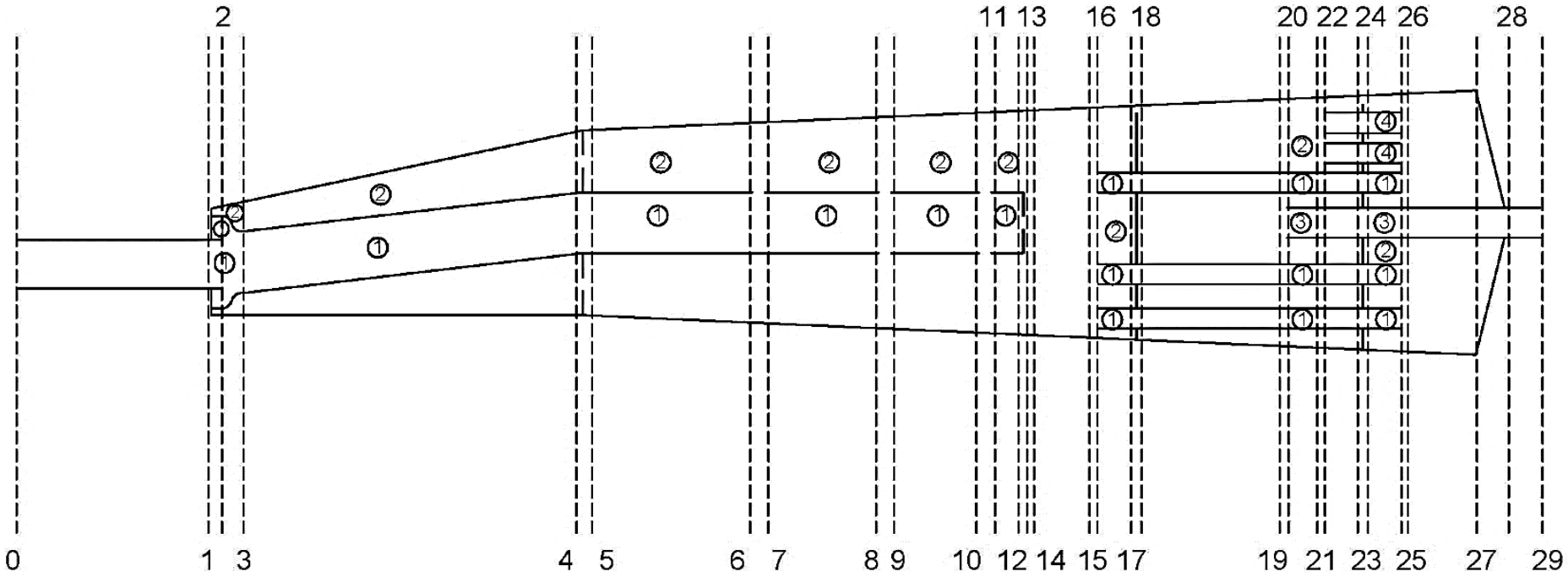

Figure 5.3. Schematic of the muffler with sections and domains used in the 1-D ITM formulation

5.2 Acoustic analysis - Integrated transfer matrix approach

The integrated transfer matrix approach [65] relates the state variables (acoustic pressure and acoustic mass velocity) across the entire cross-section of a muffler shell, as one moves along the upstream section of muffler to downstream section along the axis of muffler and partitioned appropriately in order to relate the state variables of different tubes constituting the cross-section. Division of a muffler into a number of sections depends on the relative changes in the muffler geometry such as sudden area changes, perforated pipes (or may be some concentric hole/s on a pipe), cross baffles or boundaries.

The present muffler is partitioned into 29 sections; the integrated transfer matrix approach is applied from section 3 to section 26 of the muffler of Fig. 5.3. This muffler can be divided in 10 segments from section 3 to 13 with two acoustic elements (domains) in each section, in 3 segments from section 16 to 19 with two acoustic domains, in 1 segment from section 20 to 21 with three acoustic domains, in 3 segments from section 22 to 25 with four acoustic domains, and in two segments from section 26 to 28 with two acoustic domains.

The relation between state variables at section 3 to those at section 13 is given by

$$\begin{bmatrix} \mathrm{S}_{1,3} \\ \mathrm{S}_{2,3} \end{bmatrix} = \begin{bmatrix} [P_{1,3\_4}] & [0]_{2\times2} \\ [0]_{2\times2} & [VP_{2,3\_4}] \end{bmatrix} \begin{bmatrix} [P_{1,4\_5}] & [0]_{2\times2} \\ [0]_{2\times2} & [B_{2,4\_5}] \end{bmatrix} \begin{bmatrix} [P_{1,5\_6}] & [0]_{2\times2} \\ [0]_{2\times2} & [VP_{2,5\_6}] \end{bmatrix}$$
$$[ID_{1,2,6\_7}]_{4\times4} \begin{bmatrix} [P_{1,7\_8}] & [0]_{2\times2} \\ [0]_{2\times2} & [VP_{2,7\_8}] \end{bmatrix} [ID_{1,2,8\_9}]_{4\times4} \begin{bmatrix} [P_{1,9\_10}] & [0]_{2\times2} \\ [0]_{2\times2} & [VP_{2,9\_10}] \end{bmatrix} \tag{5.12}$$
$$[ID_{1,2,10\_11}]_{4\times4} \begin{bmatrix} [P_{1,11\_12}] & [0]_{2\times2} \\ [0]_{2\times2} & [VP_{2,11\_12}] \end{bmatrix} \begin{bmatrix} [B_{1,12\_13}] & [0]_{2\times2} \\ [0]_{2\times2} & [VP_{2,12\_13}] \end{bmatrix} \begin{bmatrix} \mathrm{S}_{1,13} \\ \mathrm{S}_{2,13} \end{bmatrix}$$

where $[S_{i,j}] = [p_{i,j} \quad v_{i,j}]^T$ is the column vector of acoustic state variables of the i^{th} domain at the j^{th} section. P_{i,j_k}, VP_{i,j_k}, and B_{i,j_k} are the 2×2 transfer matrices relating the state variables of the j^{th} section to the k^{th} section of the i^{th} domain of a simple pipe, variable area pipe and baffle with some holes, respectively. ID_{i,j,k_l} is a 4×4 transfer matrix which relates the state variables of the k^{th} section to the l^{th} section of the interacting i^{th} and j^{th} domains. The 4×4 transfer matrix that relates the acoustic state variables at section 3 to those at section 13 is named as matrix [A**]**.

The state variables at sections 13 and 14 are related through the mass and momentum conservation relations.

$$p_{14} = p_{1,13} \tag{5.13}$$

$$p_{14} = p_{2,13} \tag{5.14}$$

$$v_{14} = v_{1,13} + v_{2,13} \tag{5.15}$$

The state variables at section 14 and 15 are related as

$$\begin{bmatrix} p_{14} \\ v_{14} \end{bmatrix} = \left[VP_{c,14\_15} \right]_{2\times 2} \begin{bmatrix} p_{15} \\ v_{15} \end{bmatrix} \tag{5.16}$$

where $VP_{c,14\_15}$ is the transfer matrix which relates the acoustic state variables of section 14 to those of 15 of conical segment. This transfer matrix is named as [B] for short.

The relations between the state variables at section 15 and 16 can be written by applying the mass and momentum conservation relations

$$p_{15} = p_{1,16} \tag{5.17}$$

$$p_{15} = p_{2,16} \tag{5.18}$$

$$v_{15} = v_{1,16} + v_{2,16} \tag{5.19}$$

The transfer matrix relation between the state variables at section 16 to section 19 is given by

$$\begin{bmatrix} \mathrm{S}_{1,16} \\ \mathrm{S}_{2,16} \end{bmatrix} = \begin{bmatrix} \left[P_{1,16\_17} \right] & [0]_{2\times 2} \\ [0]_{2\times 2} & \left[VP_{2,16\_17} \right] \end{bmatrix} \begin{bmatrix} \left[P_{1,17\_18} \right] & [0]_{2\times 2} \\ [0]_{2\times 2} & \left[B_{2,17\_18} \right] \end{bmatrix} \begin{bmatrix} \left[P_{1,18\_19} \right] & [0]_{2\times 2} \\ [0]_{2\times 2} & \left[VP_{2,18\_19} \right] \end{bmatrix} \begin{bmatrix} \mathrm{S}_{1,19} \\ \mathrm{S}_{2,19} \end{bmatrix} \tag{5.20}$$

The 4×4 transfer matrix that relates the acoustic state variables at section 16 to those at section 19 is termed here as matrix [C].

The relation between the state variables at section 19 and 20 can be written by applying the mass and momentum conservation relations

$$p_{1,19} = p_{1,20} \tag{5.21}$$

$$v_{1,19} = v_{1,20} \tag{5.22}$$

$$p_{2,19} = p_{2,20} \tag{5.23}$$

$$p_{2,19} = p_{3,20} \tag{5.24}$$

$$v_{2,19} = v_{2,20} + v_{3,20} \tag{5.25}$$

The matrix relation between the state variables at section 20 and 21 of domains 1 and 2 is given by

$$\begin{bmatrix} \mathrm{S}_{1,20} \\ \mathrm{S}_{2,20} \end{bmatrix} = \begin{bmatrix} [P_{1,20\_21}] & [0]_{2\times2} \\ [0]_{2\times2} & [VP_{2,20\_21}] \end{bmatrix} \begin{bmatrix} \mathrm{S}_{1,21} \\ \mathrm{S}_{2,21} \end{bmatrix} \tag{5.26}$$

The 4×4 transfer matrix that relates the acoustic state variables at section 20 to those at section 21 is termed here as matrix [D].

The relation between the state variables at section 21 and 22 for domains 1 and 2 can be written by applying the mass and momentum conservation relations

$$p_{1,21} = p_{1,22} \tag{5.27}$$

$$v_{1,21} = v_{1,22} \tag{5.28}$$

$$p_{2,21} = p_{2,22} \tag{5.29}$$

$$p_{2,21} = p_{4,22} \tag{5.30}$$

$$v_{2,21} = v_{2,22} + v_{4,22} \tag{5.31}$$

The relation between the state variables between sections 22 and 25 of domains 1, 2 and 4 is given by

$$\begin{bmatrix} \mathrm{S}_{1,22} \\ \mathrm{S}_{2,22} \\ \mathrm{S}_{4,22} \end{bmatrix} = \begin{bmatrix} \left[P_{1,22\_23}\right] & [0]_{2\times2} & [0]_{2\times2} \\ [0]_{2\times2} & \left[VP_{2,22\_23}\right] & [0]_{2\times2} \\ [0]_{2\times2} & [0]_{2\times2} & \left[P_{4,22\_23}\right] \end{bmatrix} \begin{bmatrix} \left[P_{1,23\_24}\right] & [0]_{2\times2} & [0]_{2\times2} \\ [0]_{2\times2} & \left[B_{2,23\_24}\right] & [0]_{2\times2} \\ [0]_{2\times2} & [0]_{2\times2} & \left[P_{4,23\_24}\right] \end{bmatrix} \begin{bmatrix} \left[P_{1,24\_25}\right] & [0]_{2\times2} & [0]_{2\times2} \\ [0]_{2\times2} & \left[VP_{2,24\_25}\right] & [0]_{2\times2} \\ [0]_{2\times2} & [0]_{2\times2} & \left[P_{4,24\_25}\right] \end{bmatrix} \begin{bmatrix} \mathrm{S}_{1,25} \\ \mathrm{S}_{2,25} \\ \mathrm{S}_{4,25} \end{bmatrix} \tag{5.32}$$

The 6×6 transfer matrix that relates the state variables at section 22 to those at section 25 of domains 1, 2 and 4 is termed here as matrix [E].

The relation between the state variables at sections 25 and 26 for domains 1, 2 and 4 can be written by applying the mass and momentum conservation relations

$$p_{26} = p_{1,25} \tag{5.33}$$

$$p_{26} = p_{2,25} \tag{5.34}$$

$$p_{26} = p_{4,25} \tag{5.35}$$

$$v_{26} = v_{1,25} + v_{2,25} + v_{4,25} \tag{5.36}$$

The transfer matrix relation between sections 1 and 3 for domain 2 is given by

$$\begin{bmatrix} p_{2,3} \\ v_{2,3} \end{bmatrix} = \left[VP_{2,3\_2}\right]_{2\times2} \left[VP_{2,2\_1}\right]_{2\times2} \begin{bmatrix} p_{2,1} \\ v_{2,1} \end{bmatrix} \tag{5.37}$$

The 2×2 transfer matrix that relates the acoustic state variables at section 3 to those at section 1 of the end chamber is termed as matrix $VP_{2,3\_1}$.

Since acoustic mass velocity in domain 2 at section 1 is zero, the relation between $p_{2,3}$ and $v_{2,3}$ is given by

$$Z_L = \frac{p_{2,3}}{v_{2,3}} = \frac{VP_{2,3\_2}(1,1)}{VP_{2,3\_2}(2,1)} \tag{5.38}$$

Transfer matrix relation between sections 26 to 27 for annular domain is given by

$$\begin{bmatrix} p_{26} \\ v_{26} \end{bmatrix} = \left[VP_{26\_27}\right]_{2\times2}\left[VP_{27\_28}\right]_{2\times2}\begin{bmatrix} p_{28} \\ v_{28} \end{bmatrix} \tag{5.39}$$

The 2×2 transfer matrix that relates the acoustic state variables at section 26 to those at section 28 of the end chamber is termed as matrix VP_{26_28}.

Acoustic mass velocity at section 28 for annular domain is zero. Therefore, the relation between p_{26} and v_{26} is given by

$$Z_R = \frac{p_{26}}{v_{26}} = \frac{VP_{26\_28}(1,1)}{VP_{26\_28}(2,1)} \tag{5.40}$$

The transfer matrix relation for acoustic state variables at section 20 to those at section 29 of the tail pipe is given by

$$\begin{bmatrix} p_{3,20} \\ v_{3,20} \end{bmatrix} = \left[P_{3,20\_29}\right]_{2\times2}\begin{bmatrix} p_{29} \\ v_{29} \end{bmatrix} \tag{5.41}$$

The transfer matrix relation for the acoustic state variables at section 0 to those at section 3 of exhaust pipe is given by

$$\begin{bmatrix} p_0 \\ v_0 \end{bmatrix} = \left[P_{0\_1}\right]_{2\times2}\left[P_{1,1\_2}\right]_{2\times2}\begin{bmatrix} 1 & 0 \\ 1/Z & 1 \end{bmatrix}\left[VP_{1,2\_3}\right]_{2\times2}\begin{bmatrix} p_{1,3} \\ v_{1,3} \end{bmatrix} \tag{5.42}$$

where Z is the impedance of a small cavity (excluding the exhaust pipe between sections 1 to 2) in the annular section of domain 1 that is obtained by the similar procedure as applied to obtain Z_L above.

The overall transfer matrix of the muffler relates the acoustic state variables at section 0 of exhaust pipe to those at section 29 of tail pipe. This overall transfer matrix can be obtained by knowing the relation between the state variables $[p_{1,3} \quad v_{1,3}]^T$ and $[p_{3,20} \quad v_{3,20}]^T$ that is given by a 2×2 transfer matrix termed as [T]. Thus,

$$\begin{bmatrix} p_0 \\ v_0 \end{bmatrix} = \left[P_{0\_1}\right]_{2\times2}\left[P_{1,1\_2}\right]_{2\times2}\begin{bmatrix} 1 & 0 \\ 1/Z & 1 \end{bmatrix}\left[VP_{1,2\_3}\right]_{2\times2}[T]_{2\times2}\left[P_{3,20\_29}\right]_{2\times2}\begin{bmatrix} p_{29} \\ v_{29} \end{bmatrix} \tag{5.43}$$

$$\left[\tilde{A}\right]\left\{\tilde{x}\right\}=\left\{\tilde{b}\right\}$$

$$\tilde{x}(1:10,1)=\left[\begin{array}{cccccccccc} p_{2,3} & v_{2,3} & p_{1,13} & v_{1,13} & p_{2,13} & v_{2,13} & p_{14} & v_{14} & p_{15} & v_{15}\end{array}\right]^T$$

$$\tilde{x}(11:20,1)=\left[\begin{array}{cccccccccc} p_{1,16} & v_{1,16} & p_{2,16} & v_{2,16} & p_{1,19} & v_{1,19} & p_{2,19} & v_{2,19} & p_{1,20} & v_{1,20}\end{array}\right]^T$$

$$\tilde{x}(21:30,1)=\left[\begin{array}{cccccccccc} p_{2,20} & v_{2,20} & p_{3,20} & v_{3,20} & p_{1,21} & v_{1,21} & p_{2,21} & v_{2,21} & p_{1,22} & v_{1,22}\end{array}\right]^T$$

$$\tilde{x}(31:42,1)=\left[\begin{array}{cccccccccccc} p_{2,22} & v_{2,22} & p_{4,22} & v_{4,22} & p_{1,25} & v_{1,25} & p_{2,25} & v_{2,25} & p_{4,25} & v_{4,25} & p_{26} & v_{26}\end{array}\right]^T$$

$$\tilde{b}(1:2,1)=\left[\begin{array}{cc} p_{1,3} & v_{1,3}\end{array}\right]^T,\tilde{b}(3:42,1)=zeros(40,1)$$

$$\tilde{A}(1:4,3:6)=A,\tilde{A}(3:4,1:2)=-eye(2)$$

$$\tilde{A}(5,1)=-1,\tilde{A}(5,2)=Z_L$$

$$\tilde{A}(6,3)=1,\tilde{A}(6,7)=-1$$

$$\tilde{A}(7,5)=1,\tilde{A}(7,7)=-1$$

$$\tilde{A}(8,4)=1,\tilde{A}(8,6)=1,\tilde{A}(8,8)=-1$$

$$\tilde{A}(9:10,7:8)=eye(2),\tilde{A}(9:10,9:10)=-B$$

$$\tilde{A}(11,9)=1,\tilde{A}(11,11)=-1$$

$$\tilde{A}(12,9)=1,\tilde{A}(12,13)=-1$$

$$\tilde{A}(13,10)=-1,\tilde{A}(13,12)=1,\tilde{A}(13,14)=1$$

$$\tilde{A}(14:17,11:14)=eye(4),\tilde{A}(14:17,15:18)=-C$$

$$\tilde{A}(18,15)=1,\tilde{A}(18,19)=-1$$

$$\tilde{A}(19,16)=1,\tilde{A}(19,20)=-1$$

$$\tilde{A}(20,17)=1,\tilde{A}(20,21)=-1$$

$$\tilde{A}(21,17)=1,\tilde{A}(21,23)=-1$$

$$\tilde{A}(22,18)=-1,\tilde{A}(22,22)=1,\tilde{A}(22,24)=1$$

$$\tilde{A}(23:26,19:22)=eye(4),\tilde{A}(23:26,25:28)=-D$$

$$\tilde{A}(27,25)=1,\tilde{A}(27,29)=-1$$

$$\tilde{A}(28,26)=1,\tilde{A}(28,30)=-1$$

$$\tilde{A}(29,27)=1,\tilde{A}(29,31)=-1$$

$$\tilde{A}(30,27)=1,\tilde{A}(30,33)=-1$$

$$\tilde{A}(31,28)=-1,\tilde{A}(31,32)=-1,\tilde{A}(31,34)=1$$

$$\tilde{A}(32:37,29:34)=eye(6),\tilde{A}(32:37,35:40)=-E$$

$$\tilde{A}(38,35)=1,\tilde{A}(38,41)=-1$$

$$\tilde{A}(39,37)=1,\tilde{A}(39,41)=-1 \qquad (5.44)$$

$$\tilde{A}(40,39)=1,\tilde{A}(40,41)=-1$$

$$\tilde{A}(41,36)=1,\tilde{A}(41,38)=1,\tilde{A}(41,40)=1,\tilde{A}(41,42)=-1$$

$$\tilde{A}(42,41)=-1,\tilde{A}(42,42)=Z_R$$

The aforementioned transfer matrix [T] can be obtained by solving simultaneously the 42 linear system of equations (Eqs. (5.12)–(5.36), (5.38), and (5.40)) involving 44 variables. This system of equations in a matrix form is given by Eq. (5.44). Because of the bigger size of the matrix equation it has been given in standard notation of linear system of equations and practices to define an element and submatrix in MATLAB. Inverse of the 42×42 coefficient matrix of Eq. (5.44) is named as matrix [F]. The relation between the state variables $[p_{1,3} \quad v_{1,3}]^T$ and $[p_{3,20} \quad v_{3,20}]^T$ is given by

$$\begin{bmatrix} p_{1,3} \\ v_{1,3} \end{bmatrix} = \begin{bmatrix} F_{23,1} & F_{23,2} \\ F_{24,1} & F_{24,2} \end{bmatrix}_{2\times 2} \begin{bmatrix} p_{3,20} \\ v_{3,20} \end{bmatrix} \equiv [T] \begin{bmatrix} p_{3,20} \\ v_{3,20} \end{bmatrix} \tag{5.45}$$

The overall transfer matrix of muffler, which relates the upstream acoustic state variables to the downstream state variables is obtained. This overall transfer matrix is used for computing the transmission loss of the muffler proper. The overall transfer matrix in Eq. (5.43) is named [TM].

Expression for transmission loss (TL) of muffler is given by

$$TL = 20\log_{10}\left[\frac{1+M_{ep}}{1+M_{tp}}\left(\frac{Y_{tp}}{Y_{ep}}\right)^{1/2}\left|\frac{TM_{11}+TM_{12}/Y_{tp}+Y_{ep}TM_{21}+\left(Y_{ep}/Y_{tp}\right)TM_{22}}{2}\right|\right], \quad \text{(dB)} \tag{5.46}$$

where $Y_{tp} = c_0/S_{tp}$ and $Y_{ep} = c_0/S_{ep}$ are characteristic impedances of tail pipe and exhaust pipe, respectively. Symbols M_{ep} and M_{tp} denote the mean flow Mach numbers in the exhaust pipe and tail pipe, respectively.

5.3 3-D FEM validation of the 1-D ITM acoustic analysis

The tetrahedron elements of mesh size 2.5 mm is used except from section 2 to section 3 in the annular region (domain 2 of Fig. 5.3) where the mesh size is 1 mm.

The 3-D analysis of muffler is done for with and without mean flow cases for exhaust gas of density 0.3592 kg/m^3 at 600^0 C. In this section, the validation of 1-D ITM approach plane wave analysis is done by comparing the results of transmission loss computed by the 3-D FEM analysis. Figure 5.4 shows this comparison for the stationary medium and Fig. 5.5 for the moving medium.

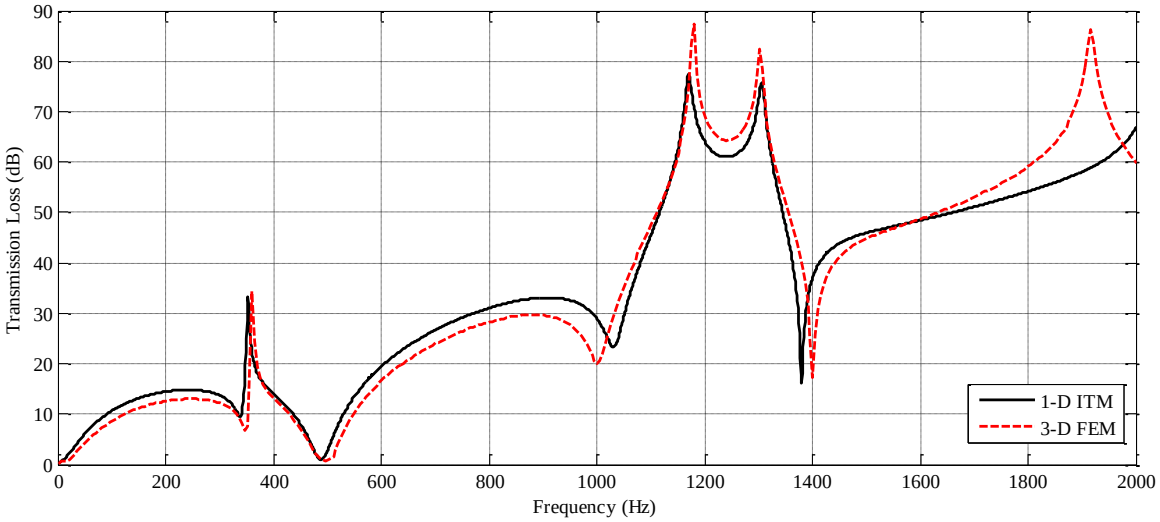

Figure 5.4. Comparison of TL spectrum of the muffler proper for exhaust gas medium without mean flow

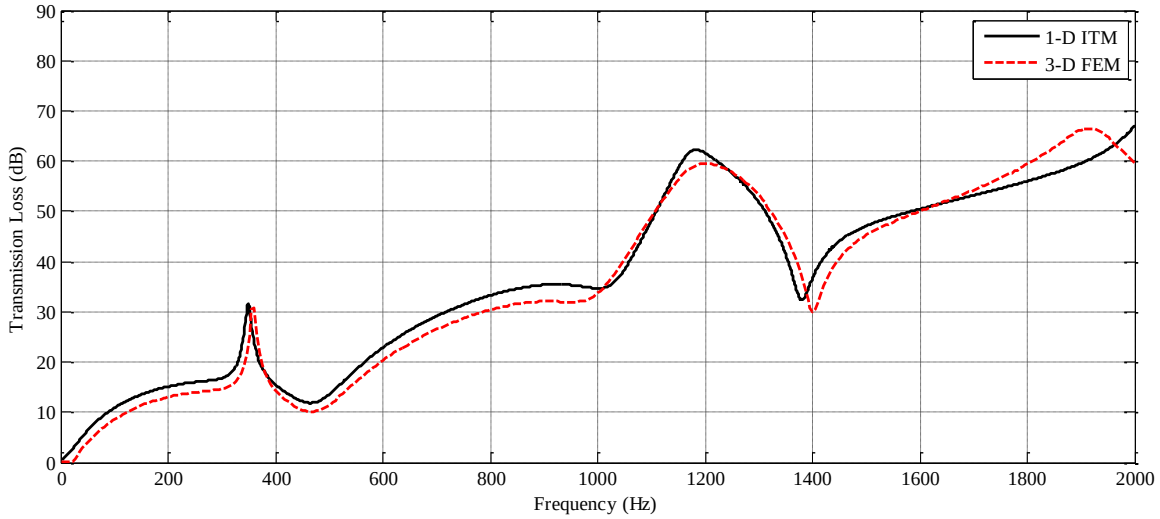

Figure 5.5. Comparison of TL spectrum of the muffler proper for exhaust gas medium with mean flow

Figures 5.4 and 5.5 show that the transmission loss computed by the 1-D ITM approach tallies well with the 3-D FEM values up to 1600 Hz. However, the cut-off frequency for the maximum diameter of muffler is 3476 Hz for exhaust gas medium. This indicates that the cut-on of the higher-order evanescent modes at much lower frequencies as well as the wave propagation in the outlet end chamber is not in the axial direction only. Nevertheless, the 1-D analysis is adequate for the engine exhaust noise analysis because most of the noise would occur at the firing frequency and a few harmonics thereof.

The first peak in the TL spectrum, with and without mean flow, is due to the cavity of annulus (domain 2) between sections 1 and 4. In this domain, flow does not enter and that is

why the first peak is still present in the TL spectrum of muffler with mean flow. All the other peaks and troughs flatten out due to the presence of mean flow, which introduces aeroacoustic resistances because of the bias flow through the holes.

IL spectrum of the muffler shown in Fig. 5.1 is computed with 0.6 *m* long exhaust pipe of 24 *mm* diameter. Figure 5.6 shows the IL spectrum of the muffler with respect to 1 *m* long reference pipe of 24 *mm* diameter computed by the 1-D ITM approach. It is evident from Fig. 5.6 that the IL spectra computed using the parametric expression developed in Chapter 2 and that assuming anechoic source compare well. Therefore, in the case of unavailability of the measured source impedance or the estimated source impedance by the present method, anechoic source can be assumed to predict the IL spectrum of mufflers.

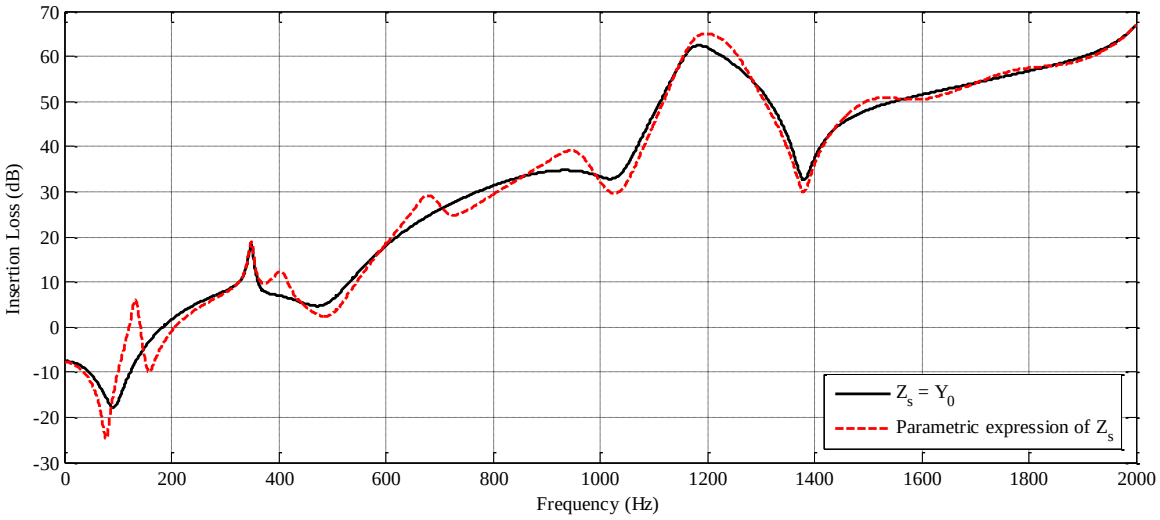

Figure 5.6. Effect of source impedance on predicted IL spectrum of the muffler with respect to 1 *m* long reference pipe of 24 *mm* diameter

5.4 Conclusion

The 1-D plane wave analysis of a double flow-reversal commercial motorcycle engine muffler is done by the ITM (integrated transfer matrix) approach in this chapter. The TL spectrum of the muffler computed by means of 1-D analysis with and without mean flow cases are compared with the 3-D FEA computed spectrum. It is shown that the 1-D plane wave analysis is good enough to do analysis of these kinds of mufflers by designers for evaluation of its acoustical attenuation performances. Holes in baffles and on pipes improve the performance of muffler in the presence of mean flow by lifting the troughs due to the bias flow through the holes. It is a reconfirmation of something that has been known vaguely for some time, and has been used in the next chapter in order to design small muffler for adequate IL.

Chapter 6

Crucial Role of Mean Flow in the Design of MCCA Perforated Element Mufflers*

Overall insertion loss (IL) and total backpressure of a muffler always play a pivotal role in the design of a muffler to reduce an automotive engine's exhaust noise. The flow-reversal interacting chambers (one such muffler is analysed in Chapter 5) have the combined advantage of phase cancellation (popularly known as the Herschel Quincke effect) due to the difference in the time taken by wave propagation through multiple paths and impedance mismatch at every discontinuity [1]. However, at every sudden area discontinuity, there is considerable stagnation pressure drop. Nowadays, the perforated element mufflers are most common for the I.C. engine applications.

The effect of mean flow on the flow-acoustic performance of four different configurations of multiply-connected co-axial (MCCA) mufflers is investigated in this chapter. The present study also shows how an ultra-small muffler can give adequate overall insertion loss (in dBA) with reasonable backpressure. The limit of Mach number in the tail pipe for jet noise is also studied in order to keep jet noise low enough so as not to compromise the overall insertion loss (IL) of a MCCA muffler.

6.1 Flow-acoustic analysis of MCCA mufflers

In this section, four different configurations of the multiply-connected coaxial (MCCA) mufflers have been analysed making use of the 1-D Integrated Transfer Matrix (ITM) approach [1,65]. The 1-D estimates of transmission loss (TL) have been validated against the 3-D Finite Element analysis in the following section.

6.1.1 Single Plug Muffler (C-1)

Figure 6.1 shows the schematic diagram of a single plug muffler along with the detailed drawings of perforated pipes and baffles as well as the distribution of flow in the muffler, and

* This chapter is generally based on the Author's publication in Noise Control Engineering Journal, vol. 65, issue 5, pp. 462–481, 2017.

the division of the muffler proper into a number of sections and domains for application of the integrated transfer matrix (ITM) approach. The flow distribution analysis in the muffler is carried out making use of the lumped flow resistance network shown in Fig. 6.2. Description of the lumped flow resistances and the percentage of total flow, which passes through these resistances, are given in Table 6.1.

Applying the Kirchhoff's loop law for stagnation pressure drop one can write

$$Q_2|Q_2|R_4 + Q_3|Q_3|R_6 - (Q_0 - Q_2)|Q_0 - Q_2|R_5 = 0 \tag{6.1}$$

$$Q_3|Q_3|R_6 - (Q_2 - Q_3)|Q_2 - Q_3|R_7 = 0 \tag{6.2}$$

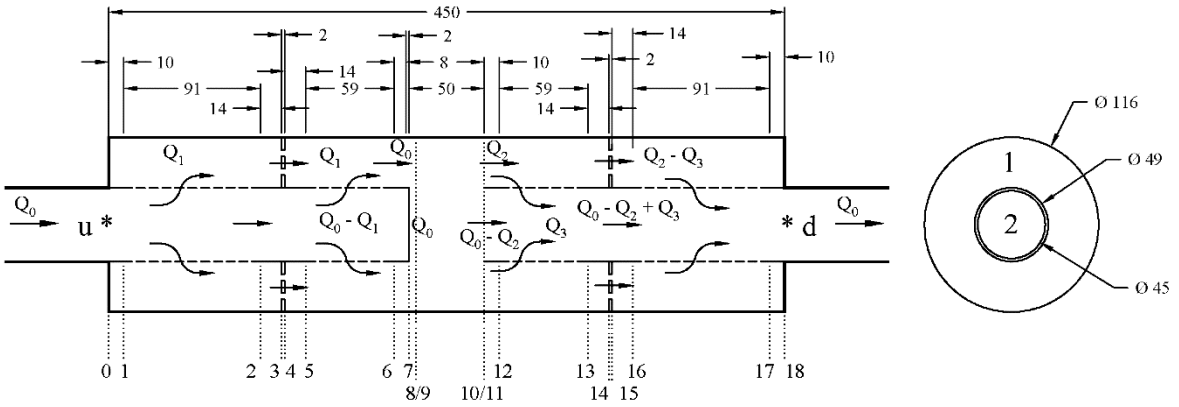

(a)

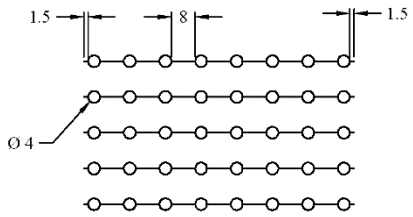

91 mm Perforated Section
Ø 4 Holes, 8 Rows
10 Holes/Row

(b)

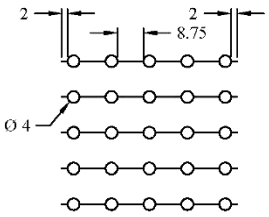

59 mm Perforated Section
Ø 4 Holes, 5 Rows
10 Holes/Row

(c)

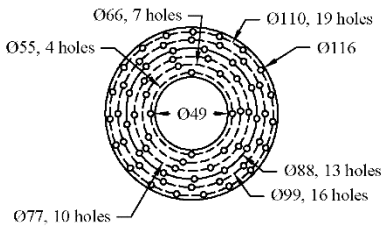

Perforated Baffle

(d)

Figure 6.1. Single plug muffler (C-1) (a) Schematic diagram of the muffler with flow distribution and sections and domains for the ITM application; (b) Details of the 91 mm perforated pipe; (c) The 59 mm perforated pipe; and (d) Perforated baffle

The total value of volume discharge rate of exhaust gas through the muffler by a 3-cylinder, 4-stroke diesel engine of 2.5 litre swept volume, running at 2250 RPM is 0.0758 m^3/s.

Equations (6.1) and (6.2) contain two unknowns, and these are solved simultaneously using the *fsolve* function in MATLAB.

It can be noticed from Table 6.1 that the flow resistances R_1 and R_2 are such that flow gets almost equally distributed through parallel paths. This helps to minimize backpressure. It may be noted from Fig. 6.2 that the total backpressure of the muffler is given by

$$\Delta P = Q_0^2\left(R_0 + R_8\right) + \left(Q_1^2 R_1 + Q_0^2 R_3 + Q_2^2 R_4 + Q_3^2 R_6\right) \tag{6.3}$$

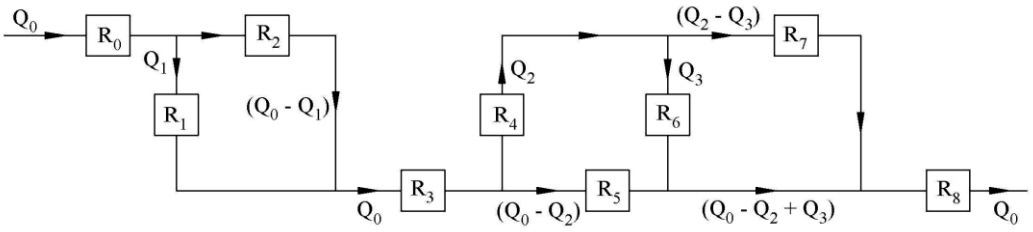

Figure 6.2. Flow-resistance network circuit of the muffler of Fig. 6.1 (C-1)

Table 6.1. Description of flow resistances and flow distribution in C-1

Resistance	Description	Q_i/Q_0(%)
R_0	Flow resistance due to friction in the exhaust pipe before the muffler proper	100
R_1	Cross flow resistance of the LHS perforate of exhaust pipe and the LHS Baffle	51.1
R_2	Cross flow resistance of the RHS perforate of the exhaust pipe	48.9
R_3	Sudden area expansion from annular region in the inlet side to the full chamber	100
R_4	Sudden area contraction from the chamber to annular region in the outlet side	30.1
R_5	Sudden area contraction from the chamber to the tail pipe	69.9
R_6	Cross flow resistance of the LHS perforate of the tail pipe	14.7
R_7	Cross flow resistance of the RHS perforate of tail pipe and the RHS Baffle	15.4
R_8	Flow resistance due to friction in the tail pipe after the muffler proper	100

The first term of the RHS of Eq. (6.3) is the stagnation pressure drop due to the pipe friction in the exhaust pipe and tail pipe, whereas the second term is the stagnation pressure drop due to the different flow resistance elements in the muffler proper. The expressions of flow resistances are given in Appendix E.

The total backpressure for the muffler shown in Fig. 6.1 works out to be 1.57 kPa. The volume flow rates for different elements are used to evaluate the mean flow Mach number needed for evaluation of acoustic impedance of perforates for carrying out the 3-D FEM as well as the 1-D ITM acoustic analysis of mufflers in the presence of mean flow.

Now, the ITM approach is applied for acoustic analysis of the single plug muffler of Fig. 6.1 [1,65]. The acoustic state variables of domains 1 and 2 at section 0 are related to those at section 7 as in Eq. (6.4).

$$\begin{bmatrix}[S_{1,0}]\\ [S_{2,0}]\end{bmatrix}=\begin{bmatrix}[P_{1,0\_1}] & [O]_{2\times2}\\ [O]_{2\times2} & [P_{2,0\_1}]\end{bmatrix}[E_{1,2,1\_2}]\begin{bmatrix}[P_{1,2\_3}] & [O]_{2\times2}\\ [O]_{2\times2} & [P_{2,2\_3}]\end{bmatrix}\begin{bmatrix}[B_{1,3\_4}] & [O]_{2\times2}\\ [O]_{2\times2} & [P_{2,3\_4}]\end{bmatrix} \times\begin{bmatrix}[P_{1,4\_5}] & [O]_{2\times2}\\ [O]_{2\times2} & [P_{2,4\_5}]\end{bmatrix}[E_{1,2,5\_6}]\begin{bmatrix}[P_{1,6\_7}] & [O]_{2\times2}\\ [O]_{2\times2} & [P_{2,6\_7}]\end{bmatrix}\begin{bmatrix}[S_{1,7}]\\ [S_{2,7}]\end{bmatrix} \tag{6.4}$$

Here, represents the acoustic state vector of the i^{th} domain at the j^{th} section. Acoustic state variables $p_{i,j}$ and $v_{i,j}$ are acoustic pressure and acoustic mass velocity, respectively. P_{i,j_k} and B_{i,j_k}, are the transfer matrices of uniform pipe and baffle of the i^{th} domain which relates the state variables of the j^{th} section to the k^{th} section, respectively. Transfer matrix E_{i,j,k_l} relates the state variables of the k^{th} section to the l^{th} section in the i^{th} domain and the j^{th} domain.

The overall transfer matrix, which relates the acoustic state variables of domains 1 and 2 at section 0 to those at section 7, is termed as [A]. The inverse of matrix [A] is termed as [B].

The rigid wall boundary conditions at sections 0 and 7 for domains 1 and 2, respectively, yield

$$v_{1,0}=0 \tag{6.5}$$

$$v_{2,7}=0 \tag{6.6}$$

Now, combining Eqs. (6.4)–(6.6) yields

$$\begin{bmatrix}\bullet & \bullet & \bullet & \bullet & 0 & 0\\ \bullet & [B]_{4\times4} & & \bullet & 0 & 0\\ \bullet & & & \bullet & -1 & 0\\ \bullet & \bullet & \bullet & \bullet & 0 & -1\\ 0 & 1 & 0 & 0 & 0 & 0\\ 0 & 0 & 0 & 0 & 0 & 1\end{bmatrix}\begin{bmatrix}p_{1,0}\\ v_{1,0}\\ p_{2,0}\\ v_{2,0}\\ p_{2,7}\\ v_{2,7}\end{bmatrix}=\begin{bmatrix}p_{1,7}\\ v_{1,7}\\ 0\\ 0\\ 0\\ 0\end{bmatrix} \tag{6.7}$$

The inverse of the 6×6 matrix in Eq. (6.7) is termed as [C]. The acoustic state variables of domain 2 at section 0 are related to those of domain 1 at section 7 as

$$\begin{bmatrix}p_{2,0}\\ v_{2,0}\end{bmatrix}=\begin{bmatrix}C_{31} & C_{32}\\ C_{41} & C_{42}\end{bmatrix}\begin{bmatrix}p_{1,7}\\ v_{1,7}\end{bmatrix} \tag{6.8}$$

State variables of domain 1 at section 7 are related to those at section 10 of the middle chamber of the muffler as

$$\begin{bmatrix} p_{1,7} \\ v_{1,7} \end{bmatrix} = \begin{bmatrix} P_{1,7\_8} \end{bmatrix} \begin{bmatrix} SAE_{8\_9} \end{bmatrix} \begin{bmatrix} P_{c,9\_10} \end{bmatrix} \begin{bmatrix} p_{c,10} \\ v_{c,10} \end{bmatrix} \tag{6.9}$$

where SAE_{i_j} represents the transfer matrix of the sudden area expansion from the i^{th} section to the j^{th} section. The transfer matrix for sudden area discontinuities (expansion as well as contraction) are given in Appendix F.

The relation between the state variables at section 10 of the central chamber and section 11 of domains 1 and 2 is obtained by applying the mass continuity and momentum conservation equations that are given by Eqs. (6.10)–(6.12).

$$p_{c,10} = p_{1,11} \tag{6.10}$$

$$p_{c,10} = p_{2,11} \tag{6.11}$$

$$v_{c,10} = v_{1,11} + v_{2,11} \tag{6.12}$$

The acoustic state variables of domains 1 and 2 at section 11 are related to those at section 18 as

$$\begin{bmatrix} \begin{bmatrix} S_{1,11} \end{bmatrix} \\ \begin{bmatrix} S_{2,11} \end{bmatrix} \end{bmatrix} = \begin{bmatrix} \begin{bmatrix} P_{1,11\_12} \end{bmatrix} & [O]_{2\times2} \\ [O]_{2\times2} & \begin{bmatrix} P_{2,11\_12} \end{bmatrix} \end{bmatrix} \begin{bmatrix} E_{1,2,12\_13} \end{bmatrix} \begin{bmatrix} \begin{bmatrix} P_{1,13\_14} \end{bmatrix} & [O]_{2\times2} \\ [O]_{2\times2} & \begin{bmatrix} P_{2,13\_14} \end{bmatrix} \end{bmatrix} \begin{bmatrix} \begin{bmatrix} B_{1,14\_15} \end{bmatrix} & [O]_{2\times2} \\ [O]_{2\times2} & \begin{bmatrix} P_{2,14\_15} \end{bmatrix} \end{bmatrix} \times \begin{bmatrix} \begin{bmatrix} P_{1,15\_16} \end{bmatrix} & [O]_{2\times2} \\ [O]_{2\times2} & \begin{bmatrix} P_{2,15\_16} \end{bmatrix} \end{bmatrix} \begin{bmatrix} E_{1,2,16\_17} \end{bmatrix} \begin{bmatrix} \begin{bmatrix} P_{1,17\_18} \end{bmatrix} & [O]_{2\times2} \\ [O]_{2\times2} & \begin{bmatrix} P_{2,17\_18} \end{bmatrix} \end{bmatrix} \begin{bmatrix} \begin{bmatrix} S_{1,18} \end{bmatrix} \\ \begin{bmatrix} S_{2,18} \end{bmatrix} \end{bmatrix} \tag{6.13}$$

The overall transfer matrix, which relates the acoustic state variables of domains 1 and 2 at section 11 to those at section 18, is termed as [D]. The inverse of matrix [D] is termed as [E].

Rigid wall boundary condition for domain 1 at section 18 is given by

$$v_{1,18} = 0 \tag{6.14}$$

Now, Eqs. (6.10)–(6.14) are combined in the matrix Eq. (6.15).

$$\begin{bmatrix} 1 & 0 & -1 & 0 & 0 & 0 & 0 & 0 \\ 1 & 0 & 0 & 0 & -1 & 0 & 0 & 0 \\ \bullet & \bullet & \bullet & \bullet & 0 & 0 & -1 & 0 \\ \bullet & & & \bullet & 0 & 0 & 0 & -1 \\ \bullet & [E]_{4\times4} & & \bullet & 0 & 0 & 0 & 0 \\ \bullet & \bullet & \bullet & \bullet & 0 & 0 & 0 & 0 \\ 0 & -1 & 0 & 1 & 0 & 1 & 0 & 0 \\ 0 & 0 & 0 & 0 & 0 & 0 & 0 & 1 \end{bmatrix} \begin{bmatrix} p_{c,10} \\ v_{c,10} \\ p_{1,11} \\ v_{1,11} \\ p_{2,11} \\ v_{2,11} \\ p_{1,18} \\ v_{1,18} \end{bmatrix} = \begin{bmatrix} 0 \\ 0 \\ 0 \\ 0 \\ p_{2,18} \\ v_{2,18} \\ 0 \\ 0 \end{bmatrix} \tag{6.15}$$

The inverse of the 8×8 matrix in Eq. (6.15) is termed as [F]. The relation between acoustic state variables of the middle chamber at section 10 is related to those of domain 2 at section 18 as

$$\begin{bmatrix} p_{c,10} \\ v_{c,10} \end{bmatrix} = \begin{bmatrix} F_{15} & F_{16} \\ F_{25} & F_{26} \end{bmatrix} \begin{bmatrix} p_{2,18} \\ v_{2,18} \end{bmatrix} \tag{6.16}$$

Finally, the overall transfer matrix [T1] between the acoustic state variables at the upstream point and those at the downstream point of the muffler configuration # 1 is obtained by combining Eqs. (6.8), (6.9) and (6.16).

6.1.2 Double-Plug Chamber-Separated Muffler (C-2)

Figure 6.3 shows the schematic diagram of a double-plug chamber-separated muffler for the lumped flow network analysis and the 1-D ITM approach for acoustical analysis. This muffler differs from the single plug muffler by a flow plug on the outlet pipe. The corresponding lumped flow resistance network is shown in Fig. 6.4.

It is apparent from Figs. 6.3 and 6.4 that the pairs of resistances, R_1 and R_2, and R_3 and R_4, are in parallel. Flow distribution among these is computed by equating the stagnation pressure drop along the parallel paths. The total backpressure of the muffler is given by

$$\Delta P = Q_0^2 \left(R_0 + R_6 \right) + \left(Q_1^2 R_1 + Q_0^2 R_3 + Q_2^2 R_4 \right) \tag{6.17}$$

Backpressure for this muffler turns out to be 2.58 kPa, which is approximately 1 kPa more than that of the single plug muffler because of the additional constraint of the second plug.

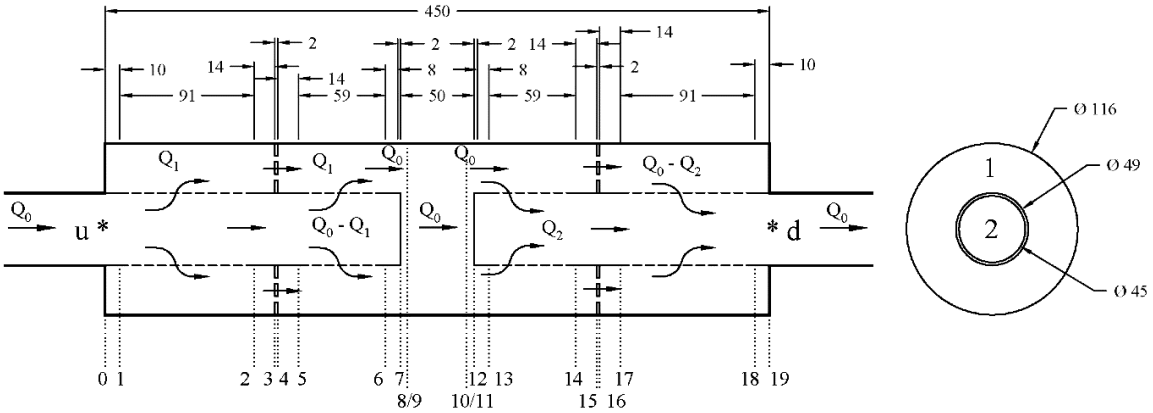

Figure 6.3. Schematic diagram of the double-plug chamber-separated muffler (C-2) with flow distribution and sections and domains for the ITM application

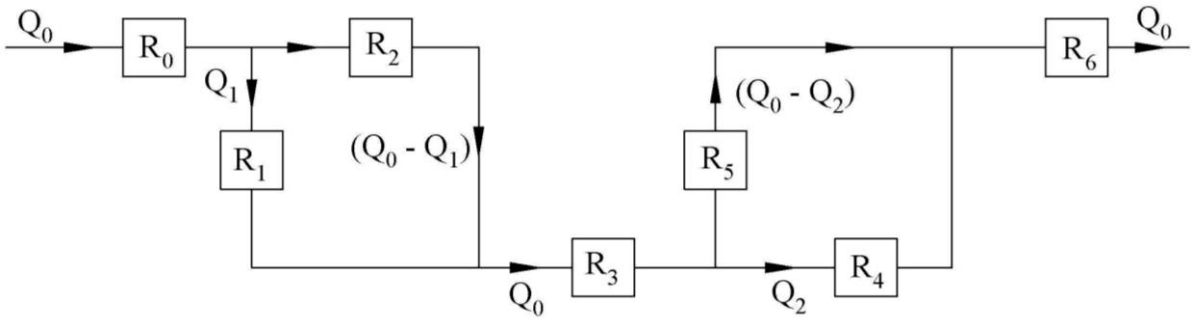

Figure 6.4. Flow-resistance network circuit of the muffler of Fig. 6.3 (C-2)

It can be seen from Fig. 6.3 that the relation between the acoustic state variables of domain 2 at section 0 and those of domain 1 at section 7 are similar to those for the single plug muffler and are governed by Eq. (6.8).

Transfer matrix relation between acoustic state variables of domain 1 at section 7 and those of domain 1 at section 12 is given by

$$\begin{bmatrix} p_{1,7} \\ v_{1,7} \end{bmatrix} = \left[P_{1,7\_8}\right]\left[SAE_{8\_9}\right]\left[P_{c,9\_10}\right]\left[SAC_{10\_11}\right]\left[P_{1,11\_12}\right]\begin{bmatrix} p_{1,12} \\ v_{1,12} \end{bmatrix} \tag{6.18}$$

where SAC_{i_j} represent the transfer matrix of sudden area contraction from the i^{th} section to the j^{th} section. The acoustic state variables of domains 1 and 2 at section 12 are related to those at section 19 as

$$\begin{bmatrix}[S_{1,12}]\\ [S_{2,12}]\end{bmatrix}=\begin{bmatrix}[P_{1,12\_13}] & [O]_{2\times2}\\ [O]_{2\times2} & [P_{2,12\_13}]\end{bmatrix}[E_{1,2,13\_14}]\begin{bmatrix}[P_{1,14\_15}] & [O]_{2\times2}\\ [O]_{2\times2} & [P_{2,14\_15}]\end{bmatrix}\begin{bmatrix}[B_{1,15\_16}] & [O]_{2\times2}\\ [O]_{2\times2} & [P_{2,15\_16}]\end{bmatrix} \times\begin{bmatrix}[P_{1,16\_17}] & [O]_{2\times2}\\ [O]_{2\times2} & [P_{2,16\_17}]\end{bmatrix}[E_{1,2,17\_18}]\begin{bmatrix}[P_{1,18\_19}] & [O]_{2\times2}\\ [O]_{2\times2} & [P_{2,18\_19}]\end{bmatrix}\begin{bmatrix}[S_{1,19}]\\ [S_{2,19}]\end{bmatrix} \tag{6.19}$$

The overall transfer matrix, which relates the acoustic state variables of domains 1 and 2 at section 12 to those at section 19, is termed as [G]. The inverse of matrix G is termed as [H].

The rigid wall boundary conditions at sections 12 and 19 for domains 2 and 1, respectively, yield

$$v_{2,12}=0 \tag{6.20}$$

$$v_{1,19}=0 \tag{6.21}$$

Equations (6.19) to (6.21) are combined in Eq. (6.22).

$$\begin{bmatrix}\bullet & \bullet & \bullet & \bullet & -1 & 0\\ \bullet & & & \bullet & 0 & -1\\ \bullet & [H]_{4\times4} & & \bullet & 0 & 0\\ \bullet & \bullet & \bullet & \bullet & 0 & 0\\ 0 & 0 & 0 & 1 & 0 & 0\\ 0 & 0 & 0 & 0 & 0 & 1\end{bmatrix}\begin{bmatrix}p_{1,12}\\ v_{1,12}\\ p_{2,12}\\ v_{2,12}\\ p_{1,19}\\ v_{1,19}\end{bmatrix}=\begin{bmatrix}0\\ 0\\ p_{2,19}\\ v_{2,19}\\ 0\\ 0\end{bmatrix} \tag{6.22}$$

The inverse of the 6×6 matrix in Eq. (6.22) is termed as [I]. Then acoustic state variables of domain 1 at section 12 would be related to those of domain 2 at section 19 as

$$\begin{bmatrix}p_{1,12}\\ v_{1,12}\end{bmatrix}=\begin{bmatrix}I_{13} & I_{14}\\ I_{23} & I_{24}\end{bmatrix}\begin{bmatrix}p_{2,19}\\ v_{2,19}\end{bmatrix} \tag{6.23}$$

The overall transfer matrix [T2] between the acoustic state variables at the upstream end and the downstream end of the muffler configuration # 2 is obtained by combining Eqs. (6.8), (6.18) and (6.23).

6.1.3 Common Plug Muffler (C-3)

Figure 6.5 shows the schematic diagram of the common plug muffler for the lumped flow resistance network analysis and the 1-D ITM approach for acoustical analysis. The lumped

flow resistance network is shown in Fig. 6.6. The flow distribution in the inlet half and the outlet half of this muffler are the same as those of the muffler shown in Fig. 6.3.

This muffler differs from the double-plug chamber-separated muffler by the fact that the flow coming out from the inlet side annular region does not have sudden contraction followed by sudden expansion. The total backpressure of the muffler is given by

$$\Delta P = Q_0^2 \left(R_0 + R_5 \right) + \left(Q_1^2 R_1 + Q_2^2 R_3 \right) \tag{6.24}$$

The backpressure for this muffler works out to be 2.58 kPa, which is nearly the same as that of the double-plug chamber-separated muffler, because the difference between the cross-sectional area of the entire chamber and the annular region of the muffler shown in Fig. 6.3 is very small.

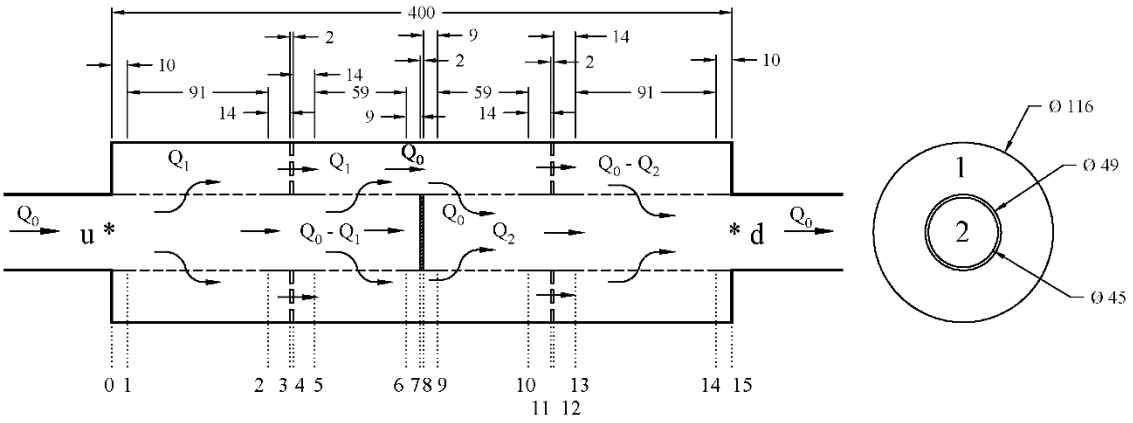

Figure 6.5. Schematic diagram of the common plug muffler (C-3) with flow distribution and sections and domains for ITM application

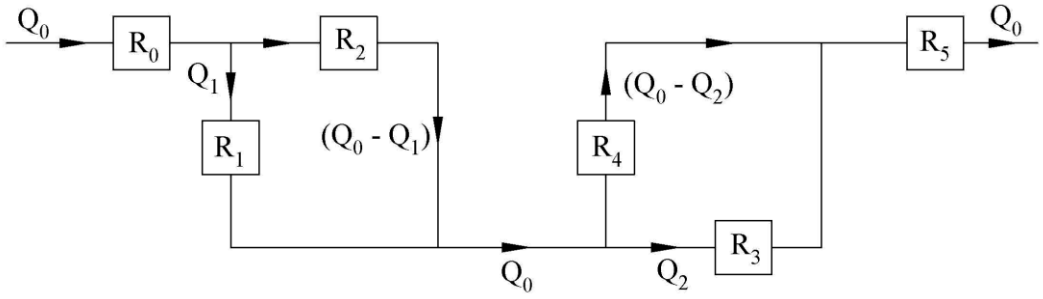

Figure 6.6. Flow-resistance network circuit of the muffler of Fig. 6.5 (C-3)

There are four fewer sections in this muffler as compared to the double-plug chamber-separated muffler of Fig. 6.3 for the ITM analysis. Except the segment between sections 8 and 11 of the muffler shown in Fig. 6.3, everything else is the same in this muffler. Equation (6.8) relates the acoustic state variables of domain 2 at section 0 to those of domain 1 at section 7.

Transfer matrix relating the acoustic state variables of domain 1 at section 7 to those of domain 1 at section 8 is given by

$$\begin{bmatrix} p_{1,7} \\ v_{1,7} \end{bmatrix} = \begin{bmatrix} P_{1,7\_8} \end{bmatrix} \begin{bmatrix} p_{1,8} \\ v_{1,8} \end{bmatrix} \tag{6.25}$$

The sections 12–19 of the double-plug chamber-separated muffler may be replaced by sections 8–15 of this muffler. The acoustic state variables of domain 1 at section 8 can be related to those of domain 2 at section 15 of this muffler as per the procedure followed from Eqs. (6.19)–(6.23) for the corresponding variables of the double-plug chamber-separated muffler (C-2).

The inverse of the 6×6 matrix similar to Eq. (6.22) of this muffler is termed as [J]. The relation between the acoustic state variables of domain 1 at section 8 and those of domain 2 at section 15 is given by

$$\begin{bmatrix} p_{1,8} \\ v_{1,8} \end{bmatrix} = \begin{bmatrix} J_{13} & J_{14} \\ J_{23} & J_{24} \end{bmatrix} \begin{bmatrix} p_{2,15} \\ v_{2,15} \end{bmatrix} \tag{6.26}$$

The overall transfer matrix [T3] between the acoustic state variables at upstream to downstream of the muffler is obtained by combining Eqs. (6.8), (6.25) and (6.26).

6.1.4 Common-Plug Muffler with End Chambers (C-4)

Figure 6.7 shows the schematic diagram of the common-plug muffler with end chambers with detailed drawing of the perforated pipes and baffles as well as the distribution of flow in the muffler, and the division of muffler proper into a number of sections and domains for the application of the integrated transfer matrix approach,

The lumped flow resistance network for the muffler is shown in Fig. 6.8. Description of the lumped flow resistances and the percentage of total flow, which passes through them, are given in Table 6.2.

As per Fig. 6.8, total backpressure of the muffler is given by

$$\Delta P = Q_0^2 \left(R_0 + R_5 \right) + \left(Q_1^2 R_1 + Q_2^2 R_3 \right). \tag{6.27}$$

Now, the ITM approach is applied for acoustic analysis of the intermediate common plug muffler. The acoustic state variables at upstream of the muffler proper are related to those at section 2 of the left end chamber as

$$\begin{bmatrix} p_u \\ v_u \end{bmatrix} = \left[SAE_{0\_1} \right] \left[P_{c,1\_2} \right] \begin{bmatrix} p_{c,2} \\ v_{c,2} \end{bmatrix} \tag{6.28}$$

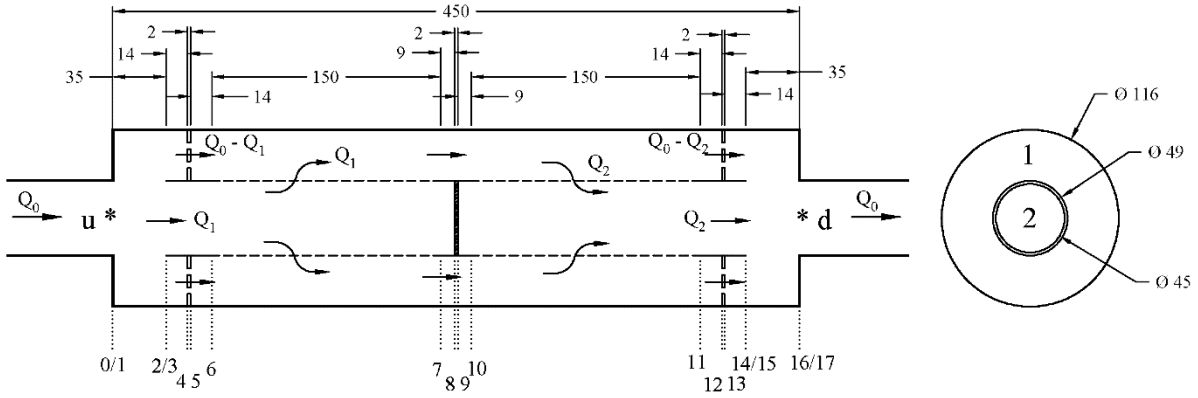

(a)

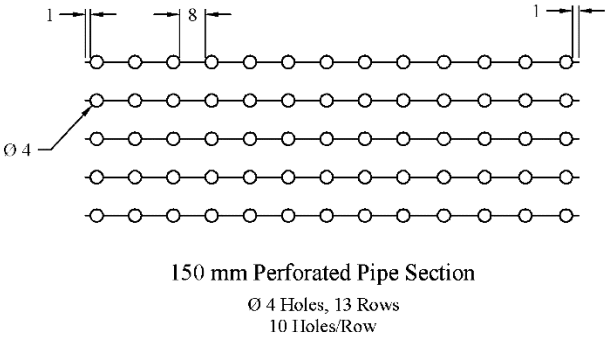

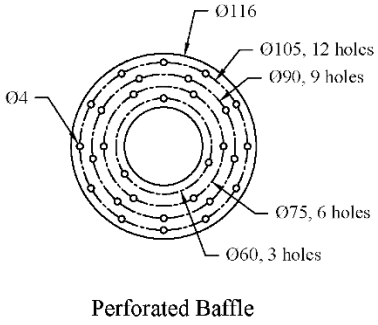

(b) (c)

Figure 6.7. Common-plug muffler with end chambers (C-4) (a) Schematic diagram with flow distribution and sections and domains for the ITM application; (b) Details of the 150 mm perforated pipe; and (c) Details of the perforated Baffle

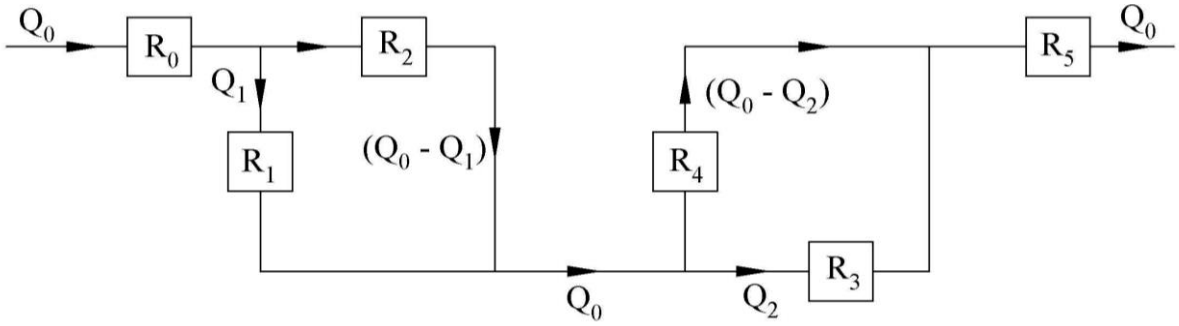

Figure 6.8. Flow-resistance network circuit of the muffler of Fig. 6.7 (C-4)

The relations between the state variables at section 2 of the left end chamber and section 3 of domains 1 and 2 are obtained by applying the mass continuity and momentum conservation equations given by

$$p_{c,2} = p_{1,3} \tag{6.29}$$

$$p_{c,2} = p_{2,3} \tag{6.30}$$

$$v_{c,2} = v_{1,3} + v_{2,3} \tag{6.31}$$

Table 6.2. Description of the flow resistances of C-4 and flow distribution

Resistance	Description	Q_i/Q_0(%)
R_0	Flow resistance due to friction in the exhaust pipe before the muffler proper and sudden expansion from the exhaust pipe to the left end chamber	100
R_1	Cross flow resistance of the perforate of the inner pipe and the sudden contraction from the left end chamber to the inner pipe	79.2
R_2	Cross flow resistance of the LHS baffle and sudden contraction from the end chamber to the annulus	20.8
R_3	Cross flow resistance of the perforate of the inner pipe and the sudden expansion from the inner pipe to the right end chamber	77.9
R_4	Cross flow resistance through the RHS baffle and sudden expansion from annulus to the end chamber	22.1
R_5	Flow resistance due to friction in the tail pipe after the muffler proper and sudden contraction from the right end chamber to the tail pipe	100

The transfer matrix relation between acoustic state variables of domains 1 and 2 at section 3 and those at section 8 is given by

$$\begin{bmatrix} [S_{1,3}] \\ [S_{2,3}] \end{bmatrix} = \begin{bmatrix} [P_{1,3\_4}] & [O]_{2\times2} \\ [O]_{2\times2} & [P_{2,3\_4}] \end{bmatrix} \begin{bmatrix} [B_{1,4\_5}] & [O]_{2\times2} \\ [O]_{2\times2} & [P_{2,4\_5}] \end{bmatrix} \begin{bmatrix} [P_{1,5\_6}] & [O]_{2\times2} \\ [O]_{2\times2} & [P_{2,5\_6}] \end{bmatrix} \times [E_{1,2,6\_7}] \begin{bmatrix} [P_{1,7\_8}] & [O]_{2\times2} \\ [O]_{2\times2} & [P_{2,7\_8}] \end{bmatrix} \begin{bmatrix} [S_{1,8}] \\ [S_{2,8}] \end{bmatrix} \tag{6.32}$$

The overall transfer matrix, which relates the acoustic state variables of domains 1 and 2 at section 3 to those at section 8, is termed as [K]. The inverse of matrix [K] is termed as [L].

Rigid wall boundary condition for domain 2 at section 8 is given by

$$v_{2,8} = 0 \tag{6.33}$$

Now, Eqs. (6.29)–(6.33) are combined in Eq. (6.34):

$$\begin{bmatrix} 1 & 0 & -1 & 0 & 0 & 0 & 0 & 0 \\ 1 & 0 & 0 & 0 & -1 & 0 & 0 & 0 \\ 0 & 0 & \bullet & \bullet & \bullet & \bullet & 0 & 0 \\ 0 & 0 & \bullet & [L]_{4\times4} & & \bullet & 0 & 0 \\ 0 & 0 & \bullet & & & \bullet & -1 & 0 \\ 0 & 0 & \bullet & \bullet & \bullet & \bullet & 0 & -1 \\ 0 & -1 & 0 & 1 & 0 & 1 & 0 & 0 \\ 0 & 0 & 0 & 0 & 0 & 0 & 0 & 1 \end{bmatrix} \begin{bmatrix} p_{c,2} \\ v_{c,2} \\ p_{1,3} \\ v_{1,3} \\ p_{2,3} \\ v_{2,3} \\ p_{2,8} \\ v_{2,8} \end{bmatrix} = \begin{bmatrix} 0 \\ 0 \\ p_{1,8} \\ v_{1,8} \\ 0 \\ 0 \\ 0 \\ 0 \end{bmatrix} \tag{6.34}$$

The inverse of the 8×8 matrix in Eq. (6.34) is termed as [M]. The relation between the acoustic state variables of the left end chamber at section 2 and those of domain 1 at section 8 is given by

$$\begin{bmatrix} p_{c,2} \\ v_{c,2} \end{bmatrix} = \begin{bmatrix} M_{13} & M_{14} \\ M_{23} & M_{24} \end{bmatrix} \begin{bmatrix} p_{1,8} \\ v_{1,8} \end{bmatrix} \tag{6.35}$$

Transfer matrix relation between acoustic state variables of domain 1 at section 8 and domain 1 at section 9 is given by

$$\begin{bmatrix} p_{1,8} \\ v_{1,8} \end{bmatrix} = \begin{bmatrix} P_{1,8\_9} \end{bmatrix} \begin{bmatrix} p_{1,9} \\ v_{1,9} \end{bmatrix} \tag{6.36}$$

Rigid wall boundary condition for domain 2 at section 9 is given by

$$v_{2,9} = 0 \tag{6.37}$$

The acoustic state variables of domains 1 and 2 at section 9 are related to those at section 14 as in Eq. (6.38):

$$\begin{bmatrix} [S_{1,9}] \\ [S_{2,9}] \end{bmatrix} = \begin{bmatrix} [P_{1,9\_10}] & [O]_{2\times2} \\ [O]_{2\times2} & [P_{2,9\_10}] \end{bmatrix} [E_{1,2,10\_11}] \begin{bmatrix} [P_{1,11\_12}] & [O]_{2\times2} \\ [O]_{2\times2} & [P_{2,11\_12}] \end{bmatrix} \begin{bmatrix} [B_{1,12\_13}] & [O]_{2\times2} \\ [O]_{2\times2} & [P_{2,12\_13}] \end{bmatrix} \times \begin{bmatrix} [P_{1,13\_14}] & [O]_{2\times2} \\ [O]_{2\times2} & [P_{2,13\_14}] \end{bmatrix} \begin{bmatrix} [S_{1,14}] \\ [S_{2,14}] \end{bmatrix} \tag{6.38}$$

The overall transfer matrix, which relates the acoustic state variables of domains 1 and 2 at section 9 to those at section 14, is termed as [N].

The relation between the state variables at section 15 of the right end chamber and section 14 of domains 1 and 2 is obtained by applying the mass continuity and momentum conservation equations given by

$$p_{c,15} = p_{1,14} \tag{6.39}$$

$$p_{c,15} = p_{2,14} \tag{6.40}$$

$$v_{c,15} = v_{1,14} + v_{2,14} \tag{6.41}$$

Now, the Eqs. (6.37)–(6.41) are combined to obtain

$$\begin{bmatrix} 1 & 0 & 0 & 0 & \bullet & \bullet & \bullet & \bullet \\ 0 & 1 & 0 & 0 & \bullet & -[N]_{4\times4} & & \bullet \\ 0 & 0 & 1 & 0 & \bullet & & & \bullet \\ 0 & 0 & 0 & 1 & \bullet & \bullet & \bullet & \bullet \\ 0 & 0 & 0 & 0 & 1 & 0 & 0 & 0 \\ 0 & 0 & 0 & 0 & 0 & 1 & 0 & 1 \\ 0 & 0 & 0 & 1 & 0 & 0 & 0 & 0 \\ 0 & 0 & 0 & 0 & 1 & 0 & -1 & 0 \end{bmatrix} \begin{bmatrix} p_{1,9} \\ v_{1,9} \\ p_{2,9} \\ v_{2,9} \\ p_{1,14} \\ v_{1,14} \\ p_{2,14} \\ v_{2,14} \end{bmatrix} = \begin{bmatrix} 0 \\ 0 \\ 0 \\ 0 \\ p_{c,15} \\ v_{c,15} \\ 0 \\ 0 \end{bmatrix} \tag{6.42}$$

The inverse of the 8×8 matrix in Eq. (6.42) is termed as [P]. Thus, the relation between acoustic state variables of domain 1 at section 9 to those of the right end chamber at section 15 is given by

$$\begin{bmatrix} p_{1,9} \\ v_{1,9} \end{bmatrix} = \begin{bmatrix} P_{15} & P_{16} \\ P_{25} & P_{26} \end{bmatrix} \begin{bmatrix} p_{c,15} \\ v_{c,15} \end{bmatrix} \tag{6.43}$$

State variables of the right end chamber at section 15 are related to those at downstream end of the muffler proper by

$$\begin{bmatrix} p_{c,15} \\ v_{c,15} \end{bmatrix} = \begin{bmatrix} P_{c,15\_16} \end{bmatrix} \begin{bmatrix} SAC_{16\_17} \end{bmatrix} \begin{bmatrix} p_d \\ v_d \end{bmatrix} \tag{6.44}$$

The overall transfer matrix [T4] between the acoustic state variables at the upstream end to the downstream end of the muffler is obtained by combining Eqs. (6.28), (6.35), (6.36), (6.43) and (6.44).

6.2 3-D FEM validation of the 1-D ITM acoustic analysis

Equation (5.46) computes the transmission loss of all four muffler configurations using the overall transfer matrix between the upstream end and the downstream end of muffler proper.

T_{11}, T_{12}, T_{21} and T_{22} are the four-pole parameters of the overall transfer matrices [T1], [T2], [T3] and [T4] of the muffler Configuration nos. 1, 2, 3 and 4, respectively.

The 3-D FEM acoustic analysis is done using LMS Virtual Lab. Tetrahedron finite elements of 3 mm size are used for all four muffler configurations. The details of 3-D finite element analysis is given in Appendix G.

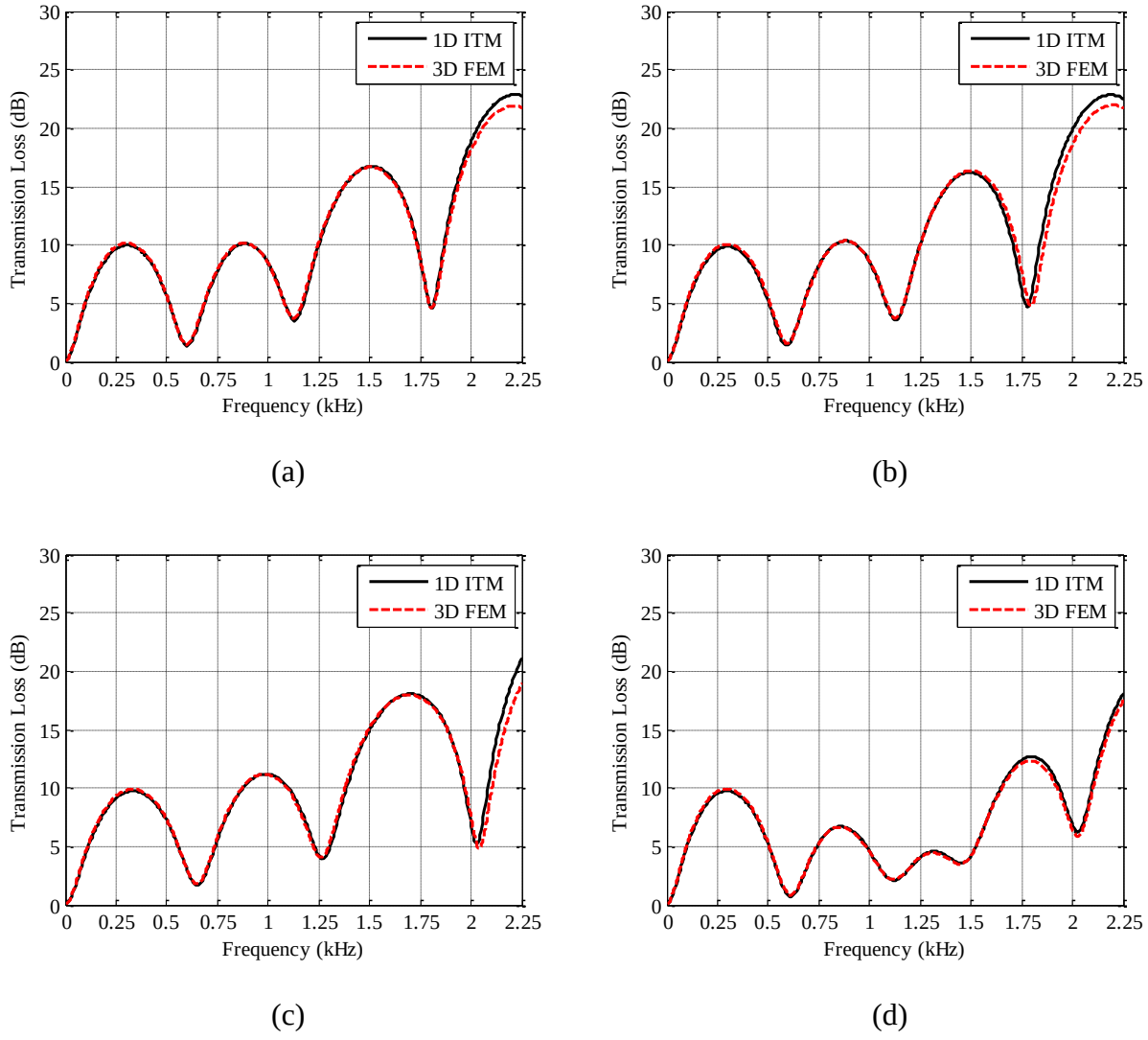

Figure 6.9. Comparison of transmission loss computed by the 1-D ITM approach and 3-D FEM for stationary medium. (a) Single plug muffler; (b) Double-plug chamber separated muffler; (c) Common plug muffler; and (d) Common-plug muffler with end chambers.

First, the 1-D acoustic analysis using the ITM approach is validated for stationary medium using the 3-D FEM acoustic analysis. Then, the validation is done for the mean flow case, and the transmission loss (TL) spectra computed by the 1-D ITM and the 3-D FEM are compared, as shown in Figs. 6.9 and 6.10, for the mean flow Mach number M = 0 and M = 0.083,

respectively. The temperature of exhaust gas is 823 K which corresponds to the speed of sound 575 m/s.

As the shell diameter of all four configurations is the same (116 mm), the cut-off frequency for all these mufflers is approximately 2903 Hz. The 1-D and 3-D computed transmission loss values may be seen to tally excellently upto 2250 Hz, which is lower than the cut-off frequency. However, the upper limit of frequency shown in plots represents the 40th engine firing frequency harmonic, which is good enough in practice.

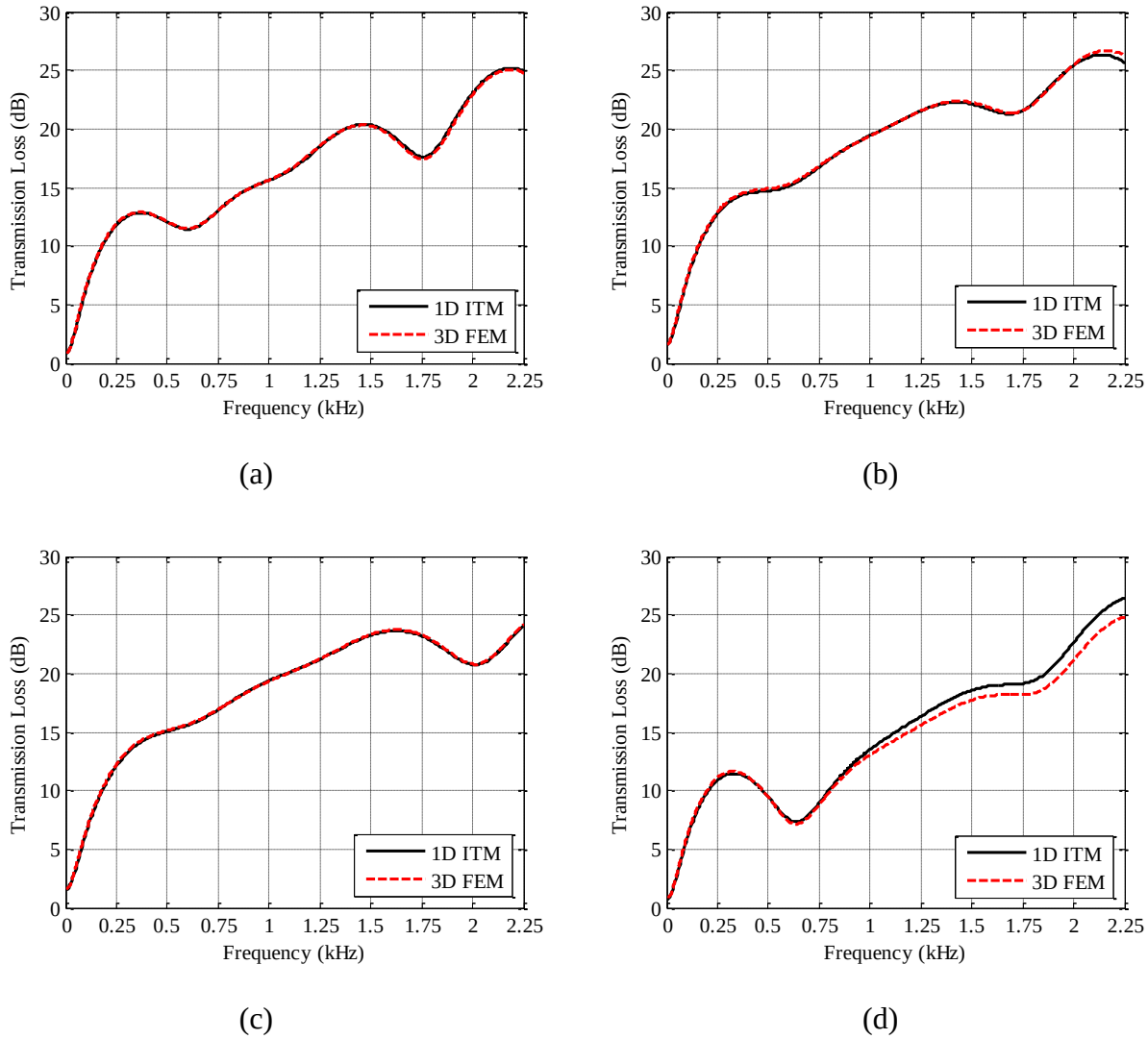

Figure 6.10. Comparison of transmission loss computed by the 1-D ITM approach and 3-D FEM for the mean flow Mach number M= 0.083. (a) Single plug muffler; (b) Double-plug chamber-separated muffler; (c) Common plug muffler; and (d) Common-plug muffler with end chambers

Length of the muffler proper of the configurations shown in Figs. 6.1, 6.3 and 6.7 is 450 mm. If a simple expansion chamber, corresponding to these configurations were

considered, then the peaks and troughs of TL would occur at odd and even multiples of 319.5 Hz, respectively [1]. Since the length of the muffler proper shown in Fig. 6.5 is 400 mm, the corresponding simple expansion chamber peaks and troughs of TL would occur at odd and even multiples of 359.4 Hz, respectively. Table 6.3 shows the first three peaks and troughs in the TL spectrum of the four coaxial muffler configurations considered here for stationary medium.

It may be noted from Table 6.3 that, in comparison with the simple expansion chamber muffler, all the peaks and troughs are shifted towards left for all the four mufflers. The periodic domes of transmission loss are present for all the mufflers for the stationary medium case. The troughs are lifted more at higher frequencies compared to the lower frequencies.

Table 6.3. Peaks and troughs in the TL spectra of the mufflers for stationary medium

Muffler	Peak Frequency (Hz)			Trough Frequency (Hz)		
	1st	2nd	3rd	1st	2nd	3rd
Configuration no. 1	304	885	1507	599	1127	1808
Configuration no. 2	303	884	1502	595	1130	1796
Configuration no. 3	334	984	1699	649	1262	2041
Configuration no. 4	296	855	1303	611	1118	1447

The mufflers shown in Figs. 6.1 and 6.3 differ by a plug on the outlet side which does not matter in the case of stationary medium. The TL spectra for these mufflers is shown in Figs. 6.9(a) and 6.9(b), whereas those for the moving medium are shown in Figs. 6.10(a) and 6.10(b), respectively.

The maximum TL of a simple expansion chamber depends on the diameter ratio, and for the diameter ratio 116/45 = 2.58 of the investigated mufflers, it is 10.6 dB. However, it can be observed from Fig. 6.9(c) that without mean flow the TL values in the frequency range 600–1600 Hz (approximately) for the common-plug muffler with end chambers are less than those of the simple expansion chamber except at the dip frequencies. The reason is that the acoustic mass velocity gets divided into parallel paths at the beginning and the equivalent acoustic impedance becomes less than the lower one. It can be better understood if one does the analysis by means of the lumped element model. For the range of frequencies mentioned above, the total acoustic impedance may be less than that of the simple expansion chamber muffler. However, the muffler performance substantially improves in the presence of mean flow.

Mean flow indeed plays a crucial role in the acoustics of multiply-connected coaxial perforated element mufflers. Its effect on the TL spectrum can be better understood by paying attention to the perforate impedance expressions. The normalized perforate resistance and reactance expressions are given by [64]:

$$\vartheta = \mathrm{Re}\left[j\frac{k}{\sigma C_D}\left(\frac{t}{F(\mu')} + \frac{\delta_{re} f_{\mathrm{int}}}{F(\mu)} \right) \right] + \frac{1}{\sigma}\left[1 - \frac{2J_1(kd)}{kd} \right] + 0.3\frac{M_g}{\sigma} + 1.15\frac{M_b}{\sigma C_D} \tag{6.45}$$

$$\chi = \mathrm{Im}\left[j\frac{k}{\sigma C_D}\left(\frac{t}{F(\mu')} + 0.5\frac{d\ f_{\mathrm{int}}}{F(\mu)} \right) \right] \tag{6.46}$$

where

$$K = \left(\frac{-j\omega}{\nu} \right)^{0.5},\ K' = \left(\frac{-j\omega}{\nu'} \right)^{0.5},\ F(Kd) = 1 - \frac{4J_1(Kd/2)}{Kd \times J_0(Kd/2)} \tag{6.47}$$

$$\delta_{re} = 0.2d + 200d^2 + 16000d^3,\ f_{\mathrm{int}} = 1 - 1.47\sigma^{0.5} + 0.47\sigma^{1.5} \tag{6.48}$$

In Eqs. (6.45)–(6.48), t is the orifice thickness, d is the orifice diameter, σ is the porosity, k is the wave number ω/c, c is the sound speed, C_D is the orifice discharge coefficient, J is the Bessel functions of the first kind, $\nu = \mu/\rho_0$ is the kinematic viscosity, ρ_0 is the fluid density, μ is the adiabatic dynamic viscosity, $\mu' = 2.179\mu$, M_g is the grazing flow Mach number, and M_b is the bias flow Mach number inside the holes of the perforate. The parameter f_{int} in Eq. (6.48) is a correction factor for the orifice interaction effects.

The maximum effect of mean flow is shown in Figs. 6.10(c) and 6.10(d) for the common plug muffler and the Common-Plug Muffler with End Chambers, respectively. It is because of higher bias flow for these mufflers due to plugs for flow on both sides. However, the division of flow for the common-plug muffler with end chambers (configuration no. 4) encounters less flow resistance as well as the lower value of acoustic impedance. An advantage of the lesser flow resistance is lesser backpressure, but it gets compromised by a little poorer acoustical performance.

It may be pointed here that the baffles should be placed in the middle, neither at the start of the inlet pipe nor at the end of the outlet pipe. Fig. 6.10(d) also reveals the importance of mean flow.

6.3 Effect of mean flow on all coaxial configurations

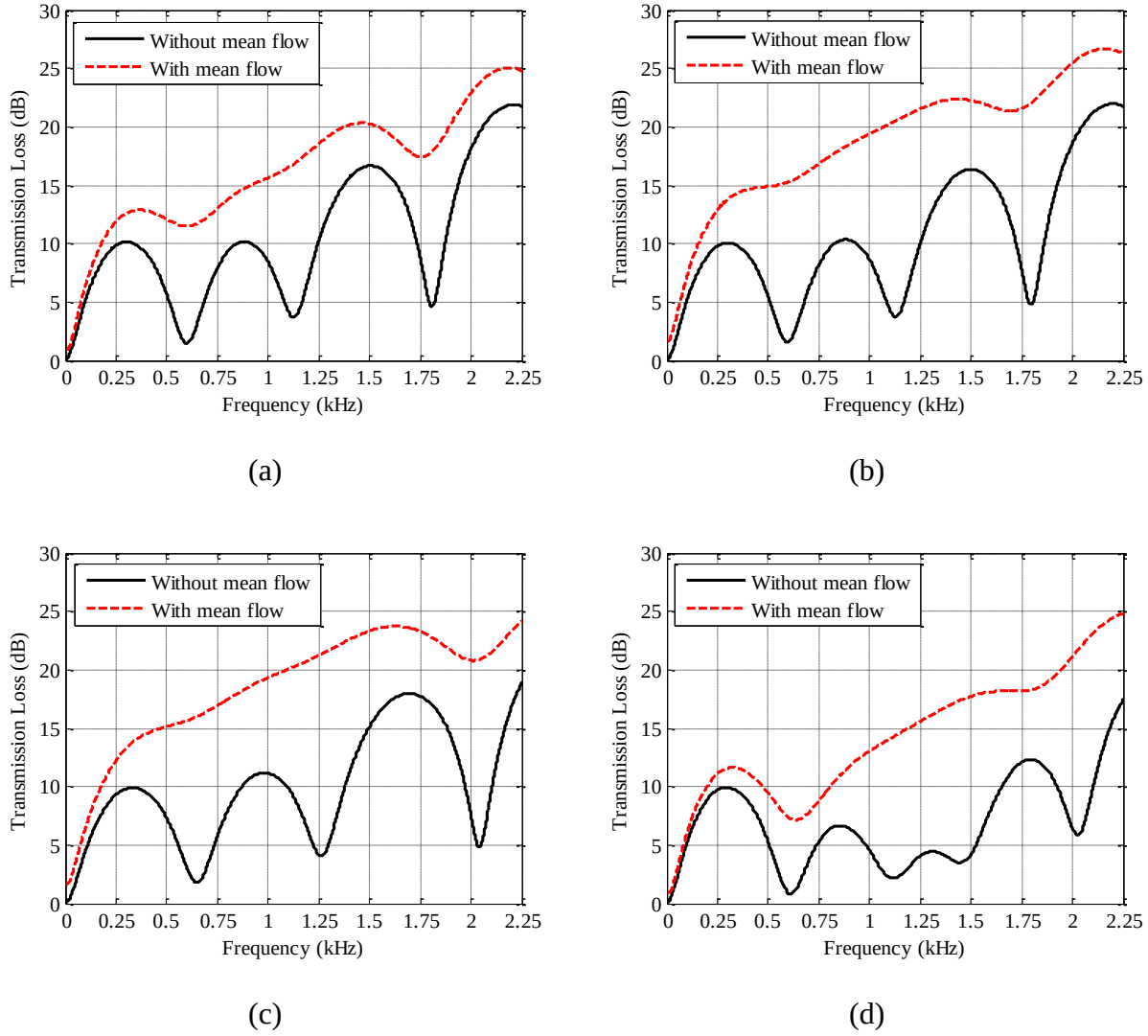

Figure 6.11. Effect of mean flow on TL spectrum of multiply-connected co-axial mufflers. (a) Single plug muffler; (b) Double-plug chamber-separated muffler; (c) Common plug muffler; and (d) Common-plug muffler with end chambers.

Figure 6.11 clearly brings out the effect of mean flow on all the four coaxial muffler configurations investigated here. The monotonically increasing trend of TL with frequency is due to the substantially augmented acoustic resistance, particularly due to the bias flow Mach number, M_b. Tuned concentric tube resonators [63] also lift up three-fourths of the TL troughs, but the extent of lifting would be comparatively much less for small values of the area expansion ratio. But, a high bias flow Mach number can make the coaxial perforated element mufflers investigated here similar to dissipative mufflers (with absorptive lining) with the additional low frequency attenuation advantage. Terms associated with grazing flow and bias

flow in Eq. (6.45) depend on Mach numbers related to these flows, porosity of perforated pipes and baffles, and the discharge coefficients. But, these terms are not dependent on frequency, and this is why the higher values of bias and grazing flow Mach numbers improve the muffler acoustic attenuation at all frequencies. This is evident from Figs. 6.11 (a)–(d).

Figures 6.11(b) and 6.11(c) (relating to the muffler configurations 2 and 3) clearly show the advantage of higher bias mean flow Mach number upto 250 Hz in contrast to Figs. 6.11(a) and 6.11(d) (relating to the muffler configurations 1 and 4) . It is important to note that the improvement in attenuation characteristics in the low-frequency regime is of crucial importance because most of the automotive noise is present at the engine firing frequency and its first few multiples.

In the next section, unmuffled SPL spectrum of a typical three-cylinder, 4-stroke diesel engine is shown, and the comparison of overall insertion loss (in dB and dBA) of these mufflers is made.

6.4 Comparative study of all four coaxial configurations on a diesel engine

The TL, IL and backpressure values of all four analysed mufflers are compared in this section. Figure 6.12 shows the comparison of the TL spectra of mufflers, and Fig. 6.13 shows the comparison of the IL spectra.

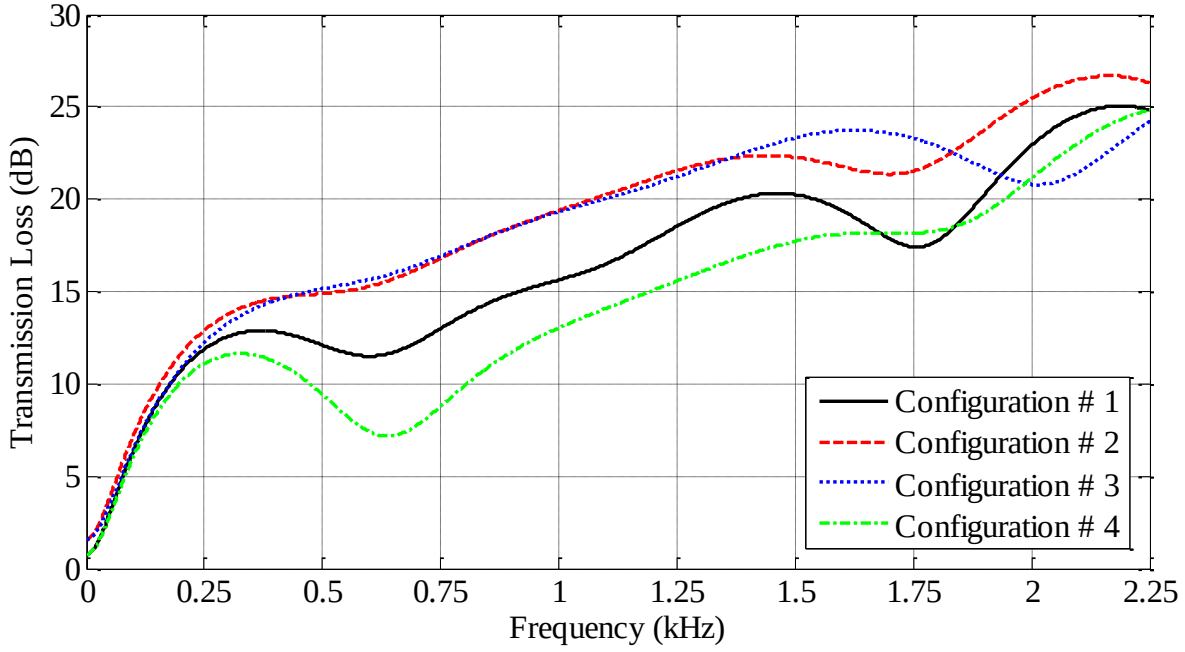

Figure 6.12. Comparison of Transmission Loss of the MCCA Mufflers (Configurations 1-4) with mean flow (M = 0.083)

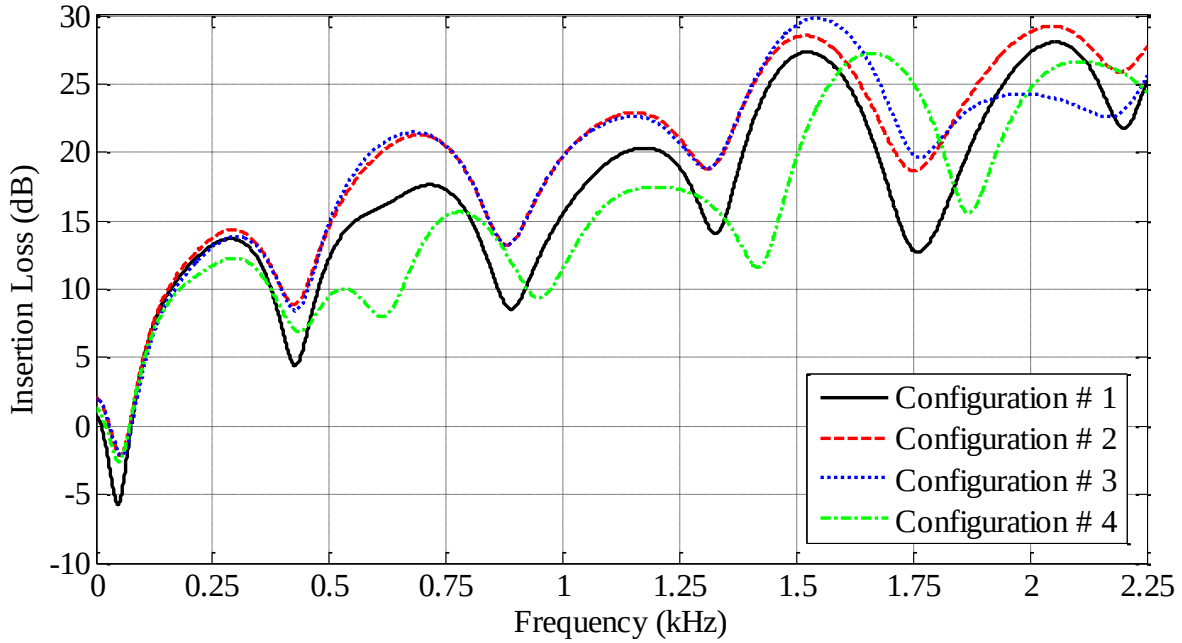

Figure 6.13. Comparison of Insertion Loss of the MCCA Mufflers (Configurations 1–4) with mean flow (M = 0.083)

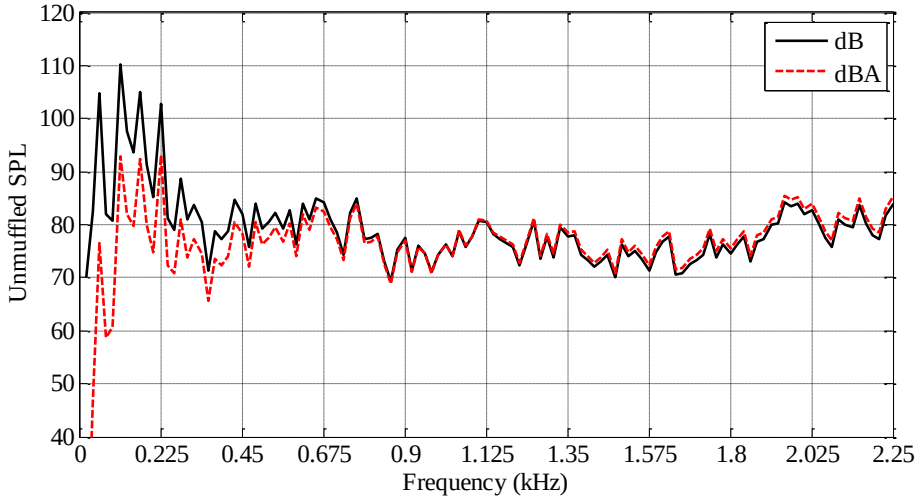

Figure 6.14. Unmuffled SPL (with 6 m long tail pipe) spectrum of a typical 3-cylinder 4-stroke diesel engine running at 2250 RPM

For a practical comparison of the implications of the IL spectra of all the four muffler configurations in this chapter, SPL spectrum of the unmuffled exhaust noise of a typical three-cylinder, 4-stroke diesel engine is shown in Fig. 6.14. Anechoic source is assumed for prediction of IL spectra. It can be observed from Fig. 6.14 that in the low frequency range the tonal noise (especially at the engine firing frequency harmonics) is sharply distinguished, and in the high-frequency range a relatively flatter SPL spectrum is observed. To appreciate the need of high insertion loss at the firing frequency and at its first few multiples, Table 6.4 gives

the unmuffled sound pressure level at its first six engine harmonics, a logarithmic addition of the same, and the overall (total) measured values of the unmuffled exhaust noise, linear as well as A-weighted.

Table 6.4. Unmuffled SPL values at first six engine harmonics and Overall SPL

Harmonics No.	SPL (dB)	SPL (dBA)
1	104.7	76.5
2	110.3	92.7
3	105.1	92.5
4	102.7	93.1
5	88.7	81.1
6	80.6	74.5
Overall	113.2	101.6
$10\log_{10}\left(\sum_{i=1}^{6} 10^{0.1L_{p,i}}\right)$	112.7	97.7

The first six harmonics contribution to the overall noise in dB is good enough. But, a good amount of overall noise contribution comes from high-frequency harmonics also. The estimated IL of all the coaxial mufflers is better at frequencies beyond 250 Hz. This is the reason of adequate overall IL in dBA.

Table 6.5. Flow-acoustic performance of all four mufflers on a diesel engine

Muffler	ΔP (kPa)			IL		Muffler to engine volume ratio	Specific IL (dBA per unit volume ratio)
	$\Delta p_{ep} + \Delta p_{tp}$	Δp_{MP}	Δp_{total}	in dB	in dBA		
Configuration 1	0.35	1.22	1.57	2.4	11.2	1.9	5.9
Configuration 2	0.35	2.23	2.58	5.5	12.4	1.9	6.5
Configuration 3	0.35	2.23	2.58	3.9	11.4	1.7	6.7
Configuration 4	0.35	1.75	2.10	5.1	10.9	1.9	5.7

Finally, Table 6.5 summarises the comparative study of all four mufflers analysed in this chapter. Common plug muffler (C-3) seems to be a better option considering specific IL defined as the overall A-weighted IL per unit volume ratio (ratio of muffler volume to engine swept volume). However, its overall IL is 1 dBA less than that of the Common-Plug Chamber-Separated Muffler (C-2), but then the volume is 11 percent lower. The muffler volume of configurations 1, 2 and 4 is 4.76 litres, and that of configuration 3 is 4.23 litres. For comparison,

the engine swept volume is 2.5 litres. Thus, all four configurations are extraordinarily small, with their muffler volume being less than two times the engine swept volume.

It is worth noting here that the specific IL of the multiply connected perforated coaxial mufflers is quite high due to the crucial role of mean flow, while backpressure is quite modest. This feature makes them ideal for design of compact efficient mufflers.

6.5 Limiting mean flow and jet noise

The effect of jet noise is often overestimated by muffler designers, who try to limit the high mean flow Mach number in the tail pipe. Before performing a parametric study on the common plug muffler (C-3, Fig. 6.5) it is necessary to examine the contribution of jet noise to total exhaust noise and thereby decide upon the limits of Mach number.

The mechanical power of a jet is given by [94]

$$W_m = \frac{1}{2}\dot{m}U^2 = \frac{1}{2}\dot{m}M_j^2 c_j^2 \tag{6.49}$$

where $\dot{m}$ is the mass flow rate of the jet, U is the mean flow velocity averaged over the cross-section of the jet, M_j is the Mach number related to the jet medium, and c_j is the speed of sound in the jet medium.

The relation between the acoustical and mechanical power of the jet is given by [98]

$$W_a = \eta W_m \tag{6.50}$$

where η is the acoustical efficiency, and an approximate expression for it is given by [98]

$$\eta \approx \left(\frac{T_j}{T_0}\right)^2 \left(\frac{\rho_j}{\rho_0}\right) K_a M_a^5 \tag{6.51}$$

Here, T_0 is the absolute temperature (in Kelvin) and ρ_0 is the mass density of the ambient medium; T_j and ρ_j are the absolute temperatures and mass density of the medium of the jet; M_a is the Mach number relative to the ambient gas; and K_a is the acoustical power coefficient which for subsonic jet is given by [98]

$$K_a \approx 5\times 10^{-5} \tag{6.52}$$

The Mach number with respect to the ambient gas M_a and the Mach number with respect to the jet medium M_j are related by

$$M_a = M_j \left(\frac{T_j}{T_0} \right)^{1/2} \tag{6.53}$$

The SPL at a distance *r* from the orifice is given by

$$L_p = 10 \log_{10} \left(W_a \Big/ \left(10^{-12} \times 4\pi r^2 \right) \right) \tag{6.54}$$

Equations (6.49)–(6.54) may be combined to get an approximate expression of the limiting Mach number, which is given by Eq. (6.55).

$$M_j = \left(10^{(0.1L_p - 7)} \times \frac{4\pi r^2}{2.5 c^2 \dot{m}} \times \left(\frac{T_0}{T} \right)^{4.5} \frac{\rho_0}{\rho} \right)^{1/7} \tag{6.55}$$

It may be noted from Eq. (6.55) that the limiting Mach number M_j (the Mach number limit) depends on the allowable jet noise SPL (L_p) and the distance of microphone from the orifice for fixed mass flow rate and temperature and density of the ambient medium and the jet medium.

For a particular application, the limit of jet SPL is taken as 69 dB. And, the distance *r* for DG sets and automotive engines are 1 m and 7.5 m, respectively. The limits for DG sets and automotive engines turn out to be 0.2 and 0.35, respectively. In practice, however, the impingement noise (aerodynamic noise generated within the muffler) may lower the limits substantially, approximately to 0.15 and 0.25 for DG sets and automotive engines, respectively.

6.6 Parametric study on the common plug muffler (C-3)

The maximum TL and IL of a simple expansion chamber (SEC) increase with an increase in the ratio of the diameter of the shell (d_s) to the diameter of inlet/outlet pipe (d_p) [1]. The perforated elements improve attenuation characteristics of the muffler on top of those of the basic SEC. To investigate the effect of the diameter ratio (d_s / d_p), three different ratios are taken while keeping the shell diameter fixed at 116 mm. The number of holes on the perforated pipes and baffles is not changed. Consequently, the value of bias flow Mach numbers through it remains fixed at M_b = 0.083, but the value of the grazing flow Mach number M_g changes.

In Table 6.6, the Mach number (M) of mean flow in the exhaust pipe and tail pipe, grazing flow Mach number (M_g) through perforated pipes, and porosity (σ) of perforated pipes and baffles are listed.

Table 6.6. Mach number of mean flow in exhaust/tail pipe M, grazing flow through perforates M_g and porosity σ for different values of the exhaust/tail pipe diameter d

d (mm)	M	M_g			σ (in %)		
		1-2	5-6	13-14	1-2	3-4	5-6
45	0.08	0.06	0.02	0.04	7.8	10	7.5
32	0.16	0.12	0.04	0.08	11	9.1	10.6
26	0.25	0.18	0.06	0.12	13.5	8.8	13

In Table 6.6, *i-j* represents the perforated pipes and baffles between the i^{th} and the j^{th} section of the muffler shown in Fig. 6.5. Grazing mean flow in the perforated pipe between sections 9-10 is similar to section 5-6. Values of the porosity of perforated pipes between sections 1-2, baffle between sections 3-4, and perforated pipe between sections 5-6 are similar to those of the perforated pipe between sections 13-14, the baffle between section 11-12, and the perforated pipe between section 9-10, respectively.

It is important to study the effects of change in pipe diameters on the perforate impedance before studying the effect of the diameter ratio on attenuation characteristics while keeping the shell diameter fixed. The normalized specific impedance of a perforate θ is given by

$$\theta = \frac{p}{\rho_0 c_0 u} = \vartheta + j\chi \tag{6.56}$$

where u is the particle velocity considered on the continuous perforated section. Thus, the acoustic impedance of the perforate is given by

$$Z_p = \frac{p}{\rho_0 S u} = \frac{c_0}{S}\left(\vartheta + j\chi\right) \tag{6.57}$$

where S is the complete perforate (pipe/baffle) open area.

In Table 6.7, the dependence of different parameters of a perforated pipe on pipe diameter is given.

Table 6.7. Dependence of the different parameters of a perforated pipe on pipe diameter, *d*

Parameter	S	σ	M_g	M_b
Dependence	$\propto d$	$\propto 1/d$	$\propto 1/d^2$	constant

It is evident from Table 6.7 and Eqs. (6.45), (6.46), and (6.57) that the perforate impedance terms, except the grazing flow Mach number (M_g) term, remain unaffected by pipe diameter, *d*. The values of the first term of perforate resistance and reactance decrease a little with a decrease in diameter of pipes because an increment in porosity would decrease the interaction factor f_{int} . The perforate resistance term associated with M_g is inversely proportional to the square of pipe diameter, and this is why the perforate impedance of pipe increases with a decrease in the pipe diameter. However, the perforate impedance of baffles remains almost constant with a decrease in pipe diameter. It is because a decrement in the pipe diameter gives an increment in the normalized impedance, but it also increases the perforate area *S* of the baffle.

In Fig. 6.15 the effect of pipe diameter and thence the diameter ratio (ratio of shell diameter to exhaust/tail pipe) is shown. The smaller exhaust/tail pipe diameter gives the added advantage of higher grazing flow Mach number which increases the perforate normalized resistance. The higher the shell-to-pipe diameter ratio, the more the insertion loss at most of the frequencies. Larger diameter ratio marginally lowers the IL dip frequency. Significantly, the value of IL at the trough increases.

It may be noted that in the negative IL region, values of the unmuffled A-weighted SPL are very low. Therefore, the negative IL values at very low frequencies are of no consequence for the overall acoustic performance (IL in dBA).

The improvement in muffler acoustic attenuation with a decrement of the exhaust/tail pipe diameter, however, suffers from the disadvantage of higher backpressure. The flow-acoustic parameters for three different values of the inlet and outlet pipe diameters are given in Table 6.8, where it is shown that the reason for higher backpressure is the flow resistance due to pipe friction in the exhaust pipe (of 300 mm length) and tail pipe (of 600 mm length), not the flow resistances faced within the muffler proper.

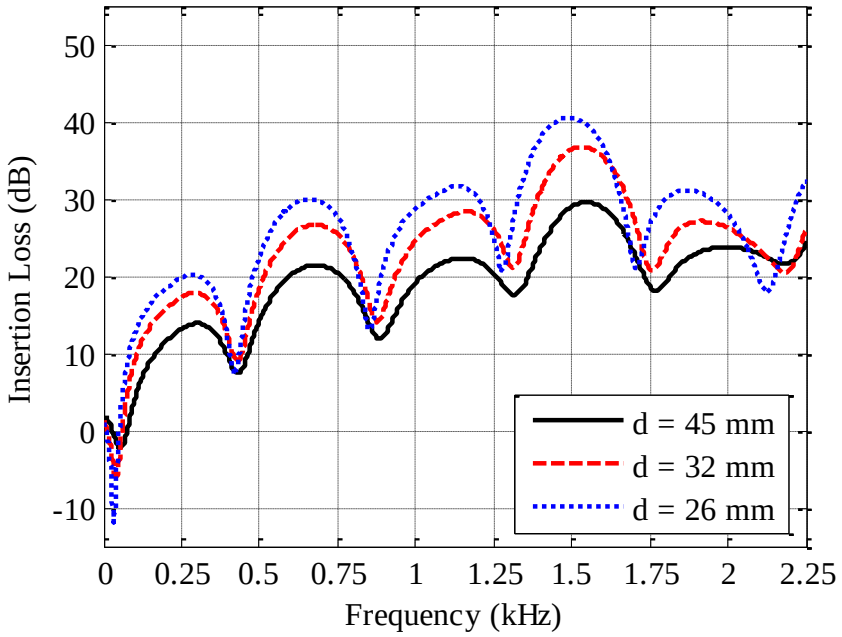

Figure 6.15. Effect of the inner pipe diameter *d* (keeping the shell diameter fixed at 116 mm) on IL of the common plug muffler (C-3, Fig. 6.5)

The frictional flow resistance of a uniform pipe is inversely proportional to the fifth power of diameter. The significant increment in backpressure due to the exhaust pipe and tail pipe is more worrisome than the jet noise. There will also be a little increase in stagnation pressure drop due to the muffler proper which is not taken into account. The increase in the stagnation pressure drop due to the pipe friction of inner pipes of the muffler proper can be neglected in comparison to that across the exhaust and tail pipes. This is because the length of muffler proper is 400 mm which is 44.4 % of summation of the lengths of the exhaust and tail pipes, and the flow gets divided in these pipe equally which reduces the stagnation pressure drop to 1/4th of the full flow passing through it.

In Table 6.8 and hereafter the subscripts *ep*, *tp*, and *MP* stand for exhaust pipe, tail pipe and muffler proper, respectively.

Table 6.8. Flow-acoustic parameters of different diameter ratio with fixed shell diameter

d_s / d_p	ΔP (kPa)			IL (dBA)	SIL (dBA per unit volume ratio)
	$\Delta p_{ep} + \Delta p_{tp}$	Δp_{MP}	Δp_{total}		
116/45	0.35	2.23	2.58	11.4	6.7
116/32	1.92	2.23	4.15	15.4	9.1
116/26	5.41	2.23	7.64	18.3	10.8

If the diameters of the exhaust pipe and tail pipe are not changed, the acoustic attenuation of a muffler can still be enhanced by increasing the shell diameter and thence the diameter ratio without facing the problem of high backpressure. In this case, the grazing mean flow Mach number through perforates does not change. The different shell diameters are taken to maintain the same diameter ratio as it is taken for the results shown in Fig. 6.15 and Table 6.8. In Fig. 6.16, the effect of diameter ratio on IL of the muffler is shown while keeping the diameter of the exhaust pipe and tail pipe fixed at 45 mm.

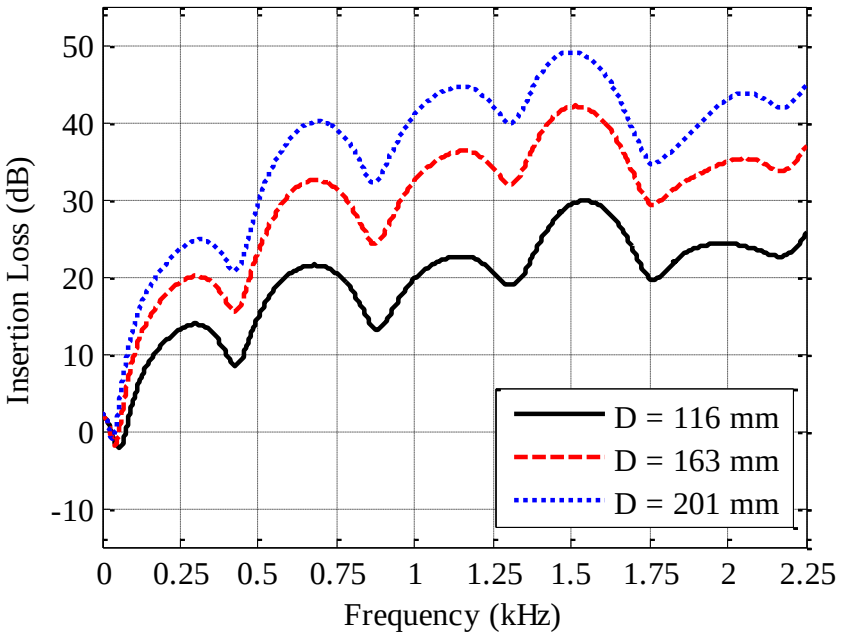

Figure 6.16. Effect of diameter ratio on IL of Double Plug Muffler with diameter of the inner pipe fixed at 45 mm

Table 6.9. Flow-acoustic parameters of mufflers for different diameter ratio with fixed pipe diameter d_p

d_s / d_p	ΔP (kPa)			IL (dBA)	SIL (dBA per unit volume ratio)
	$\Delta p_{ep} + \Delta p_{tp}$	Δp_{MP}	Δp_{total}		
116/45	0.35	2.23	2.58	11.4	6.7
163/45	0.35	2.23	2.58	17.0	5.1
201/45	0.35	2.23	2.58	20.9	3.9

It can be observed from Fig. 6.16 that an increase in diameter ratio shifts the IL dip frequency slightly towards left as seen in Fig. 6.15. But, the value of negative IL at very low frequencies decreases in this case with increment in the shell diameter and thence the diameter ratio. The IL values in this case are higher for almost the entire frequency range for all mufflers

when compared with those with similar diameter ratio in Fig. 6.15. This increase in Fig. 6.16 is due to the larger muffler shell volume. The flow-acoustic parameters for three different values of the inlet and outlet pipe diameters are given in Table 6.9. The increase in diameter ratio increases the overall IL of a muffler, but not in proportion to the muffler volume increase. The fifth column of Table 6.9 clearly shows the decrement in specific insertion loss, SIL.

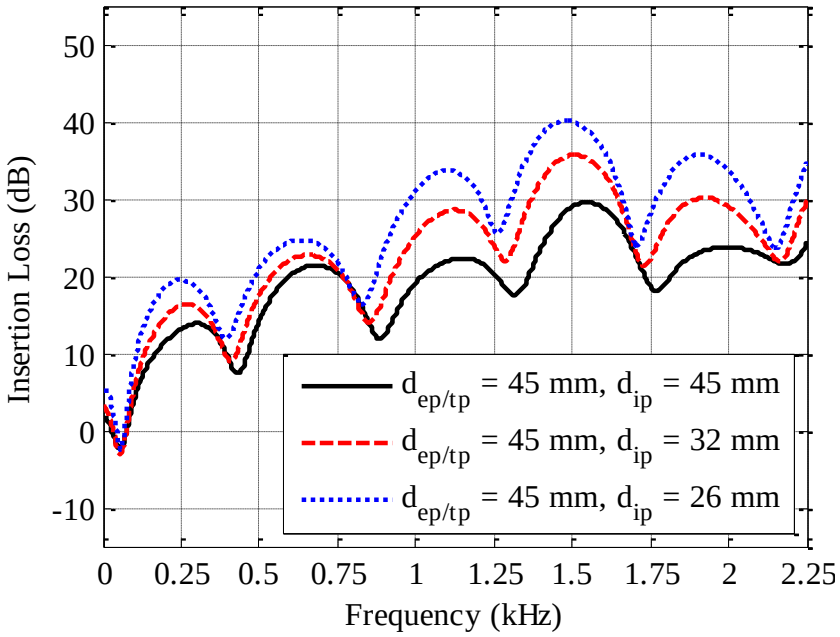

Figure 6.17. Effect of decrement in the intermediate pipe diameter on IL of the common plug muffler, keeping diameters of exhaust pipe, tail pipe and muffler shell fixed at 45 mm, 45 mm, and 116 mm, respectively.

Finally, the parametric study is done by changing the diameter of the intermediate pipes (inside the muffler proper) while the exhaust pipe and tail pipe diameters are kept constant (45 mm). The muffler shell diameter is also held constant (116 mm). The insertion loss of the common plug muffler with these dimensional changes is shown in Fig. 6.17, where it can be observed that the above mentioned geometrical changes keep the negative insertion loss low in comparison to those in Fig. 6.15.

The flow-acoustic parameters for the alterations of common plug muffler mentioned above (in Fig. 6.17) are listed in Table 6.10.

The increases in stagnation pressure drop due to the exhaust pipe and tail pipe are due to the sudden area discontinuity at both ends of the muffler proper. However, it is advantageous for overall insertion loss; the aeroacoustic resistances at sudden area discontinuities raise the overall insertion loss.

Table 6.10. Flow-acoustic parameters of different inner pipes diameter with fixed exhaust pipe, tail pipe and muffler shell diameters

d_{ip} (mm)	ΔP (kPa)			IL (dBA)	SIL (dBA per unit volume ratio)
	$\Delta p_{ep} + \Delta p_{tp}$	Δp_{MP}	Δp_{total}		
45	0.35	2.23	2.58	11.4	6.7
32	0.58	2.23	2.81	13.4	7.9
26	1.80	2.23	4.03	16.4	9.7

6.7 Conclusion

Four different configurations have been analysed using the 1-D Integrated Transfer Matrix (ITM) approach, and the results have been validated against the 3-D FEM. The lumped flow resistance networks have been used for estimation of flow distribution as well as total backpressure. It is demonstrated that mean flow plays a crucial role in the flow-acoustic performance of the multiply-connected co-axial (MCCA) mufflers. Comparison of the performance with and without mean flow demonstrates how the bias flow Mach number affects the attenuation characteristics of the MCCA mufflers. Perforated baffles on either side of the plug ensure phase cancellations due to the Herschel-Quincke tube effect, thereby raising the TL (and IL) curves, while at the same time reducing backpressure due to division of flow in parallel passages.

Configuration no. 3 (Fig. 6.5) has been shown to be the best of the set and is taken up for parametric studies. The effect of diameter ratio with and without a change in the grazing flow Mach number is investigated and it is shown that the grazing flow Mach number also plays a major role in obtaining high overall IL with a decrease in the diameter of perforated pipes. A decrease in the diameter of the comparatively long exhaust pipe and tail pipe increases the backpressure of the muffler. In a trade-off between backpressure of muffler and overall insertion loss as well as specific insertion loss (overall insertion loss (in dBA) per unit muffler to engine volume ratio), a suggestion is made to make the inner pipes (inside the muffler) diameters narrower than the tail pipe and exhaust pipe.

Expression of limiting mean flow Mach number is derived for permissible limit of jet noise. This expression can be a guideline to use the diameter of tail pipes for maximum exhaust mass flow rate from jet noise point of view. In this chapter, judicious use of perforated elements in ultra small MCCA mufflers are shown to obtain adequate insertion loss.

Chapter 7

Development of Rational Design Guidelines for Large SISO Perforated Element Mufflers*

The primary design requirements of an exhaust muffler for internal combustion (IC) engines are wideband insertion loss (IL), particularly high IL at low frequencies (of the order of the firing frequency of the engine), limited back pressure, and limited volume of the muffler proper [1]. The double tuned extended tube resonator [62], perforated concentric tube resonator [63], and side-inlet side-outlet (SISO) mufflers [99] fulfil all requirements except the requirement of high IL at low frequency which however is most crucial for ensuring sufficient overall IL. Cross-flow perforated element mufflers (plug mufflers) fulfil this latter requirement, but suffer from the disadvantage of relatively high back pressure [82]. Larger mufflers raise the transmission loss (TL) and IL spectra at all frequencies and hence the overall values of IL [1,94]. However, they cannot be accommodated under the vehicle. This would, fortuitously, not be a problem for exhaust mufflers of the diesel generator (DG) sets, which are located on the top of the acoustic enclosures of the DG sets.

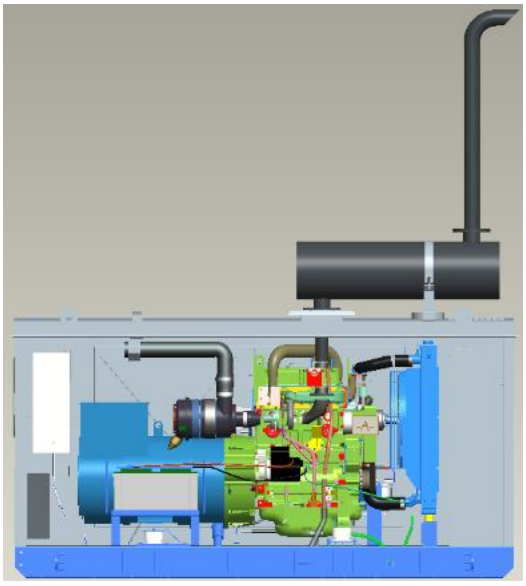

Figure 7.1. Schematic diagram of a DG set with side inlet and side outlet muffler

* This chapter is generally based on the Author's publication in Noise Control Engineering Journal, vol. 66, issue 4, pp. 308–323, 2018.

Logistics of an acoustic enclosure for a diesel generator (DG) set require mounting of the exhaust muffler on the top of the enclosure with side-inlet and side-outlet. The exhaust pipe enters the muffler vertically as a side inlet and the tail pipe leaves the muffler vertically as a side outlet, as shown in the schematic Fig. 7.1. Recently, multiply-connected perforated-element combination mufflers with side inlet/outlet have been analysed, making use of the lumped-element (0-D), the quasi-plane wave (1-D), and the FEM (3-D) approaches [84]. In the case of a side inlet/outlet perforated pipe opening into a cavity, plane wave propagation is not possible and therefore 1-D analysis is ruled out. In the present study, however, 1-D plane wave analysis has been done for such kind of mufflers, and it has been found that the plane wave analysis works better than the quasi-plane wave analysis. In the present 1-D plane wave analysis, side inlet/outlet perforate is modelled as lumped inline impedance and the chamber is modelled as distributed (continuous) element. This can be used to predict the acoustic attenuation properties faster up to 500 Hz. Fortunately, exhaust noise predominates at these frequencies, and the 1-D plane wave analysis offers a very convenient and fast method of the flow-acoustic analysis leading to ready conceptualization and development of design guidelines.

Four different, yet somewhat similar, cross-flow perforated element muffler configurations have been investigated here making use of the 1-D plane wave analysis and the same is validated against the 3-D FEM approach. The results of the two approaches for TL and IL spectra match well up to about 300 Hz, which covers the firing frequency and its first few harmonics of the DG set engine running at 1500 rpm. The number of holes for each of the perforates is designed so as to limit the overall back pressure to the prescribed value (6 kPa in this case). In fact, keeping a 10% margin, all four muffler configurations are designed for a limiting back pressure of 5.4 kPa. Procedure to compute the number of holes is illustrated in Appendix H.

These SISO perforated element mufflers can be analysed using the 0-D lumped element analysis as well and for that the transfer matrix across *n*-parallel junctions are derived in Appendix I. The application of the 1-D ITM approach between the start and end of the intermediate pipes of all four SISO mufflers are illustrated in Appendix J.

By comparing the results with the mean flow to those for the stationary medium, it is shown that mean flow plays a significant role in lifting the troughs of the TL and the IL curve very substantially. This is a very desirable feature of the cross flow perforated element mufflers.

This is in sharp contrast to the performance of the double-tuned concentric tube resonator [63] as well as extended tube resonator [62] where mean flow affects the tuning adversely.

Finally, by comparing the 3-D FEM computed TL and IL spectra of all four muffler configurations, some design guidelines have been arrived at.

7.1 Flow-acoustic analysis of large SISO mufflers

The dissipative effect of mean flow through the perforated elements being crucial, we need to carry out the mean flow distribution analysis for all four configurations. Expressions of flow resistances are given in Appendix E.

The specifications of the engine on which the muffler configurations are studied are listed in Table 7.1. The acoustic analysis is performed for estimating the TL and IL spectra up to 1000 Hz using the 1-D plane wave analysis. The 1-D estimates of TL and IL have been validated against the 3-D finite element analysis in Sec. 7.3.

Table 7.1. Engine Specifications

Parameter	Value
Number of cylinders	12
Engine capacity (litres)	32.1
Exhaust gas volume flow rate ($= Q_0$) (m^3/s)	2.98
Exhaust gas temperature (K)	793.8
Engine speed (RPM)	1500

7.1.1 Two-chamber, One-baffle and Two-perforate Muffler (C-1)

Figure 7.2 shows the schematic sectional views of the muffler configuration no. 1 with salient dimensions in mm. It may be noted that volume of the muffler is equal to 20 times the engine capacity for all four muffler configurations investigated here. The details of perforates (shown in Fig. 7.2(b)) on the intermediate pipes no. 1 and no. 2 are given in Table 7.2. The diameter of holes of each perforate of all four configurations is 6 mm.

For muffler configuration no. 1, the schematic of flow distribution is shown in Fig. 7.2(b). The flow distribution analysis is carried out by using the lumped flow resistance network shown in Fig. 7.3. Description of the lumped flow resistances and the percentage of total flow through these resistances are given in Table 7.3. The flow resistances through the two parallel paths (intermediate pipes) are such that the flow gets almost equally divided which helps to

minimise backpressure. The number of holes in the perforate of inner pipe no. 1 is less than that of inner pipe no. 2, because the stagnation pressure drop across the sudden expansion is half a dynamic head more as compared to the sudden contraction. The total backpressure of muffler configuration no. 1 is given by [1,97]:

$$\Delta p = Q_0^2 \left(R_1 + \frac{(R_2 + R_3)(R_4 + R_5)}{\left(\sqrt{(R_2 + R_3)} + \sqrt{(R_4 + R_5)}\right)^2} + R_6 \right) \tag{7.1}$$

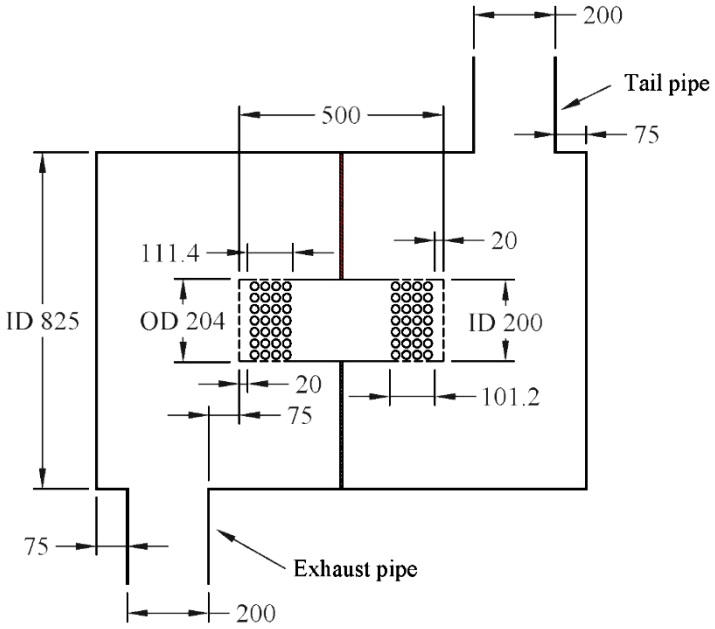

(a) Front sectional view

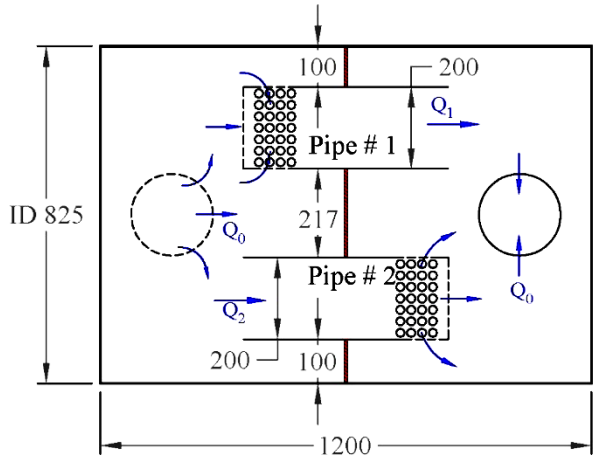

(b) Top sectional view

Figure 7.2. Schematic sectional views of muffler configuration no. 1 (two-chamber, one baffle and two-perforate Muffler) with flow distribution

The lumped flow resistance model has been verified experimentally; see for example, Refs. [64,97,100]. The total backpressure of the muffler shown in Fig. 7.2 works out to be 5.36 kPa. Mean flow Mach number in the exhaust/tail pipe of every muffler configuration is 0.168. Number of holes in perforates decides the grazing and bias flow Mach numbers which is crucial for better acoustic attenuation properties. Appendix H illustrates how the number of holes is decided in accordance with the requirement of nearly same back pressure of all muffler configurations.

Table 7.2. Details of perforates on the two parallel intermediate pipes of configuration no. 1

Perforated pipe	Number of rows of holes comprising the perforate	Number of holes in each row of the perforate	Number of holes on the end plate	Total number of holes in the perforate
Pipe no. 1	10	45	225	675
Pipe no. 2	11	45	225	720

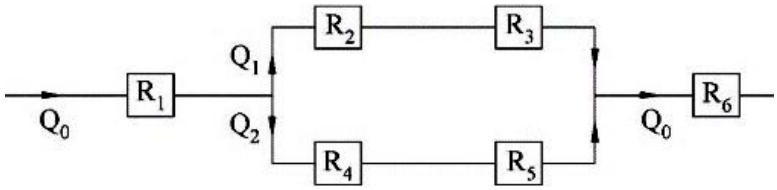

Figure 7.3. Lumped flow-resistance network diagram of configuration no. 1

Table 7.3. Description of flow resistances and flow distribution in configuration no. 1

Resistance	Description	$Q_i/Q_0(\%)$
R_1	Sudden area expansion from exhaust pipe to the left end chamber	100
R_2	Cross flow resistance of the perforated end of inner pipe no. 1	50.03
R_3	Sudden area expansion from inner pipe no. 1 to the right end chamber	50.03
R_4	Sudden area contraction from the left end chamber to inner pipe no. 2	49.97
R_5	Cross flow resistance of the perforated end of inner pipe no. 2	49.97
R_6	Sudden area contraction from the right end chamber to tail pipe	100

Table 7.4. Grazing and Bias mean flow Mach numbers in configuration no. 1

Perforated pipe	Mean grazing flow Mach number (M_g)	Mean bias flow Mach number (M_b)
Pipe no. 1	0.0551	0.1297
Pipe no. 2	0.0559	0.1381

The grazing and bias flow Mach number of different perforates of the muffler configuration shown in Fig. 7.2 are listed in Table 7.4.

The overall transfer matrix [T1] of the muffler configuration no. 1, relating the acoustic state variables at the upstream station of the muffler to the downstream station of the muffler as per electro-acoustic circuit given in Fig. 7.4 is given by:

$$\begin{bmatrix} p_u \\ v_u \end{bmatrix} = \left[P_{ep} \right]_{2\times2} \left[SAE_{ep\_LC} \right] \begin{bmatrix} 1 & 0 \\ 1/Z_{cL} & 1 \end{bmatrix} [T]_{2\times2} \begin{bmatrix} 1 & 0 \\ 1/Z_{cR} & 1 \end{bmatrix} \left[SAC_{RC\_tp} \right] \left[P_{tp} \right]_{2\times2} \begin{bmatrix} p_d \\ v_d \end{bmatrix} \quad (7.2)$$

where *P* is the transfer matrix of a uniform pipe and subscripts *ep* and *tp* represent exhaust pipe and tail pipe, respectively. SAE_{ep_LC} is the transfer matrix of sudden area expansion from the exhaust pipe to the left end chamber. SAC_{RC_tp} is the transfer matrix of sudden area contraction from the right end chamber to the tail pipe. Transfer matrices for the sudden area discontinuities are given by Eq. (F.4), and for the large sudden area contraction and expansion are given by Eqs. (F.7) and (F.8) of Appendix F, respectively. Z_{cL} and Z_{cR} are the impedances of quarter wave resonators at the left end and the right end of the muffler proper beyond the midpoint of side inlet and side outlet pipes, respectively. The transfer matrix [T] that relates the acoustic state variables at the upstream junction of the side inlet pipe in the left end chamber to those at the downstream junction of the side outlet pipe in the right end chamber is obtained using the Integrated Transfer Matrix (ITM) approach [65]. The TL spectrum of the configuration no. 1 muffler computed using the1-D plane wave analysis is compared against the 3-D FEM computed TL spectrum in Sec. 7.3.

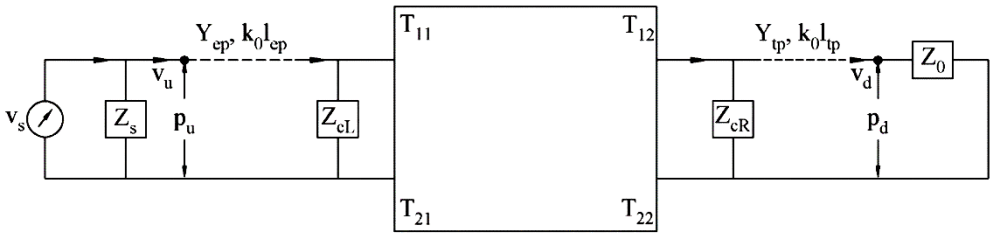

Figure 7.4. Electro-acoustic circuit diagram of configuration no. 1

7.1.2 Two-chamber, One-baffle and Four-perforate Muffler (C-2)

Figure 7.5 shows the schematic sectional views of the muffler configuration no. 2 with salient dimensions in mm. The details of perforates (shown in Fig. 7.5(b)) at the ends of the intermediate pipes no. 1 and no. 2 are given in Table 7.5.

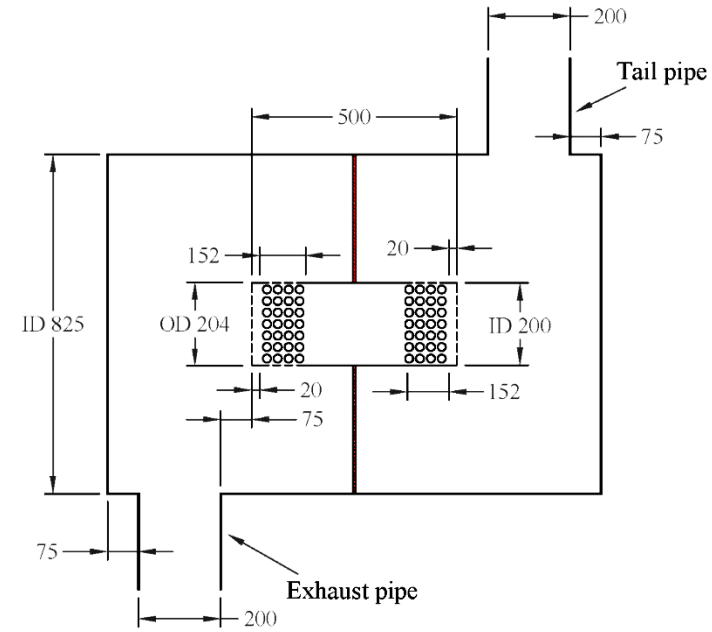

(a) Front sectional view

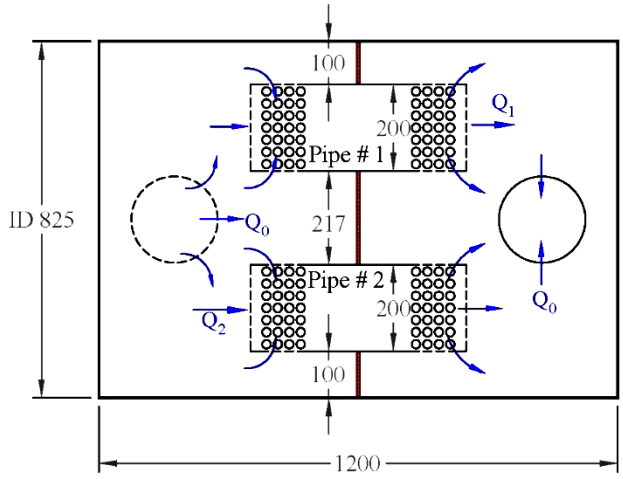

(b) Top sectional view

Figure 7.5. Schematic sectional views of configuration no. 2 (two-chamber, one-baffle and four-perforate Muffler) with flow distribution

In this muffler configuration, the flow, which enters the left end chamber of the muffler proper from the exhaust pipe, is divided into two parallel paths as shown in Fig. 7.5(b). The flow distribution analysis is carried out by using the lumped flow resistance network shown in Fig. 7.3. Description of the lumped flow resistances and the percentage of total flow through these resistances are given in Table 7.6. Equation (7.1) gives the total backpressure of the muffler configuration no. 2 and it works out to be 5.38 kPa. The grazing and bias flow Mach number of each perforate of muffler configuration shown in Fig. 7.5 are 0.0525 and 0.1037, respectively. Equation (7.2) gives the overall transfer matrix [T2] of the muffler configuration no. 2 as per electro-acoustic circuit given in Fig. 7.4. Here, the transfer matrix [T] that relates

the acoustic state variables at the upstream junction of the side inlet pipe in the left end chamber to those at the downstream junction of the side outlet pipe in the right end chamber can be obtained using the ITM approach [65].

Table 7.5. Details of perforates on perforate ends of intermediate pipes of configuration no. 2

Perforated pipe	Number of rows of holes comprising the perforate	Number of holes in each row of the perforate	Number of holes on the end plate	Total number of holes in the perforate
Pipe no. 1	15	45	225	900
Pipe no. 2	15	45	225	900

Table 7.6. Description of flow resistances and flow distribution in configuration no. 2

Resistance	Description	$Q_i/Q_0(\%)$
R_1	Sudden area expansion from exhaust pipe to the left end chamber	100
R_2	Cross flow resistance of the left end perforate of inner pipe no. 1	50
R_3	Cross flow resistance of the right end perforate of inner pipe no. 1	50
R_4	Cross flow resistance of the left end perforate of inner pipe no. 2	50
R_5	Cross flow resistance of the right end perforate of inner pipe no. 2	50
R_6	Sudden area contraction from the right end chamber to tail pipe	100

7.1.3 Two-chamber, One-baffle and Six-perforate Muffler (C-3)

Figure 7.6 shows the schematic sectional views of the muffler configuration no. 3 with salient dimensions in mm. The details of the perforates (shown in Fig. 7.6) at the end of the inlet pipe, the outlet pipe, the intermediate pipe no. 1 and the intermediate pipe no. 2 are given in Table 7.7. In contrast to the muffler configurations 1 and 2, the flow through the exhaust pipe in the muffler configuration no. 3 comes out from the perforated end, and the flow gets into the tail pipe through the perforated end, as shown in Fig. 7.6.

The flow distribution analysis is carried out by using the lumped flow resistance network shown in Fig. 7.3. Description of the lumped flow resistances and the percentage of total flow through these resistances is given in Table 7.8. Equation (7.1) gives the total backpressure of the muffler configuration no. 3 and it works out to be 5.30 kPa. The grazing and bias flow

Mach number of different perforates of the muffler configuration of Fig. 7.6 are listed in Table 7.9.

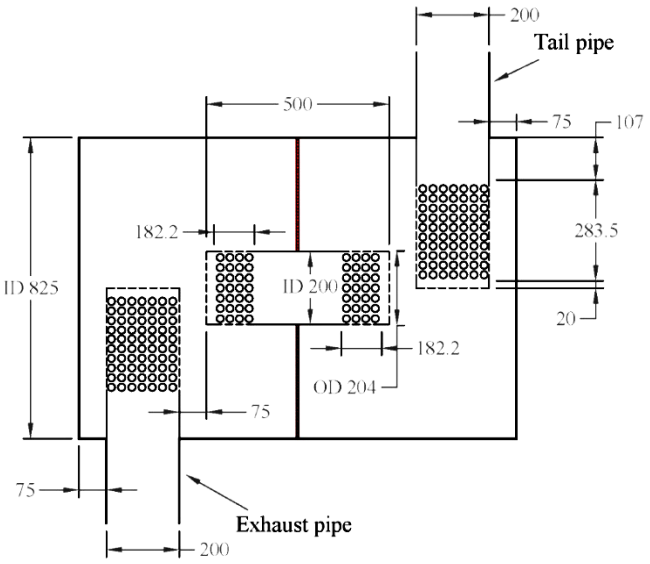

(a) Front sectional view

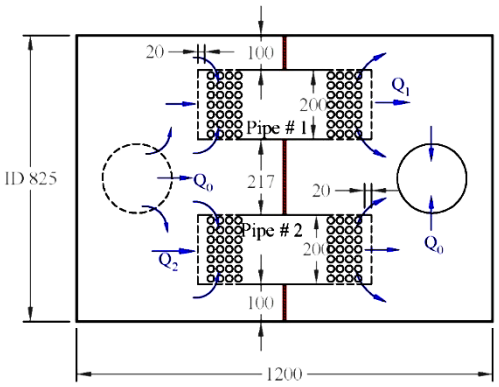

(b) Top sectional view

Figure 7.6. Schematic sectional views of configuration no. 3 (two-chamber, one baffle and six-perforate Muffler) with flow distribution

Equation (7.3) gives the overall transfer matrix [T3] of the muffler configuration no. 3 as per the electro-acoustic circuit shown in Fig. 7.7, which relates the acoustic state variables at the upstream station of the muffler to the downstream station of the muffler.

$$\begin{bmatrix} p_u \\ v_u \end{bmatrix} = \left[P_{ep}\right]_{2\times2} \begin{bmatrix} 1 & Z_{p,in} \\ 0 & 1 \end{bmatrix} \begin{bmatrix} 1 & 0 \\ 1/Z_{cL} & 1 \end{bmatrix} \left[T\right]_{2\times2} \begin{bmatrix} 1 & 0 \\ 1/Z_{cR} & 1 \end{bmatrix} \begin{bmatrix} 1 & Z_{p,out} \\ 0 & 1 \end{bmatrix} \left[P_{tp}\right]_{2\times2} \begin{bmatrix} p_d \\ v_d \end{bmatrix} \quad (7.3)$$

Here, the transfer matrix [T] that relates the acoustic state variables at the upstream junction of the side inlet pipe in the left end chamber to those at the downstream junction of the side outlet pipe in the right end chamber can be obtained using the ITM approach [65]. $Z_{p,in}$ and

$Z_{p,out}$ are the lumped perforate impedances of the side inlet and the side outlet perforate elements, respectively. In this chapter, the side inlet and the side outlet perforated elements are approximated by lumped perforate impedances. The plane wave propagation is assumed in the axial direction of chambers.

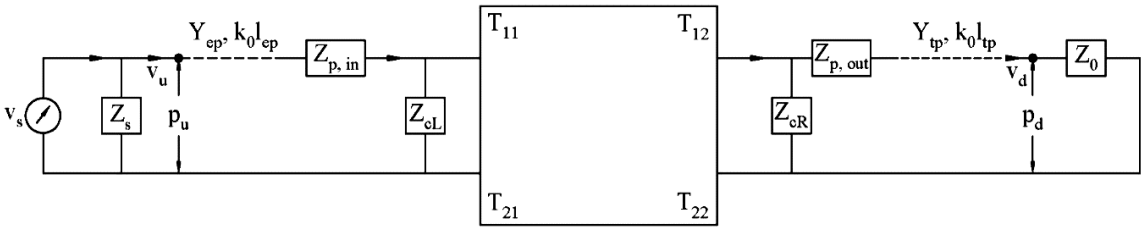

Figure 7.7. Electro-acoustic circuit diagram of configuration no. 3

Table 7.7. Details of perforates on perforated ends of inlet/intermediate/outlet pipes of configuration no. 3

Perforated pipe	Number of rows of holes comprising the perforate	Number of holes in each row of the perforate	Number of holes on the end plate	Total number of holes in the perforate
Exhaust	28	45	225	1485
Pipe no. 1	18	45	225	1035
Pipe no. 2	18	45	225	1035
Tail	28	45	225	1485

Table 7.8. Description of flow resistances and flow distribution in configuration no. 3

Resistance	Description	$Q_i/Q_0(\%)$
R_1	Cross flow resistance of the perforate on exhaust pipe	100
R_2	Cross flow resistance of the left perforated end of inner pipe no. 1	50
R_3	Cross flow resistance of the right perforated end of inner pipe no. 1	50
R_4	Cross flow resistance of the left perforated end of inner pipe no. 2	50
R_5	Cross flow resistance of the right perforated end of inner pipe no. 2	50
R_6	Cross flow resistance of the perforate on tail pipe	100

Table 7.9. Grazing and Bias mean flow Mach numbers in configuration no. 3

Perforated pipe	Mean grazing flow Mach number (M_g)	Mean bias flow Mach number (M_b)
Pipes no. 1 and no. 2 (intermediate pipes)	0.0511	0.0902
Inlet/Outlet pipes	0.0967	0.1257

7.1.4 Two-chamber, One perforated baffle and Six-perforate Muffler (C-4)

Figure 7.8 shows the schematic sectional views of the muffler configuration no. 4 with salient dimensions in mm. The details of the perforates (shown in Fig. 7.8) at the end of the inlet pipe, the outlet pipe, the intermediate pipe no. 1 and the intermediate pipe no. 2 are given in Table 7.10. The number of holes on the perforated baffle is double of the number of holes on each end of the two intermediate pipes. In contrast to the muffler configuration 3, the flow in the left end chamber of the muffler gets equally divided in two intermediate pipes and perforated baffle, as shown in Fig. 7.8(b). This muffler configuration is different from the other configurations on the basis of interaction of waves in the two end chambers.

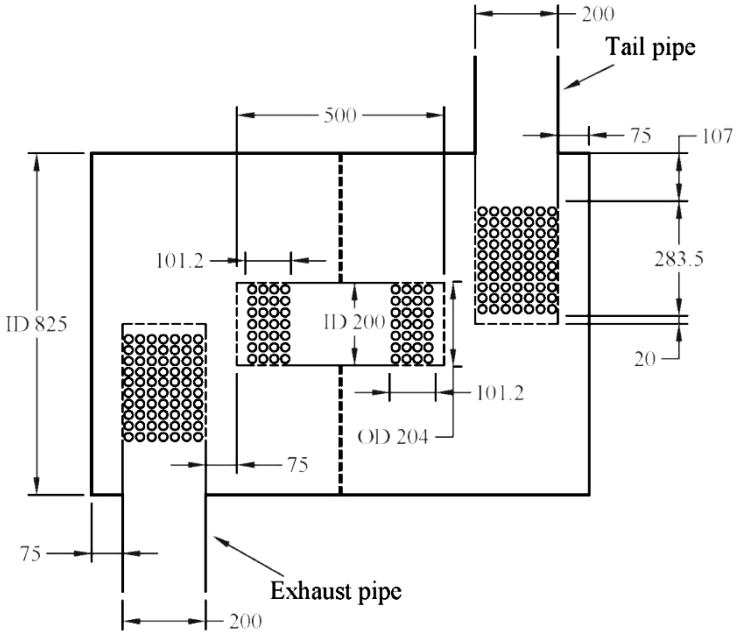

(a) Front sectional view

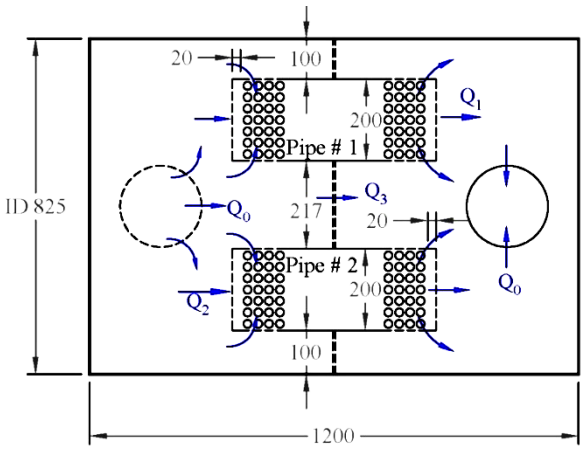

(b) Top sectional view

Figure 7.8. Schematic sectional views of configuration no. 4 (two-chamber, one perforated baffle and six perforate Muffler) with flow distribution

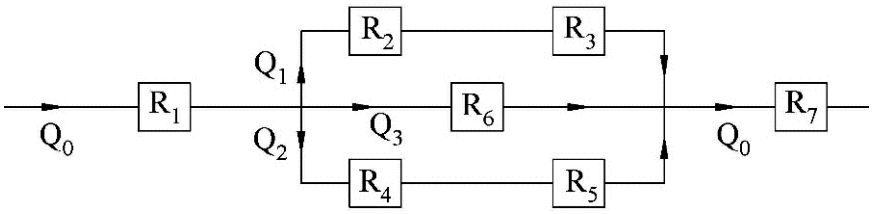

Figure 7.9. Lumped flow-resistance network diagram of configuration no. 4

Table 7.10. Details of perforates on perforated ends of inlet/intermediate/outlet pipes of configuration no. 4

Perforated pipe	Number of rows of holes comprising the perforate	Number of holes in each row of the perforate	Number of holes on the end plate	Total number of holes in the perforate
Exhaust	28	45	225	1485
Pipe no. 1	10	45	225	675
Pipe no. 2	10	45	225	675
Tail	28	45	225	1485

Table 7.11. Description of flow resistances and flow distribution in configuration no. 4

Resistance	Description	$Q_i/Q_0(\%)$
R_1	Cross flow resistance of the perforate on exhaust pipe	100
R_2	Cross flow resistance of the left perforated end of inner pipe no. 1	33.33
R_3	Cross flow resistance of the right perforated end of inner pipe no. 1	33.33
R_4	Cross flow resistance of the left perforated end of inner pipe no. 2	33.33
R_5	Cross flow resistance of the right perforated end of inner pipe no. 2	33.33
R_6	Cross flow resistance of the perforated baffle	33.33
R_7	Cross flow resistance of the perforate on tail pipe	100

The flow distribution analysis is carried out by using the lumped flow resistance network shown in Fig. 7.9. Description of the lumped flow resistances and the percentage of total flow through these resistances are given in Table 7.11. Equation (7.4) gives the total backpressure of the muffler configuration no. 4 and it works out to be 5.38 kPa. The grazing and bias flow Mach number in different perforates of the muffler configuration of Fig. 7.8 are listed in Table 7.12.

$$\Delta p = Q_0^2 \left(R_1 + \frac{1}{\left(1/\sqrt{(R_2+R_3)} + 1/\sqrt{(R_4+R_5)} + 1/\sqrt{R_6}\right)^2} + R_7 \right) \tag{7.4}$$

The overall transfer matrix [T4] of the muffler configuration no. 4 can be computed as Eq. (7.3) for muffler configuration no. 3 as per electro-acoustic circuit diagram shown in Fig. 7.7, where the transfer matrix [T] that relates the acoustic state variables at the upstream junction of the side inlet pipe in the left end chamber to those at the downstream junction of the side outlet pipe in the right end chamber can be obtained using the ITM approach [65] for the muffler configuration no. 4.

Table 7.12. Grazing and Bias mean flow Mach numbers in configuration no. 4

Perforated pipe/baffle	Mean grazing flow Mach number (M_g)	Mean bias flow Mach number (M_b)
Pipes no. 1 and no. 2 (intermediate pipes)	0.0373	0.0922
Inlet/Outlet pipes	0.0967	0.1257
Baffle	0	0.0461

7.2 3-D FEM convergence study

Transmission loss computation of any muffler using 3-D FEM by means of the commercial software package LMS Virtual Lab is discussed in the literature [63,80,84]. Computation of insertion loss (IL) calls for knowledge of the transfer matrix. In all these studies, the transmission loss computation is done by assuming anechoic termination. However, the computation of transfer matrix or the four-pole parameters of an acoustic element using the FEM by means of the LMS Virtual Lab was not reported in the literature [63,80,84]. In the present study, the computation of transfer matrix of an acoustic element using the concept of two load method is discussed in Appendix G. Once the transfer matrix of a muffler is computed using FEM, then assuming a suitable source impedance (anechoic source in the present case) and radiation impedance, the IL spectrum of a muffler can be computed.

The turnaround time for simulation by the 3-D FEM is much more than that with the 1-D plane wave analysis. For big mufflers, the computational cost of FEM using fine mesh for analysis can be too much. Fortunately, for an engine running at 1500 RPM, the maximum frequency of interest can be taken as 1000 Hz. λ is the wavelength corresponding to the maximum frequency of interest. Mesh with element size of $\lambda/6$ proved to be too coarse. In the present study, the linear (first order) tetrahedron elements of four different sizes, shown in the legend of Fig. 7.10, are taken for the convergence study. The number of nodes, the number of elements, and the

computational (CPU) time for the entire spectrum (200 frequency steps up to 1000 Hz) are given in Table 7.13.

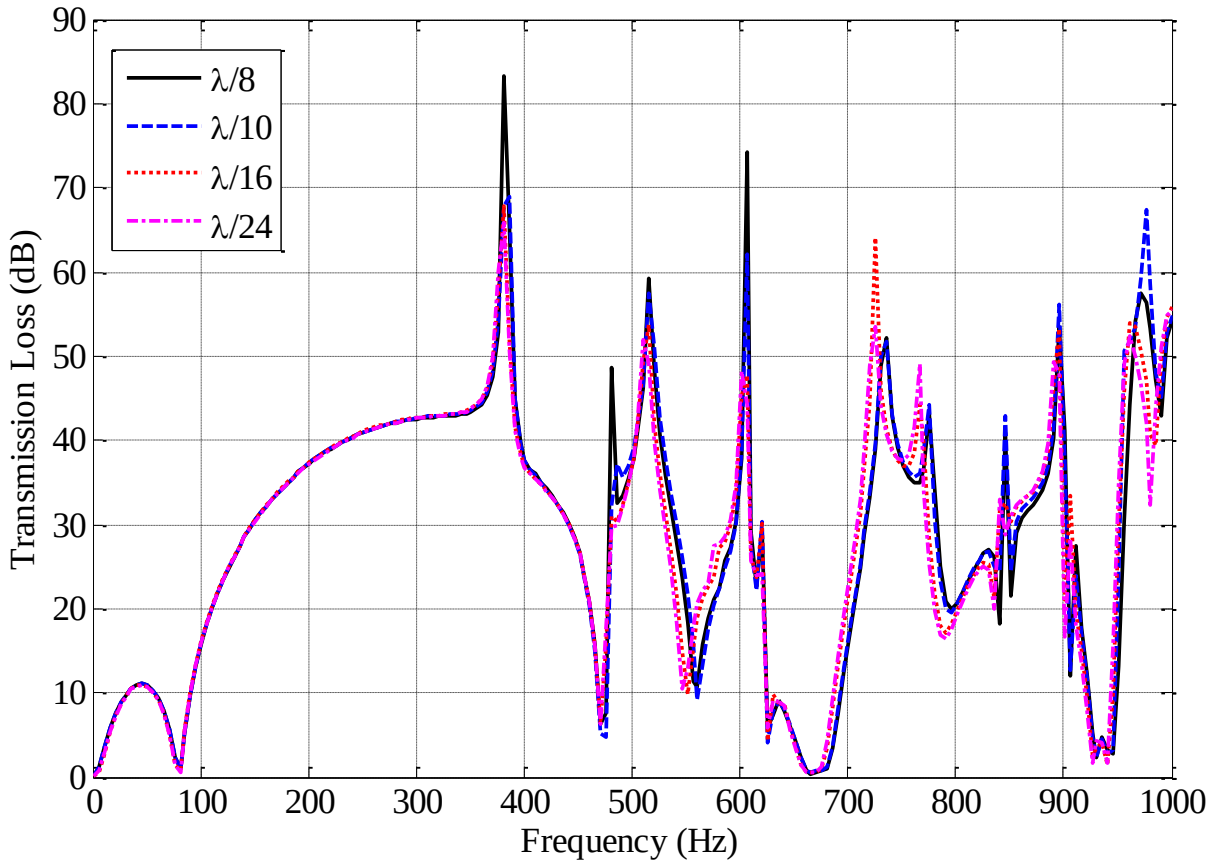

Figure 7.10. Effect of mesh size on the Transmission Loss spectra of configuration no. 1 computed by means of 3-D FEM analysis for the stationary medium case

Figures 7.11 and 7.12 show the iterations required for each frequency step and computation time for simulation at each frequency step, respectively. The relative tolerance for solving the system of linear equations generated by FEM is set at 10^{-10}. The finer the mesh size, the bigger is the size of matrices in a linear system of equations, which would require more iterations for the solution to converge.

It can be observed from Figs. 7.11 and 7.12 that with increment in frequency for each mesh size, the number of iterations and hence the computational time required at each frequency step increases in general. At the peaks and troughs of the TL spectra, the system of linear equations cannot be very stable, and that is why the computation at those frequencies takes more iterations/time for the solution to converge.

It is evident from Figs. 7.10–7.12 that the average mesh size $\lambda/10$ is a good trade-off between accuracy and computational cost. Hereafter, all 3-D simulations in this chapter are done using average mesh size of $\lambda/10$.

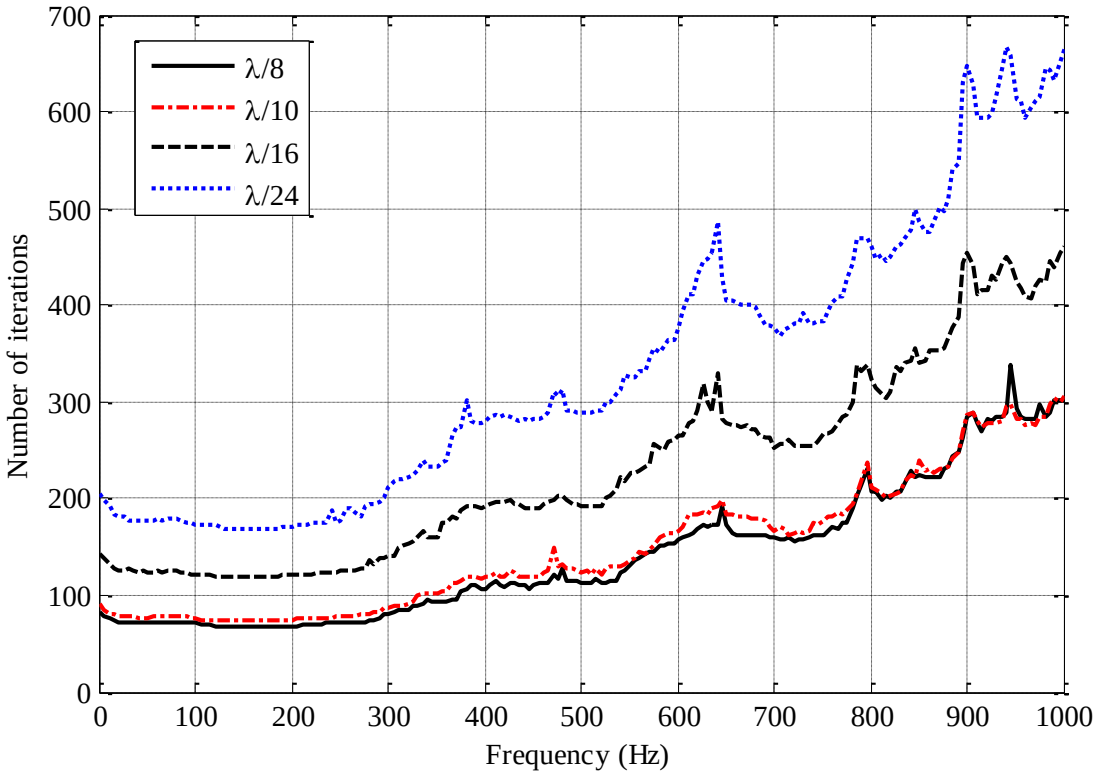

Figure 7.11. Effect of the mesh size on the number of iterations required for FEA as a function of frequency

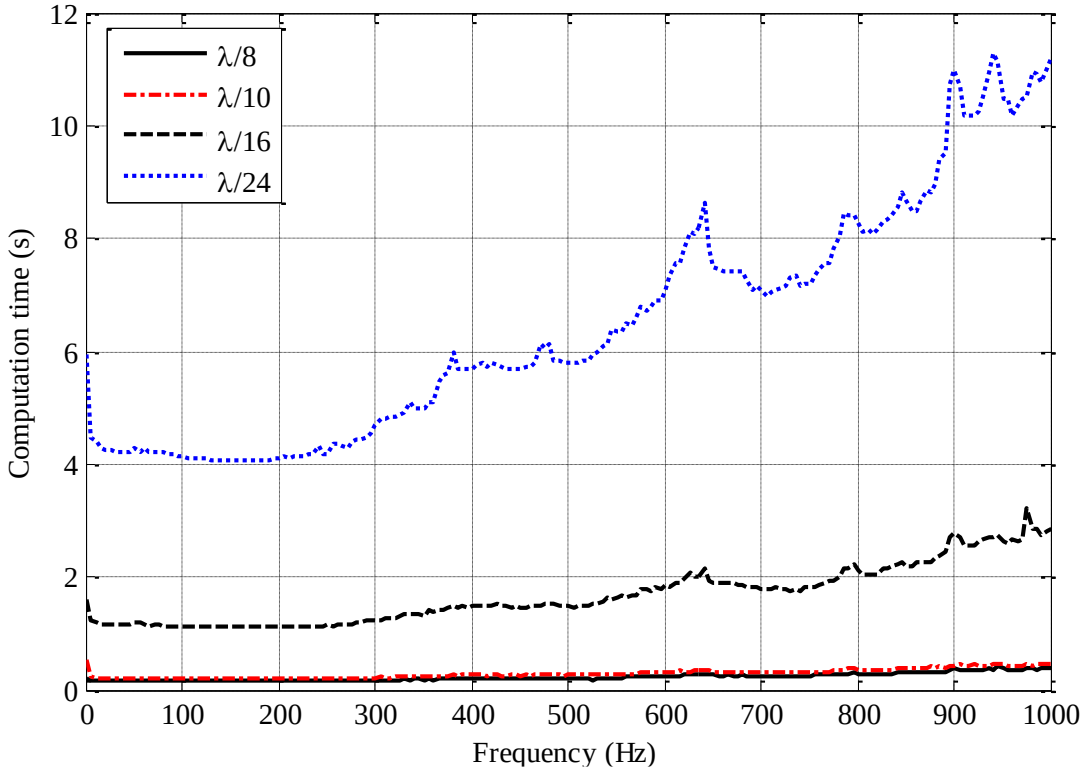

Figure 7.12. Effect of the mesh size on the computation time required for acoustic analysis as a function of frequency

Table 7.13. Description of different mesh sizes for simulation of configuration no. 1

Average mesh size	Number of nodes	Number of elements	Computational time* (in seconds)
$\lambda/8$	7022	33264	48.11
$\lambda/10$	8515	41320	64.39
$\lambda/16$	35722	184294	340.73
$\lambda/24$	101928	551844	1307.48

* A still more important consideration against the use of FEM is the turnaround time which includes the physical effort as well as the pre-processing time.

7.3 Comparison of TL spectra computed by different methods

The acoustic analysis done with the 1-D Integrated Transfer Matrix (ITM) method can be valid up to the cut-on frequency of a muffler. For the muffler configurations studied in this chapter, diameter of the shell is 825 mm, and the first azimuthal mode gets cut on at 401 Hz. It is clear from Figs. 7.13-7.15 that the 1-D ITM method predicted TL values for respective muffler configurations compare well up to the cut-on frequency except in the vicinity of first peak. This has happened because the plane wave propagation in the muffler's end chambers is assumed to be in axial direction. However, the propagation of waves is not in axial direction in the end chambers beyond 350 Hz (approximately) as observed in the 3-D FEM simulations of muffler configurations 1–3.

It can be noticed from Fig. 7.16 that the TL values computed by the 1-D ITM method compares well against 3-D FE method up to 300 Hz for muffler configuration no. 4. Figure 7.16 shows relative poor performance of muffler configuration no. 4 as compared to muffler configurations 1, 2 and 3. The reason of the relatively lower TL that the parallel paths decrease the mean flow grazing Mach numbers through perforated elements as can be noted from Subsections 7.1.1 to 7.1.4. The decrement in grazing flow Mach numbers decreases the equivalent resistance of perforated elements. Moreover, in muffler configuration no. 4, the bias mean flow Mach number through the holes on perforate is half as compared to the perforated ends of both intermediate pipes. This is a demerit of a design feature where the flow gets divided among the perforated pipe segment and the perforated baffle as indicated in Chapter 6.

It can be observed that the 1-D ITM method is not suitable for acoustic analysis of mufflers studied in this chapter beyond a couple of engine harmonics. Therefore, only the 3-D FEM

analysis should be used for analysis of large SISO perforated element mufflers. The muffler can however be synthesized using the design criteria from the 1-D ITM results.

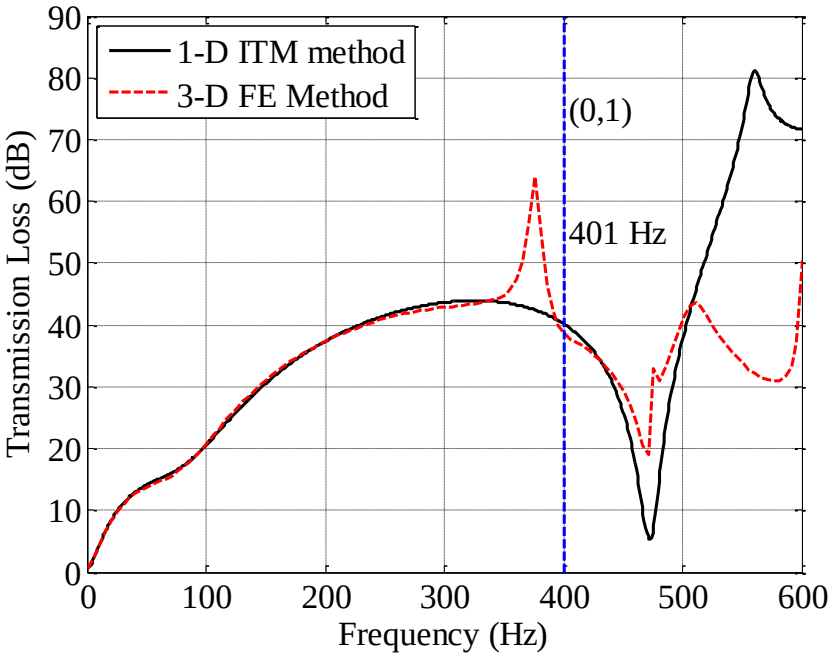

Figure 7.13. Comparison of TL spectra of configuration no. 1 computed by the 1-D ITM method and the 3-D FE method for the moving medium case (M_{ep} = 0.168).

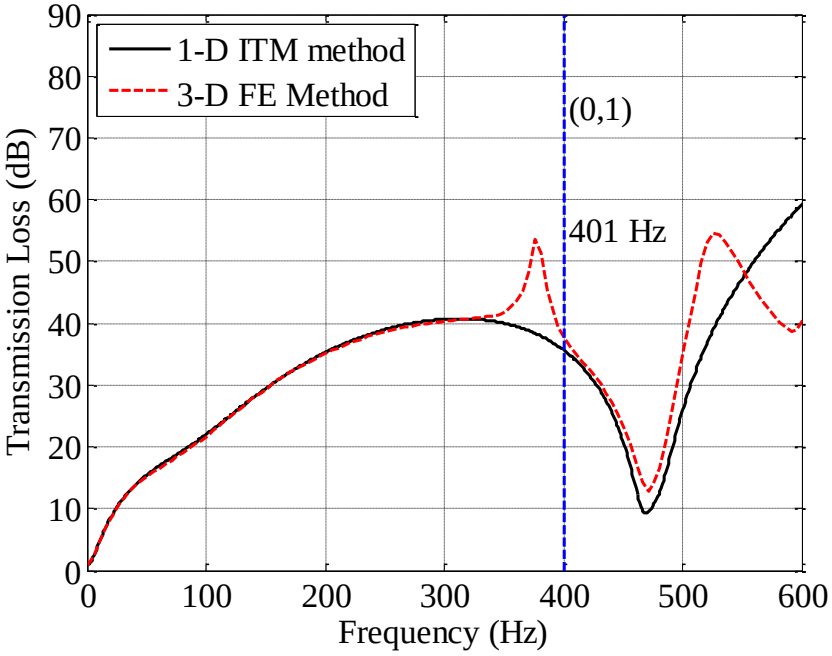

Figure 7.14. Comparison of TL spectra of configuration no. 2 computed by the 1-D ITM method and the 3-D FE method for the moving medium case (M_{ep} = 0.168).

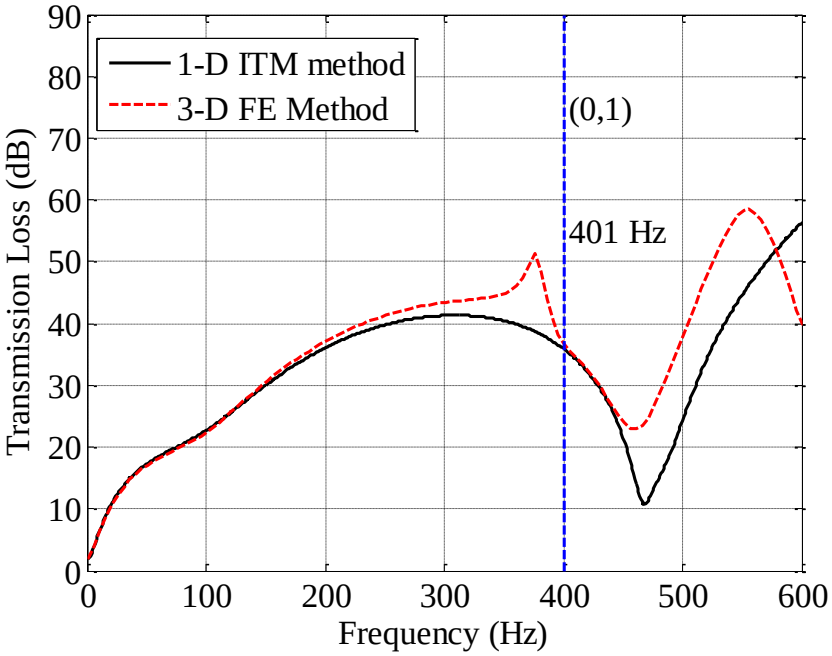

Figure 7.15. Comparison of TL spectra of configuration no. 3 computed by the 1-D ITM method and the 3-D FE method for the moving medium case (M_{ep} = 0.168).

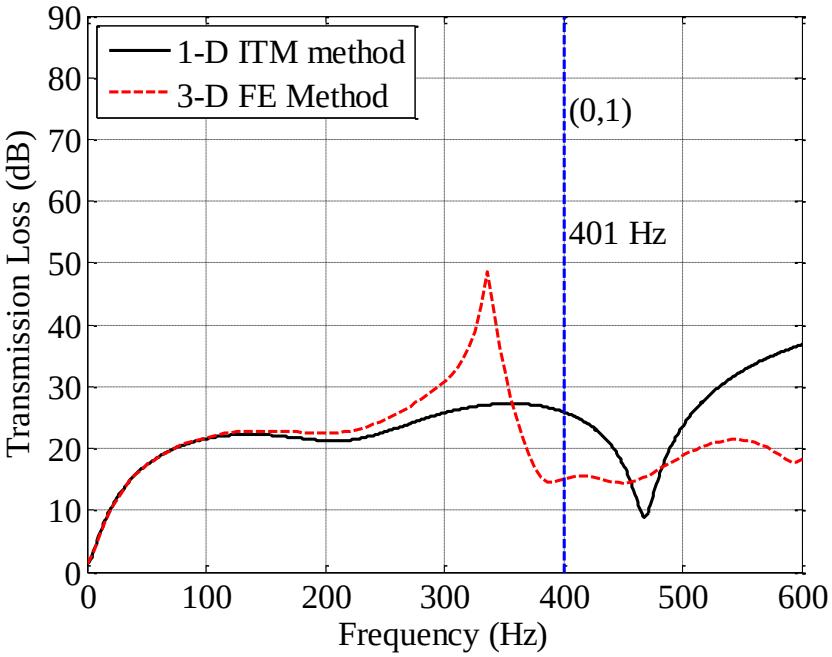

Figure 7.16. Comparison of TL spectra of configuration no. 4 computed by the 1-D ITM method and the 3-D FE method for the moving medium case (M_{ep} = 0.168).

7.4 Effect of mean flow on all SISO configurations

The true performance measure of a muffler is insertion loss, IL [1]. The effect of mean flow on acoustic attenuation properties of the cross-flow perforated element mufflers is one of the crucial factors for their usage in silencing the internal combustion engine exhaust system as illustrated in Chapter 6. The 3-D FEM computed IL spectra with respect to a reference pipe of 1 m length and 0.2 m diameter are shown in Figs. 7.17–7.20 for muffler configurations 1–4, respectively. The lengths of the exhaust pipe and tail pipe for all muffler configurations are 0.6 m and 1 m, respectively. The IL spectra of all four muffler configurations are computed with anechoic source assumption, which implies that the source impedance is equal to the characteristic impedance of the exhaust pipe [1,33].

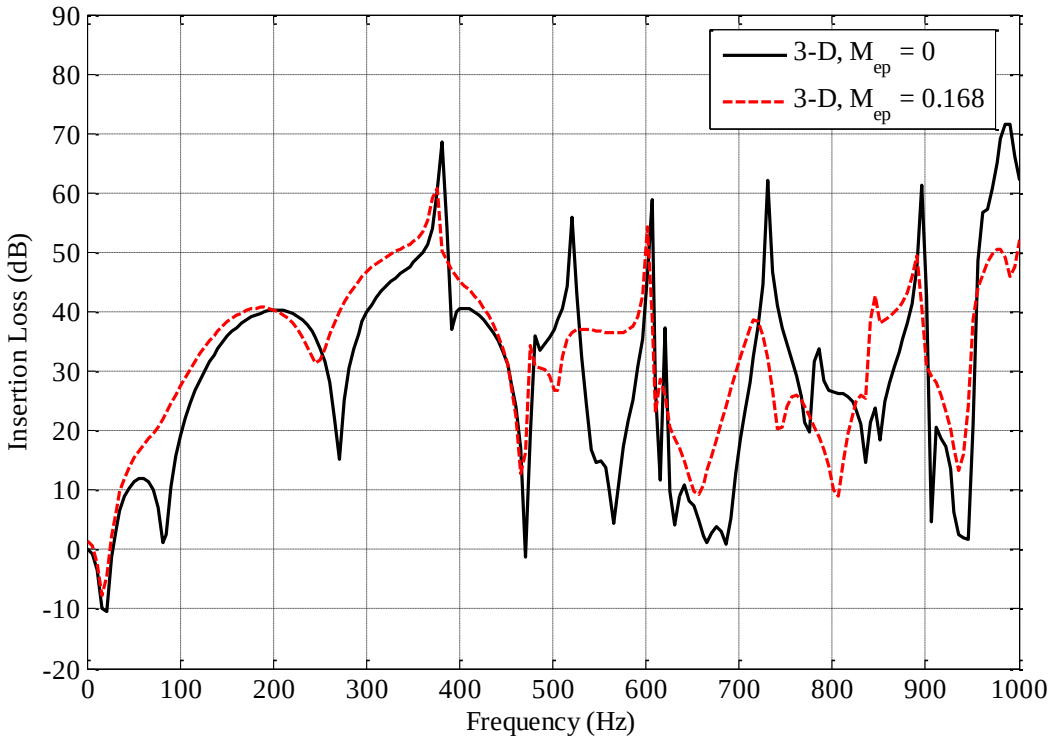

Figure 7.17. Effect of mean flow on the IL spectra of configuration no. 1.

The presence of mean flow in muffler substantially increases the perforate resistances due to aeroacoustic losses that are known to lift the troughs and lower the peaks of attenuation characteristics spectra (TL and IL spectra). This is confirmed by Figs. 7.17–7.20. Experimental validation of the effect of mean flow on the TL spectrum of a perforated element muffler has been provided by Elnady *et al*. [64]. Logarithmic (rather, anti-logarithmic) addition of decibels implies that lifting the IL troughs would increase the overall insertion loss of the muffler

notwithstanding lowering of the peaks in the IL spectrum. The effect of mean flow on the IL spectrum of muffler configuration 3 is more as compared with the other configurations.

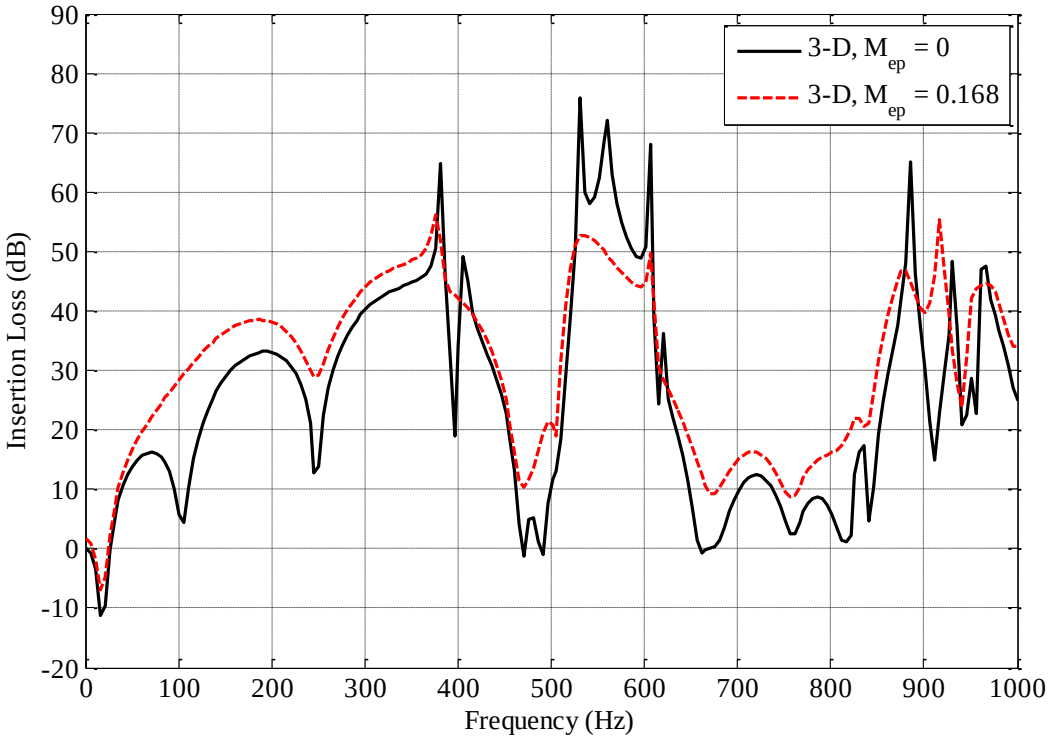

Figure 7.18. Effect of mean flow on the IL spectra of configuration no. 2.

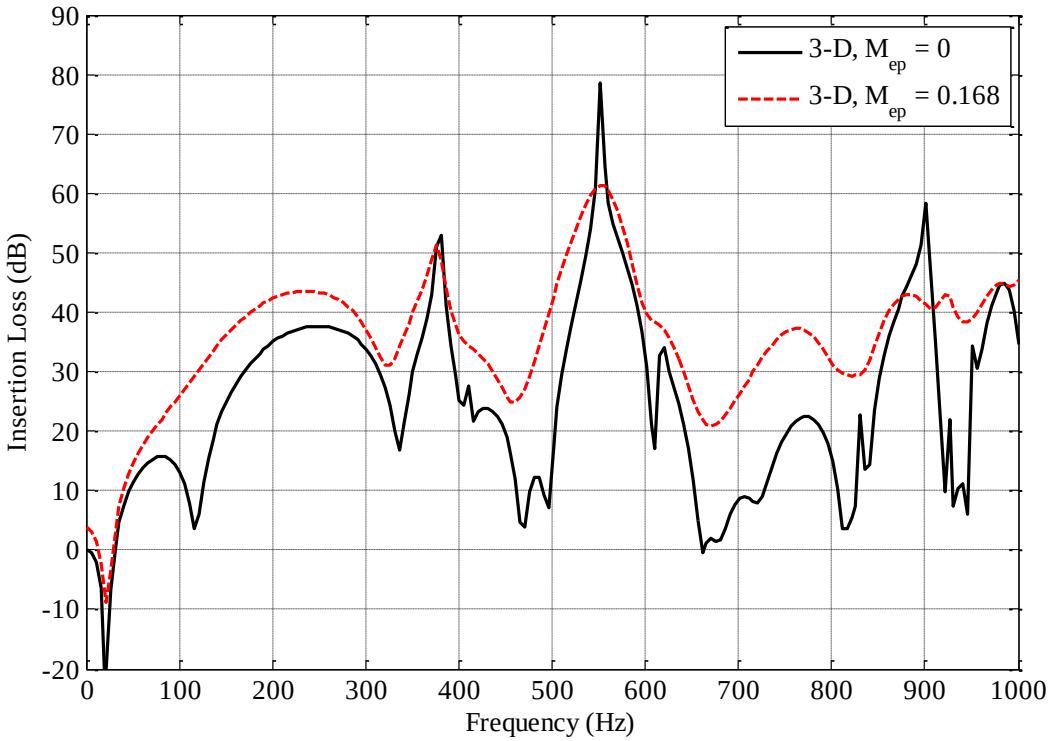

Figure 7.19. Effect of mean flow on the IL spectra of configuration no. 3.

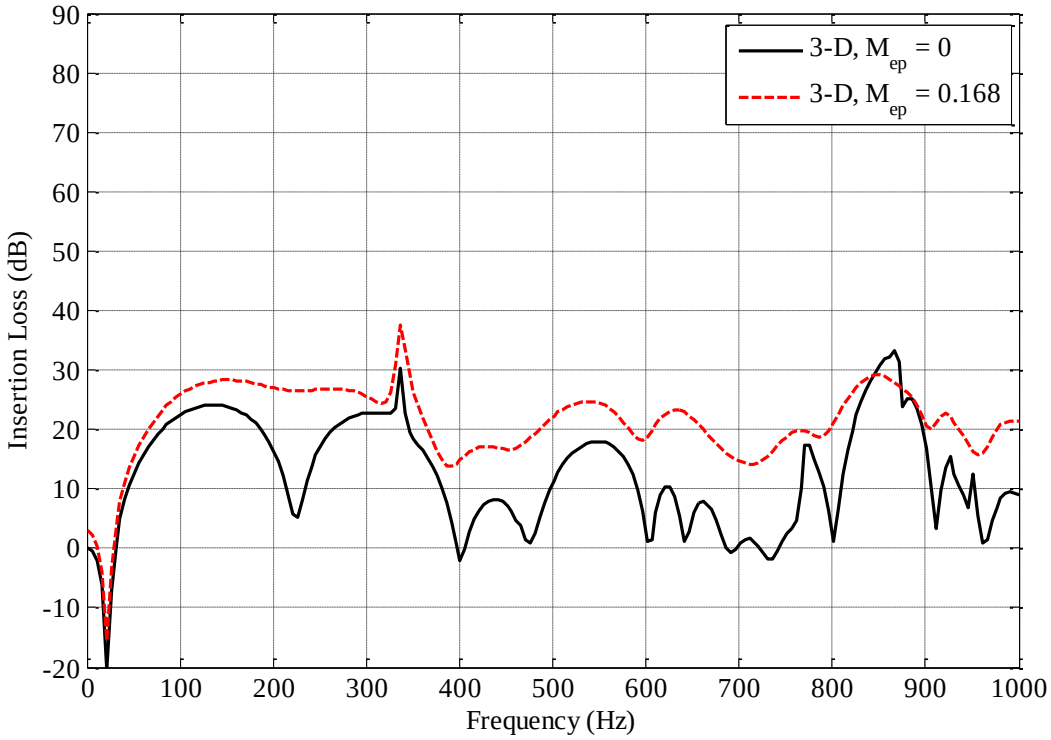

Figure 7.20. Effect of mean flow on the IL spectra of configuration no. 4.

7.5 Comparative study of all four SISO muffler configurations

It is clear from the preceding sections that dependable acoustic analysis of these mufflers in the presence of mean flow can be done by 3-D FEM only. Thus, the TL and IL spectra computed by 3-D FEM analysis of all four configurations for the moving medium (M_{ep} = 0.168) case are shown in Figs. 7.21 and 7.22, respectively. In general, the TL and IL values of muffler configuration no. 4 is inferior to the other configurations. The first peak and the first trough of the TL spectra of muffler configurations 1, 2 and 3 are in the vicinity of one another. The first peak of the TL spectrum of muffler configuration no. 4 occurs at a frequency that is about 40 Hz lower than the first peak of configurations 1, 2 and 3, because of the interaction of waves in both end chambers due to perforated baffle. It is interesting to note that TL and IL values of muffler configuration no. 3 are generally better than those of the other three configurations. Significantly, the IL values for muffler configuration no. 3 are above 20 dB for the entire frequency range from 80 Hz to 1000 Hz, and therefore this configuration should be the designer's choice.

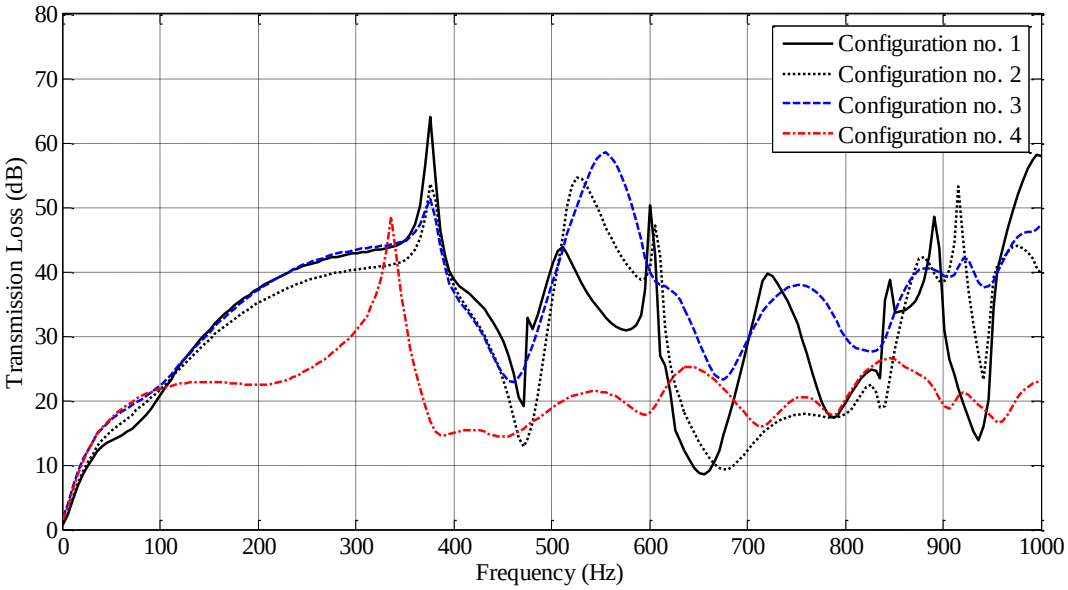

Figure 7.21. Comparison of the TL spectra of the four perforated element mufflers

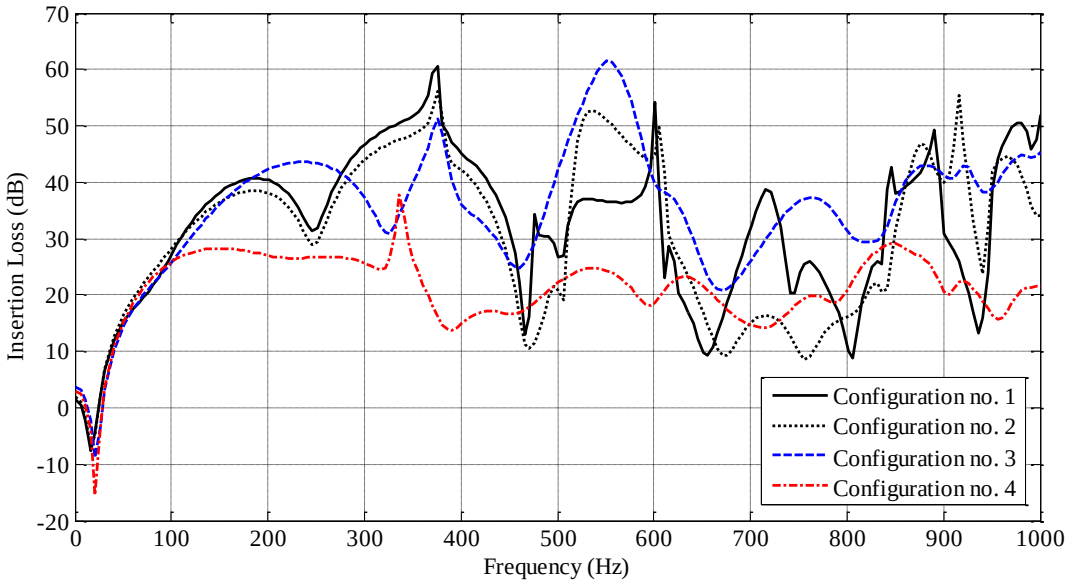

Figure 7.22. Comparison of the IL spectra of the four perforated element mufflers

7.6 Conclusions and design guidelines

- The flow-acoustic resistance due to the bias-flow through the holes of a perforate introduces high acoustic damping which substantially raises the troughs of the TL-spectrum and IL-spectrum of the muffler. This feature significantly increases the overall IL (or noise attenuation) of the muffler as implied in the algebra of anti-logarithmic addition of the muffled (and unmuffled) SPL at different speed orders. Thus, mean flow plays a crucial role in the side inlet/side outlet type muffler configuration investigated in this chapter.

- Configuration no. 1 is marginally better than configuration no. 2 in some frequency regions and vice-versa. However, for most of the frequencies configuration no. 3 is better than configurations no. 2 and no. 4 because IL troughs are raised by several decibels. This indicates that for a given overall backpressure, additional perforates at the inlet and outlet pipe, as provided in configuration no. 3, would raise the IL troughs and thence the overall IL of a muffler.
- 3-D FEM has been used here to find out the upper frequency limit of the applicability of the 1-D ITM method. This limit turns out to be about 400 Hz for the large mufflers considered here. Therefore, the muffler configuration designed from basic considerations listed above should be validated against the 3-D FEM predictions before prototyping and testing on the engine test bed.
- Having adopted configuration no. 3, for a given limit on backpressure of the muffler, the number of holes in each perforate can be calculated as illustrated in Appendix H.
- It is well known that the bigger the cavities (and thence volume of the muffler shell), the higher the overall IL of the muffler. In the absence of the space constraint above a DG set enclosure and requirement of high IL (over 25 dB), the shell volume has been taken to be as high as 20 times the engine capacity.

Chapter 8

Conclusion

8.1 Summary

In the present research work, a novel direct evaluation method is proposed for estimation of acoustic source characteristics of the internal combustion (IC) engines' exhaust systems. Design and analysis of some complex commercial muffler configurations are also carried out in this thesis. The issue of the judicious use of perforated elements to have better acoustic attenuation properties as well as modest backpressure are studied in detail.

Theory of this direct evaluation method for estimation of acoustic source impedance of a naturally aspirated (NA) single-cylinder engine is discussed in Chapter 2. The parametric expression of normalized acoustic source impedance has also been developed for prediction of insertion loss (IL) of mufflers.

Application of the direct evaluation method is extended in Chapter 3 for estimation of source characteristics of a two-cylinder engine exhaust system. It is shown to predict the unmuffled sound pressure level (SPL) spectrum which compares well with the measured spectrum. Application of the direct evaluation method is extended to turbocharged (T/C) engines using the transfer matrix of the turbine derived in terms of turbine pressure ratio in Chapter 4.

A typical double-flow reversal multiply-connected chamber muffler of a motorcycle engine is analysed in Chapter 5. It is shown that for such complex muffler the 1-D ITM approach can be used to predict TL spectrum up to 1600 Hz that compared well with 3-D computed spectrum.

Analysis of multiply-connected co-axial (MCCA) mufflers is demonstrated in Chapter 6, where it is shown that the ultra-small size mufflers can also give modest overall IL (dBA). The size of mufflers used to be a concern for the automotive engines (on-road or off-road vehicles) because of lack of sufficient space under the vehicle. However, bigger size mufflers can be used for diesel generator (DG) set engines on the top of the acoustic canopy. This location calls for the side-inlet side-outlet configuration (SISO) mufflers. The peculiar problem of the analysis of the perforated side-inlet/outlet pipes, is addressed in Chapter 7 by suggesting a 1-D ITM analysis for frequencies up to the cut-on of the first higher mode.

8.2 Salient contributions

At the end of each of the Chapters 2 to 7, conclusions of the respective Chapters were discussed. However, the notable contributions of the present research work are listed below:

1) The difficulties and demerits of direct evaluation methods and mutli-load indirect methods are removed by the method proposed in this thesis. *Normalized source resistance and reactance components of a single-cylinder engine downstream of exhaust valve turn out to be smooth functions of frequency that allow simple algebraic fits.*

2) Parametric studies have been conducted for different engine speeds and different cylinder capacities for the full engine load condition. *The source impedance of a single -cylinder engine is shown to remain almost the same for different engine speeds. The parametric expression of source impedance of a single-cylinder engine running at full load is given in terms of cylinder capacity and frequency.*

3) Computation of the exhaust gas mass flow rate discharging from cylinders to a typical exhaust system requires the acoustic pressure and acoustic mass velocity to satisfy the acoustic load impedance of typical exhaust system downstream of the exhaust valve. *The harmonic balance method is successfully applied to the IC engine for cylinders discharging to a typical exhaust system*.

4) The estimated source impedance using the results of simplified time-domain simulation for cylinders discharging to an ideal pressure release boundary condition or to a typical exhaust system turns out to be almost equal. However, the estimated source strength level is shown to differ considerably for two different discharge systems. *The source characteristics estimated even in the framework of the novel direct evaluation method presented here are not unique, as would be expected for a nonlinear time-variant source.*

5) The predicted unmuffled SPL spectra using the estimated source characteristics for two different discharge conditions have a similar trend and compare well with the measured spectrum. Therefore, *the ideal pressure release boundary condition at the downstream*

end of the exhaust valve can be used which further simplifies the estimation of the acoustic source characteristics of IC engines using the present method.

6) The acoustic modelling of the turbine and compressor of a turbocharger are done assuming the isentropic expansion and compression occurs across a planar discontinuity, respectively. This simplified acoustic model of turbocharger does not incorporate the wave propagation inside the turbine and compressor. However, it has been shown to be handy. *The simplified acoustic model of the turbine and compressor yields transfer matrices in terms of their respective static pressure ratios.*

7) *Normalized source impedance estimated just downstream of the exhaust valve of each cylinder turns out to be more or less independent of the number of cylinder constituting the engine. It indicates that the source impedance at the beginning of the exhaust pipe is a function of the geometry (physical dimensions) of the runner, manifold, turbine, etc.*

8) The source characteristics of each cylinder of an IC engine are computed using the present method. These are then combined and transferred across the manifold (runners) and turbine to estimate the source characteristics of the complete engine at any desired source-load junction. The present method requires basic geometrical details with pressure and temperature of the in-cylinder gas at the blowdown condition (exhaust valve opening). *Thus, an approximate unmuffled exhaust SPL spectrum can be known before even the prototyping of an engine, and thus design and analysis of engine and muffler can be integrated.*

9) The bias mean flow through the perforated pipes/baffles gives considerable acoustic impedance even at low frequencies which is one of the key factors for the use of perforated elements with plug flow. However, the same boon becomes a bane when stagnation pressure drop due to high flow resistance is considered. *However, the use of perforated baffle between the two different perforated segments is shown to have better acoustic attenuation properties due to Herschel-Quincke tube effect (selective phase cancellation) and lesser stagnation pressure drop due to the division of flow in parallel paths.*

10) The higher mean flow Mach number has always been associated with more jet noise. However, the expression of limiting Mach number considering a desired net insertion loss is not reported in the literature. *In the present study, the limiting Mach number values have been derived for the automotive engines as well as the DG set engines.*

11) Transfer matrix across the *n*-parallel tubes is derived in the literature. However, to the best of the Author's knowledge, no such transfer matrix relation is available for the *n*-parallel generalized acoustic elements in the literature. *An appropriate transfer matrix has now been derived in this thesis.*

12) Side-inlet side-outlet (SISO) mufflers are generally used for DG set engines. *In this thesis, the use of 1-D plane wave analysis is extended to the end chambers with side-inlet/outlet perforated pipes.*

8.3 Suggestions for future work

In the present research work, the application of the novel direct evaluation method is carried out only for the IC engine exhaust system. Parametric study on the source impedance of a single cyinder engine is done for the full load conditions for different engine capacities and engine speeds. However, no parametric study has been carried out for the source strength level (SSL).

In many engines, the intake noise also becomes the decisive factor when the exhaust noise is attenuated to a greater extent using the well-designed mufflers.

Consequently, further studies can be carried out on the following research topics:

1) Parametric study on the exhaust source characteristics of a cylinder of the naturally aspirated and turbocharged engines in terms of the engine speed (RPM), the average power delivered per cylinder and the cylinder capacity.

2) Application of the direct evaluation method presented here in order to estimate the intake source characteristics of the naturally aspirated as well as turbocharged engines.

3) A similar parameteric study for intake source characteristics as mentioned above for the exhaust source characteristics.

4) Improved analytical modelling of acoustics of the turbine and compressor of a turbocharger which would consider wave propagation in the turbine and compressor, as well as the static pressure ratio.

5) Analysis of large and medium size side-inlet side-outlet mufflers with internal absorptive lining.

Appendix A: Time Domain Simulation of the Engine Exhaust Process

The flows through poppet valves in the cylinder are modelled as one-dimensional quasi-steady isentropic compressible flow [101]. In the isentropic flow, it is assumed that the flow is brought from the stagnation state to the present state of the flow. The isentropic mass flow rate in a cross-section of area *A* is given by [101]

$$\dot{m} = A\frac{p_o}{\sqrt{RT_o}}\left[\frac{2\gamma}{\gamma-1}\left\{\left(\frac{p}{p_o}\right)^{2/\gamma} - \left(\frac{p}{p_o}\right)^{(\gamma+1)/\gamma}\right\}\right]^{1/2} \tag{A.1}$$

However, the flow through the valves of a cylinder cannot be isentropic, and thus the real gas flow effects are included by means of an experimentally determined discharge coefficient C_D. The discharge coefficient value depends on the reference area taken for the mass flow rate computation. Several different reference areas are the valve head area $\pi D_v^2/4$, the port area at the valve seat $\pi D_p^2/4$, the geometrical minimum flow area as described in Appendix B, and the valve curtain area $\pi D_v L_v$, where L_v is the valve lift. The product of reference area A_R and corresponding discharge coefficient C_D is termed as the effective flow area of the valve assembly. The expression for the mass flow rate through the valves of cylinder is given by [101]

$$\dot{m} = C_D A_R \frac{p_o}{\sqrt{RT_o}}\left[\frac{2\gamma}{\gamma-1}\left\{\left(\frac{p}{p_o}\right)^{2/\gamma} - \left(\frac{p}{p_o}\right)^{(\gamma+1)/\gamma}\right\}\right]^{1/2} \tag{A.2}$$

where p_o and T_o are the upstream stagnation pressure and temperature, respectively, and p is the downstream static pressure (assumed equal to the pressure at the valve). When the flow is choked, the Mach number of mean flow for the effective area will be unity. In fact, it will be unity at the minimum flow area in the valve section. The condition for the choked flow is given by [101]

$$\frac{p_o}{p} \geq \left(\frac{\gamma+1}{2}\right)^{\gamma/(\gamma-1)} \tag{A.3}$$

and the mass flow rate for the choked flow through valves is given by

$$\dot{m} = C_D A_R \sqrt{\frac{\gamma}{RT_o}} p_o \left(\frac{\gamma+1}{2}\right)^{0.5(1+\gamma)/(1-\gamma)} \tag{A.4}$$

For the choked flow the pressure, temperature and density at the valve are independent of the pressure, temperature and density at the downstream section, and these are given by [101]

$$p_v = p_o \left(\frac{2}{\gamma+1}\right)^{\gamma/(\gamma-1)} \tag{A.5}$$

$$T_v = T_o \left(\frac{2}{\gamma+1}\right) \tag{A.6}$$

$$\rho_v = \rho_o \left(\frac{2}{\gamma+1}\right)^{1/(\gamma-1)} \tag{A.7}$$

In the normal direction of flow out through the exhaust valve and reverse direction of flow through the intake valve, the stagnation properties are of the in-cylinder gas. However, in the reverse direction of flow through the exhaust valve and normal direction of flow through the intake valve the stagnation properties are of the respective runners. The stagnation properties of the fluid are local to the flow, and these properties of the flow in the intake and exhaust ports can be obtained using the mean flow Mach number (M) in the respective valve ports.

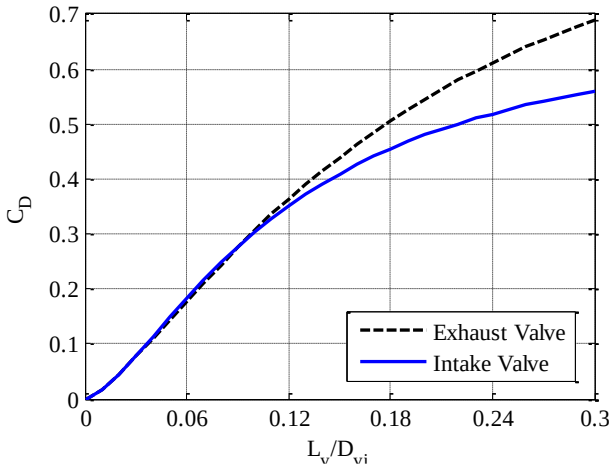

Figure A.1. The discharge coefficients of valve for inner valve seat area as reference area

In the present study, the inner valve seat area is taken as the reference area, and several engines from the AVL example manual are considered to observe the variation of discharge coefficient with respect to the normalised valve lift (ratio of valve lift to valve seat inner diameter). The CurveExpert Professional software version 2.4.0 has been used for fitting the

values of discharge coefficients of the intake and exhaust valves with DR-Hill-Zerobackground model of non-linear fits. Equation (A.8) gives the value of discharge coefficient for the intake and exhaust valves with respect to the normalised valve lift (ratio of valve lift to valve seat inner diameter). Figure A.1 shows the variation of discharge coefficients for the exhaust and intake valves.

$$C_D = \begin{cases} \dfrac{1.07\left(L_v/D_{vi}\right)^{1.3754}}{0.1054+\left(L_v/D_{vi}\right)^{1.3754}} & \text{Exhaust Valve} \\ \dfrac{0.7\left(L_v/D_{vi}\right)^{1.5055}}{0.0407+\left(L_v/D_{vi}\right)^{1.5055}} & \text{Intake Valve} \end{cases} \tag{A.8}$$

By making use of the energy balance of the cylinder, mass balance of the control volume in the cylinder, equation of state for an ideal gas, and with assumption of adiabatic flow through the exhaust and intake valves, and assuming that the specific heat constant of the in-cylinder gas is equal to that of the intake and exhaust gases, the following relation is derived in Ref. [16]:

$$\frac{\dot{p}_c}{p_c} = \gamma\left(\frac{\dot{m}_c}{m_c} - \frac{\dot{V}_c}{V_c}\right) \tag{A.9}$$

where the rate of change of the in-cylinder gas mass is given by

$$\dot{m}_c = \dot{m}_{in} - \dot{m}_{ex} \tag{A.10}$$

Assuming that the in-cylinder gas mass and its rate of change at the current step is known, and applying the forward difference scheme for the rate of change of the in-cylinder gas pressure, the current step's in-cylinder gas pressure is given by

$$p_{c,n} = \frac{p_{c,n-1}}{1-\gamma\dfrac{\Delta\theta}{\omega}\left(\dfrac{\dot{m}_{c,n}}{m_{c,n}} - \dfrac{\dot{V}_{c,n}}{V_{c,n}}\right)} \tag{A.11}$$

where $\omega = 2\pi \times RPM/60$ is the angular frequency of the crankshaft. RPM is number of revolutions per minute of the crankshaft.

As the starting point is the exhaust blowdown, the in-cylinder mass at any instant is given by

$$m_{c,n} = m_{EVO} + \int_{EVO}^{\theta_n} \frac{\dot{m}_c}{\omega} d\theta \tag{A.12}$$

The volume of a cylinder and its rate of change are analytically known, and these are given by [101]

$$V_{c,n} = \frac{V_s}{2}\left[\frac{CR+1}{CR-1} + \frac{l}{r} - \cos\theta_n - \left\{\left(\frac{l}{r}\right)^2 - \sin^2\theta_n\right\}^{1/2}\right] \tag{A.13}$$

$$\dot{V}_{c,n} = \frac{dV_c}{d\theta}\frac{d\theta}{dt} = \omega \left.\frac{dV_c}{d\theta}\right|_{\theta=\theta_n} \tag{A.14}$$

where V_s is the cylinder swept volume, *CR* is the compression ratio, *l* is the length of the connecting rod, *r* is the crank radius and θ is the crank angle with respect to the top dead centre (TDC). However, it is evident from Eqs. (A.2) and (A.10) that the rate of change of the in-cylinder gas mass depends on the current step value of the in-cylinder gas pressure. The in-cylinder gas mass depends on the current step value of change of the in-cylinder gas mass rate, as is evident from Eq. (A.12). The steps to compute the in-cylinder gas state variables and the mass flow rate through valves are given in Section 2.2.

Appendix B: Poppet Valve Geometry and Minimum Flow Area

In internal combustion engines, the exhaust valves as well as intake valves are of the poppet type. Figure B.1 shows the poppet valve schematic with the parameters defining its geometry.

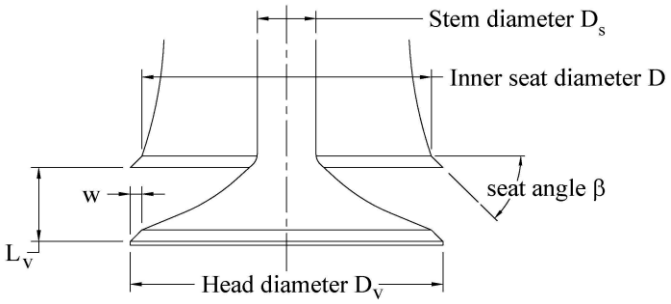

Figure B.1. Parameters defining the poppet valve geometry

The instantaneous valve flow area depends on the valve lift and the geometrical details of the valve head, seat, and stem. The flow area development has three stages as the valve lift increases, as shown in Figure B.2. The expression for valve flow area for three stages are given in Eqs. (B.1), (B.2) and (B.3) [101].

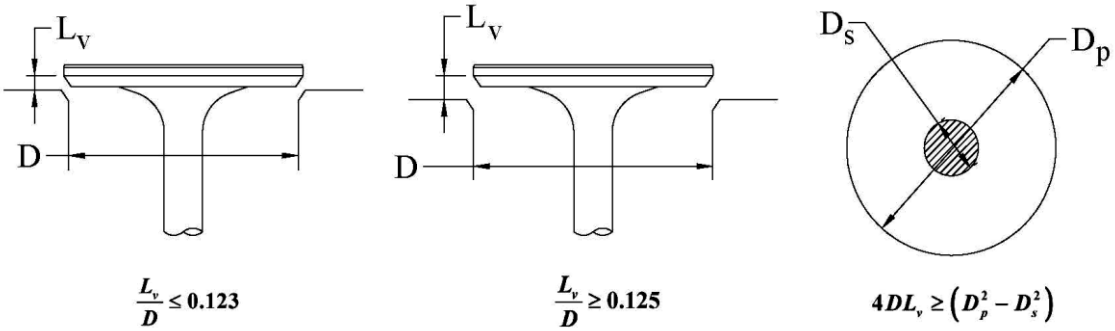

Figure B.2. Schematic showing the three stages of the valve lifts

Stage 1: $\dfrac{w}{\sin\beta\cos\beta} > L_v > 0$

$$A_m = \pi L_v \cos\beta\left(D_v - 2w + 0.5L_v \sin 2\beta\right) \tag{B.1}$$

Stage 2: $\left[\left(\dfrac{D_p^2 - D_s^2}{4D_m}\right)^2 - w^2\right]^{1/2} + w\tan\beta \ge L_v > \dfrac{w}{\sin\beta\cos\beta}$

$$A_m = \pi D_m\left[\left(L_v - w\tan\beta\right)^2 + w^2\right]^{1/2} \tag{B.2}$$

Stage 3: $L_v > \left[\left(\frac{D_p^2 - D_s^2}{4D_m} \right)^2 - w^2 \right]^{1/2} + w\tan\beta$

$$A_m = 0.25\pi\left(D_p^2 - D_s^2\right) \quad \text{(B.3)}$$

Appendix C: Engine Specifications

The specifications of the AVL BOOST example manual single-cylinder naturally aspirated (NA) 500 cc gasoline engine used in this investigation are given in Table C.1 [102].

Table C.1. Single-cylinder naturally aspirated 4-stroke gasoline engine specifications

Parameter	**Values**	**Parameter**	**Values**
Bore	84 mm	Stroke	90 mm
Connecting-rod length	174.5 mm	Compression ratio	9
Intake valve opening (IVO)	41.5^0 before TDC	Exhaust valve opening (EVO)	74.8^0 before TDC
Intake valve closing (IVC)	89.6^0 after BDC	Exhaust valve closing (EVC)	30.2^0 after BDC
Intake valve inner seat diameter	40 mm	Exhaust valve inner seat diameter	34.8 mm
Intake valve maximum lift	9.78 mm	Exhaust valve maximum lift	9.68 mm
Intake runner diameter	34 mm	Exhaust runner diameter	31 mm

The specifications of the 15 kVA diesel generator set (DG-Set) two-cylinder, naturally aspirated engine running at 1500 RPM are given in Table C.2.

Table C.2. 15 kVA DG-Set two-cylinder 4-stroke naturally aspirated engine specifications

Parameter	**Value**	**Parameter**	**Value**
Bore	100 mm	Stroke	120 mm
Connecting-rod length	206 mm	Compression ratio	18
Blowdown pressure	4.4 bar	Volumetric efficiency	90 %
Blowdown temperature	965 K	Exhaust gas temperature	691 K
Length of acoustic test load	1107 mm	Diameter of acoustic test load	76 mm
Intake valve opening (IVO)	43^0 before TDC	Exhaust valve opening (EVO)	87.5^0 before BDC
Intake valve closing (IVC)	68^0 after BDC	Exhaust valve closing (EVC)	39.5^0 after TDC
Intake valve inner seat diameter	45 mm	Exhaust valve inner seat diameter	39.5 mm
Intake port diameter	38.6 mm	Exhaust port diameter	33.1 mm
Intake valve stem diameter	7.96 mm	Exhaust valve stem diameter	7.94 mm
Intake valve seat width	1.9 mm	Exhaust valve seat width	1.95 mm
Intake valve seat angle	45 degree	Exhaust valve seat angle	45 degree
Intake valve maximum lift	10.41 mm	Exhaust valve maximum lift	10.55 mm

The specifications of the 20 kVA DG-Set two-cylinder, naturally aspirated engine running at 1500 RPM are given in Table C.3.

Table C.3. 20 kVA DG-Set two-cylinder 4-stroke naturally aspirated engine specifications

Parameter	**Value**	**Parameter**	**Value**
Bore	105 mm	Stroke	120 mm
Connecting-rod length	216 mm	Compression ratio	18
Blowdown pressure	6 bar	Volumetric efficiency	90 %
Blowdown temperature	1316 K	Exhaust gas temperature	712 K
Length of acoustic test load	829 mm	Diameter of acoustic test load	76 mm
Intake valve opening (IVO)	43^0 before TDC	Exhaust valve opening (EVO)	86.5^0 before BDC
Intake valve closing (IVC)	66^0 after BDC	Exhaust valve closing (EVC)	39.5^0 after TDC
Intake valve inner seat diameter	40.48 mm	Exhaust valve inner seat diameter	39.3 mm
Intake port diameter	38.9 mm	Exhaust port diameter	35 mm
Intake valve stem diameter	7.94 mm	Exhaust valve stem diameter	7.92 mm
Intake valve seat width	2.05 mm	Exhaust valve seat width	0.8 mm
Intake valve seat angle	30 degree	Exhaust valve seat angle	45 degree
Intake valve maximum lift	10.44 mm	Exhaust valve maximum lift	10.58 mm

The specifications of the 200 kVA DG-Set six-cylinder, 4-valve, turbocharged aftercooled engine running at 1500 RPM are given in Table C.4.

Table C.4. 200 kVA DG-Set six-cylinder 4-stroke turbocharged engine specifications

Parameter	**Value**	**Parameter**	**Value**
Bore	118 mm	Stroke	135 mm
Connecting-rod length	248 mm	Compression ratio	15.5
Blowdown pressure	9.8 bar	Blowdown temperature	1042 K
Boost pressure ratio	3.0	Turbine pressure ratio	2.2
Turbocharger shaft speed	10,900 RPM	Number of turbine blades	11
Intake valve opening (IVO)	27^0 before TDC	Exhaust valve opening (EVO)	70^0 before BDC
Intake valve closing (IVC)	39^0 after BDC	Exhaust valve closing (EVC)	24^0 after TDC
Intake valve inner seat diameter	36 mm	Exhaust valve inner seat diameter	33.6 mm
Intake port diameter	32.8 mm	Exhaust port diameter	30.6 mm
Intake valve stem diameter	7.2 mm	Exhaust valve stem diameter	6.1 mm
Intake valve seat width	2 mm	Exhaust valve seat width	1.5 mm
Intake valve seat angle	30 degree	Exhaust valve seat angle	45 degree
Intake valve maximum lift	11.09 mm	Exhaust valve maximum lift	11.07 mm

Appendix D: Transfer and Combination of Source Characteristics

Estimation of the source characteristics of a multi-cylinder engine requires the transfer of source characteristics from just downstream of the exhaust valves to the upstream end of the exhaust manifold junction and then a combination of these characteristics to evaluate the source characteristics at the downstream end of the manifold junction.

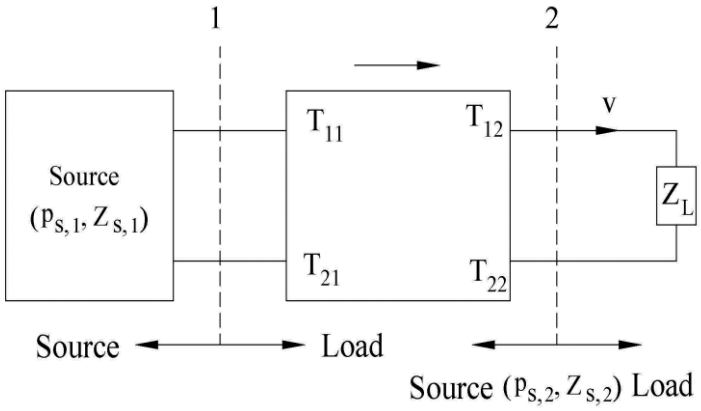

Figure D.1. Transfer of source characteristics from station 1-1 to station 2-2 [44]

The schematic of the transfer of source characteristics from upstream station 1-1 to the downstream station 2-2 is shown in Fig. D.1. The relations between the source characteristics at station 1-1 to those at station 2-2 are expressed as [44]

$$p_{s,2} = \frac{p_{s,1}}{T_{11} + T_{21} Z_{s,1}} \tag{D.1}$$

$$Z_{s,2} = \frac{T_{12} + T_{22} Z_{s,1}}{T_{11} + T_{21} Z_{s,1}} \tag{D.2}$$

Figure D.2 shows the combination of two sources into a single equivalent source. The combined source pressure and source impedance at a junction are given by [44]

$$p_{s,3} = \frac{p_{s,1} Z_{s,2} + p_{s,2} Z_{s,1}}{Z_{s,1} + Z_{s,2}} \tag{D.3}$$

$$Z_{s,3} = \frac{Z_{s,1} Z_{s,2}}{Z_{s,1} + Z_{s,2}} \tag{D.4}$$

In Figs. D.2 (b) and (c), load impedance Z_L applies at section 3-3 in Fig. D.2(a). It is related to $Z'_{L,i}$ as

$$Z_L = \frac{A_3 Z'_{L.i} + B_3}{C_3 Z'_{L.i} + D_3} \tag{D.5}$$

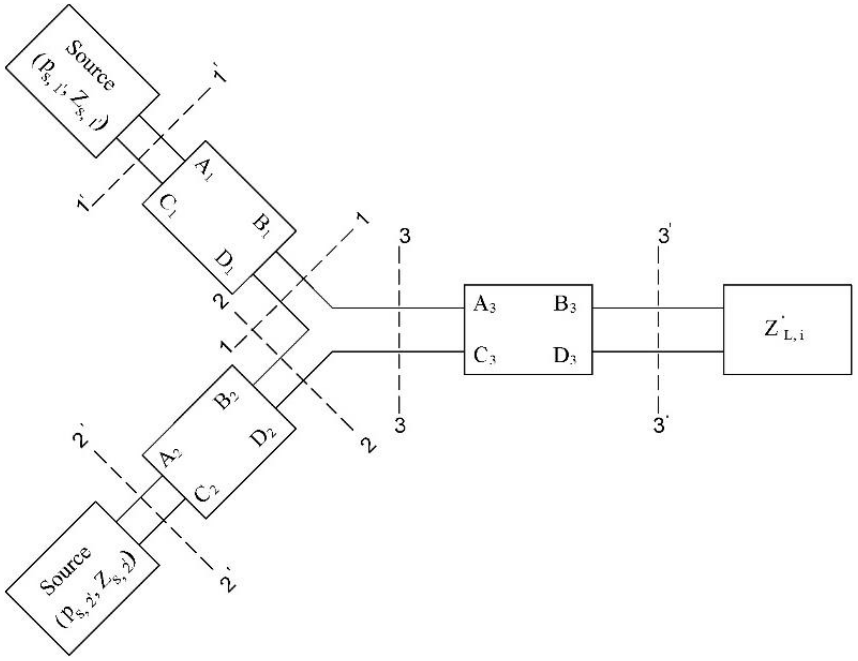

(a)

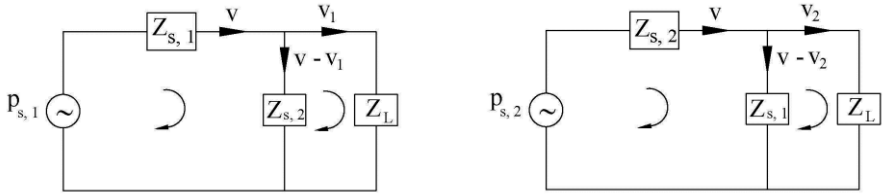

(b) (c)

Figure D.2. Combining two sources into a single-equivalent source [44]. (a) Schematic diagram of a system with two sources; (b) analogous circuit for the junction with source 1 only and (c) analogous circuit for the junction with source 2 only

Combined source pressure (p_s) and impedance (Z_s) of *n* sources at a junction are given by [44]

$$p_s = \frac{\sum_{i=1}^{n} p_{s,i} / Z_{s,i}}{\sum_{i=1}^{n} 1 / Z_{s,i}} \tag{D.6}$$

$$Z_s = \frac{1}{\sum_{i=1}^{n} 1 / Z_{s,i}} \tag{D.7}$$

Appendix E: Lumped Flow Resistances

Flow resistance for sudden area changes (contraction and expansion) are given by Eqs. (E.1) and (E.2), respectively [1].

$$R_c = \frac{1}{2}\frac{\rho_0}{S^2}\times\frac{1}{2}\left(1-\frac{S_d}{S_u}\right) \tag{E.1}$$

$$R_e = \frac{1}{2}\frac{\rho_0}{S^2}\times\left(1-\frac{S_u}{S_d}\right)^2 \tag{E.2}$$

Here, S is the smaller of the two areas S_d and S_u the cross-sectional areas of the downstream pipe and upstream pipe, respectively. ρ_0 is the density of the medium.

Perforate flow resistance for cross flow is given by [64]

$$R_{CF} = \frac{1}{2}\frac{\rho_0}{\left(C_D S_p\right)^2}, S_p = n_h \times \frac{\pi}{4} d_h^2 \tag{E.3}$$

where S_p is the perforate area, n_h is number of holes, d_h is the hole diameter, and C_D is the coefficient of discharge of hole orifices which is assumed to be 0.817, following Elnady *et al*. [64].

Flow resistance due to pipe friction is given by [1]

$$R_{PF} = \frac{1}{2}\frac{\rho_0}{S^2}\times\frac{fL}{D} \tag{E.4}$$

where S is the cross-sectional area of the uniform pipe, L is the length of pipe, D is the diameter of the pipe, and f is the frictional factor which is taken as 0.0358, following Neighuk *et al*. [103].

Appendix F: Transfer Matrix of Sudden Area Discontinuities

The sudden area contraction and expansion are shown in Fig. F.1. The upstream and downstream stations are represented by 2 and 1, respectively.

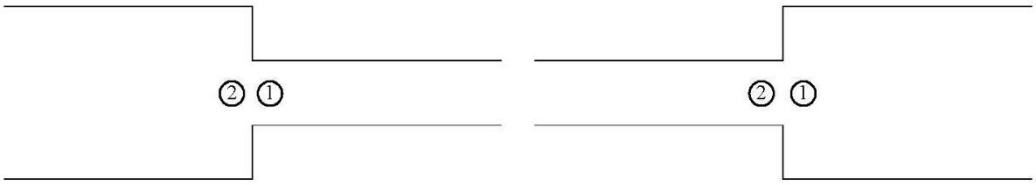

(a) (b)

Figure F.1. Sudden area discontinuities: (a) Contraction; (b) Expansion

The transfer matrix which relates the aeroacoustic variables at a sudden discontinuity is given by [1]

$$\begin{bmatrix} p_{c,2} \\ v_{c,2} \end{bmatrix} \simeq \begin{bmatrix} 1 & KM_1Y_1 \\ 0 & 1 \end{bmatrix} \begin{bmatrix} p_{c,1} \\ v_{c,1} \end{bmatrix} \tag{F.1}$$

where M_1 is the mean flow Mach number in the downstream pipe and Y_1 is the characteristic impedance of downstream pipe. K is the loss factor which is given by Eq. (F.2) for sudden contraction and sudden expansion.

$$K = \begin{cases} \frac{1}{2}\left(1 - \frac{S_d}{S_u}\right) & \text{for sudden contraction} \\ \left(\frac{S_d}{S_u} - 1\right)^2 & \text{for sudden expansion} \end{cases} \tag{F.2}$$

The relation between aeroacoustic and classical acoustic state variables is given by [1]

$$\begin{bmatrix} p_c \\ v_c \end{bmatrix} = \begin{bmatrix} 1 & MY_0 \\ M/Y_0 & 1 \end{bmatrix} \begin{bmatrix} p \\ v \end{bmatrix} \tag{F.3}$$

where M and Y_0 are the mean flow Mach number and the characteristic impedance of the pipe, respectively. Equation (F.4) gives the transfer matrix for a sudden discontinuity in terms of the classical acoustic variables [1].

$$\begin{bmatrix} p_2 \\ v_2 \end{bmatrix} = \frac{1}{1-M_2^2} \begin{bmatrix} 1 & -M_2 Y_2 \\ -M_2/Y_2 & 1 \end{bmatrix} \begin{bmatrix} 1 & KM_1 Y_1 \\ 0 & 1 \end{bmatrix} \begin{bmatrix} 1 & M_1 Y_1 \\ M_1/Y_1 & 1 \end{bmatrix} \begin{bmatrix} p_1 \\ v_1 \end{bmatrix} \tag{F.4}$$

Relation between M_1, M_2, Y_1 and Y_2 are given in Eqs. (F.5) and (F.6).

$$\frac{M_1}{Y_1} = \frac{M_2}{Y_2} \tag{F.5}$$

$$M_2 Y_2 = M_1 Y_1 \left(\frac{S_1}{S_2} \right)^2 \tag{F.6}$$

Using Eqs. (F.2), (F.4), (F.5) and (F.6) and considering $M_1^2, M_2^2 \ll 1$, after a little algebraic manipulation, transfer matrices of large sudden area contraction and expansion are given by Eqs. (F.7) and (F.8).

$$\begin{bmatrix} p_2 \\ v_2 \end{bmatrix} = \begin{bmatrix} 1 & 1.5 M_1 Y_1 \\ 0 & 1 \end{bmatrix} \begin{bmatrix} p_1 \\ v_1 \end{bmatrix} \tag{F.7}$$

$$\begin{bmatrix} p_2 \\ v_2 \end{bmatrix} = \begin{bmatrix} 1 & -M_2 Y_2 \\ 0 & 1 \end{bmatrix} \begin{bmatrix} p_1 \\ v_1 \end{bmatrix} \tag{F.8}$$

Appendix G: 3-D Finite Element Analysis

Acoustic analysis of muffler in 3-D has been done by means of the FEM based software package LMS Virtual Lab [104]. The entire acoustic domain of the muffler has been discretized into finite elements. The use of variational formulation for the acoustic system yields the governing equations [104]

$$\left\{\left[M\right]-k_0^2\left[K\right]+\mathrm{j}\rho_0\omega\left[C\right]\right\}\left\{p_n\right\}=-\mathrm{j}\rho_0\omega\left\{F\right\}, \tag{G.1}$$

where [*M*], [*K*] and [*C*] are the inertia, stiffness and damping matrices, respectively. Symbols, k_0, ω, and ρ_0 represent the wave number, angular frequency and density of the medium, respectively. **{***F***}** is the vector of the nodal acoustic forces, which is determined by the boundary conditions. Vector $\left\{p_n\right\}$ comprises of nodal acoustic pressures.

For obtaining the transmission loss of muffler using the 3-D FEM, two boundary conditions are applied:

i. u = -1 m/s (arbitrarily chosen value of the particle velocity at the inlet end, i.e., at the start of exhaust pipe, and the negative sign indicate that the outward normal is in opposite direction to the particle velocity);

ii. acoustic impedance $\xi=\rho_0 c_0$ at the outlet of tail pipe that gives the anechoic termination, where c_0 is the speed of sound.

For perforated pipes and baffles, if one wanted to do the acoustic analysis then the size of the mesh in holes has to be kept very small which would make the analysis very cumbersome and time-consuming. However, in LMS Virtual Lab, the perforated pipe and baffle can be replaced by two surfaces (inner surface and outer surface), separated by a gap equal to the thickness of pipe or baffle as the case may be. In order to maintain continuity and to capture the effect of holes, an impedance relation is applied between the inner and the outer surfaces as follows [104]:

$$Z=\left(p_1-p_2\right)/u_n, \tag{G.2}$$

where, *Z* is the holes impedance, and 1 and 2 denote the locations on the inner and the outer side of the holes, respectively.

At each frequency, the system of equations (global equations assembled from the elemental equations using the connectivity matrix) is set up and solved by using an iterative procedure to obtain pressure distribution **{** p_n **}**. The velocity field is then obtained by differentiating the pressure field at the Gauss points of the elements and then extrapolating and averaging at the nodes.

Once the solver of LMS Virtual Lab solves the global matrix equation, the acoustic pressure in the entire domain is found out at each frequency, and the pressure vector is used to find out the acoustic particle velocity. Plane wave propagation is assumed in the exhaust pipe and tail pipe of the muffler, and the transmission loss of the muffler proper is calculated by

$$TL = 20\log_{10}\left|\frac{p_i + Y_i u_i}{2Y_o u_o}\right| \tag{G.3}$$

where p is acoustic pressure, u is acoustic particle velocity and Y is characteristic impedance of the medium. Subscripts 'i' and 'o' indicate the inlet end of the exhaust pipe and outlet end of the tail pipe, respectively.

For computation of TL spectra of a muffler, only anechoic termination is required. However, the computation of IL spectra calls for the transfer matrix of a muffler. Computation of transfer matrix needs the acoustic state variables, i.e. acoustic pressure and acoustic mass velocity, at the upstream end and the downstream end of an acoustic element for two different terminations. For simplicity, these two different terminations can be rigid termination (rigid wall boundary condition) and zero radiation impedance termination (pressure release boundary condition). However, in the case of pressure release boundary condition, the author encountered a singularity in the 3-D FEM acoustic simulation using LMS Virtual Lab. Nevertheless, the four-pole parameters of a muffler can be determined using rigid termination and anechoic termination as two distinct boundary conditions at the downstream end.

The transfer matrix, which relates the acoustic state variables of the upstream station (subscript u) and the downstream station (subscript d) of an acoustic element, is given by:

$$\begin{bmatrix} p_u \\ v_u \end{bmatrix} = \begin{bmatrix} T_{11} & T_{12} \\ T_{21} & T_{22} \end{bmatrix} \begin{bmatrix} p_d \\ v_d \end{bmatrix} \tag{G.4}$$

where p and v are acoustic pressure and acoustic mass velocity at the respective stations. The relation between acoustic mass velocity, acoustic particle velocity, the density of the medium and area of the cross-section at the respective station is given by:

$$v = \rho_0 S u \tag{G.5}$$

In the case of rigid termination, the first column of the transfer matrix can be determined as follows:

$$T_{11} = \left. \frac{p_u}{p_d} \right|_{u_d = 0} \tag{G.6}$$

$$T_{21} = \rho_0 S_u \left. \frac{u_u}{p_d} \right|_{u_d = 0} \tag{G.7}$$

where u_u is known from the acoustic source boundary condition.

For the case of anechoic termination, the relation between the acoustic pressure at the downstream station, the speed of sound and the acoustic particle velocity is given by:

$$p_d = \rho_0 c_0 u_d \tag{G.8}$$

Combining Eqs. (G.4) and (G.8) and rearranging the terms, the elements of the second column of the transfer matrix are given by:

$$T_{12} = \frac{c_0}{S_d} \left(\left. \frac{p_u}{p_d} \right|_{p_d = \rho_0 c_0 u_d} - T_{11} \right) \tag{G.9}$$

$$T_{22} = \frac{c_0}{S_d} \left(\rho_0 S_u \left. \frac{u_u}{p_d} \right|_{p_d = \rho_0 c_0 u_d} - T_{21} \right) \tag{G.10}$$

TL and IL values may now be evaluated in terms of the transfer matrix parameters T_{11}, T_{12}, T_{21} and T_{22} by using the appropriate expressions derived in Ref. [1].

Appendix H: Computation of number of holes on perforates for given backpressure of SISO muffler configurations

The flow resistances of sudden area expansion, sudden area contraction and cross-flow perforates given by Eqs. (E.1)–(E.3), respectively, can be represented by one expression as [1]:

$$R = \varepsilon \frac{1}{2} \frac{\rho_0}{S^2} \tag{H.1}$$

where ε is a loss factor and S is the minimum cross-sectional area of upstream and downstream pipes in case of sudden area discontinuities and the cross-sectional area of perforated pipe in case of cross-flow perforate. Loss factors for different elements are listed in Table H.1 [1].

Table H.1. Loss factors of different elements [1]

Element	Sudden expansion	Sudden contraction	Cross flow perforate
Loss factor (ε)	$\left(1-\frac{S_u}{S_d}\right)^2$	$\frac{1}{2}\left(1-\frac{S_d}{S_u}\right)$	$\frac{1}{\left(C_D \times OAR\right)^2}$

The open area ratio (*OAR*) of a perforate is defined as the ratio of area of holes and the cross-sectional area of perforated pipe [1]:

$$OAR = \frac{n_h d_h^2}{d_p^2} \tag{H.2}$$

where n_h, d_h and d_p are number of holes, diameter of holes, and diameter of perforated pipe, respectively.

The stagnation pressure drop across any flow resistance is $Q^2 R$, where Q is the volume flow rate through the flow resistance. Thus, the stagnation pressure drop across any flow resistance element is given as:

$$\Delta p = \varepsilon \left(\frac{1}{2} \rho_0 U^2 \right) \tag{H.3}$$

where U is the mean flow velocity corresponding to the cross-sectional area S. The term $0.5\rho_0 U^2$ is called the dynamic head.

Cross-sectional areas of the inlet pipe, the outlet pipe and the intermediate pipes in the all three muffler configurations are same. Therefore, the number of dynamic head (N) corresponding to the exhaust pipe for maximum allowable backpressure can be expressed as:

$$N = \frac{\Delta P_{\text{allowable}}}{H}, \quad H = \frac{1}{2}\rho_0 U_{ep}^2 \tag{H.4}$$

The values of parameters in Eq. (H.4) are given in Table H.2.

Table H.2. Flow velocity and stagnation pressure drop parameters

Parameter	$\Delta P_{allowable}$ (kPa)	U_{ep} (m/s)	$H = 1/2\rho_0 U_{ep}^2$ (kPa)	N
Value	5.4	94.8	2.0	2.7

Thus, the limiting value of backpressure $\Delta P_{\text{allowable}}$ is 2.7 H, where H is the dynamic head in exhaust pipe.

H.1 SISO C-1 muffler

In order to have, minimum backpressure the flow resistance of two parallel paths (intermediate pipes) are kept same for all three muffler configurations. The flow loss factors for flow through inner pipe no. 1 and no. 2 are ε_I and ε_{II}, respectively, being equal, these are denoted by a common symbol ε_{ip}. Flow loss factors of flow through the inlet and outlet pipes are denoted by ε_{in} and ε_{out}, respectively. Thus, the total backpressure of muffler configurations can be written as:

$$\Delta p = \frac{1}{2}\rho_0 U_{ep}^2 \left(\varepsilon_{in} + \varepsilon_{ip} + \varepsilon_{out}\right) \tag{H.5}$$

The area ratio at sudden area discontinuities are quite high, therefore the loss factor for expansion and contraction are taken as 1 and 0.5, respectively. Thus, the value of loss factor across the intermediate pipes becomes

$$\varepsilon_{ip} = N - 1.5 = 2.7 - 1.5 = 1.2 \tag{H.6}$$

The flow loss factor for each parallel paths is four times ε_{ip} because the flow velocity in each parallel path is half of U_{ep}. Flow loss factors of perforates of inner pipes no. 1 and no. 2, ε_I and ε_{II}, respectively, are given as:

$$\varepsilon_I = 4\varepsilon_{ip} - 1 = 3.8 \tag{H.7}$$

$$\varepsilon_{II} = 4\varepsilon_{ip} - 0.5 = 4.3 \tag{H.8}$$

Use of Eq. (H.2) in the cross-flow perforate loss factor from Table H.1 yields the following expressions for the number of holes on the perforate of inner pipes nos. 1 and 2, n_{h1} and n_{h2}, respectively for the muffler configuration no. 1:

$$n_{h1} = \frac{d_p^2}{d_h^2}\frac{1}{C_D\sqrt{\varepsilon_I}} = \frac{200^2}{6^2}\frac{1}{0.8\sqrt{3.8}} \cong 712 \tag{H.9}$$

$$n_{h2} = \frac{d_p^2}{d_h^2}\frac{1}{C_D\sqrt{\varepsilon_{II}}} = \frac{200^2}{6^2}\frac{1}{0.8\sqrt{4.3}} \cong 670 \tag{H.10}$$

The number of holes may not be an integer, and even if it is integer, yet it may not be arranged in a regular pattern. Thus, the number of holes are adjusted in such a way that it can be arranged nicely in a pattern. The porosity of perforated pipes and end plates are adjusted to be approximately 20 %.

H.2 SISO C-2 muffler

The value of ε_{ip} for this configuration is also given by Eq. (H.6). The flow resistances at each end of each intermediate pipe are in series. Thus, the value of flow loss factors of perforates at each end of intermediate pipes should be equal to $2\,\varepsilon_{ip}$. The number of holes (n_{hc}) in each end perforate of muffler configuration no. 2 is given by:

$$n_{hc} = \frac{d_p^2}{d_h^2}\frac{1}{C_D\sqrt{2\varepsilon_{ip}}} = \frac{200^2}{6^2}\frac{1}{0.8\sqrt{2.4}} \cong 897 \tag{H.11}$$

H.3 SISO C-3 muffler

For muffler configuration no. 3, the perforates are on each end of intermediate pipes as well as at the ends of inlet/outlet pipes inside the muffler shell. The flow loss factors ε_{in}, ε_{ip} and ε_{out} are kept the same ($=N/3$). Thus, number of holes on perforate of inlet/outlet pipes $n_{h,in/out}$ and number of holes on each perforate end of intermediate pipes n_{ip} are given as:

$$n_{h,in/out} = \frac{d_p^2}{d_h^2}\frac{1}{C_D\sqrt{\varepsilon_{ip}}} = \frac{200^2}{6^2}\frac{1}{0.8\sqrt{0.9}} \cong 1464 \tag{H.12}$$

$$n_{h,ip} = \frac{d_p^2}{d_h^2}\frac{1}{C_D\sqrt{2\varepsilon_{ip}}} = \frac{200^2}{6^2}\frac{1}{0.8\sqrt{1.8}} \cong 1035 \tag{H.13}$$

H.4 SISO C-4 muffler

The baffle of muffler configuration no. 4 is perforated. The flow loss factor ε_{ip} is for the combination of holes on intermediate pipes and the perforated baffle. Since the volume flow rate through three parallel paths as well as the stagnation pressure are same. The value of loss factor of each parallel path is 9 times of ε_{ip}. The perforates on intermediate pipes are in series. Thus, the loss factor of each perforate end of intermediate pipes is 4.5 times of ε_{ip}. The number of holes on each perforate end of intermediate pipes $n_{h,ip}$ and the number of holes on perforated baffle are given as:

$$n_{h,ip} = \frac{d_p^2}{d_h^2}\frac{1}{C_D\sqrt{4.5\varepsilon_{ip}}} = \frac{200^2}{6^2}\frac{1}{0.8\sqrt{4.05}} \cong 690 \tag{H.14}$$

$$n_{h,baffle} = 2n_{ip} \cong 1380 \tag{H.15}$$

Appendix I: Transfer Matrix Across *n* Parallel Paths

Selamet and Easwaran [105] derived the transfer matrix relation between the upstream and downstream junction of *n* parallel tubes modified Herschel Quincke-Tube. Here the derivation is done for the most generalized *n*-parallel paths as shown in Fig. I.1.

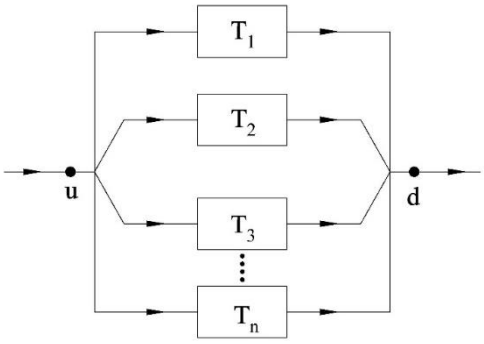

Figure I.1: The schematic diagram of *n* parallel paths emanating from the upstream junction and merging at the downstream junction

Momentum conservation and mass continuity at the upstream junction yield:

$$p_u = p_{1u} = p_{2u} = \cdots = p_{nu} \qquad \text{(I.1) – (I.n)}$$

$$v_u = v_{1u} + v_{2u} + \cdots + v_{nu} \qquad \text{(I.n+1)}$$

Similarly, at the downstream junction:

$$p_d = p_{1d} = p_{2d} = \cdots = p_{nd} \qquad \text{(I.n+2) – (I.2n+1)}$$

$$v_d = v_{1d} + v_{2d} + \cdots + v_{nd} \qquad \text{(I.2n+2)}$$

The transfer matrix relation between the upstream and the downstream station for the m^{th} path is given by:

$$\begin{bmatrix} p_{mu} \\ v_{mu} \end{bmatrix} = \begin{bmatrix} T_{m,11} & T_{m,12} \\ T_{m,21} & T_{m,22} \end{bmatrix} \begin{bmatrix} p_{md} \\ v_{md} \end{bmatrix}, \quad m = 1, 2, ..., n. \qquad \text{(I.2n+3)}$$

Using Eq. (I.2n+3), Eqs. (I.1) – (I.n) can be written as

$$p_u = T_{m,11} p_{md} + T_{m,12} v_{md}, \quad m = 1, 2, ..., n. \qquad \text{(I.2n+4) – (I.3n+3)}$$

Equation (I.n+1) can be written as

$$v_u = \sum_{m=1}^{n} T_{m,21} p_{md} + \sum_{m=1}^{n} T_{m,22} v_{md} \qquad \text{(I.3n+4)}$$

Equations (I.n+2) – (I.2n+1) and (I.2n+2) can be written as

$$p_d = p_{md}, \quad m = 1, 2, ..., n. \qquad \text{(I.3n+5) – (I.4n+4)}$$

$$v_d = \sum_{m=1}^{n} v_{md} \qquad \text{(I.4n+5)}$$

Inverting the matrix Eq. (I.2n+3) yields

$$\begin{bmatrix} p_{md} \\ v_{md} \end{bmatrix} = \begin{bmatrix} U_{m,11} & U_{m,12} \\ U_{m,21} & U_{m,22} \end{bmatrix} \begin{bmatrix} p_{mu} \\ v_{mu} \end{bmatrix}, \text{ where } m = 1, 2, ..., n. \qquad \text{(I.4n+6)}$$

Dividing both sides of Eqs. (I.2n+4) – (I.3n+3) by the corresponding $T_{m,12}$ and summing up yields

$$p_u \sum_{m=1}^{n} \frac{1}{T_{m,12}} = p_d \sum_{m=1}^{n} \frac{T_{m,11}}{T_{m,12}} + v_d \qquad \text{(I.4n+7)}$$

Similar procedure applied to Eq. (I.4n+6) yields

$$p_d \sum_{m=1}^{n} \frac{1}{U_{m,12}} = p_u \sum_{m=1}^{n} \frac{U_{m,11}}{U_{m,12}} + v_u \qquad \text{(I.4n+8)}$$

Substituting the value of p_u from Eq. (I.4n+7) into Eq. (I.4n+8) and rearranging yields

$$v_u = p_d \left(\sum_{m=1}^{n} \frac{1}{U_{m,12}} - \frac{\sum_{m=1}^{n} \left(T_{m,11} / T_{m,12} \right)}{\sum_{m=1}^{n} \left(1 / T_{m,12} \right)} \sum_{m=1}^{n} \frac{U_{m,11}}{U_{m,12}} \right) - v_d \frac{\sum_{m=1}^{n} \left(U_{m,11} / U_{m,12} \right)}{\sum_{m=1}^{n} \left(1 / T_{m,12} \right)} \qquad \text{(I.4n+9)}$$

Finally, Eqs. (I.4n+7) and (I.4n+9) yield the desired transfer matrix relation between the acoustic state variables at the upstream junction and the downstream junction as

$$\begin{bmatrix} p_u \\ v_u \end{bmatrix} = \begin{bmatrix} \dfrac{\sum_{m=1}^{n} \left(T_{m,11} / T_{m,12} \right)}{\sum_{m=1}^{n} \left(1 / T_{m,12} \right)} & \dfrac{1}{\sum_{m=1}^{n} \left(1 / T_{m,12} \right)} \\ \sum_{m=1}^{n} \dfrac{1}{U_{m,12}} - \dfrac{\sum_{m=1}^{n} \left(T_{m,11} / T_{m,12} \right)}{\sum_{m=1}^{n} \left(1 / T_{m,12} \right)} \sum_{m=1}^{n} \dfrac{U_{m,11}}{U_{m,12}} & -\dfrac{\sum_{m=1}^{n} \left(U_{m,11} / U_{m,12} \right)}{\sum_{m=1}^{n} \left(1 / T_{m,12} \right)} \end{bmatrix} \begin{bmatrix} p_d \\ v_d \end{bmatrix} \qquad \text{(I.4n+10)}$$

Appendix J: Application of the 1-D ITM Approach to the SISO Muffler Configurations

In all four muffler configurations studied in Chapter 7, the 1-D ITM approach [64] can be applied for the section between the upstream and the downstream of the intermediate pipes. The transfer matrix [T] can now relate the acoustic state variables of the end chambers at the upstream section and the downstream section of the intermediate pipes.

J.1 SISO muffler configuration no. 1

Figure J.1 shows the schematic diagram of the section of muffler configuration no. 1 where the 1-D ITM approach can be applied. Domains 1, 2 and 3 represent annular region, inner pipe no. 1 and inner pipe no. 2, respectively.

The acoustic state variables of domains 1, 2 and 3 at section 0 are related to those at section 4 as in Eq. (J.1).

$$\begin{bmatrix}[S_{1,0}]\\ [S_{2,0}]\\ [S_{3,0}]\end{bmatrix} = \begin{bmatrix}[P_{1,0\_1}] & [O]_{2\times2} & [O]_{2\times2}\\ [O]_{2\times2} & [B_{2,0\_1}] & [O]_{2\times2}\\ [O]_{2\times2} & [O]_{2\times2} & [P_{3,0\_1}]\end{bmatrix}\begin{bmatrix}[P_{1,1\_2}] & [O]_{2\times2} & [O]_{2\times2}\\ [O]_{2\times2} & [P_{2,1\_2}] & [O]_{2\times2}\\ [O]_{2\times2} & [O]_{2\times2} & [P_{3,1\_2}]\end{bmatrix}$$
$$\times\begin{bmatrix}E_{1,2,2\_3}(1:2,1:2) & E_{1,2,2\_3}(1:2,3:4) & [O]_{2\times2}\\ E_{1,2,2\_3}(3:4,1:2) & E_{1,2,2\_3}(3:4,3:4) & [O]_{2\times2}\\ [O]_{2\times2} & [O]_{2\times2} & [P_{3,2\_3}]\end{bmatrix} \tag{J.1}$$
$$\times\begin{bmatrix}[P_{1,3\_4}] & [O]_{2\times2} & [O]_{2\times2}\\ [O]_{2\times2} & [P_{2,3\_4}] & [O]_{2\times2}\\ [O]_{2\times2} & [O]_{2\times2} & [P_{3,3\_4}]\end{bmatrix}\begin{bmatrix}[S_{1,4}]\\ [S_{2,4}]\\ [S_{3,4}]\end{bmatrix}$$

Here, $S_{i,j} = [p_{i,j} \quad v_{i,j}]^T$ represents the acoustic state vector of the i^{th} domain at the j^{th} section. Acoustic state variables $p_{i,j}$ and $v_{i,j}$ are acoustic pressure and acoustic mass velocity, respectively. P_{i,j_k} and B_{i,j_k}, are the transfer matrices of uniform pipe and baffle of i^{th} domain which relates the state variables of the j^{th} section to the k^{th} section, respectively. Transfer matrix E_{i,j,k_l} relates the state variables of the k^{th} section to the l^{th} section in interacting i^{th} domain and j^{th} domain.

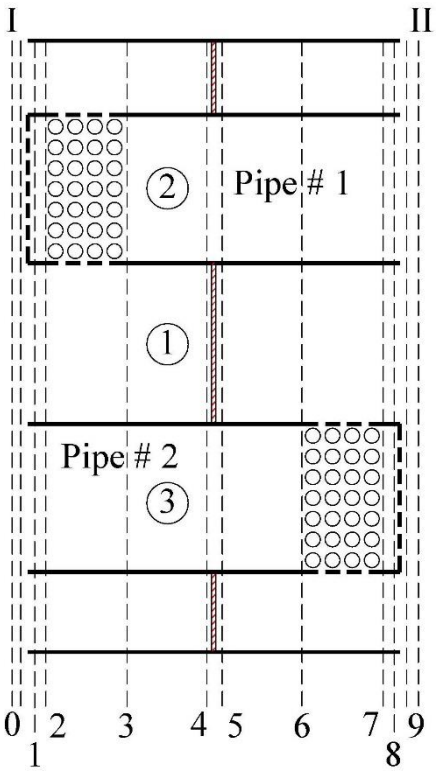

Figure J.1. Schematic diagram of the section of SISO muffler C-1 for 1-D ITM approach

The overall transfer matrix, which relates the acoustic state variables of domains 1, 2 and 3 at section 0 to those at section 4, is termed as [A].

The relation between the acoustic state variables at section I of left end chamber and section 0 of domains of 1, 2 and 3 is obtained by applying the mass continuity and momentum conservation equations that are given by Eqs. (J.2)–(J.5).

$$p_I = p_{1,0} = p_{2,0} = p_{3,0} \qquad \text{(J.2) – (J.4)}$$

$$v_I = v_{1,0} + v_{2,0} + v_{3,0} \qquad \text{(J.5)}$$

The rigid wall boundary conditions at sections 4 and 5 for domain are given by Eqs. (J.6) and (J.7), respectively.

$$v_{1,4} = 0 \qquad \text{(J.6)}$$

$$v_{1,5} = 0 \qquad \text{(J.7)}$$

The acoustic state variables of domains 2 and 3 at section 4 are related to those at section 5 as in Eq. (J.8).

$$\begin{bmatrix}[S_{2,4}]\\ [S_{3,4}]\end{bmatrix}=\begin{bmatrix}[P_{2,4\_5}] & [O]_{2\times2}\\ [O]_{2\times2} & [P_{3,4\_5}]\end{bmatrix}\begin{bmatrix}[S_{2,5}]\\ [S_{3,5}]\end{bmatrix} \tag{J.8}$$

The overall transfer matrix, which relates the acoustic state variables of domains 2 and 3 at section 4 to those at section 5, is termed as [B].

The acoustic state variables of domains 1, 2 and 3 at section 5 are related to those at section 9 as in Eq. (J.9).

$$\begin{bmatrix}[S_{1,5}]\\ [S_{2,5}]\\ [S_{3,5}]\end{bmatrix}=\begin{bmatrix}[P_{1,5\_6}] & [O]_{2\times2} & [O]_{2\times2}\\ [O]_{2\times2} & [P_{2,5\_6}] & [O]_{2\times2}\\ [O]_{2\times2} & [O]_{2\times2} & [P_{3,5\_6}]\end{bmatrix}\begin{bmatrix}E_{1,3,6\_7}(1:2,1:2) & [O]_{2\times2} & E_{1,3,6\_7}(1:2,3:4)\\ [O]_{2\times2} & [P_{2,6\_7}] & [O]_{2\times2}\\ E_{1,3,6\_7}(3:4,1:2) & [O]_{2\times2} & E_{1,3,6\_7}(3:4,3:4)\end{bmatrix}$$
$$\times\begin{bmatrix}[P_{1,7\_8}] & [O]_{2\times2} & [O]_{2\times2}\\ [O]_{2\times2} & [P_{2,7\_8}] & [O]_{2\times2}\\ [O]_{2\times2} & [O]_{2\times2} & [P_{3,7\_8}]\end{bmatrix}\begin{bmatrix}[P_{1,8\_9}] & [O]_{2\times2} & [O]_{2\times2}\\ [O]_{2\times2} & [P_{2,8\_9}] & [O]_{2\times2}\\ [O]_{2\times2} & [O]_{2\times2} & [B_{3,8\_9}]\end{bmatrix}\begin{bmatrix}[S_{1,9}]\\ [S_{2,9}]\\ [S_{3,9}]\end{bmatrix} \tag{J.9}$$

The overall transfer matrix, which relates the acoustic state variables of domains 1, 2 and 3 at section 5 to those at section 9, is termed as [C].

The relation between the acoustic state variables at section II of right end chamber and section 0 of domains of 1, 2 and 3 is obtained by applying the mass continuity and momentum conservation equations that are given by Eqs. (J.10)–(J.13).

$$p_{II}=p_{1,0}=p_{2,0}=p_{3,0} \tag{J.10) – (J.12}$$

$$v_{II}=v_{1,0}+v_{2,0}+v_{3,0} \tag{J.13}$$

Equations (J.1) – (J.13) contains 28 variables and 26 linear system of equations. Thus, the 26 variables can be expressed in terms of the acoustic state variables p_{II} and v_{II} as given by the matrix equation (J.14). The inverse of the 26×26 matrix in Eq. (J.14) is termed as *U*. Thus, the acoustic state variables at the upstream of the intermediate pipes in the left end chamber can be related to those at the downstream of intermediate pipes in the right end chamber as:

$$\begin{bmatrix}p_I\\ v_I\end{bmatrix}=\begin{bmatrix}U_{1,25} & U_{2,25}\\ U_{1,26} & U_{2,26}\end{bmatrix}\begin{bmatrix}p_{II}\\ v_{II}\end{bmatrix} \tag{J.15}$$

$$
\begin{bmatrix}
-1 & 0 & 1 & 0 & 0 & 0 & 0 & 0 & 0 & 0 & 0 & 0 & 0 & 0 & 0 & 0 & 0 & 0 & 0 & 0 & 0 & 0 & 0 & 0 & 0 & 0 \\
-1 & 0 & 0 & 0 & 1 & 0 & 0 & 0 & 0 & 0 & 0 & 0 & 0 & 0 & 0 & 0 & 0 & 0 & 0 & 0 & 0 & 0 & 0 & 0 & 0 & 0 \\
-1 & 0 & 0 & 0 & 0 & 0 & 1 & 0 & 0 & 0 & 0 & 0 & 0 & 0 & 0 & 0 & 0 & 0 & 0 & 0 & 0 & 0 & 0 & 0 & 0 & 0 \\
0 & -1 & 0 & 1 & 0 & 1 & 0 & 1 & 0 & 0 & 0 & 0 & 0 & 0 & 0 & 0 & 0 & 0 & 0 & 0 & 0 & 0 & 0 & 0 & 0 & 0 \\
0 & 0 & 1 & 0 & 0 & 0 & 0 & 0 & \bullet & \bullet & \bullet & \bullet & \bullet & \bullet & 0 & 0 & 0 & 0 & 0 & 0 & 0 & 0 & 0 & 0 & 0 & 0 \\
0 & 0 & 0 & 1 & 0 & 0 & 0 & 0 & \bullet & & & & & \bullet & 0 & 0 & 0 & 0 & 0 & 0 & 0 & 0 & 0 & 0 & 0 & 0 \\
0 & 0 & 0 & 0 & 1 & 0 & 0 & 0 & \bullet & & -[A] & & & \bullet & 0 & 0 & 0 & 0 & 0 & 0 & 0 & 0 & 0 & 0 & 0 & 0 \\
0 & 0 & 0 & 0 & 0 & 1 & 0 & 0 & \bullet & & & & & \bullet & 0 & 0 & 0 & 0 & 0 & 0 & 0 & 0 & 0 & 0 & 0 & 0 \\
0 & 0 & 0 & 0 & 0 & 0 & 1 & 0 & \bullet & & & & & \bullet & 0 & 0 & 0 & 0 & 0 & 0 & 0 & 0 & 0 & 0 & 0 & 0 \\
0 & 0 & 0 & 0 & 0 & 0 & 0 & 1 & \bullet & \bullet & \bullet & \bullet & \bullet & \bullet & 0 & 0 & 0 & 0 & 0 & 0 & 0 & 0 & 0 & 0 & 0 & 0 \\
0 & 0 & 0 & 0 & 0 & 0 & 0 & 0 & 0 & 1 & 0 & 0 & 0 & 0 & 0 & 0 & 0 & 0 & 0 & 0 & 0 & 0 & 0 & 0 & 0 & 0 \\
0 & 0 & 0 & 0 & 0 & 0 & 0 & 0 & 0 & 0 & 0 & 0 & 0 & 0 & 0 & 1 & 0 & 0 & 0 & 0 & 0 & 0 & 0 & 0 & 0 & 0 \\
0 & 0 & 0 & 0 & 0 & 0 & 0 & 0 & 0 & 0 & 1 & 0 & 0 & 0 & 0 & 0 & \bullet & \bullet & \bullet & \bullet & 0 & 0 & 0 & 0 & 0 & 0 \\
0 & 0 & 0 & 0 & 0 & 0 & 0 & 0 & 0 & 0 & 0 & 1 & 0 & 0 & 0 & 0 & \bullet & -[B] & & \bullet & 0 & 0 & 0 & 0 & 0 & 0 \\
0 & 0 & 0 & 0 & 0 & 0 & 0 & 0 & 0 & 0 & 0 & 0 & 1 & 0 & 0 & 0 & \bullet & & & \bullet & 0 & 0 & 0 & 0 & 0 & 0 \\
0 & 0 & 0 & 0 & 0 & 0 & 0 & 0 & 0 & 0 & 0 & 0 & 0 & 1 & 0 & 0 & \bullet & \bullet & \bullet & \bullet & 0 & 0 & 0 & 0 & 0 & 0 \\
0 & 0 & 0 & 0 & 0 & 0 & 0 & 0 & 0 & 0 & 0 & 0 & 0 & 0 & 1 & 0 & 0 & 0 & 0 & 0 & \bullet & \bullet & \bullet & \bullet & \bullet & \bullet \\
0 & 0 & 0 & 0 & 0 & 0 & 0 & 0 & 0 & 0 & 0 & 0 & 0 & 0 & 0 & 1 & 0 & 0 & 0 & \bullet & & & & & & \bullet \\
0 & 0 & 0 & 0 & 0 & 0 & 0 & 0 & 0 & 0 & 0 & 0 & 0 & 0 & 0 & 0 & 1 & 0 & 0 & \bullet & & -[C] & & & & \bullet \\
0 & 0 & 0 & 0 & 0 & 0 & 0 & 0 & 0 & 0 & 0 & 0 & 0 & 0 & 0 & 0 & 0 & 1 & 0 & \bullet & & & & & & \bullet \\
0 & 0 & 0 & 0 & 0 & 0 & 0 & 0 & 0 & 0 & 0 & 0 & 0 & 0 & 0 & 0 & 0 & 0 & 1 & \bullet & & & & & & \bullet \\
0 & 0 & 0 & 0 & 0 & 0 & 0 & 0 & 0 & 0 & 0 & 0 & 0 & 0 & 0 & 0 & 0 & 0 & 0 & 1 & \bullet & \bullet & \bullet & \bullet & \bullet & \bullet \\
0 & 0 & 0 & 0 & 0 & 0 & 0 & 0 & 0 & 0 & 0 & 0 & 0 & 0 & 0 & 0 & 0 & 0 & 0 & -1 & 0 & 1 & 0 & 0 & 0 & 0 \\
0 & 0 & 0 & 0 & 0 & 0 & 0 & 0 & 0 & 0 & 0 & 0 & 0 & 0 & 0 & 0 & 0 & 0 & 0 & -1 & 0 & 0 & 0 & 1 & 0 & 0 \\
0 & 0 & 0 & 0 & 0 & 0 & 0 & 0 & 0 & 0 & 0 & 0 & 0 & 0 & 0 & 0 & 0 & 0 & 0 & 1 & 0 & 0 & 0 & 0 & 0 & 0 \\
0 & 0 & 0 & 0 & 0 & 0 & 0 & 0 & 0 & 0 & 0 & 0 & 0 & 0 & 0 & 0 & 0 & 0 & 0 & 0 & 1 & 0 & 1 & 0 & 0 & 1
\end{bmatrix}
\begin{bmatrix}
p_I \\ v_I \\ p_{1,0} \\ v_{1,0} \\ p_{2,0} \\ v_{2,0} \\ p_{3,0} \\ v_{3,0} \\ p_{1,4} \\ v_{1,4} \\ p_{2,4} \\ v_{2,4} \\ p_{3,4} \\ v_{3,4} \\ p_{1,5} \\ v_{1,5} \\ p_{2,5} \\ v_{2,5} \\ p_{3,5} \\ v_{3,5} \\ p_{1,9} \\ v_{1,9} \\ p_{2,9} \\ v_{2,9} \\ p_{3,9} \\ v_{3,9}
\end{bmatrix}
=
\begin{bmatrix}
0 \\ 0 \\ 0 \\ 0 \\ 0 \\ 0 \\ 0 \\ 0 \\ 0 \\ 0 \\ 0 \\ 0 \\ 0 \\ 0 \\ 0 \\ 0 \\ 0 \\ 0 \\ 0 \\ 0 \\ 0 \\ 0 \\ 0 \\ 0 \\ 0 \\ p_{II} \\ v_{II}
\end{bmatrix}
\tag{J.14}
$$

J.2 SISO muffler configurations nos. 2 and 3

The section between the upstream and the downstream of the intermediate pipes of the muffler configuration nos. 2 and 3 as shown in Fig. J.2 are different from the muffler configuration no. 1 in following aspects:

i. In muffler configuration nos. 2 and 3, the perforated end plates are on both ends of intermediate pipes whereas in muffler configuration no. 1 it is at inlet end of intermediate pipe no. 1 and at outlet end of intermediate pipe no. 2.

ii. The segments between 2 and 3 as well as 6 and 7 are three interacting ducts in muffler configurations nos. 2 and 3, whereas in muffler configuration no. 1 these segments are two interacting ducts.

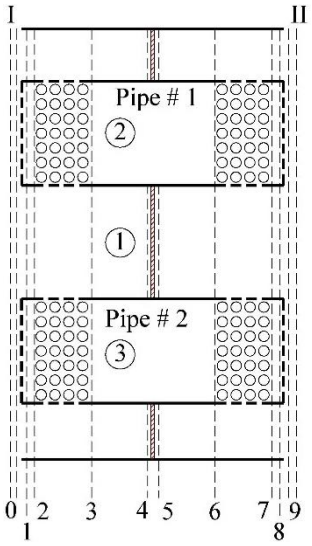

Figure J.2. Schematic diagram of the section of SISO muffler C-2 and C-3 for 1-D ITM approach

The acoustic state variables of domains 1, 2 and 3 at section 5 are related to those at section 9 as in Eq. (J.17). This equation is corresponding to Eq. (J.9) of muffler configuration no. 1.

$$\begin{bmatrix}[S_{1,0}]\\ [S_{2,0}]\\ [S_{3,0}]\end{bmatrix}=\begin{bmatrix}[P_{1,0\_1}] & [O]_{2\times2} & [O]_{2\times2}\\ [O]_{2\times2} & [B_{2,0\_1}] & [O]_{2\times2}\\ [O]_{2\times2} & [O]_{2\times2} & [B_{3,0\_1}]\end{bmatrix}\begin{bmatrix}[P_{1,1\_2}] & [O]_{2\times2} & [O]_{2\times2}\\ [O]_{2\times2} & [P_{2,1\_2}] & [O]_{2\times2}\\ [O]_{2\times2} & [O]_{2\times2} & [P_{3,1\_2}]\end{bmatrix}$$
$$\times[E_{1,2,3,2\_3}]\begin{bmatrix}[P_{1,3\_4}] & [O]_{2\times2} & [O]_{2\times2}\\ [O]_{2\times2} & [P_{2,3\_4}] & [O]_{2\times2}\\ [O]_{2\times2} & [O]_{2\times2} & [P_{3,3\_4}]\end{bmatrix}\begin{bmatrix}[S_{1,4}]\\ [S_{2,4}]\\ [S_{3,4}]\end{bmatrix} \quad \text{(J.16)}$$

$$\begin{bmatrix}[S_{1,5}]\\ [S_{2,5}]\\ [S_{3,5}]\end{bmatrix}=\begin{bmatrix}[P_{1,5\_6}] & [O]_{2\times2} & [O]_{2\times2}\\ [O]_{2\times2} & [P_{2,5\_6}] & [O]_{2\times2}\\ [O]_{2\times2} & [O]_{2\times2} & [P_{3,5\_6}]\end{bmatrix}[E_{1,2,3,6\_7}]$$
$$\times\begin{bmatrix}[P_{1,7\_8}] & [O]_{2\times2} & [O]_{2\times2}\\ [O]_{2\times2} & [P_{2,7\_8}] & [O]_{2\times2}\\ [O]_{2\times2} & [O]_{2\times2} & [P_{3,7\_8}]\end{bmatrix}\begin{bmatrix}[P_{1,8\_9}] & [O]_{2\times2} & [O]_{2\times2}\\ [O]_{2\times2} & [B_{2,8\_9}] & [O]_{2\times2}\\ [O]_{2\times2} & [O]_{2\times2} & [B_{3,8\_9}]\end{bmatrix}\begin{bmatrix}[S_{1,9}]\\ [S_{2,9}]\\ [S_{3,9}]\end{bmatrix} \quad \text{(J.17)}$$

All other equations are similar to those of muffler configuration no. 1. And, following the similar procedure given for muffler configuration no. 1 a 2×2 overall transfer matrix between the upstream of the intermediate pipes in the left end chamber and the downstream of the intermediate pipes in the right end chamber can be obtained as given in Eq. (J.15).

J.3 SISO muffler configuration no. 4

It can be observed from Fig. J.3 that the baffle between sections 4 and 5 are perforated. Thus, the 1-D ITM approach can be directly applied between section 0–9. The acoustic state variables of domains 1, 2 and 3 at section 0 are related to those at section 9 as in Eq. (J.18). The overall transfer matrix, which relates the acoustic state variables of domains 1, 2 and 3 at section 0 to those at section 9, is termed as [D].

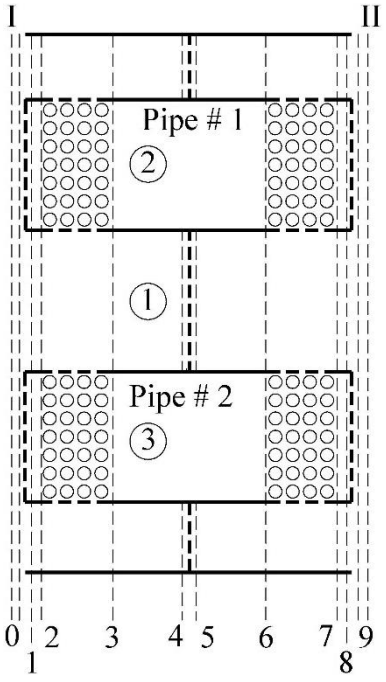

Figure J.3: Schematic diagram of the section of SISO muffler C-4 for 1-D ITM approach

$$\begin{bmatrix}[S_{1,0}]\\[S_{2,0}]\\[S_{3,0}]\end{bmatrix}=\begin{bmatrix}[P_{1,0\_1}] & [O]_{2\times2} & [O]_{2\times2}\\ [O]_{2\times2} & [B_{2,0\_1}] & [O]_{2\times2}\\ [O]_{2\times2} & [O]_{2\times2} & [B_{3,0\_1}]\end{bmatrix}\begin{bmatrix}[P_{1,1\_2}] & [O]_{2\times2} & [O]_{2\times2}\\ [O]_{2\times2} & [P_{2,1\_2}] & [O]_{2\times2}\\ [O]_{2\times2} & [O]_{2\times2} & [P_{3,1\_2}]\end{bmatrix}[E_{1,2,3,2\_3}]$$
$$\times\begin{bmatrix}[P_{1,3\_4}] & [O]_{2\times2} & [O]_{2\times2}\\ [O]_{2\times2} & [P_{2,3\_4}] & [O]_{2\times2}\\ [O]_{2\times2} & [O]_{2\times2} & [P_{3,3\_4}]\end{bmatrix}\begin{bmatrix}[B_{1,4\_5}] & [O]_{2\times2} & [O]_{2\times2}\\ [O]_{2\times2} & [P_{2,4\_5}] & [O]_{2\times2}\\ [O]_{2\times2} & [O]_{2\times2} & [P_{3,4\_5}]\end{bmatrix}$$
$$\times\begin{bmatrix}[P_{1,5\_6}] & [O]_{2\times2} & [O]_{2\times2}\\ [O]_{2\times2} & [P_{2,5\_6}] & [O]_{2\times2}\\ [O]_{2\times2} & [O]_{2\times2} & [P_{3,5\_6}]\end{bmatrix}[E_{1,2,3,6\_7}]\begin{bmatrix}[P_{1,7\_8}] & [O]_{2\times2} & [O]_{2\times2}\\ [O]_{2\times2} & [P_{2,7\_8}] & [O]_{2\times2}\\ [O]_{2\times2} & [O]_{2\times2} & [P_{3,7\_8}]\end{bmatrix}$$
$$\times\begin{bmatrix}[P_{1,8\_9}] & [O]_{2\times2} & [O]_{2\times2}\\ [O]_{2\times2} & [B_{2,8\_9}] & [O]_{2\times2}\\ [O]_{2\times2} & [O]_{2\times2} & [B_{3,8\_9}]\end{bmatrix}\begin{bmatrix}[S_{1,9}]\\[S_{2,9}]\\[S_{3,9}]\end{bmatrix} \tag{J.18}$$

The relation between the acoustic state variables at section I of left end chamber and section 0 of domains of 1, 2 and 3 is obtained by applying the mass continuity and momentum conservation equations that are given by Eqs. (J.19)–(J.22).

$$p_I = p_{1,0} = p_{2,0} = p_{3,0} \tag{J.19) – (J.21}$$

$$v_I = v_{1,0} + v_{2,0} + v_{3,0} \tag{J.22}$$

The relation between the acoustic state variables at section II of right end chamber and section 0 of domains of 1, 2 and 3 is obtained by applying the mass continuity and momentum conservation equations that are given by Eqs. (J.23)–(J.26).

$$p_{II} = p_{1,0} = p_{2,0} = p_{3,0} \tag{J.23) – (J.25}$$

$$v_{II} = v_{1,0} + v_{2,0} + v_{3,0} \tag{J.26}$$

Equations (J.18)–(J.26) contains 16 variables and 14 linear system of equations. Thus, the 14 variables can be expressed in terms of the acoustic state variables p_{II} and v_{II} as given by Eq. (J.27).

$$\begin{bmatrix} -1 & 0 & 1 & 0 & 0 & 0 & 0 & 0 & 0 & 0 & 0 & 0 & 0 & 0 \\ -1 & 0 & 0 & 0 & 1 & 0 & 0 & 0 & 0 & 0 & 0 & 0 & 0 & 0 \\ -1 & 0 & 0 & 0 & 0 & 0 & 1 & 0 & 0 & 0 & 0 & 0 & 0 & 0 \\ 0 & -1 & 0 & 1 & 0 & 1 & 0 & 1 & 0 & 0 & 0 & 0 & 0 & 0 \\ 0 & 0 & 1 & 0 & 0 & 0 & 0 & 0 & \bullet & \bullet & \bullet & \bullet & \bullet & \bullet \\ 0 & 0 & 0 & 1 & 0 & 0 & 0 & 0 & \bullet & & & & & \bullet \\ 0 & 0 & 0 & 0 & 1 & 0 & 0 & 0 & \bullet & & -[D] & & & \bullet \\ 0 & 0 & 0 & 0 & 0 & 1 & 0 & 0 & \bullet & & & & & \bullet \\ 0 & 0 & 0 & 0 & 0 & 0 & 1 & 0 & \bullet & & & & & \bullet \\ 0 & 0 & 0 & 0 & 0 & 0 & 0 & 1 & \bullet & \bullet & \bullet & \bullet & \bullet & \bullet \\ 0 & 0 & 0 & 0 & 0 & 0 & 0 & 0 & -1 & 0 & 1 & 0 & 0 & 0 \\ 0 & 0 & 0 & 0 & 0 & 0 & 0 & 0 & -1 & 0 & 0 & 0 & 1 & 0 \\ 0 & 0 & 0 & 0 & 0 & 0 & 0 & 0 & 1 & 0 & 0 & 0 & 0 & 0 \\ 0 & 0 & 0 & 0 & 0 & 0 & 0 & 0 & 0 & 1 & 0 & 1 & 0 & 1 \end{bmatrix} \begin{bmatrix} p_I \\ v_I \\ p_{1,0} \\ v_{1,0} \\ p_{2,0} \\ v_{2,0} \\ p_{3,0} \\ v_{3,0} \\ p_{1,9} \\ v_{1,9} \\ p_{2,9} \\ v_{2,9} \\ p_{3,9} \\ v_{3,9} \end{bmatrix} = \begin{bmatrix} 0 \\ 0 \\ 0 \\ 0 \\ 0 \\ 0 \\ 0 \\ 0 \\ 0 \\ 0 \\ 0 \\ 0 \\ p_{II} \\ v_{II} \end{bmatrix} \tag{J.27}$$

The inverse of the 14×14 matrix in Eq. (J.27) is termed as [V]. Thus, the acoustic state variables at the upstream of intermediate pipes in the left end chamber can be related to those at the downstream of the intermediate pipes in the right end chamber as:

$$\begin{bmatrix} p_I \\ v_I \end{bmatrix} = \begin{bmatrix} V_{1,13} & V_{1,14} \\ V_{2,13} & V_{2,14} \end{bmatrix} \begin{bmatrix} p_{II} \\ v_{II} \end{bmatrix} \tag{J.28}$$

References:

[1] M.L. Munjal, Acoustics of Ducts and Mufflers, Second Edition, Wiley, Chichester, UK, 2014.

[2] A.D. Jones, Noise Characteristics and Exhaust Process Gas Dynamics of a Small 2-Stroke Engine, PhD Thesis, University of Adelaide, 1978.

[3] D.D. Davis Jr., G.M. Stokes, D. Moore, G.L. Stevens Jr., Theoretical and Experimental Investigation of Mufflers with Comments on Engine-Exhaust Muffler Design, 1954.

[4] M. Fukuda, A study on the exhaust muffler of internal combustion engine, Bull. JSME. 6 (1963) 255–269.

[5] C.M. Harris, Handbook of Noise Control, McGraw-Hill, New York, 1957.

[6] A. V. Sreenath, M.L. Munjal, Evaluation of noise attenuation due to exhaust mufflers, J. Sound Vib. 12 (1970) 1–19.

[7] G.D. Callow, K.S. Peat, Insertion Loss of engine inflow and exhaust silencers, I Mech. E. C19/88 (1988) 39–46.

[8] M.L. Munjal, A.V. Sreenath, M.V. Narasimhan, Velocity ratio in the analysis of linear dynamical systems, J. Sound Vib. 26 (1973) 173–191.

[9] M.L. Munjal, A.V. Sreenath, M.V. Narasimhan, An algebraic algorithm for the design and analysis of linear dynamical systems, J. Sound Vib. 26 (1973) 193–208.

[10] R.J. Alfredson, P.O.A.L. Davies, The radiation of sound from an engine exhaust, J. Sound Vib. 13 (1970) 389–408.

[11] M.L. Munjal, Velocity ratio-cum-transfer matrix method for the evaluation of a muffler with mean flow, J. Sound Vib. 39 (1975) 105–119.

[12] M.L. Munjal, A.G. Doige, On the relation between convective source characteristics and their acoustic counterparts, J. Sound Vib. 136 (1990) 343–346.

[13] S. Howe, Attenuation of Sound in a Low Mach Number Nozzle Flow Attenuation of Sound in a Low Mach Number Nozzle Flow, J. Fluid Mech. 91 (1979) 209–229.

[14] M.L. Kathuriya, M.L. Munjal, A method for the experimental evaluation of the acoustic characteristics of an engine exhaust system in the presence of mean flow, J. Acoust. Soc. Am. 60 (1976) 745–751.

[15] M.L. Kathuriya, M.L. Munjal, Experimental evaluation of the aeroacoustic characteristics of a source of pulsating gas flow, J. Acoust. Soc. Am. 65 (1979) 240–248.

[16] V.H. Gupta, M.L. Munjal, On numerical prediction of the acoustic source characteristics of an engine exhaust system, J. Acoust. Soc. Am. 92 (1992) 2716–2725.

[17] M.G. Prasad, A four load method for evaluation of acoustical source impedance in a duct, J. Sound Vib. 114 (1987) 347–356.

[18] B.S. Sridhara, Error analysis for the four-load method used to measure the source impedance in ducts, J. Acoust. Soc. Am. 92 (1992) 2924–2931.

[19] S.-H. Jang, J.-G. Ih, Refined multiload method for measuring acoustical source characteristics of an Intake or Exhaust System, J. Acoust. Soc. Am. 107 (2000) 3217–3225.

[20] L. Desmons, J. Hardy, A Least Squares Method for Evaluation of Characteristics of Acoustical Sources, J. Sound Vib. 175 (1994) 365–376.

[21] L. Desmons, J. Hardy, Y. Auregan, Determination of the acoustical source characteristics of an internal combustion engine by using several calibrated loads, J. Sound Vib. 179 (1995) 869–878.

[22] H. Bodén, On multi-load methods for determination of the source data of acoustic one-port sources, J. Sound Vib. 180 (1995) 725–743.

[23] S.-H. Jang, J.-G. Ih, On the selection of loads in the multiload method for measuring the acoustic source parameters of duct systems, J. Acoust. Soc. Am. 111 (2002) 1171–1176.

[24] S. Zheng, H. Liu, J. Dan, X. Lian, Analysis of the load selection on the error of source characteristics identification for an engine exhaust system, J. Sound Vib. 344 (2015) 126–137.

[25] J.-G. Ih, K.S. Peat, On the causes of negative source impedance in the measurement of intake and exhaust noise sources, Appl. Acoust. 63 (2002) 153–171.

[26] H. Bodén, H. Bodén, The multiple load method for measuring the source characteristics of time-variant sources, J. Sound Vib. 148 (1991) 437–453.

[27] K.S. Peat, J.-G. Ih, An analytical investigation of the indirect measurement method of estimating the acoustic impedance of a time-varying source, J. Sound Vib. 244 (2001) 821–835.

[28] H. Rämmal, H. Bodén, Modified multi-load method for nonlinear source characterisation, J. Sound Vib. 299 (2007) 1094–1113.

[29] T.-K. Kim, J.-G. Ih, S.-H. Jang, On the nonlinear and time-varying acoustic modeling of the simplified intake or exhaust silencing system, Int. J. Automot. Technol. 15 (2014) 165–173.

[30] J. Lavrentjev, H. Bodén, M. Åbom, A linaerity test for acoustic one-port sources, J. Sound Vib. 155 (1992) 534–539.

[31] H. Bodén, F. Albertson, Linearity tests for in-duct acoustic one-port sources, J. Sound Vib. 237 (2000) 45–65.

[32] V. Macián, A.J. Torregrosa, A. Broatch, P.C. Niven, S.A. Amphlett, A view on the internal consistency of linear source identification for I.C. engine exhaust noise prediction, Math. Comput. Model. 57 (2013) 1867–1875.

[33] M.G. Prasad, M.J. Crocker, Acoustical source characterization studies on a multi-cylinder engine exhaust system, J. Sound Vib. 90 (1983) 479–490.

[34] J.Y. Chung, D.A. Blaser, Transfer function method of measuring in-duct acoustic properties. I. Theory, J. Acoust. Soc. Am. 68 (1980) 907–913.

[35] J.Y. Chung, D.A. Blaser, Transfer function method of measuring in-duct acoustic properties. II. Experiment, J. Acoust. Soc. Am. 68 (1980) 914–921.

[36] D.F. Ross, M.J. Crocker, Measurement of the acoustic internal source impedance of an internal combustion engine, J. Acoust. Soc. Am. 74 (1983) 18–27.

[37] M.G. Prasad, M.J. Crocker, Studies of acoustical performance of a multi-cylinder engine exhaust muffler system, J. Sound Vib. 90 (1983) 491–508.

[38] K.S. Peat, An analytical investigation of the direct measurement method of estimating the acoustic impedance of a time-varying source, J. Sound Vib. 256 (2002) 271–285.

[39] Y. Sathyanarayana, M.L. Munjal, A hybrid approach for aeroacoustic analysis of the engine exhaust system, Appl. Acoust. 60 (2000) 425–450.

[40] R.N. Hota, A new hybrid approach for thermo-acoustic modeling of engine exhaust system, Indian Institute of Science, 2008.

[41] R.N. Hota, Acoustic Source Characterization of the Exhaust and Intake Systems of I. C. Engines, PhD Thesis, Indian Institute of Science, 2008.

[42] R.N. Hota, M.L. Munjal, Approximate empirical expressions for the aeroacoustic source strength level of the exhaust system of compression ignition engines, Int. J. Aeroacoustics. 7 (2008) 349–371.

[43] R.N. Hota, M.L. Munjal, Acoustic source characteristics of the exhaust and intake systems of a spark ignition engine, in: INTER-NOISE, 2010: pp. 443–452.

[44] M.L. Munjal, A.G. Doige, On uniqueness, transfer and combination of acoustic sources in one-dimensional systems, J. Sound Vib. 121 (1988) 25–35.

[45] K.S. Peat, M. Elasari, S. Dequand, A linear acoustic model of the passive acoustic effect of the turbine in an automotive turbocharger, in: Int. Congr. Sound Vib., Stockholm, Sweden, 2003.

[46] K.S. Peat, A.J. Torregrosa, A. Broatch, T. Fernández, An investigation into the passive acoustic effect of the turbine in an automotive turbocharger, J. Sound Vib. 295 (2006) 60–75.

[47] H. Tiikoja, H. Rämmal, M. Åbom, H. Bodén, Investigations of Automotive Turbocharger Acoustics, SAE Int. J. Engines. 4 (2011) 2531–2542.

[48] H. Tiikoja, H. Rämaal, M. Åbom, H. Bodén, Test-rig for complete acoustic characterization of turbochargers, in: Proc. 16th AIAA/CEAS Aeroacoustics Conf., 2010.

[49] J. Igarashi, M. Toyama, Fundamentals of Acoustical Silencers (I) Theory and experiment of low-pass filters, Tokyo, 1958.

[50] T. Miwa, J. Igarashi, Fundamentals of Acoustical Silencers (II) Determination of four terminal constants of acoustical elements, Tokyo, 1959.

[51] J. Igarashi, M. Arai, Fundamentals of Acoustical Silencers (III) Attenuation charaeteristics studied by an electric simulator, Tokyo, 1960.

[52] M.L. Munjal, M. V. Narasimhan, A. V. Sreenath, A rational approach to the synthesis of one-dimensional acoustic filters, J. Sound Vib. 29 (1973) 263–280.

[53] J.W. Sullivan, M.J. Crocker, Analysis of concentric-tube resonators having unpartitioned cavities, J. Acoust. Soc. Am. 64 (1978) 207–215.

[54] J.W. Sullivan, A method for modeling perforated tube muffler components. I. Theory, J. Acoust. Soc. Am. 66 (1979) 772–778.

[55] J.W. Sullivan, A method for modeling perforated tube muffler components. II. Applications, J. Acoust. Soc. Am. 66 (1979) 779–788.

[56] K. Jayaraman, K. Yam, Decoupling approach to modeling perforated tube muffler components, J. Acoust. Soc. Am. 69 (1981) 390–396.

[57] M.L. Munjal, K.N. Rao, A.D. Sahasrabudhe, Aeroacoustic analysis of perforated muffler components, J. Sound Vib. 114 (1987) 173–188.

[58] K.S. Peat, A numerical decoupling analysis of perforated pipe silencer elements, J. Sound Vib. 123 (1988) 199–212.

[59] E. Dokumaci, Matrizant approach to acoustic analysis of perforated multiple pipe mufflers carrying mean flow, J. Sound Vib. 191 (1996) 505–518.

[60] G.R. Gogate, M.L. Munjal, Analytical and experimental aeroacoustic studies of open-ended three-duct perforated elements used in mufflers, J. Acoust. Soc. Am. 97 (1995) 2919–2927.

[61] T. Kar, M.L. Munjal, Generalized analysis of a muffler with any number of interacting ducts, J. Sound Vib. 285 (2005) 585–596.

[62] P. Chaitanya, M.L. Munjal, Effect of wall thickness on the end corrections of the extended inlet and outlet of a double-tuned expansion chamber, Appl. Acoust. 72 (2011) 65–70.

[63] E. Ramya, M.L. Munjal, Improved tuning of the extended concentric tube resonator for wide-band transmission loss, Noise Control Eng. J. 62 (2014) 252–263.

[64] T. Elnady, M. Åbom, S. Allam, Modeling perforates in mufflers using two-ports, J. Vib. Acoust. 132 (2010) 06101-1–11.

[65] N.K. Vijayasree, M.L. Munjal, On an Integrated Transfer Matrix method for multiply connected mufflers, J. Sound Vib. 331 (2012) 1926–1938.

[66] C.J. Young, M.J. Crocker, Prediction of transmission loss in mufflers by the finite−element method, J. Acoust. Soc. Am. 57 (1975) 144–148.

[67] C.I.J. Young, M.J. Crocker, Acoustical analysis, testing, and design of flow-reversing muffler chambers, J. Acoust. Soc. Am. 60 (1976) 1111–1118.

[68] D.F. Ross, A finite element analysis of perforated component acoustic systems, J. Sound Vib. 79 (1981) 133–143.

[69] K.S. Peat, Evaluation of four-pole parameters for ducts with flow by the finite element method, J. Sound Vib. 84 (1982) 389–395.

[70] C.N. Wang, C.C. Tse, Y.N. Chen, Analysis of three dimensional muffler with boundary element method, Appl. Acoust. 40 (1993) 91–106.

[71] C.-N. Wang, C.-C. Tse, Y.-N. Chen, A boundary element analysis of a concentric-tube resonator, Eng. Anal. Bound. Elem. 12 (1993) 21–27.

[72] C.N. Wang, A numerical scheme for the analysis of perforated intruding tube muffler components, Appl. Acoust. 44 (1995) 275–286.

[73] Z. Ji, Q. Ma, Z. Zhang, Application of the boundary element method to predicting acoustic performance of expansion chamber mufflers with mean flow, J. Sound Vib. 173 (1994) 57–71.

[74] A. Selamet, P.M. Radavich, The Effect of Length on the Acoustic Attenuation Performance of Concentric Expansion Chambers: An Analytical, Computational and Experimental Investigation, J. Sound Vib. 201 (1997) 407–426.

[75] A. Selamet, Z.L. Ji, Acoustic Attenuation Performance of Circular Expansion Chambers With Offset Inlet/Outlet: I. Analytical Approach, J. Sound Vib. 213 (1998) 601–617.

[76] A. Selamet, Z.L. Ji, P.M. Radavich, Acoustic Attenuation Performance of Circular Expansion Chambers With Offset Inlet/Outlet: II. Comparison With Experimental and Computational Studies, J. Sound Vib. 213 (1998) 619–641.

[77] Z.L. Ji, A. Selamet, Boundary element analysis of three-pass perforated duct mufflers, Noise Control Eng. 48 (2000) 151–156.

[78] Z.L. Ji, Boundary element acoustic analysis of hybrid expansion chamber silencers with perforated facing, Eng. Anal. Bound. Elem. 34 (2010) 690–696.

[79] A. Verma, M.L. Munjal, Flow-acoustic analysis of the perforated-baffle three-chamber hybrid muffler configurations, SAE Int. J. Passeng. Cars - Mech. Syst. 8(2015-26-(2015) 370–381.

[80] V. Sagar, M.L. Munjal, Design and analysis of a novel muffler for wide-band transmission loss, low back pressure and reduced flow-induced noise, Noise Control Eng. J. 64 (2016) 208–216.

[81] V. Sagar, M.L. Munjal, Analysis and design guidelines for fork mufflers with H-connection, Appl. Acoust. 125 (2017) 49–58.

[82] M.L. Munjal, S. Krishnan, M.M. Reddy, Flow-acoustic performance of the perforated elements with application to design, Noise Control Eng. J. 40 (1993) 159–167.

[83] V. Kumar, M.L. Munjal, Design and Analysis of a Plug-Muffler Modified for Low Back-Pressure and Improved Acoustic Performance, J. Veh. Dyn. Stability, NVH. 1 (2017) 44–57.

[84] V. Kumar, M.L. Munjal, Flow-acoustic lumped element analysis of the side-inlet / outlet combination mufflers and 1-D and FEM validation thereof, Noise Control Eng. J. 65 (2017) 197–211.

[85] V. Kumar, M.L. Munjal, Flow-acoustic lumped element analysis of the side-inlet and axial-outlet combination muffler, J. Acoust. Soc. India. 44 (2017) 61–70.

[86] F. Albertson, H. Bodén, J. Gilbert, Comparison of different methods to couple nonlinear source descriptions in the time domain to linear system descriptions in the frequency domain - Application to a simple valveless one-cylinder cold engine, J. Sound Vib. 291 (2006) 963–985.

[87] W.M. Wang, Matrix Formulation in Acoustical Analysis of Mechanically Driven Fluid Systems, J. Acoust. Soc. Am. 41 (1967) 1418–1423.

[88] Y. Zhang, J. Liu, D.W. Herrin, G. Kadlaskar, J. Liu, Using the Moebius transformation to predict the effect of source impedance on insertion loss, Noise Control Eng. J. 66 (2018) 105–116.

[89] W. Soedel, E. Padilla-Navas, B.D. Kotalik, On Helmholtz resonator effects in the discharge system of a two-cylinder compressor, J. Sound Vib. 30 (1973) 263–277.

[90] J.P. Elson, W. Soedel, Simulation of the interaction of compressor valves with acoustic back pressures in long discharge lines, J. Sound Vib. 34 (1974) 211–220.

[91] ISO 8528-10. Reciprocating internal combustion engine driven alternating current generating sets - Part 10: Measurement of airborne noise by the enveloping surface method; 1998.

[92] A. Bies, C.H. Hansen, Engineering noise control: theory and practice, 4th edition, Spon Press, London, 2009.

[93] Joint Departments of the Army, Air Force and Navy, USA, Noise and Vibration control for mechanical equipment, Washington, DC: Technical manual TM 5–805- 4/AFJMAN 32–1090; 1995.

[94] M.L. Munjal, Noise and Vibration Control, 1st edition, World Scientific in association with IISc Press, Singapore, 2013.

[95] ANSI Standard S1.4-1983. Specifications for Sound Level Meters; 1983.

[96] ANSI Standard S1.42-2001. Design Response of Weighting Networks for Acoustical Measurements; 2001.

[97] M.L. Munjal, N.K. Vijayasree, P. Chaitanya, Flow resistance network analysis of the back-pressure of automotive mufflers, Indian J. Eng. Mater. Sci. 20 (2013) 339–349.

[98] I. Heitner, How to estimate plant noises, Hydrocarb. Process. 47 (1968) 67–74.

[99] M.L. Munjal, Plane wave analysis of side inlet/outlet chamber mufflers with mean flow, Appl. Acoust. 52 (1997) 165–175.

[100] T. Elnady, S. Elsaadany, M. Åbom, Flow and Pressure Drop Calculation Using Two-Ports, J. Vib. Acoust. 133 (2011) 041016-1–8.

[101] J.B. Heywood, Internal combustion engine fundamentals, McGraw-Hill, New York, 1988.

[102] BOOST Version 17, AVL LIST GmbH, Graz, Austria. BOOST Examples manual Version 17; 2017.

[103] D. Neighuk, M.L. Munjal, A. Prasad, Pressure drop characteristics of perforated pipes with particular application to the concentric tube resonators, SAE Tech. Pap. 2015-01-23 (2015).

[104] LMS Virtual Lab 12-SL1, Technical Documentation, LMS International, Belgium, (2012).

[105] A. Selamet, V. Easwaran, Modified Herschel – Quincke tube: Attenuation and resonance for n-duct configuration, J. Acoust. Soc. Am. 102 (1997) 164–169.

List of Publications Constituting the Thesis

Journal Publications

[1] K. M. Kumar and M. L. Munjal, "On the crucial role of mean flow in the design of multiply-connected coaxial perforated element mufflers," *Noise Control Engineering Journal*, **65(5)**, 462–481, 2017.

[2] K. M. Kumar and M. L. Munjal, "Direct estimation and experimental validation of the acoustic source characteristics of two-cylinder naturally aspirated diesel engine exhaust system," *Applied Acoustics*, **135**, 70–84, 2018.

[3] K. M. Kumar and M. L. Munjal, "On development of rational design guidelines for large side-inlet side-outlet perforated element mufflers," *Noise Control Engineering Journal*, **66(4)**, 308–323, 2018.

[4] K. M. Kumar and M. L. Munjal, "Direct estimation and experimental validation of the acoustic source characteristics of turbocharged diesel engine exhaust system," *Applied Acoustics*, **149**, 171–180, 2019.

Conference Proceedings

[1] K. M. Kumar and M. L. Munjal, "Direct Evaluation of the Engine Acoustic Source Characteristics and Validation Thereof," *3rd Automotive Noise and Vibration Congress*, Pune, 2016, 28th–29th January, pp. 1–17.

[2] K. M. Kumar and M. L. Munjal, "A Simple Novel Method for Direct Evaluation of the Acoustic Source Impedance of the Exhaust System of a Single Cylinder Engine," *24th International Congress On Sound and Vibration*, London, 2017, 23rd–27th July, pp. 1–8. (**Peer reviewed conference**)

[3] K. M. Kumar and M. L. Munjal, "1-D Acoustical Analysis of a Typical Double Flow-Reversal Commercial Muffler of a Motorcycle Engine and 3-D Validation Thereof," *4th Automotive Noise and Vibration Congress*, Pune, 2017, 8th–9th November, pp. 1–11.